1. Report No. FHWA/TX-09/0-5123-3	2. Government Accession No.	3. Recipient's Catalog No.
4. Title and Subtitle MECHANISTIC-EMPIRICAL ASPHALT OVERLAY THICKNESS DESIGN AND ANALYSIS SYSTEM		5. Report Date November 2008 Resubmitted: February 2009 Resubmitted: July 2009 Published: October 2009
		6. Performing Organization Code
7. Author(s) Fujie Zhou, Sheng Hu, Xiaodi Hu, and Tom Scullion		8. Performing Organization Report No. Report 0-5123-3
9. Performing Organization Name and Address Texas Transportation Institute The Texas A&M University System College Station, Texas 77843-3135		10. Work Unit No. (TRAIS)
		11. Contract or Grant No. Project 0-5123
12. Sponsoring Agency Name and Address Texas Department of Transportation Research and Technology Implementation Office P. O. Box 5080 Austin, Texas 78763-5080		13. Type of Report and Period Covered Technical Report: September 2007-August 2008
		14. Sponsoring Agency Code

15. Supplementary Notes
Project performed in cooperation with the Texas Department of Transportation and the Federal Highway Administration.
Project Title: Development of an Advanced Overlay Design System Incorporating Both Rutting and Reflection Cracking Requirements
URL: http://tti.tamu.edu/documents/0-5123-3.pdf

16. Abstract
   The placement of an asphalt overlay is the most common method used by the Texas Department of Transportation (TxDOT) to rehabilitate existing asphalt and concrete pavements. The type of overlay and its required thickness are important decisions that TxDOT engineers make on a daily basis. To perform well, an asphalt overlay must have a balance of both good rut and crack resistance. Furthermore, overlay performance is highly influenced by many factors, such as existing pavement conditions, traffic loading, and environmental conditions. It has also recently become common practice to use two different materials in an overlay, the first being a crack resistant level up course and the second being a wearing surface. The properties of both overlay types have a big impact on performance. The main objective of the Research Project 0-5123 was to develop a comprehensive mechanistic-empirical (M-E) asphalt overlay design system to assist TxDOT engineers to make these design decisions.
    The design system developed incorporates models for both rutting and reflection cracking of the proposed overlay. The Paris' law-based reflection cracking model was evaluated and recommended for use in this study. This model requires the use of both stress intensity factors (SIF) and fracture properties (*A* and *n*) for predicting crack propagation caused by both traffic loading and thermal effects. For practical implementation of the SIF concept, a total of 34 SIF regression equations were developed based on more than 1.6 million finite element computations. The required fracture properties can be easily determined using the Overlay Tester. The proposed reflective cracking model was calibrated using performance data from three HMA overlay field case studies and then verified using the California's Heavy Vehicle Simulator test results. To predict asphalt overlay rutting, the well-known VESYS layer rutting model was used and later calibrated using the field rutting data from the National Center for Asphalt Technology (NCAT) test track 2006. The material properties required for this model are obtained from repeated load tests. The reasonableness and accuracy of the calibrated rutting was further verified by the field rutting data from NCAT test track 2000. Finally, the calibrated reflective cracking and rutting models were integrated into an asphalt overlay thickness design and analysis program. To assist in implementation, default values of material properties have been provided for all the overlay types currently used in Texas. The program provides the designer with a tool to evaluate on a project-level basis the impact of load transfer efficiency (LTE) on predicted life and to determine what level of LTE must be repaired in order to achieve adequate performance.
    In summary this study has developed a comprehensive overlay thickness design and analysis system based on solid engineering principles. The software package developed in this study has been provided to TxDOT. Based on the evaluations made in this study its predictions appear rational and reasonable. This system is ready for state-wide pilot implementation.

17. Key Words Reflective Cracking, Rutting, Stress Intensity Factor, Overlay Test, Repeated Load Test, Asphalt Overlay Design	18. Distribution Statement No restrictions. This document is available to the public through NTIS: National Technical Information Service Springfield, Virginia 22161 http://www.ntis.gov		
19. Security Classif.(of this report) Unclassified	20. Security Classif.(of this page) Unclassified	21. No. of Pages 154	22. Price

Form DOT F 1700.7 (8-72)   **Reproduction of completed page authorized**

MECHANISTIC-EMPIRICAL ASPHALT OVERLAY THICKNESS DESIGN AND ANALYSIS SYSTEM

by

Fujie Zhou, Ph.D., P.E.
Assistant Research Engineer
Texas Transportation Institute

Sheng Hu
Associate Transportation Researcher
Texas Transportation Institute

Xiaodi Hu
Research Associate
Texas Transportation Institute

and

Tom Scullion, P.E.
Research Engineer
Texas Transportation Institute

TEXAS TRANSPORTATION INSTITUTE
The Texas A&M University System
College Station, Texas   77843-3135

DISCLAIMER

The contents of this report reflect the views of the authors, who are responsible for the facts and the accuracy of the data presented herein. The contents do not necessarily reflect the official view or policies of the Texas Department of Transportation (TxDOT) or the Federal Highway Administration (FHWA). This report does not constitute a standard, specification, or regulation. The engineer in charge was Dr. Fujie Zhou, P.E. (Texas, # 95969).

There is no invention or discovery conceived or first actually reduced to practice in the course of or under this contract, including any art, method, process, machine, manufacture, design or composition of matter, or any new useful improvement thereof, or any variety of plant, which is or may be patentable under the patent laws of the United States of America or any foreign country.

ACKNOWLEDGMENTS

TABLE OF CONTENTS

TABLE OF CONTENTS (Continued)

LIST OF FIGURES

LIST OF FIGURES (Continued)

LIST OF FIGURES (Continued)

LIST OF FIGURES (Continued)

LIST OF TABLES

CHAPTER 1

INTRODUCTION

The construction of a hot-mix asphalt (HMA) overlay is the most common method used by the Texas Department of Transportation (TxDOT) to rehabilitate existing asphalt and concrete pavements. Selecting the appropriate overlay type and thickness are important decisions that TxDOT engineers make on a routine basis. However, this selection is a difficult balancing act, because for an HMA overlay to perform well it must have a balance of both good rut and crack resistance. Furthermore, asphalt overlay performance is highly influenced by many factors, such as existing pavement conditions, traffic volume, environmental condition, and asphalt overlay mixes. Therefore, there is a need to develop an advanced asphalt overlay design system considering all these influential factors and both rutting and reflective cracking requirements to assist TxDOT engineers in making decisions.

The three primary objectives of Research Project 0-5123 were to 1) develop an HMA overlay mix design balancing rutting and reflective cracking requirements, 2) develop guidelines for evaluating existing pavements focusing on identifying repair locations and collecting information needed for the HMA overlay thickness design in which the primary concern is reflective cracking, and 3) develop an HMA overlay thickness design system focusing on reflective cracking and rutting. The first two objectives have been completed and documented in the Year 1 report 0-5123-1 entitled "Integrated Asphalt (Overlay) Mixture Design, Balancing Rutting and Cracking Requirements," and the Year 2 report 0-5123-2 entitled "Guidelines for Evaluation of Existing Pavements for HMA Overlay," respectively. In the last two years the research team focused on the third objective of this research project and developed asphalt overlay thickness design system, which is documented in this report.

Chapter 2 discusses the development and calibration of a reflective cracking model for asphalt overlays, and similar development for asphalt overlay rutting is described in Chapter 3. Chapter 4 documents the asphalt overlay thickness design and analysis system and associated software incorporating both reflective cracking and rutting models developed in Chapters 2 and 3. Chapter 5 presents the sensitivity analysis of the asphalt overlay thickness design system. Finally, Chapter 6 summarizes the report and makes some recommendations.

CHAPTER 2

DEVELOPMENT AND CALIBRATION OF THE M-E REFLECTIVE CRACKING MODEL FOR ASPHALT OVERLAYS

INTRODUCTION

An HMA overlay is one of the primary options for rehabilitating existing HMA concrete pavements and Portland cement concrete (PCC) pavements. HMA overlays often exhibit a cracking pattern similar to that which had previously existed in the old pavement shortly after opening to traffic. This propagation of a crack from the existing pavement into and through a new HMA overlay is known as reflective cracking. Reflective cracking is most common in HMA overlays placed on PCC pavements, but it also occurs in overlays on cracked asphalt concrete pavements as well as in asphalt pavements with stabilized bases. It is well known that when reflective cracking occurs, the infiltration of water can cause rapid deterioration of the underlying pavement structure including the foundation, thus, reducing the pavement service life. However, a rational reflective cracking model for HMA overlay design and analysis is still missing. The reflective cracking model in the Mechanistic-Empirical Design Guide (MEPDG) developed under the NCHRP Project 1-37A is a pure empirical model (*1*). Therefore, there is a need to develop an M-E reflective crack model for routine HMA overlay thickness design and analysis.

The basic mechanism for reflective cracking is strain concentration in the overlay due to the movement in the existing pavement at the vicinity of joints and/or cracks. This movement may be induced by bending or shearing action resulting from traffic loads or daily and seasonal temperature changes, as shown in Figure 2-1. In fact, the majority of reflective cracking is caused by the combination of all these mechanisms. As shown in Figure 2-1b, every pass of a traffic load will induce two shear plus one bending action on the HMA overlay. Also, these bending and shear actions are affected by the daily temperature variations. Thus, the combination of all these three mechanisms (bending, shearing, and thermal) is crucial to successfully model reflective cracking. In addition, reflective crack propagation is also influenced by other factors such as the existing pavement's structural geometry and HMA overlay fracture properties, specifically, the load transfer efficiency at joints and cracks. Therefore, all the three mechanisms and associated influencing factors must be addressed in the M-E reflective cracking model. Based on this background, the main objective of this chapter was to develop such an M-E reflective cracking model for HMA overlay design and analysis.

The research approach utilized to achieve the above objective includes three steps:

1) reflective cracking model review and recommendations;

2) development of the Paris' law-based fracture mechanics approach for predicting reflective cracking of HMA overlays; and

3) preliminary calibration of the developed reflective cracking model.

The detailed work conducted is presented in the subsequent text.
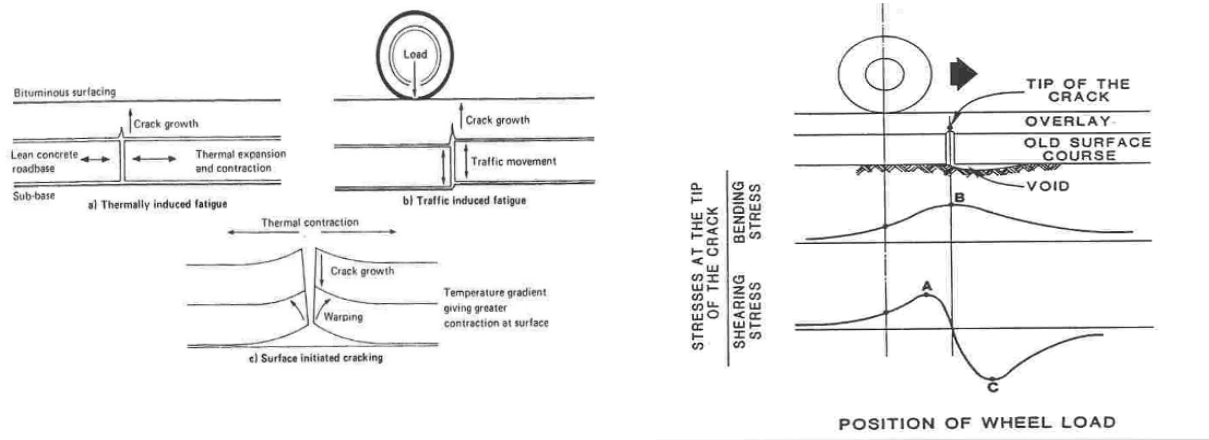
(a) (Nunn (*2*))   (b) (Lytton (*3*))

Figure 2-1. Mechanisms of Reflective Cracking.

REFLECTIVE CRACKING MODEL REVIEW AND RECOMMENDATION

Reflective cracking has been a serious concern associated with HMA overlay over existing pavements from as early as 1932, when Gary and Martin (*4*) studied this problem. Since then, many studies have been conducted to address this problem. Various models have been developed to analyze or predict reflective cracking. In general, these models can be categorized as follows:

1) empirical model (*1, 5*),

2) extended multi-layer linear elastic model (*6, 7*),

3) equilibrium equations-based models (*8, 9*),

4) finite element (FE) plus traditional fatigue equation model,

5) Paris' law-based fracture mechanics model,

6) cohesive cracking/zone model, and

7) non-local continuum damage mechanics-based model.

The first three models are considered too simple to accurately model the reflective cracking phenomenon. Thus, the following discussion will focus on the last four reflective cracking models.

FE + Traditional Fatigue Equation Model

Monismith and Coetzee (*10*) made a comprehensive review on reflective cracking in 1980. One of their recommendations was to use the FE to examine the state of strain of HMA overlay around the crack in the existing pavement. The computed strain can then be used with standard fatigue analysis methods for prediction of the HMA overlay life. In 2002, Sousa et al. (*11*) improved this approach using the critical Von Mises strain instead of tensile strain at the crack tip and developed a statistical model to evaluate the critical Von Mises strain, which makes this approach possible for routine applications. However, the major limitation of this approach is no consideration of the crack propagation, as noted by Wu (*12*).

4

Most recently, Wu (*12*) proposed an M-E design procedure to mitigate reflective cracking; see Figure 2-2. The proposed procedure depends on three models: 1) the statistical critical strain model, 2) the regression model that links the initial conditions of an HMA overlay to its crack through time N_{CDM}, and 3) the model for calculating the shift factor C accounting for traffic wander, aging, etc. Wu (*12*) just established the first statistical critical strain model. The other two models were left for future study. Note that the second model requires the use of the first model as well as collecting damage evolution law parameters for typical HMA mixes and running FE simulations with non-local continuum damage mechanics model for thousands of overlay structures. The third model requires the use of the first two models as well as collecting extensive field performance data. Significant efforts are still needed to accomplish this work.
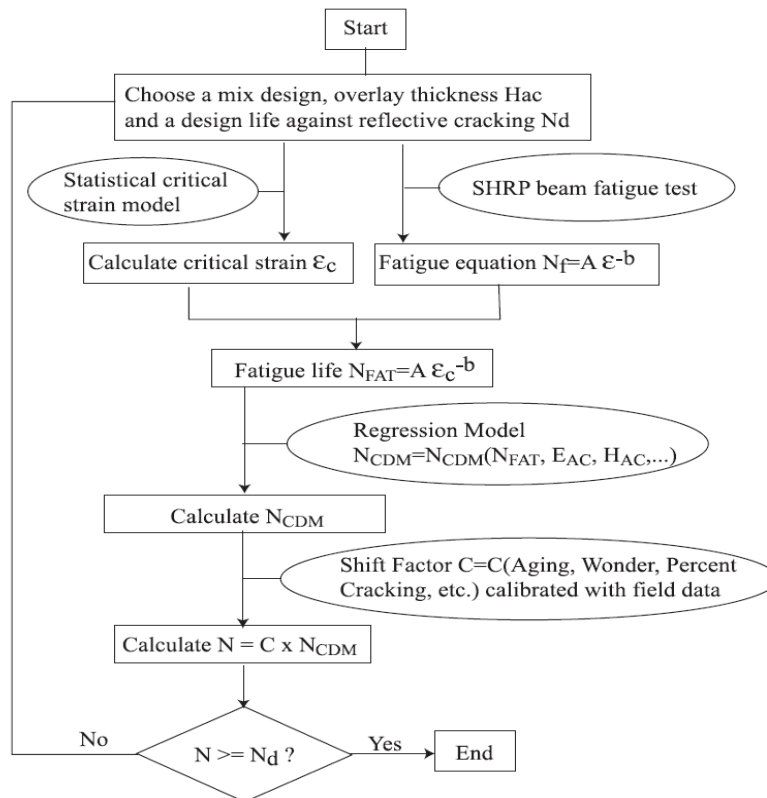
Figure 2-2. Overlay Design Flow Chart Proposed by Wu (*12*).

Paris' Law-Based Fracture Mechanics Model

Since Majidzadeh (*13*) introduced the fracture mechanics concepts into the field of asphalt pavements in 1970, the fracture mechanics approach has been widely used in predicting pavement cracking. Different from continuum mechanics, the fracture mechanics approach focuses on crack propagation. The crack propagation process can be caused by Modes I, II, III, or a combination of two or all the three modes of loading (see Figure 2-3).

Mode I: Opening mode   Mode II: Shearing mode   Mode III: Tearing mode
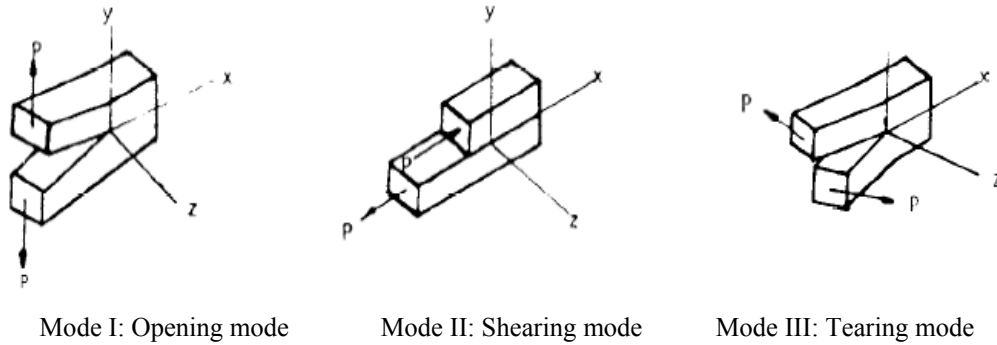
Figure 2-3. Three Modes of Crack Opening Displacement (*13*).

The fact that the combined mechanisms of reflective crack propagation (bending, shearing, and thermal stress) can be exactly modelled by fracture Modes I and II makes the fracture mechanics approach very attractive for modelling reflective cracking.

The most widely used crack propagation law was proposed by Paris and Erdogan (*14*) in the form of Equation 2-1.

$$\frac{dc}{dN} = A \times (\Delta K)^n \qquad (2\text{-}1)$$

where *c* is the crack length; *N* is the number of loading cycles; *A* and *n* are fracture properties of the HMA mixture often determined by laboratory tests; and *ΔK* is the stress intensity factor (SIF) amplitude, depending on the geometry of the pavement structure, fracture mode, and crack length.

The use of Paris' law for describing the crack growth process in visco-elastic materials, such as HMA mixtures, has been theoretically justified by Schapery (*15, 16*). Also, it has been successfully applied to predict reflective cracking of HMA overlays (*17-24*) and low temperature cracking (*25*). Apparently, the key for using Paris' law is to establish a simple way to calculate the SIF under various traffic loads and daily temperature variations and to practically determine HMA fracture properties (*A* and *n*), which are the main focus of this chapter.

Cohesive Crack/Zone Model

HMA concrete fracture is a complex phenomenon; there is a strongly nonlinear fracture process zone (FPZ) around the crack tip in the HMA concrete. In order to account for a relatively large plastic yield zone ahead of a crack tip, the cohesive cracking model (CCM) has been adopted to characterize HMA concrete fracture (*26-35*). Buttlar and his associates (*33-35*) have simulated the reflective cracking development using the CCM. The simulation results showed that the CCM is very promising with great potential. However, the application of the CCM to HMA concrete is still in the preliminary stage. Most of the above studies only applied the CCM to cracking under monotonic loading. To extend the CCM to repeated loading and crack propagation, additional material parameters describing damage accumulation under unloading and reloading cycles are needed. To the knowledge of the authors, there has not been much work done on this subject yet. In general, the CCM is still in its infancy and not readily applicable for routine HMA overlay designs and analyses. More research is still needed in this area.

Non-Local Continuum Damage Mechanics Model for Reflective Cracking

Another advanced mechanics-based model used for modelling reflective cracking is the non-local Continuum Damage Mechanics (CDM) model (*12, 36*). The ultimate state of local CDM corresponds generally to macroscopic crack initiation upon which it becomes a crack propagation problem and should be considered in the framework of fracture mechanics. If the local CDM is used to describe crack propagation (such as reflective cracking), the spurious mesh dependency then comes into play. Fortunately, this mesh-dependency can be avoided by introducing non-local mechanics. Bazant and Jirasek (*37*) made a comprehensive, state-of-the-research review of non-local formulations and provided a series of causes as well as motivations for introducing non-local continuum. However, the non-local CDM for HMA reflective cracking is relatively rare, and the results presented by Wu et al. (*36*) are promising, but just like the CCM, is still under development.

In summary, both the CCM and non-local CDM, compared to the FE+traditional fatigue equation model and the Paris' law-based fracture mechanics model are more advanced with great potential. However, both models are still under development. Thus, these two advanced models are not ready for practical application on a daily basis. As noted previously, development of the FE+traditional fatigue equation model has not been completed yet (*12*). Therefore, the best choice for the reflective cracking model at present is the Paris' law-based fracture mechanics model. In the past, the Paris' law-based fracture mechanics model was used to a limited extent because of the difficulties of calculating the SIFs and determining HMA fracture properties (*A* and *n*). However, these two difficulties have been recently resolved through development of the *SA-CrackPro* program specifically tailored for pavement SIF analysis and an upgraded Overlay Tester (OT) for the HMA fracture properties (*38, 39*).

Recommended Reflective Cracking Model

The recommended reflective cracking model in this research project includes three components: reflective crack propagation model, reflective cracking damage model, and reflective cracking amount model. The format of each of these models is presented in the following discussion.

- **Reflective Crack Propagation Model**

The general reflective crack propagation model (Equation 2-2) is based on Paris' law with the combination of bending, shearing, and thermal loading.

$$\Delta C = k_1 A \left(K_{bending} \right)^n \Delta N_i + k_2 A \left(K_{shearing} \right)^n \Delta N_i + k_3 A \left(K_{thermal} \right)^n \qquad (2\text{-}2)$$

where ΔC is the daily crack length increment; ΔN is the daily load repetitions; A and n are the HMA fracture properties; $K_{bending}$, $K_{shearing}$, and $K_{thermal}$ are the SIF caused by bending, shearing, and thermal loading, respectively; and k_1, k_2, and k_3 are the calibration factors.

- **Reflective Cracking Damage Model**

$$D = \sum \Delta C / h \qquad (2\text{-}3)$$

where D is the damage ratio; h is the overlay thickness; and $\sum \Delta C$ is the total crack length.

- **Reflective Cracking Amount Model**

A sigmoidal model as presented in Equation 2-4 is used to describe the development of the reflective cracking amount:

$$RCR = \frac{100}{1 + e^{C_1 \log D}} \tag{2-4}$$

where RCR is the reflective cracking rate (%); $C_1 = -7.0$ is used based on the relationship between the observed fatigue distress vs. damage (*39*); and D is the damage from Equation 2-3.

It is clear that the two key issues of the recommended reflective cracking model are how to quickly compute the SIFs under various traffic and thermal loads and to practically determine HMA fracture properties (*A* and *n*). It is worth noting that the traffic loading is often very fast and within a very short period of time so that the HMA mixes can be assumed to be quasi-elastic materials represented by the elastic (dynamic) modulus and Poisson's ratio. In contrast, the thermal loading often lasts several hours (or days) so that the HMA mixes are better represented using a visco-elastic model. In this study, a hybrid thermal reflective crack propagation model, similar to the low-temperature cracking model (*25*), is proposed. More detailed information is presented in the following sections.

TRAFFIC LOAD RELATED SIF AND ASSOCIATED REGRESSION EQUATIONS

As noted previously, the SIF calculation is a very critical and difficult aspect of reflective crack propagation analysis. To make the SIF calculations easy and practical, the authors have developed a semi-analytical (*SA*) FE-based crack propagation program named *SA-CrackPro* (*38*). The *SA-CrackPro* is essentially a 2D SIF calculation program that incorporates an SA method so that the *SA-CrackPro* can provide the same satisfactory computations and results as a 3D FE program, but at a much faster speed. Also, an accuracy verification of the *SA-CrackPro* with the commercial *ANSYS* FE program (*40*) yielded comparable results, as shown in Table 2-1 (*38*). For an old pavement being overlaid, it is reasonable to assume that the load transfer at the joint/crack is only contributed by the aggregate interlock (shearing). This shearing load transfer at a joint/crack is modelled using the thin-layer element and shearing modulus (log*k*) in the *SA-CrackPro* program. After substantial analyses, reasonable log*k* values corresponding to different load transfer conditions were established and listed in Table 2-2. More detailed information about the *SA-CrackPro* program, FE mesh, pavement structure and boundary conditions, and the comparison with the *ANASYS* FE program can be found in reference *38*.

Table 2-1. SIF Comparison between *SA-CrackPro* and ANSYS-3D (*38*).

Crack Length (inch)	K_I (MPa* mm$^{0.5}$)			K_{II} (MPa* mm$^{0.5}$)		
	SA-CrackPro	ANSYS-3D	Error (%)	SA-CrackPro	ANSYS-3D	Error (%)
0.3	1.724	1.641	4.8	2.560	2.694	5.3
0.9	0.280	0.278	0.7	3.482	3.658	5.1
1.5	-2.115	-1.959	7.4	4.512	4.569	1.3
2.1	-5.786	-5.401	6.7	5.736	5.796	1.0
2.7	-13.652	-12.446	8.8	8.485	8.191	-3.5

Table 2-2. log*k* Values for Load Transfer Simulation.

Joint/crack load transfer condition	log*k* (MPa/m)	
	AC/PCC	AC/AC
90 %	7.0	7.0
50 %	3.5	5.5
10 %	1.0	1.0

With this verified *SA-CrackPro* program, four factors including structural and material parameters (i. e., layer modulus and thickness), multi-layer base and/or subbase (equivalent layer thickness), multi-HMA overlays, and various load spectrums are discussed. Numerous SIF computations on various pavement structures under different traffic loads were subsequently conducted. The findings from the SIF analyses are presented below.

Effect of Structural and Material Parameters on SIF

A four-layered pavement structure consisting of an HMA overlay, existing joint PCC concrete layer, base, and subgrade was used to identify the significant influential parameters on shearing SIFs. Table 2-3 provides the pavement structural thickness and material properties used for computing the SIF values and the associated statistical analyses. The total factorial combinations for shearing SIFs ($K_{shearing}$) were 11,664. The purpose of the statistical analysis was to determine the parameters that have significant influence on $K_{shearing}$. The Pearson correlation statistical analysis results are listed in Table 2-4. Because 99 percent of the $K_{bending}$ for HMA over PCC pavements were negative values that have no contribution to the reflective crack propagation, HMA overlay over existing HMA pavement structures were used for $K_{bending}$ analyses. Also, as noted previously, the load transfer at cracks (or joints) is simulated through pure shearing. Thus, zero load transfer was used for $K_{bending}$ analyses. Similar runs were also conducted, and the results are also presented in Table 2-4.

From Table 2-4, it can be seen that all the variables except the subgrade modulus have significant influence on both the $K_{bending}$ and $K_{shearing}$, and accordingly should be incorporated into the SIF regression equations being developed.

This finding about the subgrade does not mean that the subgrade has no influence on pavement responses. As reported by Huang (*41*), the main influence of the subgrade is on pavement surface deflections, vertical compression stress in the layer lying directly above the subgrade, and compressive strain of the subgrade itself. According to Table 2-4, the subgrade modulus did not significantly influence both $K_{bending}$ and $K_{shearing}$ and accordingly reflective crack propagation. Therefore, a fixed 7 ksi subgrade modulus was utilized for the rest of the SIF analyses in this study.

Table 2-3. Structural and Material Properties for $K_{shearing}$.

Parameters	Range	Selected values	Count number
H1: HMA layer thickness (inch)	2-8	2, 4, 8	3
E1: HMA layer modulus (ksi)	290-2200	290, 870, 2200	3
H2: existing PCC layer thickness (inch)	8-14	8, 10, 14	3
E2: existing PCC layer modulus (ksi)	2900-5800	2900, 5800	2
Load transfer condition-LTC (%)	10-90	10, 50, 90	3
H3: base layer thickness (inch)	6-18	6, 18	2
E3: base layer modulus (ksi)	15-500	15, 100, 500	3
E4: subgrade modulus (ksi)	4-17	4, 7, 17	3
c/H1 (c-crack length)	0.2-0.8	0.2, 0.4, 0.6, 0.8	4

Note: total runs for $K_{shearing}$ =3*3*3*2*2*3*3*3*4=11,664.

Table 2-4. Statistic Analysis Results.

Parameters	$K_{bending}$		$K_{bending}$	
	Pearson correlation	Significance	Pearson correlation	Significance
H1	.129(**)	.000	-.263(**)	.000
E1	.311(**)	.000	.340(**)	.000
H2	-.080(**)	.000	-.059(**)	.000
E2	-.067(**)	.000	-.066(**)	.000
LTC	N/A		-.578(**)	.000
H3	-.052(**)	.000	-.018(*)	.048
E3	-.206(**)	.000	-.141(**)	.000
E4	-.019	.110	-.007	.453
Crack length	-.165(**)	.000	.124(**)	000

Note: ** Correlation is significant at the 0.01 level (2-tailed).

Consideration of a Multi-Layered Base and/or Subbase

Pavement structures often include more than one base and/or subbase layers with different moduli values. If this is the case, it is desirable to transfer the multi-layer base and/or subbase into an equivalent single layer with only one composite modulus value using Odemark's method of equivalent layer thickness (MET) (*42*). Note that the application of MET and use of a single composite modulus value was necessary in order to reduce the amount of SIF computations. This approach has been widely used for pavement response analyses (*43*) and FWD backcalculation (*44*). However, whether or not this layer thickness equivalent concept works for SIF has not been fully explored in the literature. To verify this concept, one pavement structure consisting of an HMA overlay, an existing HMA layer with a crack having no load transfer, one base layer, two subbase layers, and the subgrade was analyzed, as shown in Figure 2-4. More than 15,000 SIF computations ($K_{bending}$ and $K_{shearing}$) were run using the *SA-CrackPro* program. Figure 2-5 shows the SIF comparisons between un-transformed and transformed pavement structures. It is obvious from the results shown in Figure 2-5 that Odemark's equivalent thickness concept is still applicable to SIF computations. With this verification, the pavement structures below the existing HMA (or PCC) layer can be simplified as only a base layer plus the subgrade.

HMA overlay: H_1, E_1		HMA overlay: H_1, E_1
Existing HMA layer: H_1, E_1	← Crack/joint →	Existing HMA layer: H_1, E_1
Base: H_2, E_2		Base: Equivalent H_2', E_2
Subbase1: H_3, E_3		$H_2' = H_2 + H_3\sqrt[3]{\dfrac{E_3}{E_2}} + H_4\sqrt[3]{\dfrac{E_4}{E_2}}$
Subbase2: H_4, E_4		
Subgrade: E_5		Subgrade: E_5
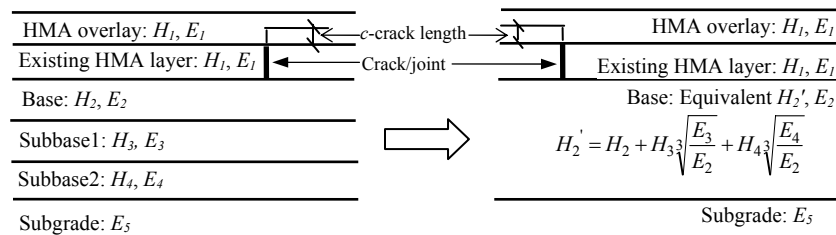
Figure 2-4. HMA Overlay Pavement Structures (LTC=10%) and Associated Odemark's Transformation.

(a) $K_{bending}$ *verification*   (b) $K_{shearing}$ *verification*
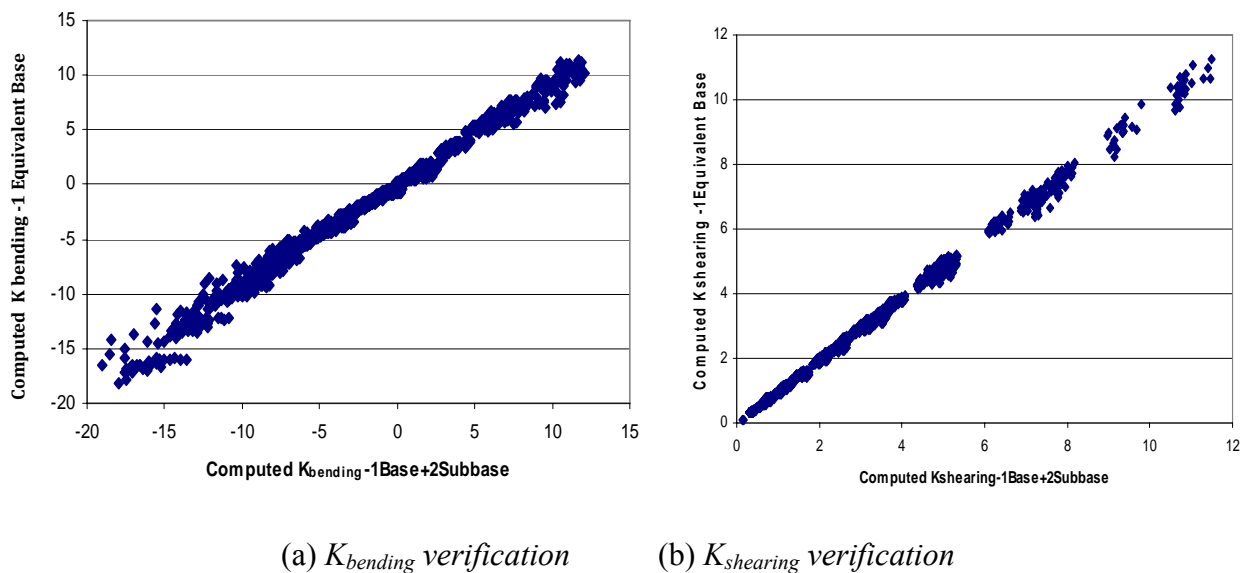
Figure 2-5. Verification of the MET Approach for Multi-Base Pavement Structures.

Consideration of a Multi-Layered HMA Overlay

Similarly, it is expected that the MET approach may be also applicable to HMA overlays. To check its validity, pavement structures with three and two HMA overlays over existing HMA (for bending) and PCC concrete pavements (for shearing with three levels of load transfer) and associated equivalent structures, as shown in Figure 2-6, were analyzed. Part of the analysis results are presented in Figure 2-7. It is clear that the MET approach is also applicable for multi-HMA overlays. Similar results have been observed for HMA over PCC pavements with 50 percent and 90 percent load transfers as well. Therefore, multi-layered HMA overlay can also be treated as one HMA overlay using the MET approach, which significantly simplifies the SIF computations and regression equation development.
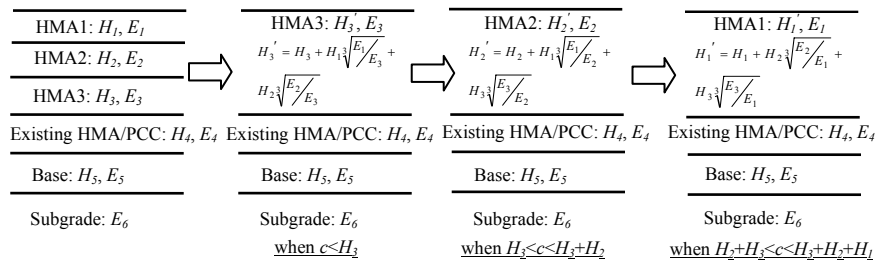
Figure 2-6. Three-Layer Overlay Structure and Its Transformation.

(a) $K_{bending}$ verification   (b) $K_{shearing}$-LTE=0.1 verification
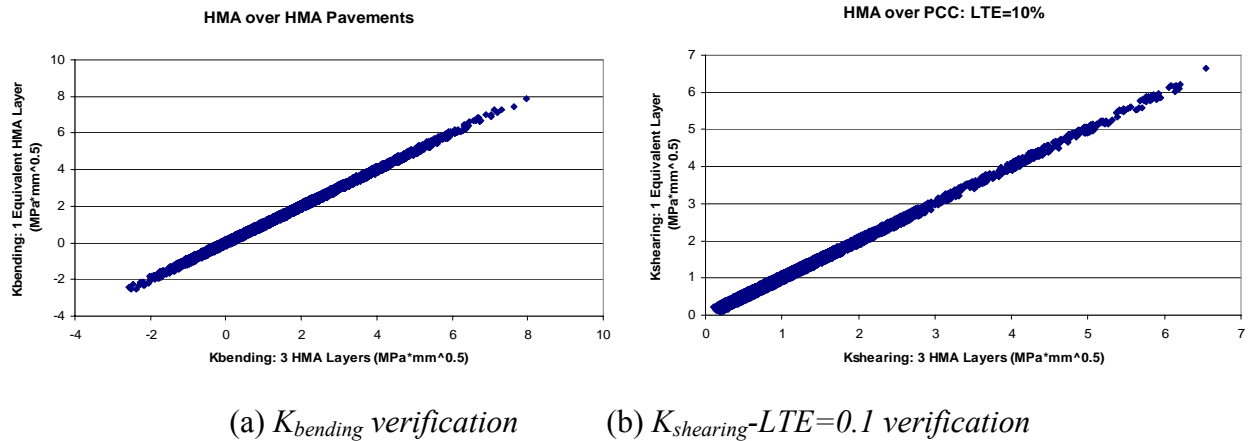
Figure 2-7. Verification of the MET Approach for Multi-HMA Pavement Structures.

Consideration of the Traffic Load Spectrum

For simplicity purposes, the multi-axle and multi-level traffic loading is often handled through the equivalent single axle load (ESAL) concept in different pavement design procedures around the world. However, this is not the case any more. The impact of a full load spectrum on pavement response and associated performance is directly considered in the MEPDG (1). Therefore, it is also desirable to fully consider the influence of a varied traffic load spectrum when analyzing reflective crack propagation. In particular, the influence of multi-axle and multi-

level traffic loading on both the bending and shearing SIFs needs to be investigated. Detailed information is presented below.

- Multi-axle traffic loading analysis

The influence of multi-axle traffic loading on the tensile strain at the bottom of the HMA layer has been well discussed by Huang (*41*). Figure 2-8 shows a tandem-axle load and associated tensile strain responses at different locations. The effect of this tandem-axle load on fatigue damage and the associated crack initiation is often taken into account by considering both ε_a and ε_a-ε_b (ε_a-ε_b is the strain for the second axle load); see Figure 2-8. This is considered a reasonable approach because the damage caused by the horizontal tensile strains in both the traffic direction and perpendicular to the traffic direction contribute to fatigue damage including the associated crack initiation process. Note that a similar approach has been used in VESYS (*45*), KENLAYER (*41*), and even in the MEPDG (*1*).
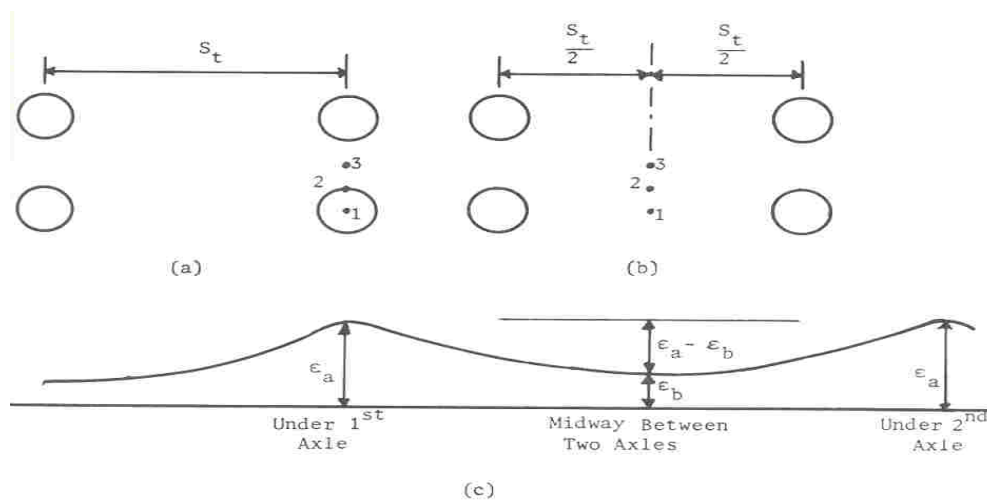
Figure 2-8. Tandem Traffic Loading (*41*).

However, this approach may not be applicable to crack propagation because of the existence of macro-cracks. In the stage of crack propagation, a macro-crack in the direction perpendicular to traffic exists and ideally propagates in the vertical direction towards the pavement surface. The main contributions to the crack propagation are from $K_{bending}$ and $K_{shearing}$ in the traffic direction. As an example, an HMA overlay pavement structure consisting of an HMA overlay, an existing HMA concrete layer, a base layer, and the subgrade was used for investigating the $K_{bending}$ and $K_{shearing}$ values corresponding to different crack lengths under a moving tridem-axle load passing over a crack. Figure 2-9 shows the $K_{bending}$ and $K_{shearing}$ development at different crack lengths under a 54 kip tridem-axle load with a tire pressure of 100 psi. For comparison purposes, the $K_{bending}$ and $K_{shearing}$ development at different crack lengths under an 18 kip single axle load with a pressure of 100 psi is also presented in Figure 2-9. It can be seen that the maximum $K_{bending}$ and $K_{shearing}$ values under the tridem-axle load are almost the same as those under the single axle load. Extensive analysis results show that this observation is also true for other pavement structures under different types of multi-axle loads. Therefore, multi-axle loads, for simplicity, can be handled through multiple applications of the single axle load. Thus, the varied traffic loading spectrum can be easily analyzed as a multi-level single axle load, which is discussed in the subsequent section.

13
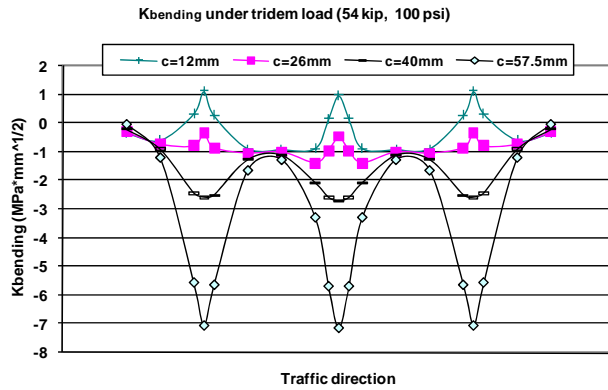
(a) $K_{bending}$ under a tridem-axle load
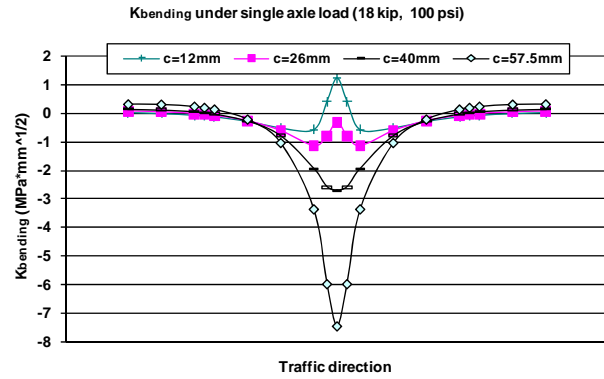
(b) $K_{bending}$ under a single axle load
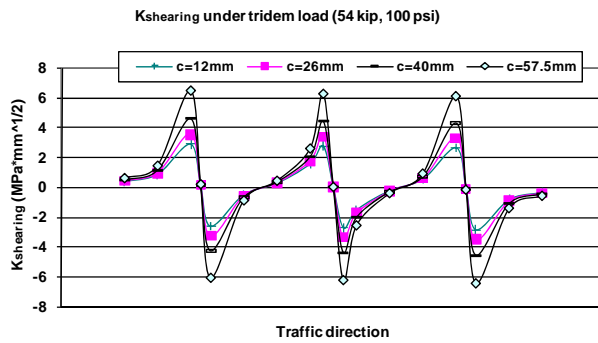
(c) $K_{shearing}$ under tridem-axle load
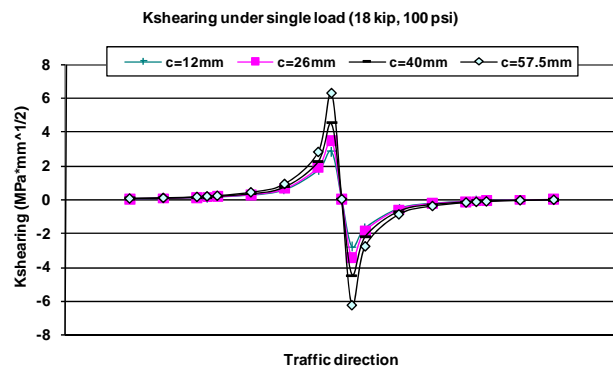
(d) $K_{shearing}$ under single axle load

Figure 2-9. $K_{bending}$ and $K_{shearing}$ Comparison: Tridem vs. Single Axle Load.

- Multi-level single axle load configuration

For a single axle traffic load, its load levels vary in a very wide range, which may result from variations in the tire pressure, contact area, and/or both. Both $K_{bending}$ and $K_{shearing}$ are linearly proportional to the tire pressure for the same contact area. Thus, only one tire pressure of 100 psi was used in this analysis. $K_{bending}$ and $K_{shearing}$ can be readily determined under other tire pressures

In the case of varying contact area but keeping tire pressure constant, $K_{bending}$ and $K_{shearing}$ must be specifically calculated for each contact area (= effective tire width × tire length). It also has been reported that the tire length and associated contact area increases with an increase in the load level while keeping the tire pressure constant; however the effective tire width hardly varies with the load level (*46*). Therefore, increasing the contact area is actually equal to an increase in the tire length, since the effective tire width does not vary with the load level.

After reviewing the default load spectrum in the MEPDG (*1*), four levels of single axle loads listed in Table 2-5 were selected for developing SIF regression equations. Note that a constant effective tire width of 6.2 inches was chosen based on the text book "Pavement Analysis and Design" by Huang (*41*). The SIF values corresponding to the other load level (or contact area/tire length) can be interpolated or extrapolated based on these SIF values.

14

Table 2-5. Four Single Axle Loads Recommended for SIF Analysis.

Axle load	Tire pressure	Effective tire width	Tire length
4 kip	100 psi	6.2 inch	1.6 inch
11 kip	100 psi	6.2 inch	4.4 inch
18 kip	100 psi	6.2 inch	7.2 inch
25 kip	100 psi	6.2 inch	10.0 inch

Note: a standard single axle consists of 2 dual tires.

Based on the above discussions, SIF regression equations were developed and presented in the next section.

SIF Regression Equations

Since the MET approach is validated for SIF, only pavement structures with an HMA layer, an existing HMA or PCC layer, a base layer, and the subgrade ($E=7$ ksi), as shown in Figure 2-10, were analyzed to develop SIF regression equations. For each pavement structure, the SIF in both bending and shearing modes under four load levels (see Table 2-5) were calculated. Note that the bending mode refers to the loading center just at the top of the crack, and the shearing mode refers to the loading edge at the top of the crack. For the shearing mode, three load transfer levels were analyzed: very poor, fair, and good. Therefore, a total of 32 SIF regression equations (= 4 load levels × 2 existing pavements × 4 SIFs) have been developed based on more than 1,600,000 runs. Only the SIF ($K_{bending}$ and $K_{shearing}$) regression equations under 18 kip single axle load are presented below. The goodness of fit is shown in Figure 2-11, in which all SIF data computations are plotted. All the other regression equations are listed in Appendix A. Note that the $K_{bending}$ and $K_{shearing}$ equations have the same polynomial expression format (Equation 2-5):

$$K_{bending\,/\,shearing} = K_a \left[K_b \left(\frac{c}{H_1} \right)^3 + K_c \left(\frac{c}{H_1} \right)^2 + K_d \left(\frac{c}{H_1} \right) + K_e \right]$$ (2-5)

HMA Overlay: H_1, E_1 c-crack length

Existing HMA or PCC: H_2, E_2 Joint or crack

Base: H_3, E_3

Subgrade: $E_4= 7$ ksi
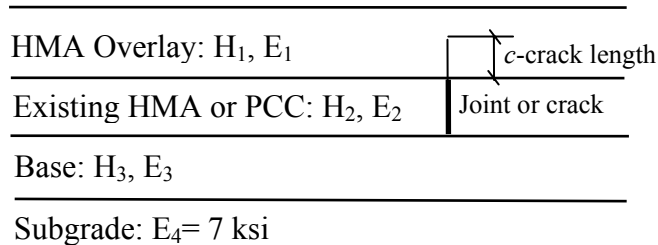
Figure 2-10. Four-Layered Pavement Structures Used for Developing the SIF Equations.

15

- ## HMA/PCC: $K_{bending}$ under single axle load of 18 kip

$$K_a = \left(-1.5900\log H_3 + 7.5670(\log E_3)^{-0.6674} + 2.9689(\log H_2)^2 - 20.2856\log H_2 - 0.6100(\log E_2)^2 + 4.0389\log E_2 + 31.0721\right) \times \quad (2\text{-}6)$$
$$\left(1.9882\log H_1 - 0.1908(\log E_1)^2 + 1.0080\log E_1 - 7.6964\right)$$

$$K_b = 7.1018 \times 10^{-6}\left(12.4974(\log E_1)^2 - 76.5328\log E_1 + 0.2502 f_1^2 - 16.9600 f_1 + 110.5739\right) \times \quad (2\text{-}7)$$
$$\left((\log E_3)^{0.5383} \times (\log E_2)^{7.7583} \times (\log E_1)^{-3.6878} - 22.2688\right) \times \left(-5.9056(f_0 c)^{-0.8594} + 1.0855\right) \times \left(-18.4093 f_0 - 1.3660 \times 10^{-6}\right)$$

$$K_c = 0.0035\left(-8.9941(\log E_1)^2 + 102.1921\log E_1 - 3.4384 f_1^2 + 17.7353 f_1 - 196.7209\right) \times \quad (2\text{-}8)$$
$$\left((\log E_3)^{-1.6440} \times (\log E_2)^{-9.2183} \times (\log E_1)^{7.8892} - 0.0595\right) \times \left(0.1618(f_0 c)^{1.1273} + 1.0769\right) \times \left(27.6264 f_0 + 4.4900\right)$$

$$K_d = 0.0014\left(-13.6682(\log E_1)^2 + 57.5807\log E_1 + 3.0213 f_1^2 - 90.3137 f_1 - 89.0447\right) \times \quad (2\text{-}9)$$
$$\left((\log E_3)^{0.0535} \times (\log E_2)^{4.7219} \times (\log E_1)^{-2.0160} + 21.3984\right) \times \left(-0.3612(f_0 c)^{0.0255} + 0.4002\right) \times \left(9.0514 f_0 - 0.3287\right)$$

$$K_e = \left(0.0253(\log E_1)^2 - 0.2021\log E_1 + 0.3703\right) \times \left((\log E_3)^{-1.6612} \times (\log E_2)^{-7.5751} \times (\log E_1)^{9.8212} - 2.8501\right) + 0.1013 \quad (2\text{-}10)$$

where $f_0, f_1, Y,$ and I are defined below:

$$f_0 = (H_1 + H_2)^2 \times \left(1 - \frac{c + H_2}{(H_1 + H_2)}\right)^2 \times \left(\frac{YE_1}{6I}\right) \quad (2\text{-}11)$$

$$f_1 = YE_1\frac{(H_1 + H_2)^2}{I} \quad (2\text{-}12)$$

$$Y = \frac{0.5E_1H_1^2 + E_2H_2H_1 + 0.5E_2H_2^2}{E_1H_1 + E_2H_2} \quad (2\text{-}13)$$

$$I = E_1\left(\frac{H_1^3}{12} + H_1(Y - 0.5H_1)^2\right) + E_2\left(\frac{H_2^3}{12} + H_2(Y - H_1 - 0.5H_2)^2\right) \quad (2\text{-}14)$$

- ## HMA/PCC: $K_{shearing}$@LTE=10 % under single axle load of 18 kip

$$K_a = \left(-0.1070\log H_3 + 10.6812(\log E_3)^{-0.0835} - 0.5013(\log H_2)^2 + 2.5971\log H_2 - 0.2433(\log E_2)^2 + 1.9193\log E_2 - 15.7217\right) \times \quad (2\text{-}15)$$
$$\left(-2.9156\log H_1 + 0.7873(\log E_1)^2 - 6.3932\log E_1 + 22.6415\right)$$

$$K_b = 0.1304\left(28.8189(\log E_1)^2 - 136.1341\log E_1 - 0.3764 f_1^2 + 6.9661 f_1 + 174.7384\right) \times \quad (2\text{-}16)$$
$$\left((\log E_3)^{-6.0501} \times (\log E_2)^{-2.2051} \times (\log E_1)^{-9.2409} + 1.3280\right) \times \left(-5.8771(f_0 c)^{-0.0043} \times (f_0(c + H_2))^{0.0073} + 5.8969\right)$$

$$K_c = 0.0942\left(-0.2358(\log E_1)^2 + 1.8967\log E_1 + 0.0176 f_1^2 - 0.2746 f_1 - 2.5255\right) \times \quad (2\text{-}17)$$
$$\left((\log E_3)^{1.8761} \times (\log E_2)^{-0.3751} \times (\log E_1)^{2.3863} + 26.2623\right) \times \left(1.1298(f_0 c)^{2.9561} \times (f_0(c + H_2))^{-3.1189} - 0.0637\right)$$

$$K_d = 0.0020\left(1.2828(\log E_1)^2 + 13.3342\log E_1 - 0.3373 f_1^2 + 4.8902 f_1 - 35.7626\right) \times \quad (2\text{-}18)$$
$$\left((\log E_3)^{3.3716} \times (\log E_2)^{0.4688} \times (\log E_1)^{-3.5661} + 3.8379\right) \times \left(-0.0850(f_0 c)^{-0.7944} \times (f_0(c + H_2))^{1.6155} + 2.2735\right)$$

$$K_e = \left(18.8600(\log E_1)^2 - 102.7152\log E_1 + 135.3821\right) \times \left((\log E_3)^{0.0122} \times (\log E_2)^{-0.0183} \times (\log E_1)^{-0.0447} - 0.9054\right) + 0.3806 \quad (2\text{-}19)$$

- ## HMA/ PCC: $K_{shearing}$@LTE=50 % under single axle load of 18 kip

$$K_a = \left(-0.0193\log H_3 + 4.9483(\log E_3)^{-0.0624} - 0.0307(\log H_2)^2 + 0.3039\log H_2 - 0.0895(\log E_2)^2 + 0.7615\log E_2 - 6.3603\right) \times \quad (2\text{-}20)$$
$$\left(-1.1037\log H_1 + 0.4444(\log E_1)^2 - 4.3627\log E_1 + 14.2575\right)$$

$$K_b = 0.0479\left(16.3162(\log E_1)^2 - 74.5807\log E_1 - 0.3493 f_1^2 + 5.1949 f_1 + 104.3394\right) \times \quad (2\text{-}21)$$
$$\left((\log E_3)^{-6.0480} \times (\log E_2)^{-2.1959} \times (\log E_1)^{-9.2398} + 0.5858\right) \times \left(-1.0782(f_0 c)^{-0.7523} \times (f_0(c + H_2))^{1.0398} + 0.2234\right)$$

$$K_c = 0.1147\left(-0.1138(\log E_1)^2 + 3.3902\log E_1 + 0.2248 f_1^2 - 2.4644 f_1 - 1.9205\right) \times \quad (2\text{-}22)$$
$$\left((\log E_3)^{1.4164} \times (\log E_2)^{-0.2297} \times (\log E_1)^{2.4083} + 12.2319\right) \times \left(0.5305(f_0 c)^{3.2861} \times (f_0(c + H_2))^{-3.5690} + 0.0072\right)$$

$$K_d = 0.0714 \left(2.3439 \left(\log E_1 \right)^2 - 14.9453 \log E_1 - 0.0899 \ f_1^{\ 2} + 1.7984 \ f_1 + 25.4835 \right) \times$$
$$\left(\left(\log E_3 \right)^{0.2434} \times \left(\log E_2 \right)^{0.2683} \times \left(\log E_1 \right)^{1.1088} - 0.0513 \right) \times \left(- 0.0463 \ \left(f_0 c \right)^{-0.6751} \times \left(f_0 \left(c + H_2 \right) \right)^{1.3926} + 1.2505 \right) \qquad (2\text{-}23)$$

$$K_e = \left(0.4222 \ \left(\log E_1 \right)^2 - 2.0511 \ \log E_1 + 3.0481 \right) \times \left(\left(\log E_3 \right)^{0.3937} \times \left(\log E_2 \right)^{-1.8482} \times \left(\log E_1 \right)^{1.9661} + 0.5951 \right) - 0.5145 \qquad (2\text{-}24)$$

- ### HMA/ PCC: $K_{shearing}$@LTE=90 % under single axle load of 18 kip

$$K_a = \left(- 0.0188 \log H_3 + 0.5024 \left(\log E_3 \right)^{-0.2161} + 3.1986 \left(\log H_2 \right)^2 - 13.0886 \log H_2 - 0.1223 \left(\log E_2 \right)^2 + 1.3986 \log E_2 + 10.8510 \right) \times$$
$$\left(- 0.9860 \log H_1 - 0.0648 \left(\log E_1 \right)^2 + 0.3831 \log E_1 + 2.8800 \right) \qquad (2\text{-}25)$$

$$K_b = 0.0217 \left(4.9516 \left(\log E_1 \right)^2 - 54.7835 \log E_1 - 0.5966 \ f_1^{\ 2} + 9.3622 \ f_1 + 147.0602 \right) \times$$
$$\left(\left(\log E_3 \right)^{-6.0473} \times \left(\log E_2 \right)^{-2.1943} \times \left(\log E_1 \right)^{-9.2388} + 0.6254 \right) \times \left(- 0.2440 \left(f_0 c \right)^{-1.0470} \times \left(f_0 \left(c + H_2 \right) \right)^{1.2675} - 1.9551 \right) \qquad (2\text{-}26)$$

$$K_c = 0.1235 \left(1.0241 \left(\log E_1 \right)^2 - 9.6486 \ \log E_1 - 0.0019 \ f_1^{\ 2} + 0.0120 \ f_1 + 24.0502 \right) \times$$
$$\left(\left(\log E_3 \right)^{0.0189} \times \left(\log E_2 \right)^{-2.0171} \times \left(\log E_1 \right)^{4.9114} + 11.3397 \right) \times \left(0.4827 \ \left(f_0 c \right)^{2.0212} \times \left(f_0 \left(c + H_2 \right) \right)^{-2.1467} + 0.0851 \right) \qquad (2\text{-}27)$$

$$K_d = 0.1022 \left(0.9361 \left(\log E_1 \right)^2 - 11.9066 \log E_1 - 0.1813 \ f_1^{\ 2} + 3.1740 \ f_1 + 32.4907 \right) \times$$
$$\left(\left(\log E_3 \right)^{0.0034} \times \left(\log E_2 \right)^{0.0235} \times \left(\log E_1 \right)^{0.6653} - 1.2802 \right) \times \left(- 0.5207 \left(f_0 c \right)^{1.2473} \times \left(f_0 \left(c + H_2 \right) \right)^{-0.8294} + 0.7923 \right) \qquad (2\text{-}28)$$

$$K_e = \left(- 0.0046 \left(\log E_1 \right)^2 + 0.0407 \ \log E_1 - 0.0849 \right) \times \left(\left(\log E_3 \right)^{-0.0480} \times \left(\log E_2 \right)^{0.9499} \times \left(\log E_1 \right)^{1.2294} - 13.1255 \right) + 0.0465 \qquad (2\text{-}29)$$

(a) $K_{bending}$ plot

(b) $K_{shearing}$ with LTE=10% plot

(c) $K_{shearing}$ with LTE=10% plot

(d) $K_{shearing}$ with LTE=10% plot
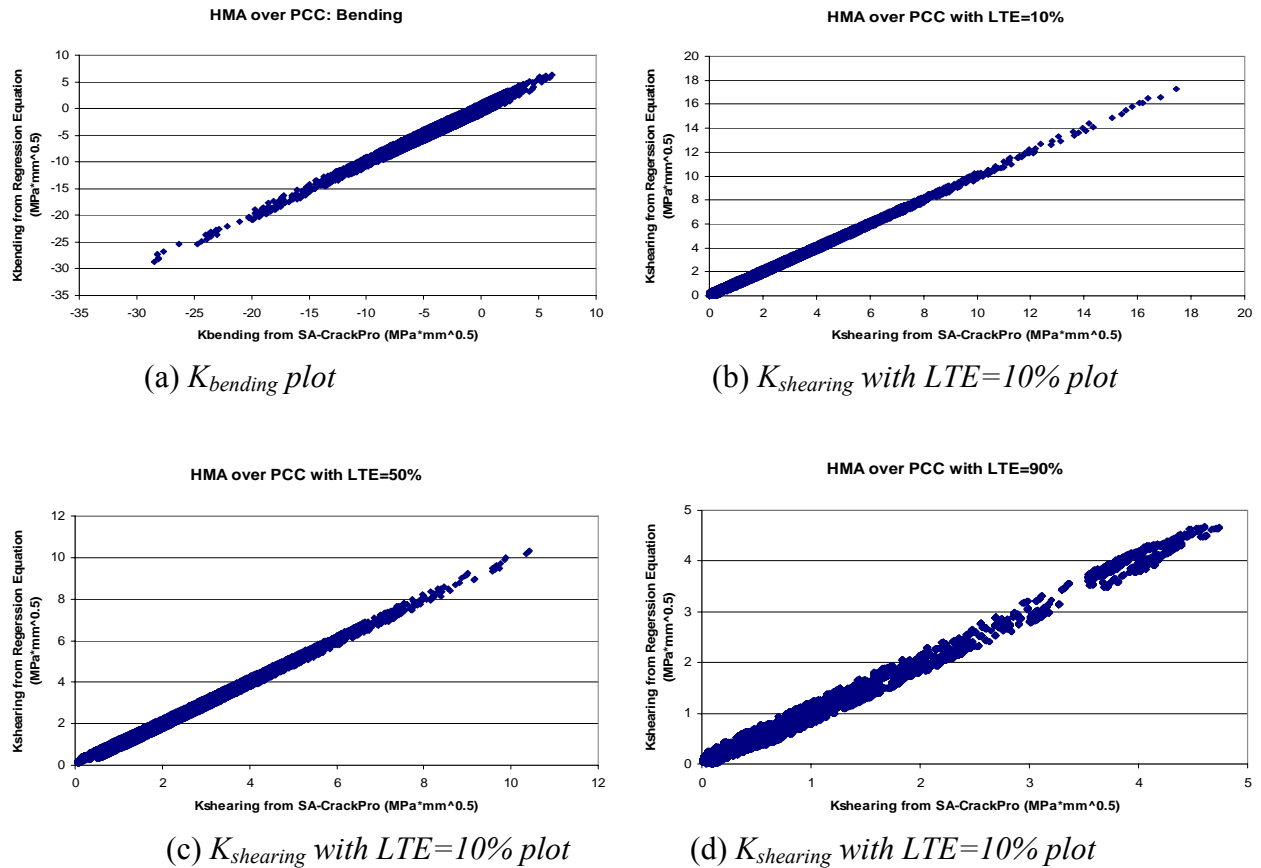
Figure 2-11. SIF Values Predicted by Regression Equation vs. SIF Calculated by SA-CrackPro Program.

17

THERMAL RELATED SIF AND ASSOCIATED REGRESSION EQUATIONS

As discussed previously, HMA overlay(s) under thermal loading often shows strong visco-elastic behavior due to long loading times, which makes the well, known Paris' law for crack propagation not applicable. Fortunately, Hiltunen and Roque (*25*) successfully developed a "hybrid" approach for low-temperature cracking, which includes: 1) establishment of the relationship between SIF at the crack tip and the thermal stress at the far field at the same height of the crack tip in the HMA layer, 2) calculation of thermal stress based on the 1D visco-elastic constitutive equation, and 3) estimation of crack propagation based on Paris' law. This approach is theoretically sound and practically applicable. Thus, a similar approach is used in this research project to analyze thermal reflective crack propagation.

However, it should be noted that some differences exist between the low-temperature cracking and the thermal reflective cracking. For example, the crack propagates upward for the thermal reflective cracking. In contrast, for the low-temperature cracking, the crack propagates downward. Additionally, the pavement structure modeled in the low-temperature cracking model included one HMA layer only. However, for the reflective cracking, at least two layers (HMA overlay plus cracked HMA (or PCC) layer) must be considered. These differences make it impossible to directly use the relationship between the SIF and the thermal stress ($\sigma_{VE\text{-}far}$) at the middle of crack spacing developed for the low-temperature cracking, although the other two components (thermal stress calculation and Paris' law-based crack propagation) can still be used. Thus, new SIF versus thermal stress relationships must be developed for HMA overlays.

A two-layer pavement structure with a continuous interface between the HMA overlay and the existing HMA/PCC pavements, as shown in Figure 2-12, was used to develop such relationships. For HMA/existing HMA pavements, the continuous interface between the existing HMA layer and base layer was assumed. However, a semi-continuous condition was assigned to the interface between PCC slabs and the base/foundation layer. After extensive FE analysis, the $K_{thermal}$ versus $\sigma_{VE\text{-}far}$ relationships were developed in the form of Equations 2-30. Detailed equations are presented below:
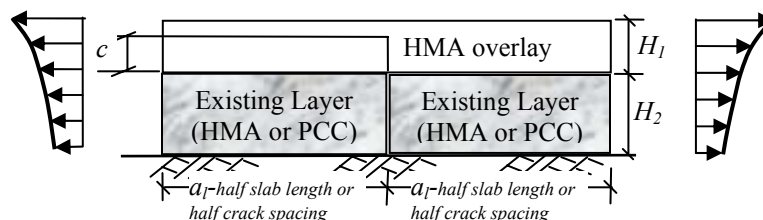
Figure 2-12. HMA Overlay Structure Model.

$$K_{thermal} = K_a \times \left[K_b \left(\frac{c}{H_1} \right)^3 + K_c \left(\frac{c}{H_1} \right)^2 + K_d \left(\frac{c}{H_1} \right) + K_e \right] \times \sigma_{VE-far} \qquad (2\text{-}30)$$

- HMA/existing HMA pavements: $K_{thermal}$

$$K_a = 3.6420 + 0.07842\ c^{-0.7797} - 0.31227\ \log\ H_1 + 0.8752\ \log\ H_2 - 2.0487 \left(\frac{\alpha_1}{\alpha_2}\right)^{-0.4629} \quad (2\text{-}31)$$

$$K_b = 14.5875 + 5.5684\ c^{-0.5925} + 6.1821\ \log\ H_1 + 1.3763\ \log\ H_2 + 0.5038 \left(\frac{\alpha_1}{\alpha_2}\right)^{-2.2239} \quad (2\text{-}32)$$

$$K_c = -52.9503 - 11.7451\ c^{-1.6459} - 3.8025\ \log\ H_1 + 0.5818\ \log\ H_2 + 16.4145 \left(\frac{\alpha_1}{\alpha_2}\right)^{-0.0619} \quad (2\text{-}33)$$

$$K_d = 15.7190 - 0.0187\ c^{0.9529} + 1.6661\ \log\ H_1 - 0.9903\ \log\ H_2 + 9.3276 \left(\frac{\alpha_1}{\alpha_2}\right)^{-0.0076} \quad (2\text{-}34)$$

$$K_e = -10.4517 + 5.3405\ c^{-0.4428} + 3.4569\ \log\ H_1 + 0.2696\ \log\ H_2 + 1.1080 \left(\frac{\alpha_1}{\alpha_2}\right)^{-1.5815} \quad (2\text{-}35)$$

where α_1 and α_2 are the thermal coefficients of expansion of HMA overlay and existing HMA layer, respectively.

- HMA/existing PCC pavements: $K_{thermal}$

$$K_a = -11.3047 + 2.5879\ c^{-0.0381} + 1.0807\ \log\ H_1 - 0.1025\ \log\ H_2 + 12.5827 \left(\frac{\alpha_1}{\alpha_2}\right)^{-1.3114} + 0.9506\ \log\ E_2 + 1.1409\ \log\ a_l \quad (2\text{-}36)$$

$$K_b = 248.0027 + 0.7731\ c^{0.3632} - 23.1703\ \log\ H_1 - 11.5524\ \log\ H_2 + 6.3684 \left(\frac{\alpha_1}{\alpha_2}\right)^{-0.7647} + 32.9654\ \log\ E_2 - 5.2321\ \log\ a_l \quad (2\text{-}37)$$

$$K_c = -450.4962 + 156.6284\ c^{-1.0367} + 28.3712\ \log\ H_1 + 19.6787\ \log\ H_2 + 3.9451 \left(\frac{\alpha_1}{\alpha_2}\right)^{-1.1741} + 68.1561\ \log\ E_2 + 9.3027\ \log\ a_l \quad (2\text{-}38)$$

$$K_d = 273.4490 - 0.9679\ c^{-0.4409} - 9.0602\ \log\ H_1 - 9.5789\ \log\ H_2 + 0.9256 \left(\frac{\alpha_1}{\alpha_2}\right)^{1.0394} - 48.3917\ \log\ E_2 - 5.4138\ \log\ a_l \quad (2\text{-}39)$$

$$K_e = -62.2704 + 11.4673\ c^{-0.8511} - 2.0765\ \log\ H_1 + 1.2882\ \log\ H_2 - 1.4467 \left(\frac{\alpha_1}{\alpha_2}\right)^{-0.7924} + 14.1434\ \log\ E_2 + 1.5225\ \log\ a_l \quad (2\text{-}40)$$

where α_1 and α_2 are the thermal coefficients of expansion of HMA overlay and existing HMA layer, respectively.

Regarding the $\sigma_{VE\text{-}far}$ (at middle of crack spacing or slab) calculation, the key is to develop a master curve of relaxation modulus $E(t)$ for the HMA overlay material. In this research project, the dynamic modulus ($|E^*|$) of HMA material is the main input for the asphalt overlay thickness design so that the relaxation modulus $E(t)$ is estimated from the dynamic modulus ($|E^*|$) through inter-conversion between linear visco-elastic functions (47). With known $E(t)$, the $\sigma_{VE\text{-}far}$ can be calculated based on the 1D visco-elastic constitutive equation. Detailed steps used in this research project to calculate the $\sigma_{VE\text{-}far}$ are presented below.

- Step 1: Develop the storage modulus E' ($= |E^*|\cos\theta$) master curves with reduced angular frequency ω. Note that $\omega = 2\pi f = 2\pi / T$, where f is the frequency and T is the time period. The master curve formula is given in Equation 2-41:

$$\log E' = \delta + \frac{\alpha}{1 + e^{\beta + \gamma \log \omega_r}} \quad (2\text{-}41)$$

19

where δ, α, β, and γ are material parameters; $\omega_r = \omega \times a_T$ is the reduced angular frequency; and a_T is the shift factor as a function of temperature T (Equation 2-42) in which a, b, and c are regression coefficients.

$$\log a_T = aT^2 + bT + c \tag{2-42}$$

- Step 2: Determine relaxation modulus $E(t)$ from the storage modulus $E'(\omega)$ through the Prony series of representation.

The storage modulus $E'(\omega)$ developed in Step 1 can be further represented below:

$$E'(\omega) = E_e + \sum_{i=1}^{m} \frac{\omega^2 \rho_i^2 E_i}{\omega^2 \rho_i^2 + 1} \tag{2-43}$$

where E_e (the equilibrium modulus), E_i (relaxation strengths), and ρ_i (relaxation time) are all positive constants. The series expression in Equation 2-43 is often referred to as a Prony series. As demonstrated later, using the Prony series expression can significantly simplify the $\sigma_{VE\text{-}far}$ calculation.

Meanwhile, the same Prony series used in Equation 2-43 can be used to represent the relaxation modulus, $E(t)$:

$$E(t) = E_e + \sum_{i=1}^{m} E_i e^{-\frac{t}{\rho_i}} \tag{2-44}$$

- Step 3: Calculate the $\sigma_{VE\text{-}far}$ based on the Boltzmann superposition principle using the following equation.

$$\sigma(t) = \int_{0}^{t} E(t - \tau) \frac{\partial \varepsilon}{\partial \tau} d\tau \tag{2-45}$$

where $\sigma(t)$ is stress at time t (or $\sigma_{VE\text{-}far}$); $E(t-\tau)$ is relaxation modulus at time $t-\tau$; ε is stain at time t ($= \alpha \times (T(t) - T_0)$); α is coefficient of thermal expansion, $T(t)$ is pavement temperature at time t; T_0 is pavement reference temperature when σ=0; and τ is variable of integration.

If a direct integration of the convolution function represented in Equation 2-45 is performed, the entire history of strains has to be stored. In order to avoid the need of storing the strain histories, the convolution representation was transformed into a two-step recurrence formula which involves internal variables. Detailed theoretical background can be found in the literature (48). The formula used in this research for computing strain response is given below:

$$\sigma(t) = E_e \varepsilon(t) + \sum_{i=1}^{m} E_i h^i(t) \tag{2-46}$$

where $h^i(t)$ is an internal variable for the specific Voigt element, i, at time t, and its definition is given below.

$$h^i(t) = e^{-\frac{\Delta t}{\rho_i}} \times h^i(t - \Delta t) - e^{-\frac{\Delta t}{2\rho_i}} \times (\varepsilon(t) - \varepsilon(t - \Delta t)) \qquad (2\text{-}47)$$

Note that if the creep compliance data from the indirect tension test (IDT) are available, relaxation modulus $E(t)$ can also be determined through inter-conversion, which has been well documented in reference *25* and others.

HMA FRACTURE PROPERTIES: *A* AND *n*

As noted previously, another aspect of the Paris' law-based reflective cracking model is to determine HMA fracture properties: *A* and *n*. Since Majidzadeh et al. initiated the work in this area in the early 1970s (*13*), the HMA fracture properties have been studied for a long time (*17-19, 49-54*). Different test setups, such as the repeated direct tension test, IDT, and semicircular bending test have been tried. However, the common difficulties such as specimen preparation and long testing time still exist. To overcome some of these difficulties, Zhou et al. recently developed an Overlay Tester (OT)-based HMA fracture properties test procedure (*39*). The three main innovative features of the OT-based test procedure for HMA fracture determination are:

1. Specimen size (6 inch by 3 inch wide by 1.5 inch high): this size of specimen can be easily cut from samples compacted by the Superpave Gyratory Compactor or from field cores or HMA slabs (either lab fabricated or cut from the field).

2. Lab specimen preparation (Figure 2-13): neither a hole in the center nor a notch at the bottom of the specimen is required, since a crack is always initiated in the first cycle.
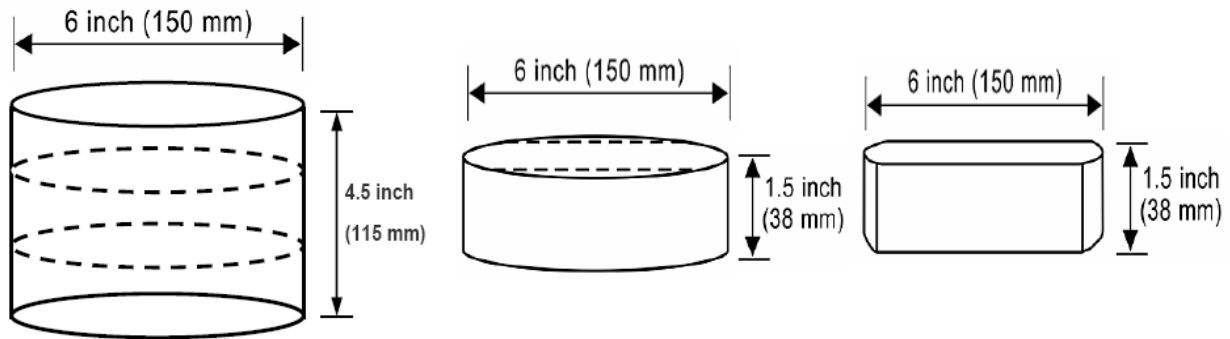
Figure 2-13. OT Specimen Preparation.

3. Short testing time: in contrast to other fracture types of tests (i.e., IDT, semicircular bending test, or repeated direct tension test) which generally take a long testing time, the OT test for determining fracture properties (*A* and *n*) can generally be done within 20 minutes, because only the first 100 cycles of data are necessary for fracture properties determination.

The detailed OT-based HMA fracture property test procedure is presented in Appendix B. It is worth noting that all test procedures including the OT-based procedure addresses only Mode I fracture (opening and/or bending mode loading). Regarding the Mode II fracture (shearing mode loading), there is no simple performance test available to date to adequately characterize this fracture mode. In most cases, it is assumed that Modes I and II share the same fracture properties (*A* and *n*) (*3, 13, 19, 20*).

PRELIMINARY CALIBRATION OF THE REFLECTIVE CRACKING MODEL

The reflective cracking model developed above was calibrated with three field case studies: 1) a pure thermal loading case, 2) a 1 inch HMA overlay over a jointed PCC pavement, and 3) a 4 inch HMA overlay over a badly cracked CRCP on Interstate Highway (IH) 20. Detailed information is presented as follows.

Case 1: Thermal reflective cracking model verification

The study on pure thermal reflective cracking is generally not practical and is also rare since the roads are built for traffic. Fortunately, an overlay test section with long-term performance data is available for this calibration. Buttlar et al. (*55*) constructed several test sections on Runway 18-36 and Taxiway F at the Rantoul National Aviation Center (RNAC) with an initial purpose of identifying cost-effective rehabilitation strategies to mitigate reflective cracking in 1999. However, there is no (or very few) aircraft loading on the control test section. Thus, it is reasonable to use it for calibrating the pure thermal reflective cracking model.

The control overlay section shown in Figure 2-14 consists of 2.5-4 inch asphalt overlay over a jointed PCC pavement, and an average overlay thickness of 3.25 inches was used in later reflective cracking prediction. Two surface mixes with the same aggregate gradation were used in the control section, one mix with a PG58-22 binder and the other with a PG64-22 binder. The IDT creep compliance test results from Buttlar et al. (*55*) are shown in Table 2-6. As reported by Buttlar (*56*), after seven years in the field, zero reflective cracking was observed.
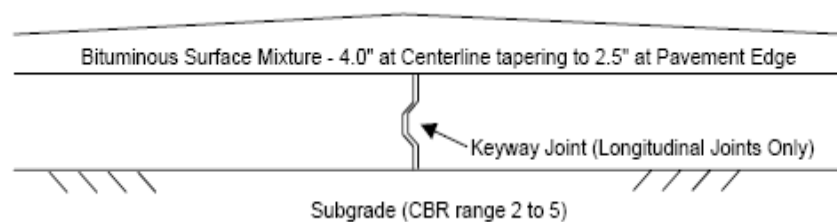
Figure 2-14. Cross-Section for Control Section at RNAC (*55*).

Since no test was performed to determine the HMA fracture properties of these two mixes, the following relationships were used to estimate *A* and *n* values for the analysis:

$$n = 2/m \qquad (16)$$
$$\log A = -2.36 - 1.14n \qquad (49)$$

22

The *m* values determined from the creep compliance are 0.3712 and 0.4661 for PG58-22 and PG64-22 mixes, respectively. The assumed thermal coefficients of expansion are 13.5×10^{-6} and 5.5×10^{-6} for HMA mixes and the existing PCC, respectively. Additionally, the required temperature profiles of HMA overlays for calculating $\sigma_{VE\text{-}far}$ were predicted through the EICM (*1*) in which the weather station at Champaign/Urbana, Illinois, was used. After numerous trials, the calibration factor for thermal reflective cracking was determined to be k_3=1200 in Equation 2-2, and the associated reflective cracking development for these two sections are shown in Figure 2-15.

Table 2-6. HMA Mix Properties Used for Thermal Analysis (*55*).

Parameter	Temp. (ºC)	Time(s)	PG58-22	PG64-28
		Creep Test Results		
Creep Compliance (1/GPa)	-20	1	0.039	0.056
		2	0.042	0.06
		5	0.048	0.067
		10	0.046	0.072
		20	0.049	0.081
		50	0.052	0.098
		100	0.054	0.104
	-10	1	0.064	0.07
		2	0.063	0.07
		5	0.071	0.095
		10	0.081	0.094
		20	0.091	0.116
		50	0.111	0.142
		100	0.126	0.164
	0	1	0.076	0.089
		2	0.096	0.104
		5	0.117	0.128
		10	0.124	0.174
		20	0.15	0.206
		50	0.192	0.289
		100	0.243	0.377
m			0.3712	0.4661
A			3.1401E-9	5.6018E-8
n			5.3887	4.2909
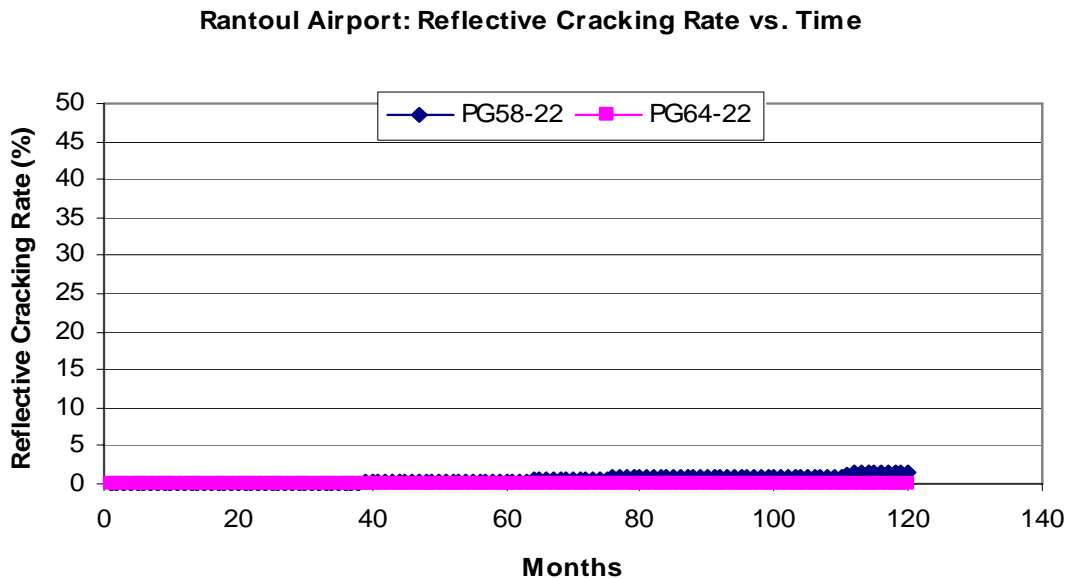
Figure 2-15. Predicted Reflective Cracking Development at RNAC.

Case 2: 1 inch HMA overlay over a jointed PCC pavement

A 1 inch HMA overlay over an 8 inch jointed PCC pavement was constructed on Pumphrey Street, Fort Worth, Texas, in July 2007. The overall conditions of the main lane of the existing PCC pavement were good, and the load transfer efficiency at the joints was more than 90 percent. But joints at all the ramps had very poor load transfer efficiency (less than 30 percent). The estimated 20-year traffic loading is 0.5 million ESALs. Two mixes specifically designed for this overlay project were dense-graded Type F mixes, which have the same gradation but two different binders: crumb rubber modified binder and 3 percent latex modified binder. Both mixes passed TxDOT's requirements for Hamburg wheel tracking test and OT (*57*) and were expected to have the same or similar performance. Figure 2-16 shows the existing pavement conditions and a plan view after HMA overlay. Three site visits had been made to this overlay project on December 14, 2007, April 2, 2008, and July 30, 2008, respectively. Cracking was not observed on the main lane for both mixes (see Figure 2-17a), but the ramps had 30-50 percent reflective cracking for both mixes and as an example, Figure 2-17b shows a reflected crack through the section with the two mixes at ramp R1.

During construction, the plant mixes were sampled for a series of lab characterization including dynamic modulus, OT, Hamburg, and repeated load permanent deformation tests. Figure 2-18a shows the dynamic modulus master curves of these two mixes, and the fracture properties measured at room temperature are also presented in Figure 2-18a. With all this information plus the weather station at Fort Worth, Texas, the reflective cracking performance of these two test sections on both the main lane and the ramps were predicted and compared to the observed reflective cracking (see Figure 2-18b). The calibration factor for shearing is k_2=40 in Equation 2-2. Note that the calibration factor for bending, k_1 could not be determined in this case because the 1 inch overlay is under compression and consequently, all the $K_{bending}$ values are negative. Thus, the k_1 value has to be determined in the next case (i.e., Case 3).

24
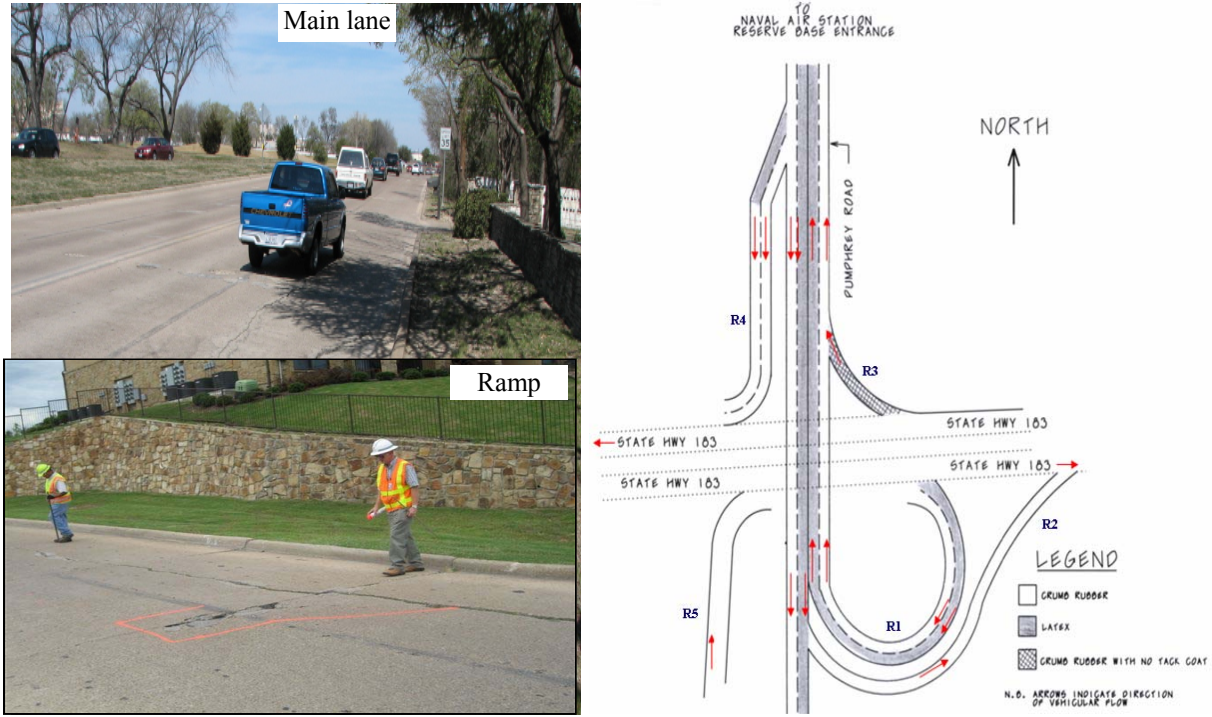
Figure 2-16. Plan View of the Pumphrey Street Project.

(a)   (b)
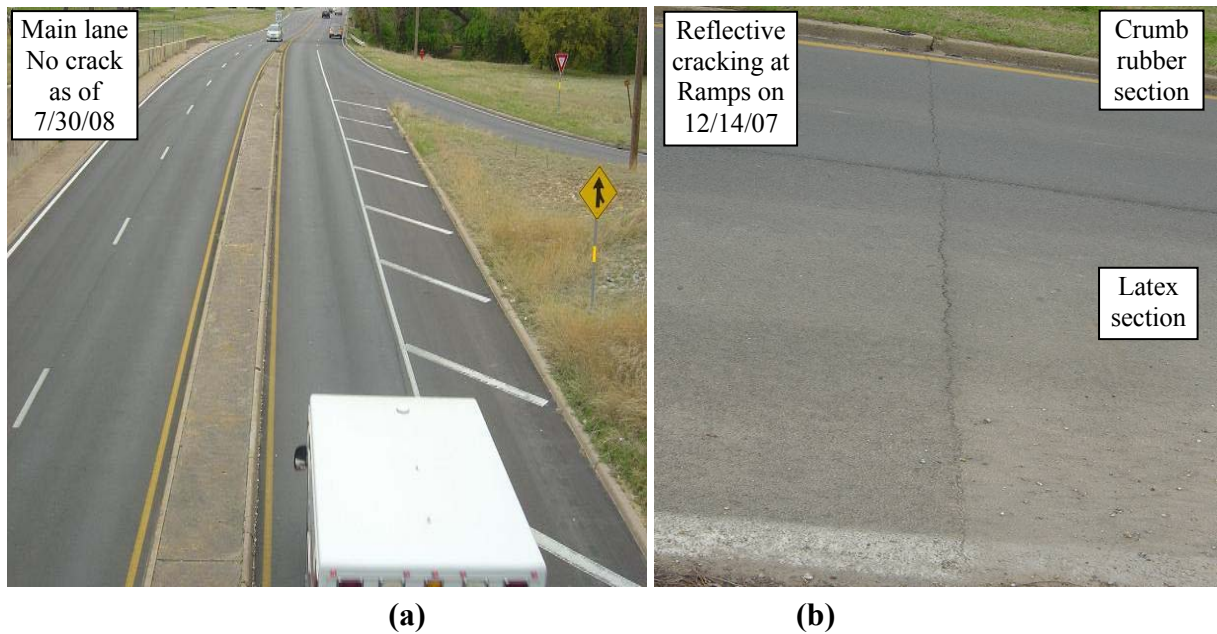
Figure 2-17. Observed Reflective Cracking.
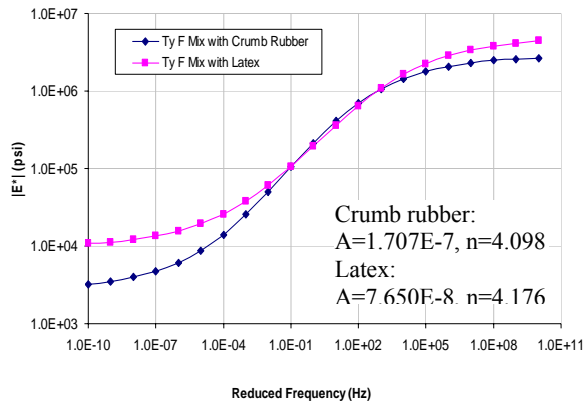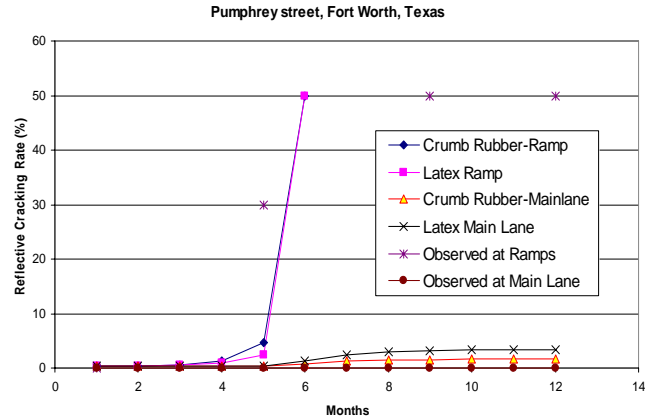
(18a)   (18b)

Figure 2-18. Pumphrey Street: Reflective Cracking Prediction.

Case 3: 4 inch HMA overlay at IH20

The IH 20 is one of the busiest truck-traveled highways in Texas. Based on 2004 traffic data, the estimated 20-year design traffic for this pavement is 87.2 million equivalent single axle loads (ESALs), with an average annual daily traffic (AADT) of 32,810 vehicles (with trucks constituting over 33 percent of the total). After years of heavy traffic, this section of highway needed to be rehabilitated. The main reason for the rehabilitation was the severe transverse cracks that caused poor ride quality. The pavement structure before the new HMA overlay consisted of 4 inch HMA overlay, 8 inch CRCP, 7 inch cement-stabilized base, 6 inch cement-treated base, and 6 inch select material over subgrade. The rehabilitation scheme included 1) milling off the 4 inch existing HMA overlay, 2) full-depth repair of the CRCP at selected locations, and 3) placement of a new 4 inch HMA overlay. After milling the existing 4 inch HMA overlay, the rolling dynamic deflectometer (RDD), which can continuously measure pavement deflection, was used to evaluate the load transfer conditions at the transverse cracks of the CRCP. Figure 2-19, as an example, shows the RDD deflection data with two sensors: Sensors 1 and 3. In this case, 10 locations have significant spikes that exceed 10 mils. These significant spikes indicate locations with poor load transfer (less than 50 percent). A total of seven reflective cracks corresponding to these spikes were observed within 25 months after opening to traffic, which are shown at the bottom in Figure 2-19 (*58*). It is clear that the load transfer had significant influence on reflective cracking.

26
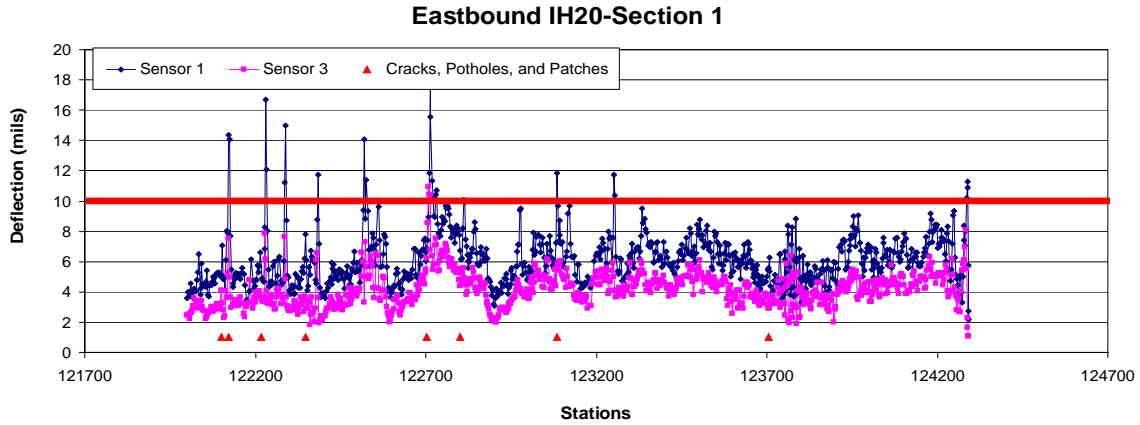
Figure 2-19. RDD Deflection Data at Test Section 1.

A total of nine mixes with the same PG76-22 binder (3 aggregate sources × 3 mix types) were used in this rehab project. These nine mixes were very stiff and had the same or very similar performance in terms of dynamic modulus (*59*), rutting resistance (Hamburg wheel tracking test), cracking resistance (Overlay test), and field performance. Thus, only test Section 1 consisting of 2 inch Superpave 12.5 mm mix and 2 inch dense-graded Type B mix was used to calibrate the reflective cracking model. The dynamic modulus and fracture properties of both mixes are presented in Figure 2-20a, and the observed reflective cracking at this section is shown in Figure 2-20b. After several trials, the calibration factor for bending load was found to be k_1=20. The predicted and the observed reflective cracking are shown in Figure 2-20b.
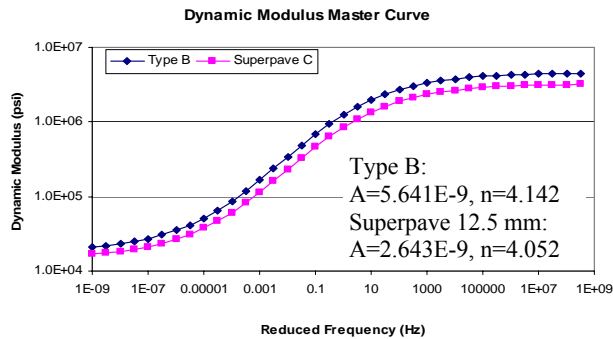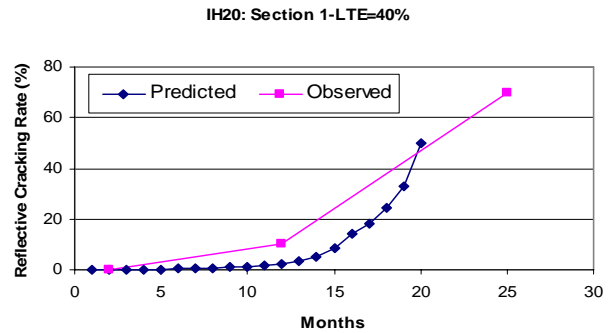
(20a) (20b)

Figure 2-20. IH20 Section 1: Reflective Cracking Prediction.

In summary, the Paris' law-based reflective cracking model has been preliminarily calibrated using three field case studies, and the three calibration factors, k_1, k_2, and k_3 for bending, shearing, and thermal loading, respectively, have been separately determined. To verify the calibrated reflective cracking model, six HMA overlays over cracked asphalt pavements tested under CalTrans accelerated pavement testing (APT) are employed and presented next.

27

VERIFICATION OF THE CALIBRATED REFLECTIVE CRACKING MODEL

A comprehensive APT study has recently been completed on the use of modified binders to limit reflective cracking in thin asphalt concrete overlays at the University of California Pavement Research Center (*60*). The experiment entailed the construction of a 90 m test road consisting of compacted clay subgrade, a 410 mm aggregate base, and 90 mm dense graded asphalt concrete surface. A Heavy Vehicle Simulator (HVS) was used to induce fatigue cracking on six, 8×1 m sections. Trafficking on each section was stopped when crack density exceeded 2.5 m/m^2. Six different overlays, including a dense graded asphalt concrete control section and five different rubber modified binder sections, were then placed on the road, as shown in Figure 2-21. The overlaid pavement structure is shown in Figure 2-22. Pavement temperatures were controlled to be around 68 ºF (20 ºC) using a temperature chamber. The HVS test results are presented in Table 2-7. The original six section locations were precisely mapped onto the overlays and the HVS used to assess reflective cracking in each. The reflective cracking conditions of Sections 587 and 588 after the HVS test are presented in Figure 2-23.
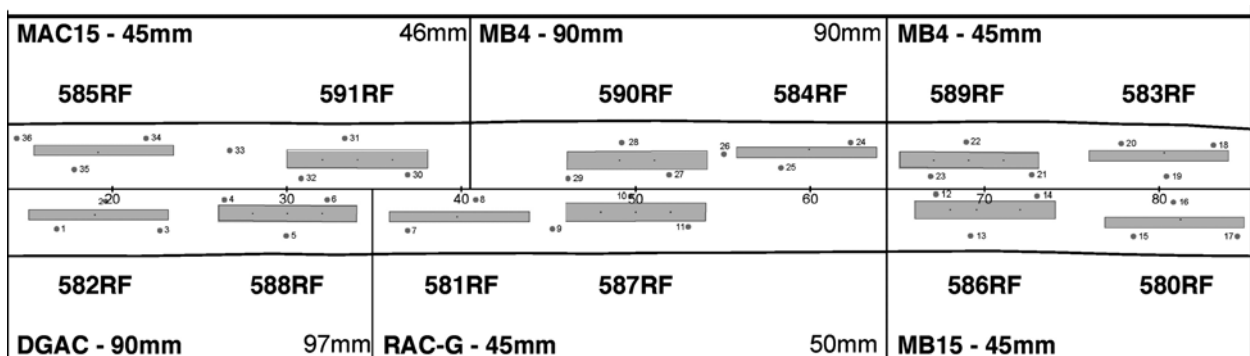
Figure 2-21. Layout of Six Overlay Test Sections (*60*).
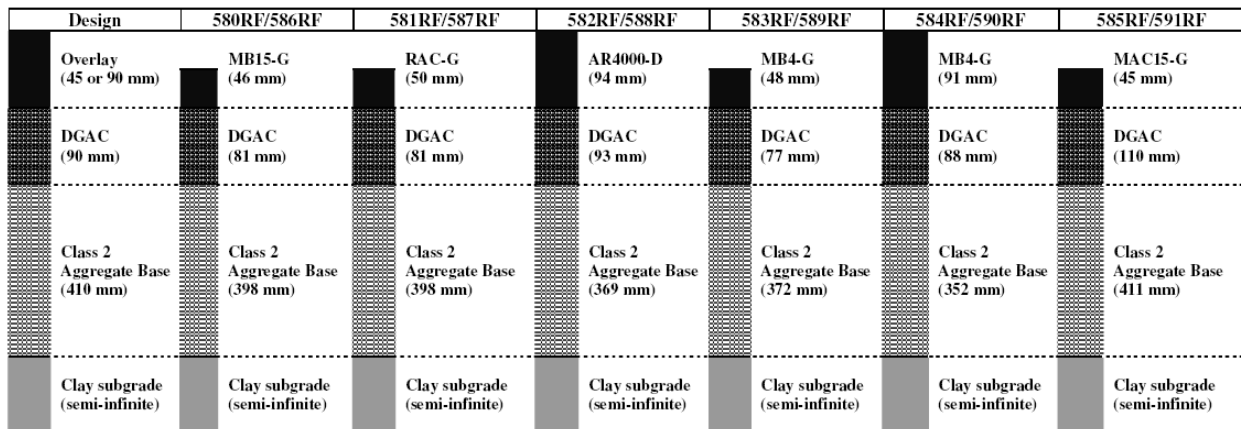
Figure 2-22. Pavement Structures of Six HVS Asphalt Overlay Test Sections (*60*).

Table 2-7. HVS Test Results of Six Asphalt Overlay Sections.

Section ID	Section brief description	No. of ESALs to 2.5 m/m^2 cracking	Regular overlay test results
586	45 mm MB4-G with 15% rubber	None after 88 million ESALs	>2000
587	45 mm RAC-G	60 million	396
588	Control section with 90 mm AR-4000-D (Dense graded asphalt concrete)	16 million	16
589	45 mm MB4-G	None after 66 million ESALs	>2000
590	90 mm MB4-G	None after 37 million ESALs	>2000
591	45mm MAC15-G	None after 91 million ESALs	>2000
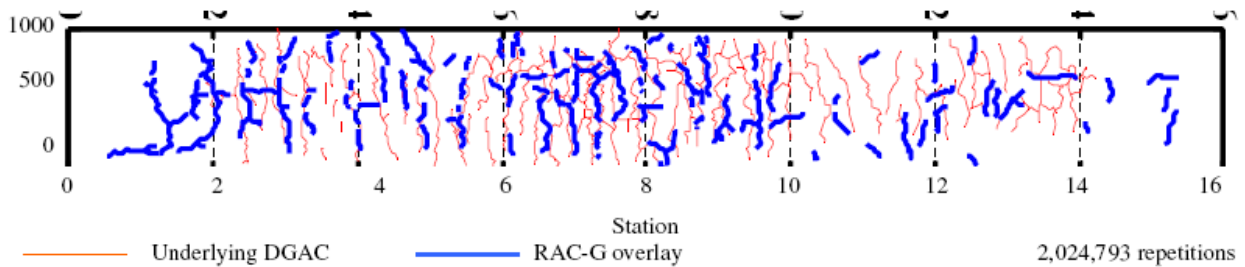
(a) Section 587
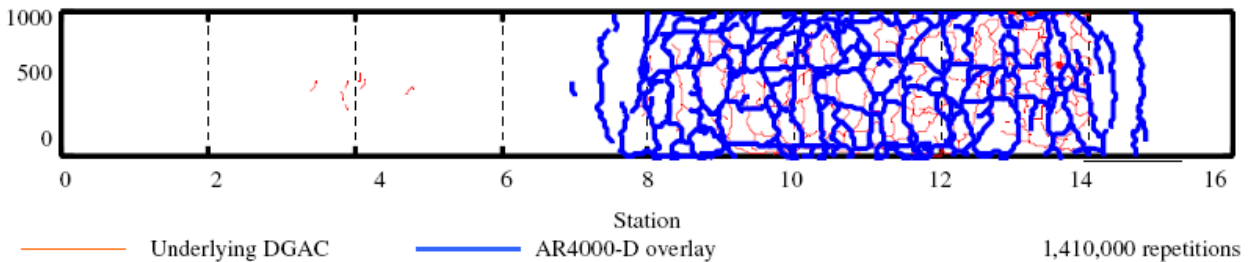
(b) Section 588

Figure 2-23. Reflective Cracking Conditions of Sections 587 and 588 after HVS Testing (*60*).

29

A total of 18 cores (3 cores from each section) were taken and shipped to TTI for the overlay testing. Two series of testing were conducted: 1) regular overlay test following Tex-248-F conducted at 77 ºF with a 0.025 inch maximum opening displacement, and 2) dynamic modulus and fracture properties (*A* and *n*) test. The regular overlay test results are shown in Table 2-8. Comparing with the HVS test results, it is apparent that the overlay test can clearly differentiate the poor reflective cracking resistance sections from the good ones. Note that the specimens of Sections 585, 586, 589, and 590 did not break at all after 2000 cycles. The measured dynamic modulus and fracture properties of each Section are shown in Figure 2-24 and Table 2-8, respectively. Furthermore, the reflective cracking rate for each HVS Section was predicted based on all this information and the preliminary calibrated reflective cracking model, as shown in Table 2-8. For comparison, HVS test results are also presented in Table 2-8. Clearly, the predicted reflective cracking rate matches what has been observed under the HVS test which is further shown in Figure 2-25 (*61*). Note that the cores shown in Figure 2-25 were taken after the HVS test. Apparently, the existing cracks at Sections 587 and 588 reflected through the HMA overlay, but almost no crack propagated at Sections 586, 589, 590, and 591 at all, which is what has been predicted from the calibrated reflective cracking model (Table 2-8). Therefore, the calibrated reflective cracking model is basically valid.
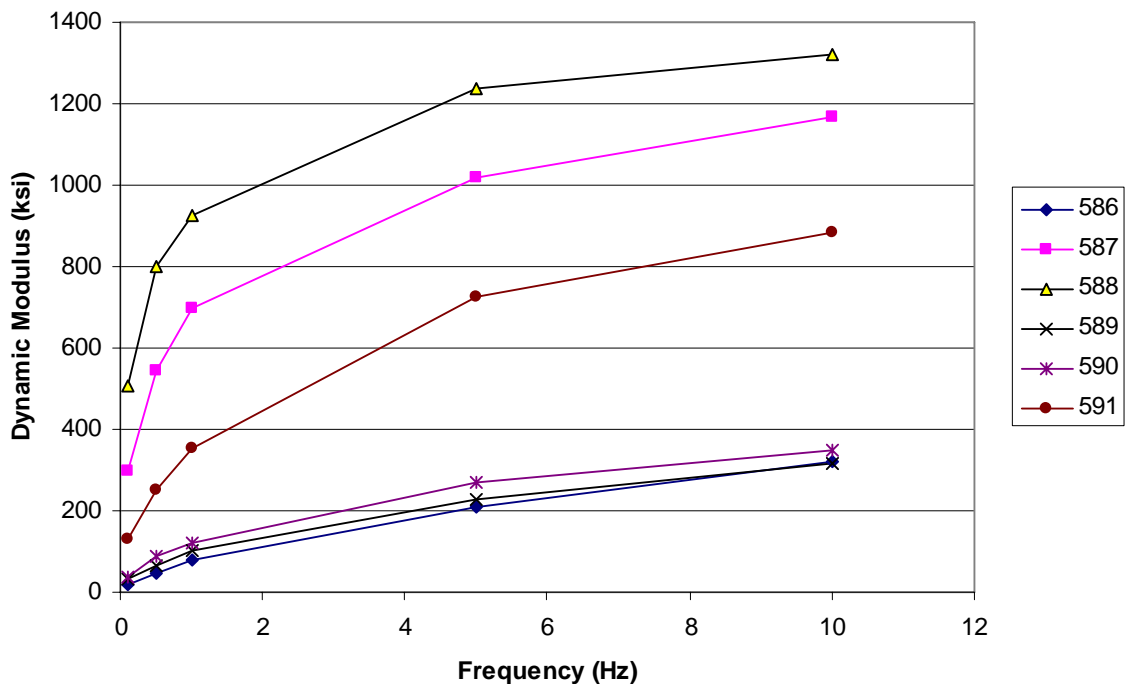
Figure 2-24. Dynamic Modulus Test Results of HVS Overlay Sections.

Table 2-8. HVS Overlay Fracture Properties and Reflective Cracking Prediction.

Section ID	Fracture Properties		Cracking Model Predicted No. of ESALs to 50 Percent Reflective Cracking	HVS Observed No. of ESALs to 2.5 m/m^2 Cracking
	A	n		
586	2.77E-06	4.974703	No crack propagation after 91 million ESALs	None after 88 million ESALs
587	3.41E-09	4.003453	50.4 million	60 million
588	6.10E-10	4.9019	8.3 million	16 million
589	2.44E-08	5.543798	No crack propagation after 66 million ESALs	None after 66 million ESALs
590	6.52E-08	5.184681	No crack propagation after 37 million ESALs	None after 37 million ESALs
591	3.44E-10	4.763871	None after 91 million ESALs	None after 91 million ESALs
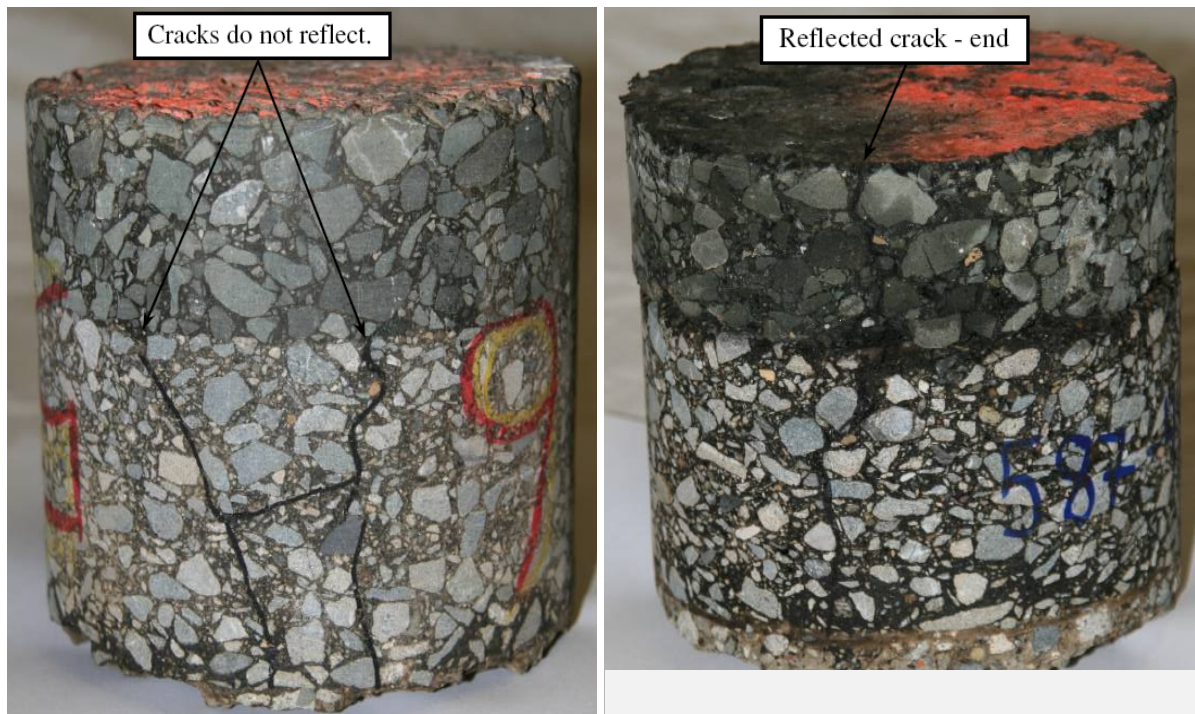
(a) Section 586   (b) Section 587

Figure 2-25. Field Cores Conditions after the HVS Testing (*61*).

(c) Section 588   (d) Section 589

(e) Section 590   (f) Section 591

Figure 2-25. Field Cores Conditions after the HVS Testing (*61*) (Continued).

SUMMARY AND CONCLUSIONS

This chapter discussed the M-E reflective cracking models for HMA overlay thickness design and analysis. Based on the work presented in this chapter, the following conclusions and recommendations are made.

- For simplicity and practical routine applications, the well-known Paris' law-based fracture mechanics model still is a rational choice to model reflective cracking induced by both traffic loading (bending and shearing) and thermal effects. This was the basis of the M-E models proposed in this study for modelling reflective cracking in asphalt overlays.

- Based on extensive SIF computations and statistical analysis, a total of 32 SIF regression equations were developed for asphalt overlays over existing flexible pavements and asphalt overlays over existing PCC pavements with three levels of load transfers efficiencies (10, 50, and 90 percent) at joints/cracks. These developed equations make it possible and practical to directly analyze the reflective crack propagation caused by variable traffic load spectrum. It was also found that the MET approach is valid for multi-layered asphalt overlays and bases (and/or subbases).

- For the thermal reflective cracking, a "hybrid" approach, similar to the SHRP low temperature cracking model, was proposed. In this hybrid approach, the viscoelastic properties of HMA mixes are considered through the thermal stress at the far field ($\sigma_{VE\text{-}far}$), which then ties with the stress intensity factor ($K_{thermal}$). Regression equations were accordingly developed for asphalt overlays over existing flexible pavements and asphalt overlays over existing PCC pavements, respectively.

- The HMA fracture properties (A and n), which are the fundamental input parameters required in the proposed M-E reflective cracking model, can be easily and directly determined in the laboratory using the simple and rapid OT test. The main innovative features of the OT for fracture property determination are the moderately small and convenient specimen size, easy specimen preparation, and short testing time (within 20 minutes). To assist in implementation the default values of fracture parameters (A and n) have been provided for typical overlay mixes (such as Type C, D, and SMAs), as presented in Chapter 4.

- The proposed reflective cracking model was preliminarily calibrated using three HMA overlay field case studies, and the calibrated model has been verified using the reflective cracking data of six asphalt overlay sections collected from California's HVS test site. Thus far, satisfactory results have been obtained. However, more field performance data are definitely needed for further model calibration and verification.

Overall, the M-E models proposed in this chapter offer great promise potential for rationally modelling and accurately predicting the reflective cracking potential of HMA overlays. Based on the data presented herein, both traffic loading (bending and shearing) and thermal effects, over flexible or rigid PCC pavements can satisfactorily be characterized. Additionally, the OT proved to be an ideal laboratory test for rapidly determining the HMA fracture properties that are required as some of the input parameters in the proposed M-E models for reflective cracking. However, although comparable results with field measurements were obtained in this study, further model validation and calibration with more field data, varied traffic load spectrums, different environmental conditions, and different materials (HMA mix types) are still required.

CHAPTER 3

DEVELOPMENT AND CALIBRATION OF M-E RUTTING MODEL FOR ASPHALT OVERLAYS

INTRODUCTION

Rutting is another potential major distress and concern for asphalt overlays for at least two reasons: 1) if the surface is impervious, the ruts trap water, and at depths of about 0.2 inch, hydroplaning (particularly for passenger cars) is a definite threat; and 2) as the ruts progress in depth, steering becomes increasingly difficult, leading to added safety concerns. Therefore, it is important to make efforts to minimize rutting, and at the same time it is necessary to develop a model to predict the potential rutting development when designing an HMA overlay.

Different from new asphalt pavement in which rutting may be from each pavement layer (i.e., asphalt layer, granular base, or subgrade), the HMA overlay rutting is mainly confined to the overlay itself, because rutting from the old pavements, in most cases, had already occurred before the HMA overlay. Several field trench studies on US281 and US175 clearly showed that the rutting was coming primarily from the top 2 inches of HMA layers, as shown in Figures 3-1 and 3-2. Thus, the rutting prediction in this research project focused only on the HMA overlay itself.

Regarding HMA overlay rutting, it is commonly accepted that rutting (permanent deformation) is a manifestation of two different mechanisms and is a combination of densification (volume change) and repetitive shear deformation (plastic flow with no volume change). It is difficult to determine the relative amounts of rutting occurring in each HMA layer, and the relative proportions of rut depth that can be attributed to densification and shear, because many factors, such as binder type, binder content, mix type, load level, temperature, initial compacted density, etc., have are influence on rutting. To adequately consider all these influential factors, it is necessary to develop an M-E rutting model. Based on this background, the main objective of this chapter was to develop an M-E rutting model for HMA overlay design and analysis.

The research approach utilized to achieve the above objective includes four steps:

1) Rutting model review and recommendation;

2) Development of HMA overlay rutting model;

3) Calibration of the developed HMA overlay rutting model; and

4) Verification of the calibrated HMA overlay rutting model.

The detailed work conducted is presented in the subsequent text.

Figure 3-1. Trench Profiles for Sections 161 (Top) and 162 (Bottom) on US281.

Figure 3-2. Trench Wire Lines for Overlay Sections 508 (Top) and 507 (Bottom) on US175.

RUTTING MODEL REVIEW AND RECOMMENDATION

Rutting prediction and modeling have been studied for a long time. Various models have been developed to predict rutting (or permanent deformation). In general, these models can be categorized as 1) layer strain rutting model and 2) shear strain rutting model. Detailed information is presented below.

Category 1: Layer Strain Rutting Model

The most often used approach for the rutting prediction is based on the use of elastic theory and the results of plastic strains determined by repeated load tests on pavement materials. The approach was initially introduced by Heukelom and Klomp (*62*). Since then, research has been conducted by others such as Monismith (*63*), McLean (*64*), Romain (*65*), Barksdale (*66*), and Morris and Hass (*67*) for soils, granular materials, and asphalt concrete. The fundamental concept of this approach is the assumption that the plastic strain ε_p is functionally proportional to the elastic state of stress (or strain) and number of load repetitions. This constitutive deformation law is considered applicable for any material type and at any point within the pavement system. The response of any material must be experimentally determined from laboratory tests for conditions (times, temperature, stress state, moisture, density, etc.) expected to occur *in situ*.

Provided the plastic deformation response is known, elastic theory (either linear or non-linear) is then used to determine the expected stress state within the pavement. By subdividing each layer into convenient thickness (Δz_j) and determining the average stress state at each layer increment, the permanent deformation within the ith layer, δ_i^p may be found by summing the $(\varepsilon_i^p) \times (\Delta z_i)$ products. This process is done for each layer present in the pavement so that it is termed "layer strain" rutting model. The total permanent deformation of the pavement is found from:

$$\delta_t^p = \sum_{i=1}^{n} \delta_i^p \tag{3-1}$$

where δ_{t}^p is total permanent deformation of the pavement, δ_{i}^p is permanent deformation within the ith layer, and n is number of layers.

Obviously, such a summation process is done along a vertical axis (constant horizontal plane coordinates). While different permanent deformation models have been proposed, only three most promising layer strain rutting models, MEPDG rutting model (*68*), NCHRP 1-40B rutting model (*69*), and VESYS rutting model (*70, 71*), are discussed below.

- MEPDG rutting model

The final MEPDG HMA rutting model is presented below:

$$\frac{\varepsilon_p}{\varepsilon_r} = k_1 \times 10^{-3.4488} T^{1.5606} N^{0.479244} \tag{3-2}$$

where ε_p is permanent strain, ε_r is resilient strain, T is temperature (ºF), N is number of load repetitions, and k_1 is depth adjustment coefficient and defined as follows:

$$k_1 = (C_1 + C_2 \times D) \times 0.328196^D \tag{3-3}$$

$$C_1 = -0.1039 h_{ac}^2 + 2.4868 h_{ac} - 17.342 \tag{3-4}$$

$$C_2 = 0.0172 h_{ac}^2 - 1.7331 h_{ac} + 27.428 \tag{3-5}$$

where h_{ac} is total HMA thickness (inch) and D is depth below the surface (inch).

- NCHRP 1-40B rutting model

NCHRP 1-40B rutting model has the same format as the MEPDG rutting model. The enhancement is to adjust permanent deformation constants based on HMA volumetric properties.

$$\frac{\varepsilon_p}{\varepsilon_r} = k_1 \left(10^{k_{r1}} T^{k_{r2}} N^{k_{r3}} \right) \tag{3-6}$$

where k_1 is depth adjustment function defined in the MEPDG rutting model. k_{r1}, k_{r2}, and k_{r3} are material properties and defined below.

Constant k_{r1} is defined as follows:

$$k_{r1} = \log\left[1.5093 \times 10^{-3} \times K_{r1} \times V_a^{0.5213} \times V_{beff}^{1.0057} \right] - 3.4488 \tag{3-7}$$

where V_{beff} is effective asphalt content in volume (%), and K_{r1} is intercept coefficient shown in Figure 3-3.
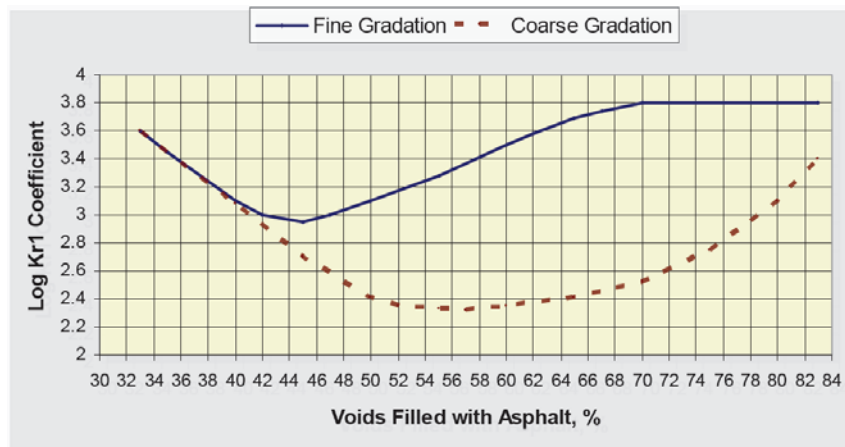
Figure 3-3. LogKr_1 Coefficient vs. Voids Filled with Asphalt (%) (69).

Constant k_{r2} is defined below:

$$k_{r2} = 1.5606 \left(\frac{V_a}{V_{a(design)}} \right)^{0.25} \left(\frac{P_b}{P_{b(opt)}} \right)^{1.25} F_{index} C_{index} \tag{3-8}$$

where $V_{a(design)}$ is design air voids; P_b is asphalt content by weight; $P_{b(opt)}$ is design asphalt content by weight; F_{index} is fine aggregate angularity index (Table 3-1); and C_{index} is coarse aggregate angularity index (Table 3-2).

Table 3-1. Fine Aggregate Angularity Index Used to Adjust F_{index}.

Gradation – External to Restricted Zone	Fine Aggregate Angularity	
	<45	>45
Dense Grading – External to Restricted Zone	1.00	0.90
Dense Grading – through Restricted Zone	1.05	1.00

38

Table 3-2. Coarse Aggregate Angularity Index Used to Adjust C_{index}.

Type of Gradation	Percent Crushed Material with Two Faces				
	0	25	50	75	100
Well Graded	1.1	1.05	1.0	1.0	0.9
Gap Graded	1.2	1.1	1.05	1.0	0.9

Constant k_{r3} is presented below:

$$k_{r3} = 0.4791 \times K_{r3} \times \frac{P_b}{P_{b(opt)}} \tag{3-9}$$

where K_{r3} is slope coefficient; for fine-graded mixes with GI<20, K_{r3} is 0.40; for coarse-graded mixes with 20<GI<40, K_{r3} is 0.70; for coarse-graded mixes with GI>40, K_{r3} is 0.80; and GI is gradation index and defined below:

$$GI = \sum_{i=3/8}^{\#50} \left| P_i - P_{i(0.45)} \right| \tag{3-10}$$

- VESYS rutting model

The VESYS rutting model is based on the assumption (or laboratory permanent deformation law) that the permanent strain per loading pulse occurring in a material specimen can be expressed by:

$$\frac{\Delta \varepsilon_p(N)}{\varepsilon} = \mu N^{-\alpha} \tag{3-11}$$

where $\Delta \varepsilon_p(N)$ is vertical permanent strain at load repetition, N; ε is peak haversine load strain for a load pulse of duration of 0.1 sec measured on the 200th repetition; and μ and α are material properties depending on stress state, temperature, etc.

The above equation assumes that ε remains relatively constant throughout the test, and thus, the permanent strain increment, $\Delta \varepsilon_p(N)$, at any load cycle is:

$$\Delta \varepsilon_p(N) = \varepsilon - \varepsilon_r(N) \tag{3-12}$$

where $\varepsilon_r(N)$ is the resilient or rebound strain taking place at cycle N. Then, the rut depth for any single layer after N load cycles can be written as:

$$R_D = H \times \varepsilon_p = H \times \varepsilon \frac{\mu}{1-\alpha} N^{1-\alpha} \tag{3-13}$$

where H is layer thickness.

The VESYS layer rutting model estimates the permanent deformation in each finite layer as the product of the elastic compression in that layer and the layer material permanent deformation law associated with that layer. The layer rutting model is expressed by:

39

$$R_D = \int_{N_1}^{N_2} U_s^+ \; \frac{e_t}{e_s} \; \mu_{sub} \; N^{-\alpha_{sub}} + \sum_{i=1}^{n-1} \int_{N_1}^{N_2} (U_i^+ - U_i^-) \, \mu_i N^{-\alpha_i} \qquad (3\text{-}14)$$

where U_s^+ is the deflection at the top of the subgrade due to single axle load; U_i^+ and U_i^- are deflections at the top and bottom of finite layer i due to axle group; e_t is strain at top of subgrade due to the axle group; e_s is strain at top of subgrade due to a single axle; μ_{sub} and α_{sub} are permanent deformation parameters of the subgrade; and μ_i and α_i are permanent deformation parameters of layer i.

The major feature of the VESYS rutting model is to characterize layer properties rather than global parameters used by the MEPDG. For each layer, the VESYS rutting model requires permanent deformation parameters: μ and α_i.

Category 2: WesTrack Shearing Strain Rutting Model

An alternative to the layer strain approach has been recently proposed to model the rutting behavior of the WesTrack test sections (*72*). In this approach, the pavement is modeled as a multi-layered elastic system with the asphalt concrete modulus determined from the repeated simple shear test at constant height (RSST-CH) tests. Rutting in AC is assumed to be controlled by shear deformations. Computed elastic shear stress and strain (τ, γ^e) at a depth of 50 mm beneath the edge of the tire are used for rutting estimates. Densification of the asphalt concrete is excluded in the rutting estimates since it has a comparatively small influence on surface rutting.

In simple loading, permanent shear strain in the AC is assumed to accumulate according to the following expression:

$$\gamma^i = a \times \exp(b\tau) \times \gamma^e \times n^c \qquad (3\text{-}15)$$

where τ is shear stress determined at this depth using elastic analysis; γ^e is corresponding elastic shear strain; n is number of axle load repetitions; and a, b, c are regression coefficients obtained from field data, RSST-CH laboratory test data, and the elastic simulations.

Rutting in AC layer due to the shear deformation is determined from the following:

$$RD_{AC} = K * \gamma_j^i \qquad (3\text{-}16)$$

For a 150 mm (6 inch) layer, the value of K is 5.5 where the rut depth (RD) is expressed in inches.

Rutting Model Selection and Recommendation

As noted previously, the WesTrack shearing rutting model requires the RSST-CH to characterize permanent deformation properties of HMA mixes and predict pavement rutting using empirical shift factors. The feature of the WesTrack shearing rutting model is that only the HMA layer located at 2 inches below the pavement surface, regardless of how many HMA layers exist in the pavement structure, is required to be evaluated under the RSST-CH. The disadvantages of the WesTrack shearing rutting model are 1) high variability of RSST-CH and 2) very limited uses and validation.

Regarding the layer strain models, both MEPDG and NCHRP 1-40B rutting models have specific parameters and do not need to run laboratory testing. While the NCHRP 1-40B rutting model is an enhanced MEPDG model and considers many more factors (e.g., asphalt binder content, angularity, gradation) influencing rutting, asphalt binder PG grade (a parameter that most affects rutting of HMA pavement based on accelerated load testing) is not directly considered in the NCHRP 1-40B rutting model. It is worth noting that not requiring laboratory testing is both advantageous and disadvantageous for these two models, because while it makes the models simple to implement, not using laboratory characterization of HMA mixes may lead to inaccurate rutting prediction. However, HMA mixes are very complex, and laboratory characterization of permanent deformation properties is critical to adequately predict field rutting performance.

Different from both the MEPDG and NCHRP 1-40B rutting models, the major feature of the VESYS layer rutting model is to characterize layer properties rather than global parameters used by the MEPDG. For each layer, the VESYS rutting model requires permanent deformation parameters: α_i and μ_i. Its disadvantage also is acquiring these layer properties and running repeated load tests for each layer. However, recognizing the complexity of HMA mixes, it is necessary to characterize each HMA layer's permanent deformation properties in order to make a more accurate prediction. Therefore, the VESYS layer rutting model was finally selected for modeling HMA overlays rutting. The detailed rutting model for asphalt overlays is presented below.

$$R_D = \sum_{i=1}^{N} k_{RD} \int \left(U_i^+ - U_i^- \right) \mu_i N^{-\alpha_i} \qquad (3\text{-}17)$$

where, k_{RD} is calibration factor, U_i^+ and U_i^- are deflection at top and bottom of finite layer i due to axle group; N is number of overlays; and μ_i and α_i are permanent deformation parameters of overlay layer i.

It is clear that the two key issues of the recommended rutting model are to 1) calculate the deflection of each HMA overlay and 2) determine permanent deformation parameters for each HMA overlay: μ_i and α_i in the lab. Additionally, rutting accumulation principle under different traffic loads and environmental conditions should also be addressed. All these three issues will be discussed in the next section.

DEVELOPMENT OF HMA OVERLAY RUTTING MODEL

As noted above, the VESYS layer rutting model has been recommended for predicting HMA overlay rutting. However, there are three issues needing to be further addressed. The following text will further discuss each one.

Calculation of HMA Overlay Deflection

Currently, different multi-layer linear elastic programs are available for calculating pavement deflection. To be consistent with current TxDOT's pavement design program, FPS19W in which the well-known multi-layer elastic program, Weslea, is used, the Weslea program was chosen to calculate the HMA overlay deflections for rutting prediction.

Laboratory Determination of HMA Overlay Rutting Properties: μ and α

The most often used laboratory test for determining the permanent deformation properties of HMA materials is repeated load test. Generally, the test is run without confining pressure with 0.1 second loading and 0.9 second rest period. After reviewing historical reference about the repeated load test in the literature, Zhou and Scullion (*73*) have standardized the repeated load test (or VESYS test) protocol. It was recommended that the test be conducted at three temperatures: 77, 104, and 122 ºF. For each temperature, the applied load is listed in Table 3-3. Detailed test protocol can be found in reference *73*.

Table 3-3. Repeated Load Test Temperatures and Load Levels.

Test temperature (ºF)	77	104	122
Applied deviator stress (psi)	30	20	10

Rutting Accumulation Principle

To consider the effects of stresses of different magnitudes on the development of rutting, which result from variations in *traffic loads* and *environmental conditions*, an accumulative damage hypothesis is required, just as for fatigue. A **"*time-hardening*"** procedure appears to provide a reasonable approach (*72, 74*).

For each season i, ε_i^p is computed from:

$$\varepsilon_i^p = \varepsilon_i^p (at N=1)\left[\left(N_{eqi} + n_i\right)^S - N_{eqi}^S\right]$$ (3-18)

where ε_i^p(at N=1) is permanent strain at the first load repetition; n_i is number of load repetitions during season i; N_{eqi} is equivalent total number of load repetitions at beginning of season i; and S is slope of $\log\varepsilon^p$ –$\log N$ curve derived from laboratory test results.

The N_{eq} is obtained for each element k with the time-hardening matching scheme as follows:

Season 1
$$N_{eq} = 0$$
$$\varepsilon_1^p = \varepsilon_1^p (N = 1)N_1^{S_1}$$ (3-19)

Season 2
$$N_{eq2} = \left[\frac{\varepsilon_1^p}{\varepsilon_2^p (N = 1)}\right]^{\frac{1}{S_2}}$$ (3-20)

$$\varepsilon_2^p = \varepsilon_2^p (N = 1)\left[\left(N_{eq2} + n_2\right)^{S_2} - N_{eq2}^{S_2}\right]$$ (3-21)

$$\text{Season } l \qquad N_{eql} = \left[\frac{\varepsilon_{l-1}^p}{\varepsilon_l^p (N=1)} \right]^{\frac{1}{S_l}} \qquad\qquad (3\text{-}22)$$

$$\varepsilon_l^p = \varepsilon_l^p (N=1) \left[\left(N_{eql} + n_l \right)^{S_l} - N_{eql}^{S_l} \right] \qquad\qquad (3\text{-}23)$$

With the above developed HMA overlay rutting, the next step is to calibrate it using field rutting data and then verify it using different field rutting data.

CALIBRATION OF THE HMA OVERLAY RUTTING MODEL

The purpose of calibration is to determine the calibration factor k_{RD} in the HMA overlay rutting model. As shown previously, the calibration factor in the MEPDG rutting model is a function of pavement temperature and asphalt layer thickness. Additionally, it has also been recognized that permanent strain (ε_p) may not be directly proportional to resilient strain (ε_r) but related to both resilient strain and modulus (*75*), so that a modulus (or strain) factor is necessary for the calibration. Therefore, it is anticipated that k_{RD} is also related to pavement temperature (T), HMA modulus, and HMA overlay thickness (h_{OL}), as presented below:

$$k_{RD} = f_1(T) \times f_2(E) \times f_3(h_{OL}) \qquad\qquad (3\text{-}24)$$

Therefore, the calibration process was to determine pavement temperature factor, $f_1(T)$, modulus factor, $f_2(E)$, and HMA overlay thickness factor, $f_3(h_{OL})$, using field rutting data.

Determination of Calibration Factors: $f_1(T)$ and $f_2(E)$

In this research project, the field rutting data from the NCAT (National Center for Asphalt Technology) pavement test track were used to determine both $f_1(T)$ and $f_2(E)$. As noted below, the sections of the NCAT test track selected for the model calibration are thin sections and most of them are less than 3 inches. Based on the national rutting trench studies conducted by NCAT (*76*) and the trench studies in Texas (Figures 3-1 and 3-2), most of the rutting occurred only in the top 4 inch HMA layers. Therefore, the thickness factor for the sections of the NCAT test track was assumed to be 1.0 when determining the calibration factors $f_1(T)$ and $f_2(E)$.

Figure 3-4 shows the 2006 experimental sections of the test track, which were constructed in October 2006 and trafficked in November 2006. The ESALs were applied with four fully loaded trucks at 45 mph with 3 trailers per tractor. Each tractor pulled a load of approximately 152,000 pounds for each of 7 loaded axles, and approximately 12,000 pounds for the front steer axle. The cumulative ESALs for NCAT Test Track are plotted in Figure 3-5.
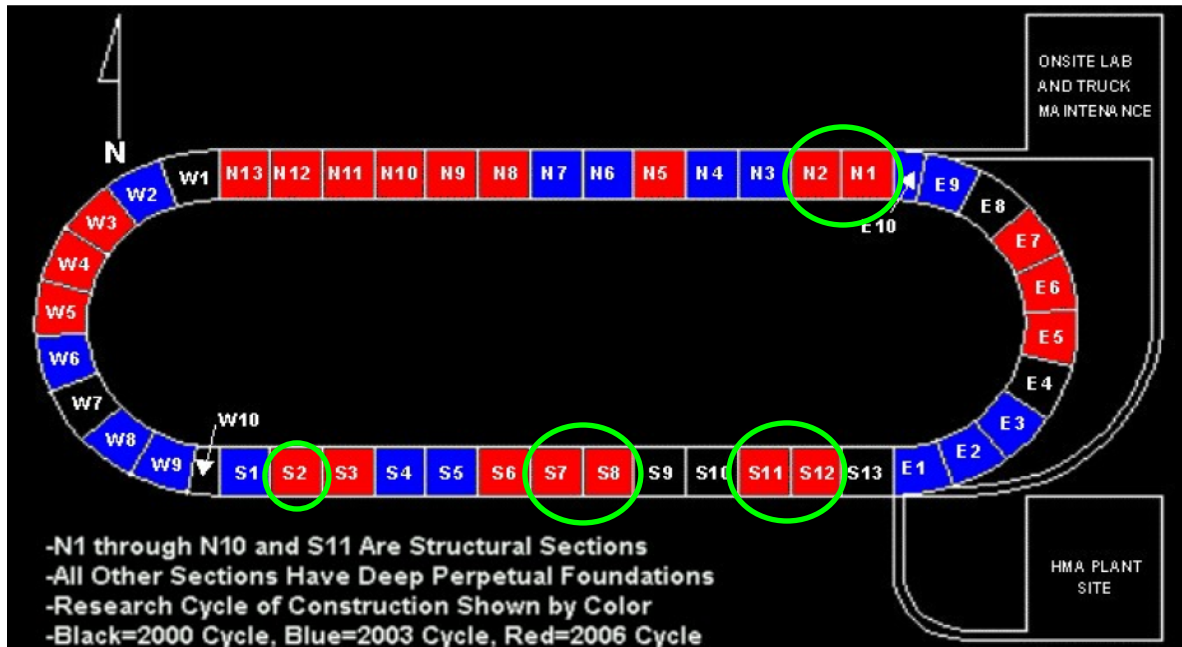
Figure 3-4. 2006 Experimental Sections of the NCAT Test Track.
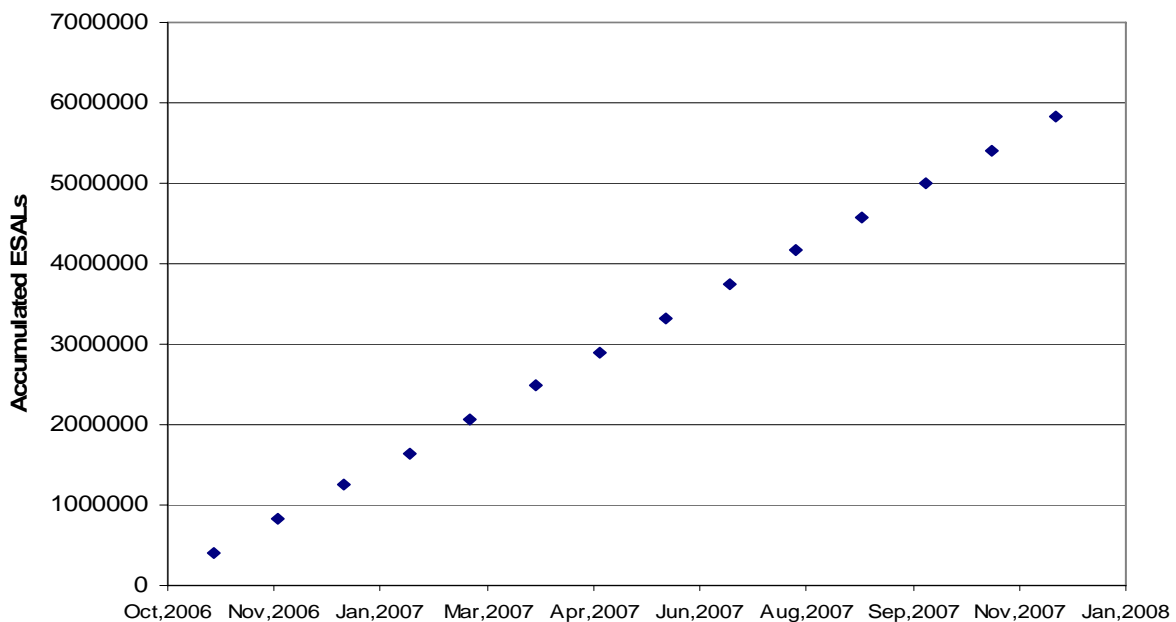
Figure 3-5. Accumulated Traffic Loads in ESALs at the NCAT Test Track.

A total of 9 sections, N1, N2, S2, S7A, S7B, S8A, S8B, S11, and S12 were selected for determining the calibration factors $f_1(T)$ and $f_2(E)$. As shown in Figure 3-6, rut depths of these 9 sections after around 6 million ESALs loading ranged from small rutting (Sections N1, N2, and S2), intermediate rutting (Sections S11 and S12), and very deep rutting (Sections 7A, 7B, 8A, and 8B). Plant mixes from these 9 test sections were compacted using the Superpave Gyratory

44

Compactor (SGC) to mold samples for both dynamic modulus test and repeated load test. Figure 3-7 shows an example of prepared samples (4 inch diameter by 6 inch height) for both tests. The dynamic modulus test was conducted over five different temperatures of 14, 40, 70, 100, and 130 °F and six loading frequencies of 25, 10, 5, 1, 0.5, and 0.1 Hz for each test temperature, respectively. Figure 3-8 shows the dynamic modulus master curves for the selected HMA mixes. Additionally, the repeated load test was run at three temperatures: 77, 104, and 122 °F. The permanent deformation properties (μ, α) for each selected section determined from the repeated load test are tabulated in Table 3-4.

Figure 3-6. Measured Rut Depths of Test Track Sections.

Figure 3-7. Examples of Prepared Specimens for Dynamic Modulus Test and Repeated Load Test.
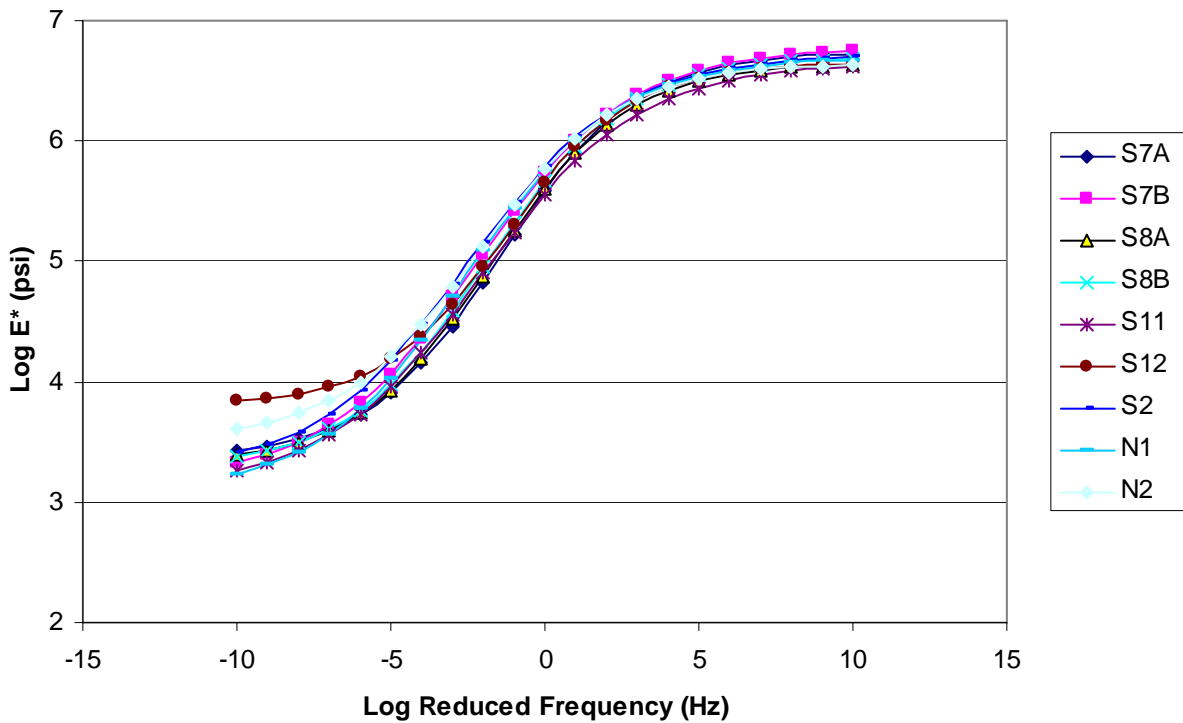
Figure 3-8. Dynamic Modulus Master Curves of the HMA Mixes Used for Calibration.

Table 3-4. μ and α Values of Selected Sections Determined from the Repeated Load Test.

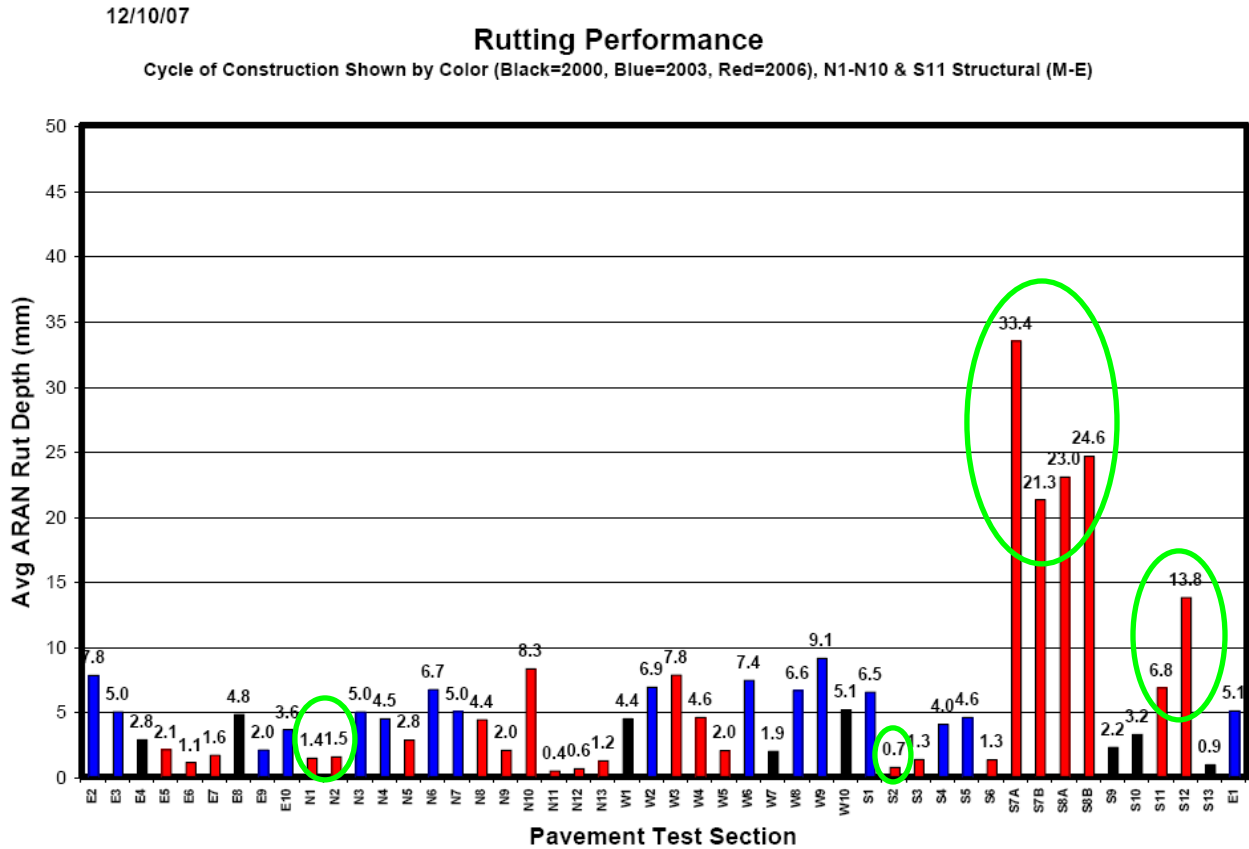| Mixes	77 ºF		104 ºF		122 ºF	
	α	μ	α	μ	α	μ
7A	0.752	0.987	0.744	1.179	0.725	1.139
7B	0.754	1.025	0.766	1.255	0.762	1.040
8A	0.797	0.850	0.786	0.988	0.774	1.000
8B	0.782	0.970	0.789	1.245	0.802	1.195
S11	0.580	0.152	0.761	0.726	0.855	1.167
S12	0.750	0.638	0.838	0.873	0.830	0.820
S2	0.708	0.372	0.781	0.681	0.802	0.958
N1	0.600	0.236	0.821	1.143	0.877	1.377
N2	0.667	0.211	0.832	0.872	0.878	1.126

In the calibration process, the climate data from the weather station at Opelika, Alabama, where the test track is located were used as input to the EICM model to predict HMA layer temperature. Note that the modulus E value used for determining $f_2(E)$ during the calibration was chosen at 130 ºF and 10 Hz. There are two reasons for choosing such a specific temperature and frequency; one reason is that rutting in most cases occurs at high temperatures (beyond 100 ºF), and the other is that dynamic modulus at 130 ºF and 10 Hz had good correlations with field rut depth, as shown in the NCHRP Report 465 (*77*). A trial and error approach was to determine both $f_1(T)$ and $f_2(E)$ meanwhile minimizing the difference between the predicted and the measured rut depth, as shown in Figure 3-9. The final temperature factor and modulus factor are presented below:

$$f_1(T) = 0.191112 + \frac{3.643124}{1 + e^{18.3009 - 0.204437\,T}} \tag{3-25}$$

$$f_2(E) = 0.30787 + \frac{1.27860}{1 + e^{-8.28248 + 0.09239\,E}} \tag{3-26}$$

where T is HMA overlay temperature, ºF; and E is HMA overlay modulus measured at 130 ºF and 10 Hz, ksi.
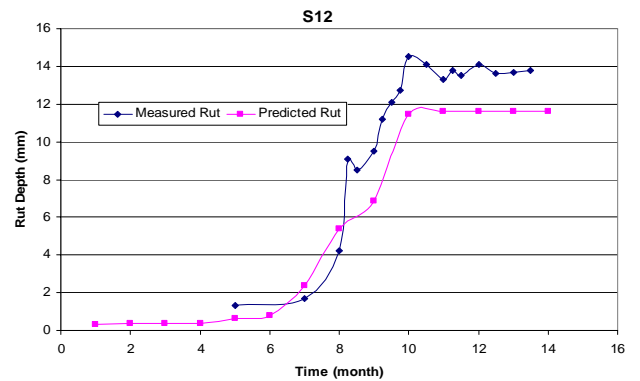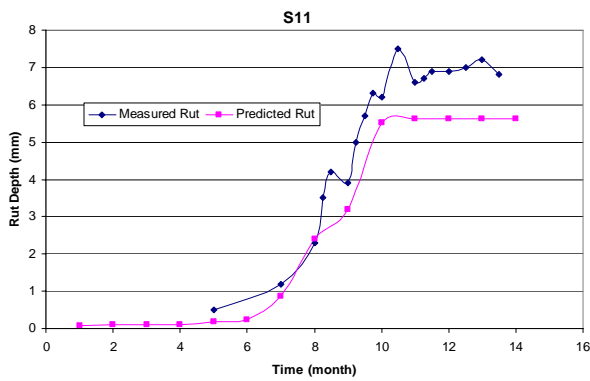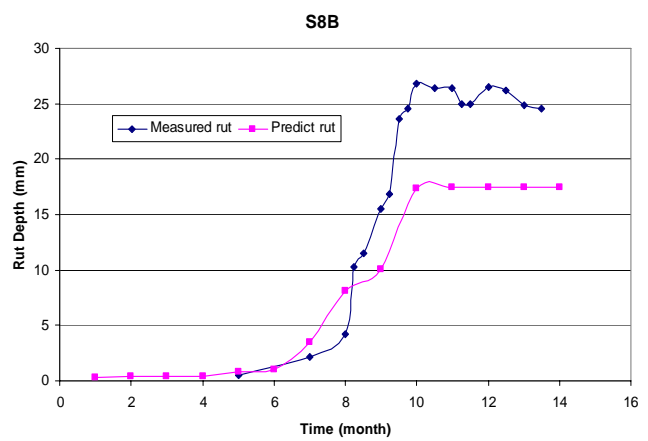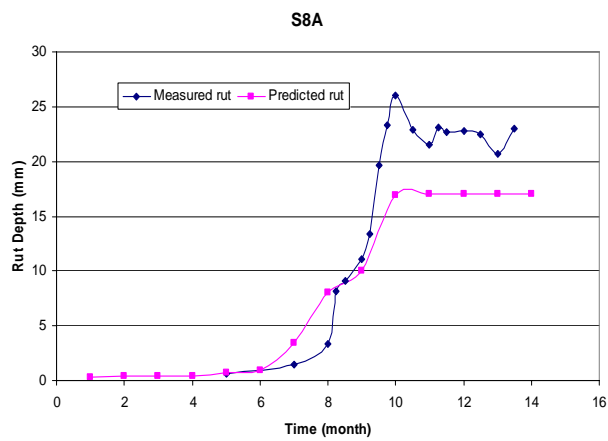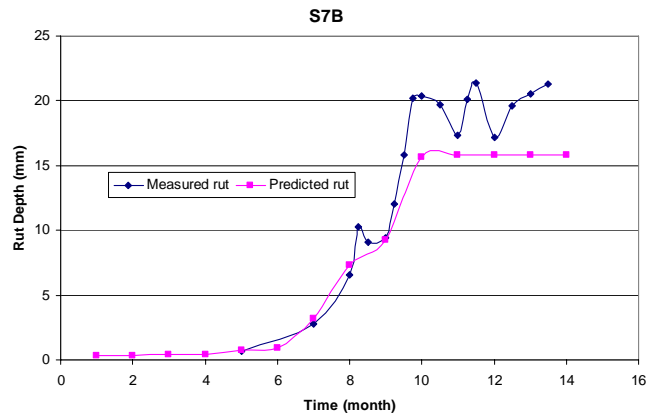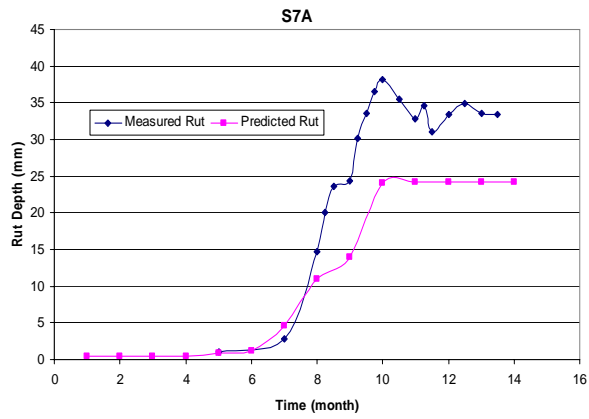
Figure 3-9. Comparisons between the Measured and Predicted Rut Development.
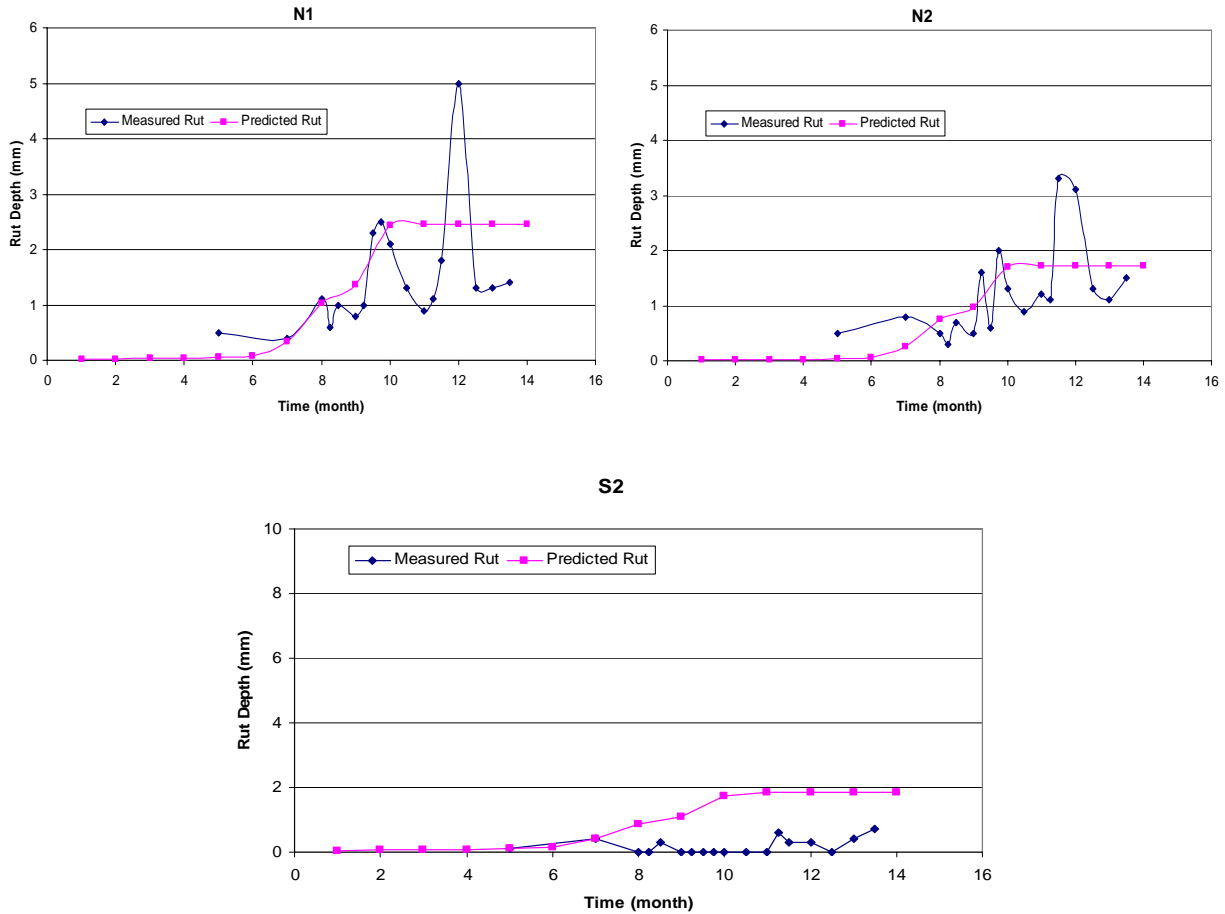
Figure 3-9. Comparisons between the Measured and Predicted Rut Development (Continued).

Determination of HMA Overlay Thickness Factor

Currently, all layer strain-based rutting models including the model used in this study predict higher and higher rut depth with increasing HMA overlay thickness, but the reality in the field is that the rutting will continually increase with thicker and thicker HMA overlay until the HMA overlay thickness reaches a certain value (normally around 5 inches). After that, the HMA overlay rutting normally does not change much with increasing the overlay thickness. Based on this general observation and field trench data shown in Figures 3-1 and 3-2 and the thickness adjustment factor used in the MEPDG program, a pure empirical factor, $f_3(h_{OL})$ was developed for adjusting the influence of the HMA overlay thickness on the predicted rut depth. The recommended HMA overlay thickness factor is presented in Equation 3-27. Figure 3-10 shows the difference of the rutting development before and after thickness adjustment. Ideally, this empirical factor, $f_3(h_{OL})$ will be replaced when more thick HMA overlay rutting data and trench information are available.

49

$$f_3\left(h_{OL}\right) = \left(0.01445272\ h_1{}^3 - 0.12471319\ h_1{}^2 + 0.22193794\ h_1 + 1.37640722\right)\times$$
$$\left(0.00567302\ h_2{}^3 + 0.07104301\ h_2{}^2 - 0.49592553\ h_2 + 2.12378879\right)\times \quad (3\text{-}27)$$
$$\left(0.00199314 + \frac{0.54035153}{1 + e^{-2.61478586\ +\ 0.58494148\ \left(h_1 + h_2\right)}}\right)$$

HMA Overlay with a PG64-22 Binder over PCC at Dallas District under 10 Million ESALs (20 Years)
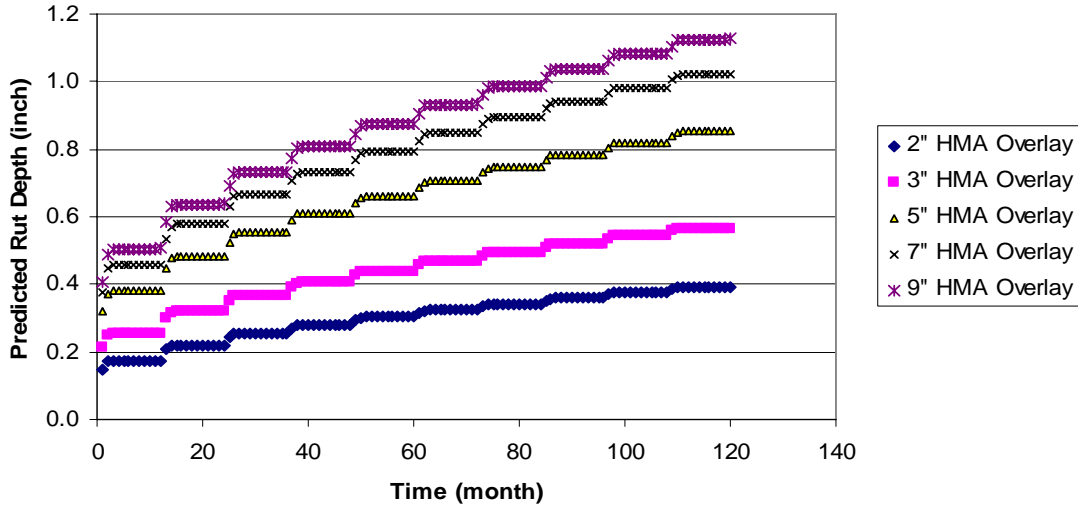
(a) Predicted HMA Overlay Rutting before Thickness Adjustment

HMA Overlay with a PG64-22 Binder over PCC at Dallas District under 10 Million ESALs (20 Years)
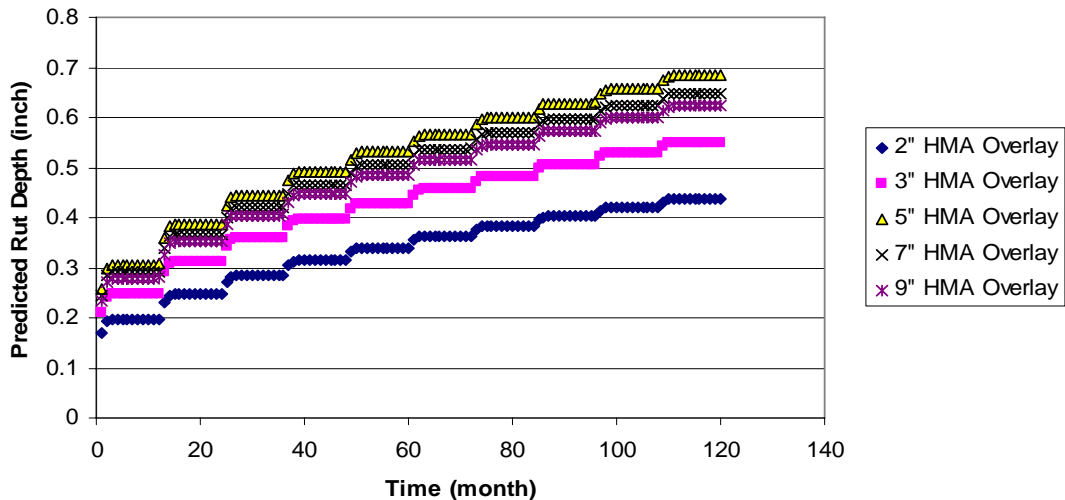
(b) Predicted HMA Overlay Rutting after Thickness Adjustment

Figure 3-10. Rutting Development Comparison before and after Thickness Adjustment.

VERIFICATION OF THE CALIBRATED HMA OVERLAY RUTTING MODEL

It is well known that it is necessary and important to verify the accuracy and reasonableness of the calibrated HMA overlay rutting model using an independent data source. In this study, the NCAT Test Track 2000 rutting data were employed for this verification process. Note that the rutting model was calibrated using the NCAT Test Track 2006 rutting data.

Since the NCAT Test Track 2000 had finished before the Research Project 0-5123 started, neither plant mixes nor raw material were available to this study. After carefully reviewing the literature, some useful information about the NCAT Test Track 2000 was found in one of the NCHRP 9-19 reports: Field Validation of the Simple Performance Test in which the measured rutting data, traffic loading conditions, dynamic modulus test and repeated load test results of several test sections were well documented (78). Three test sections, N02, N12, and N13, were identified for the purpose of rutting model verification. Figure 3-11 shows the dynamic modulus master curves of the three test sections, and Table 3-5 lists the permanent deformation parameters (μ, α) determined from the repeated load test, at 100 ºF. The comparisons between the predicted and the measured rutting development are shown in Figure 3-12. Generally, the predicted rutting matches the measured rutting in the field. Thus, the calibrated HMA overlay rutting model is valid.

NCAT Test Track 2000
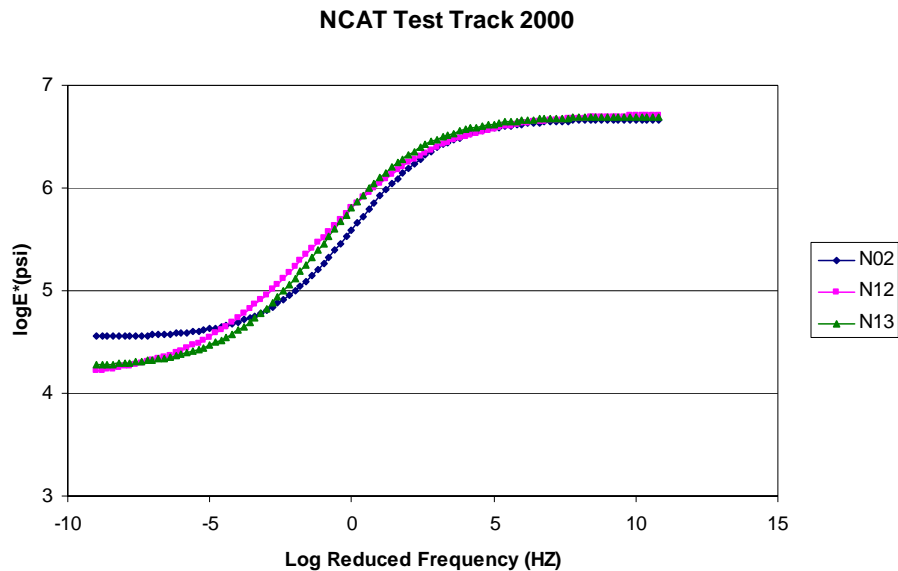
Figure 3-11. Dynamic Modulus Master Curves of Sections N02, N12, and N13.

Table 3-5. Permanent Deformation Properties of Sections N02, N12, and N13 at 100 ºF.

Section	N02	N12	N13
μ	0.478	0.182	0.840
α	0.720	0.548	0.780

51

N02

N12

N13
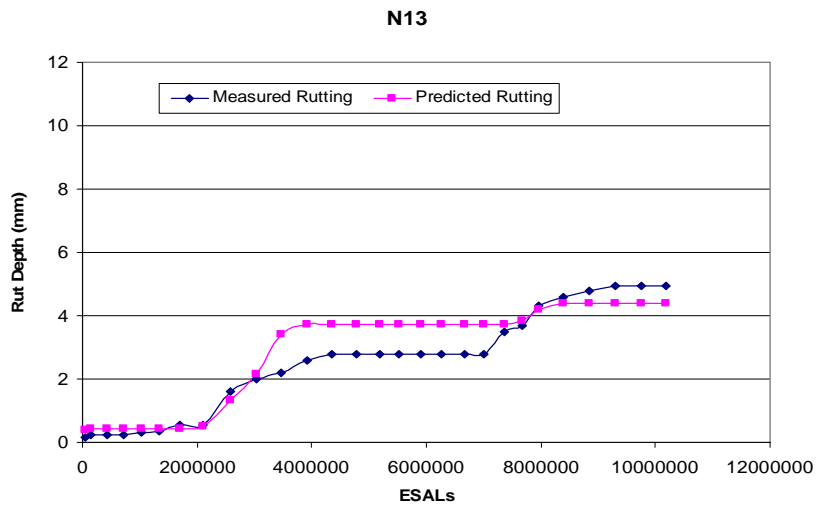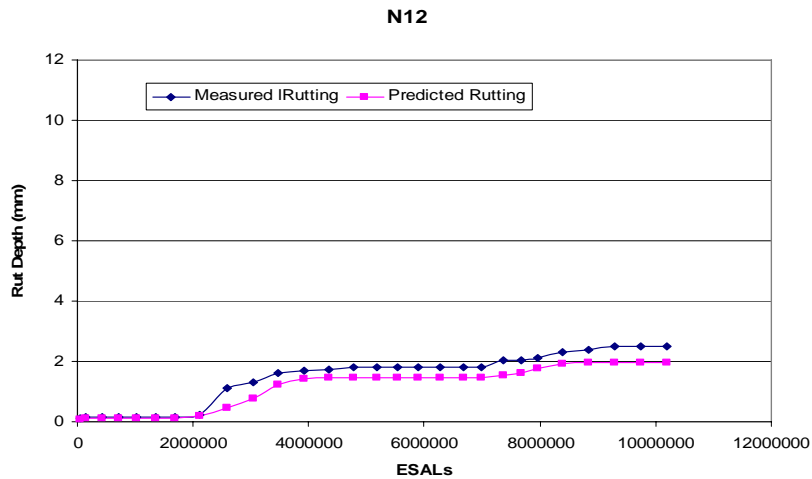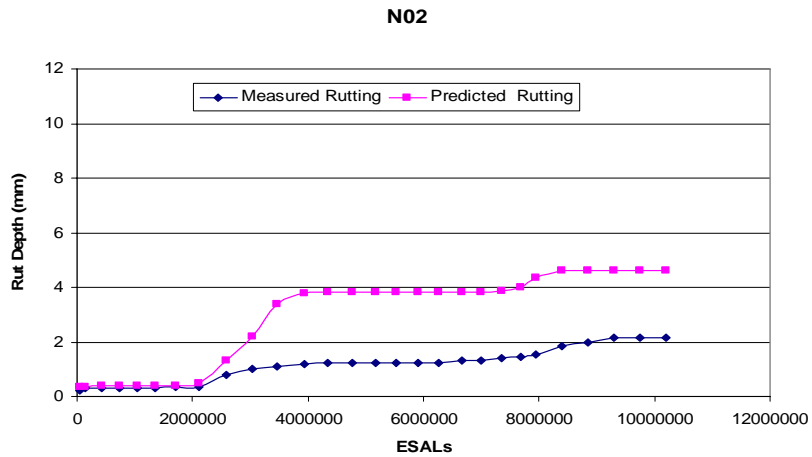
Figure 3-12. Comparisons between the Predicted and the Measured Rutting Development of Sections N02, N12, and N13.

52

SUMMARY AND CONCLUSIONS

This chapter discussed the M-E rutting models for HMA overlay thickness design and analysis. Based on the work presented in this chapter, the following conclusions and recommendations are made.

- After reviewing existing rutting models in the literature, it was found that the well-known VESYS layer rutting model still is a rational choice to model HMA overlay rutting development. The main feature of the VESYS layer rutting model is to characterize layer properties rather than global parameters used in the MEPDG. For each layer, the VESYS rutting model requires rutting parameters: α_i and μ_i. The HMA rutting parameters (α and μ), which are some of the fundamental input parameters required in the proposed M-E rutting model, can be directly determined from the repeated load test. To assist with implementation the default values of rutting parameters α and μ have been provided for typical overlay mixes (such as Type C, D, and SMAs), as presented in the next chapter.

- The proposed HMA overlay rutting model was preliminarily calibrated using 11 test sections of the NCAT Test Track 2006, and the calibrated model was further verified using the rutting data of 3 test sections of the NCAT Test Track 2000. Thus far, satisfactory results have been obtained. However, more field performance data are definitely needed for further model calibration and verification.

Overall, the M-E rutting model proposed in this chapter offers greater promising potential for rationally modeling and accurately predicting the rutting potential of HMA overlays. Although comparable results with field measurements were obtained in this study, further model validation and calibration with more field data, varied traffic load spectrums, different environmental conditions, and different materials (HMA mix types) are still required.

CHAPTER 4

HMA OVERLAY THICKNESS DESIGN AND ANALYSIS SYSTEM AND ASSOCIATED SOFTWARE

INTRODUCTION

The reflective cracking model preliminarily calibrated above has been integrated into an HMA overlay thickness design and analysis system and associated software. This chapter discusses the flowchart of the HMA overlay thickness design and analysis system. Specifically, the HMA overlay thickness design software is presented in detail.

HMA OVERLAY THICKNESS DESIGN AND ANALYSIS SYSTEM

Figure 4-1 shows the flowchart of the HMA overlay thickness design and analysis system in which both the reflective cracking and rutting models were integrated. As shown in Figure 4-1, there are four main components in the HMA overlay design and analysis system: 1) HMA overlay, 2) existing pavement conditions, 3) climatic condition, and 4) traffic loading condition. More detailed description of these four components is provided as follows.

HMA Overlay

Different HMA overlay alternatives have been provided in the design system. For example, the design system allows users to choose either single-layer or double-layer overlay. Also, for each specific layer, users can select different types of mixes, such as Type C and D, SMA-C, SMA-F, CAM, etc.; for each specific mix type, users can choose different binder types, such as a Type D mix with PG76-22 binder or a Type D mix with PG70-22 binder. Therefore, the overlay design system provides users a significant amount of combinations of designing HMA overlays for a specific project.

For each specific overlay mix, the required material properties are dynamic modulus, fracture properties A and n, and permanent deformation properties α and μ. For simplicity and easy application, default values for the required material properties for the most often used overlay mixes have been provided in the design system. Figure 4-2 shows the dynamic modulus master curves of the overlay mixes, and Table 4-1 presents the default fracture properties and permanent deformation properties of the overlay mixes. Additionally, test protocols have also been developed to directly measure these material properties if necessary:

- Dynamic modulus test: AASHTO TP62-03, Standard Method of Test for Determining Dynamic Modulus of Hot-Mix Asphalt Concrete Mixtures;

- Fracture properties: Overlay Test for Fracture Properties A and n, Appendix A; and

- Permanent deformation properties α and μ: VESYS Test Protocol for Asphalt Mixes, Report 0-5798-1.

Traffic loading:
- ESAL
- Load spectrum

Climate effect: EICM

Project level NDT
- GPR
- FWD/RDD

- Layer thickness
- Layer modulus
- Load transfer

Existing pavement structure
- Crack/joint space
- Other properties

Overlay material properties
- Asphalt overlay $(E^*, A, n, \ldots)$

Overlay alternatives
- CAM bottom layer
- Overlay thickness
- Multiple overlays

Pavement geometry and layer materials properties

Pavement "cracking response" analysis
- K_b: Stress intensity factor due to bending load
- K_s: Stress intensity factor due to shearing load
- K_T: Stress intensity factor due to temperature

Pavement "rutting response" analysis
- Overlay deflection (U^+, U^-) calculated from the WesLea Program

Rutting analysis
$$R_D = \sum_{i=1}^{N} f_1(T) f_2(E) f_3(h_{OL}) \int \left(U_i^+ - U_i^-\right) \mu_i N^{-\alpha_i}$$

Crack propagation and reflection cracking analysis
- Daily crack propagation: $\Delta C = k_1 * \Delta N * A(K_b)^n + k_2 * \Delta N * A(K_s)^n + k_3 * A(K_T)^n$
- Damage (D): $D = \Delta C / H_{AC}$
- Reflective cracking rate (RCR): $RCR = 100 / \left(1 + e^{C_1 + \log D}\right)$

Predicted life of overlay pavement

Desired asphalt overlay structure

Outputs:
- Life of overlay pavement
- Overlay performance in terms of reflective cracking and rutting.

Is predicted life ≥required life?

Yes

No

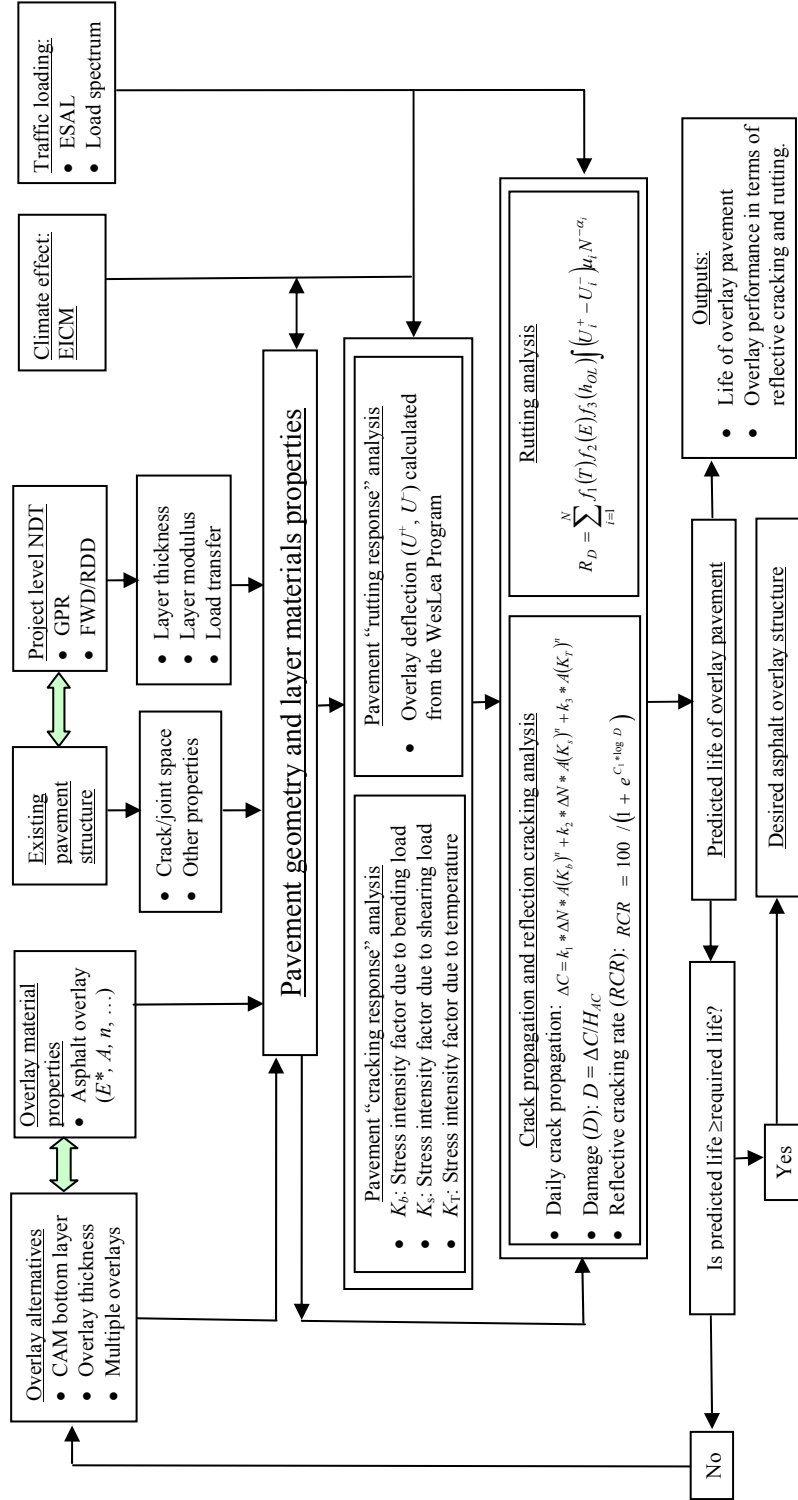**Figure 4-1. Flowchart of the HMA Overlay Thickness Design and Analysis System.**

Type D Mixes

Type C Mixes

SuperPave D Mixes

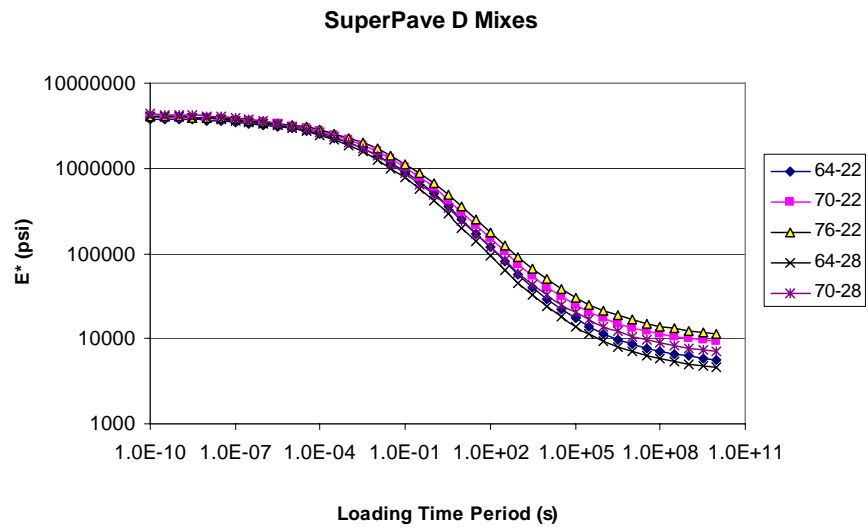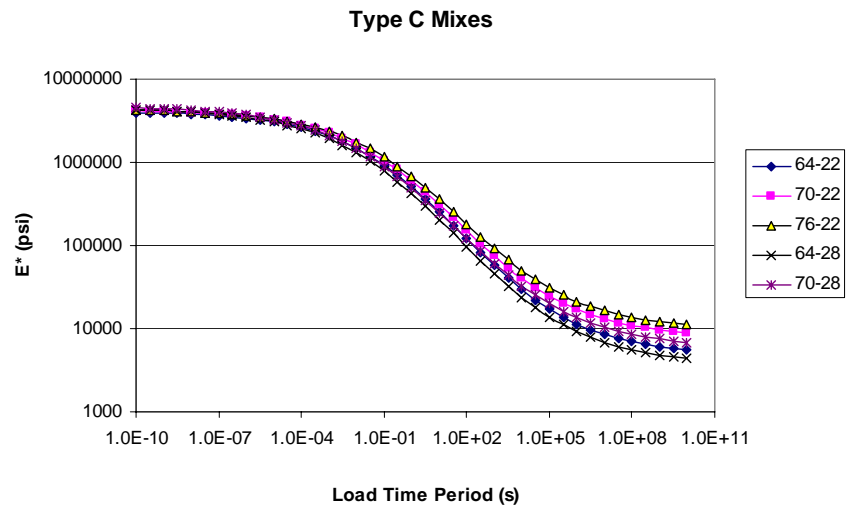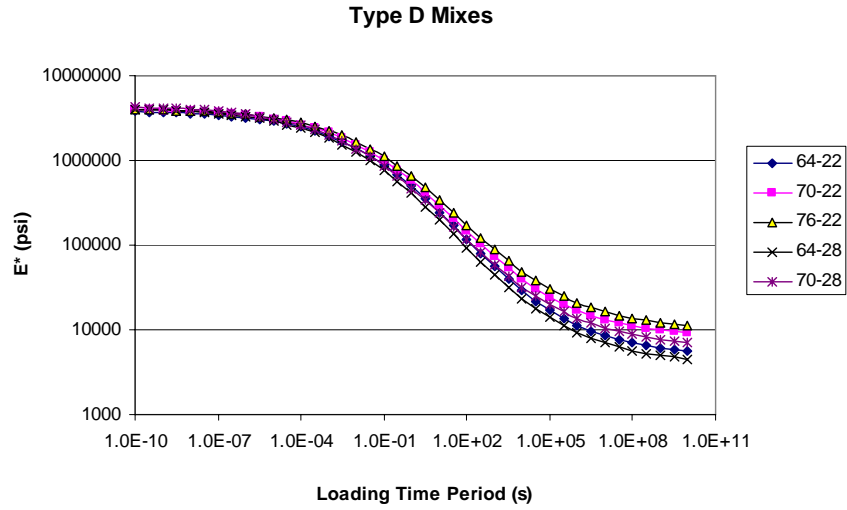**Figure 4-2. Default Dynamic Modulus Master Curves of the Overlay Mixes.**

SuperPave C Mixes
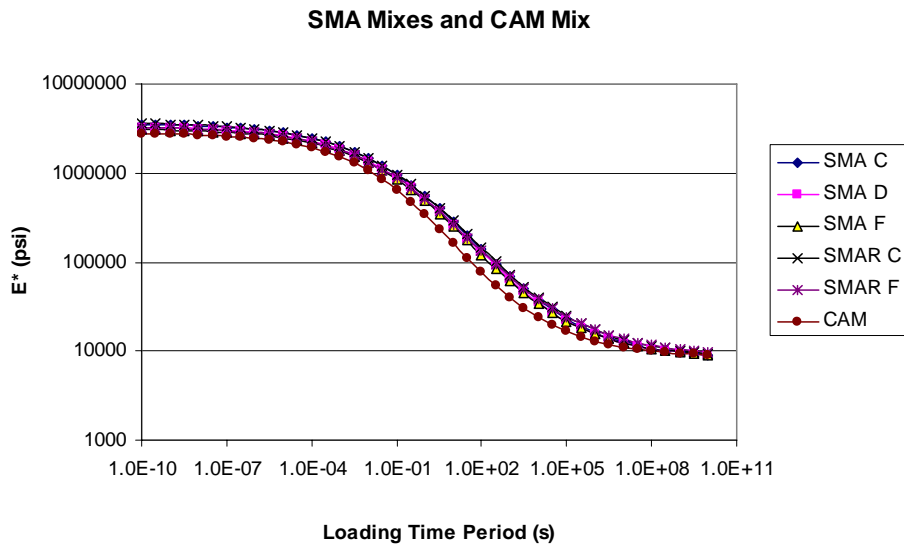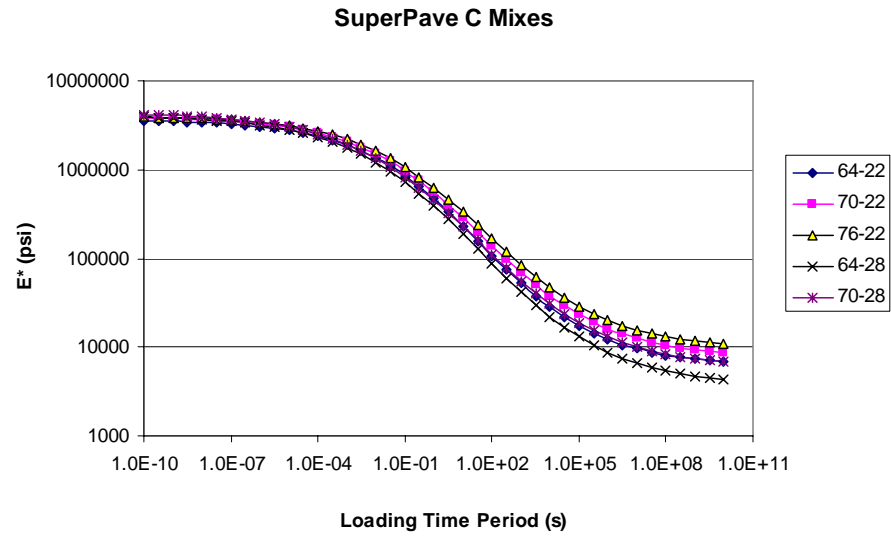

SMA Mixes and CAM Mix

Figure 4-2. Default Dynamic Modulus Master Curves of the Overlay Mixes (Continued).

58

Table 4-1. Default Rutting and Cracking Parameters of the Overlay Mixes.

Mix Type	Binder Type	Rutting parameters		Cracking Parameters	
		α	μ	A	n
Type C	64-22	0.7315	0.7234	2.29E-08	4.1475
	70-22	0.7423	0.7014	2.29E-08	4.1475
	76-22	0.7485	0.6756	2.29E-08	4.1475
	64-28	0.7315	0.7306	2.29E-08	4.1475
	70-28	0.7423	0.6986	2.29E-08	4.1475
Type D	64-22	0.7465	0.8102	2.09E-08	4.3475
	70-22	0.7521	0.7792	2.09E-08	4.3475
	76-22	0.7609	0.7265	2.09E-08	4.3475
	64-28	0.7465	0.8202	2.09E-08	4.3475
	70-28	0.7521	0.7892	2.09E-08	4.3475
SP C	64-22	0.7315	0.7234	2.29E-08	4.1475
	70-22	0.7423	0.7014	2.29E-08	4.1475
	76-22	0.7485	0.6756	2.29E-08	4.1475
	64-28	0.7315	0.7306	2.29E-08	4.1475
	70-28	0.7423	0.6986	2.29E-08	4.1475
SP D	64-22	0.7465	0.8102	2.09E-08	4.3475
	70-22	0.7521	0.7792	2.09E-08	4.3475
	76-22	0.7609	0.7265	2.09E-08	4.3475
	64-28	0.7465	0.8202	2.09E-08	4.3475
	70-28	0.7521	0.7892	2.09E-08	4.3475
SMA C	76-22	0.7106	0.7761	1.06E-08	4.2350
SMA D	76-22	0.7106	0.7856	1.06E-08	4.2350
SMA F	76-22	0.7106	0.8004	1.06E-08	4.2350
SMAR C	76-22	0.7106	0.5406	1.06E-08	4.2350
SMAR F	76-22	0.7106	0.5514	1.06E-08	4.2350
CAM	76-22	0.7670	1.3540	1.55E-08	4.1891

Existing Pavement Conditions

It has been well recognized that existing pavement conditions are very critical to HMA overlay design. To address this issue, guidelines for evaluation of existing pavements for HMA overlay were developed under this research project and published in the Year 2 Report 0-5123-2. In general, both in-situ survey and the non-destructive tests (NDT) are needed for the evaluation. The NDT testing includes the radar for determining the layer thickness of existing pavement

layers, the falling weight deflectometer (FWD) for backcalculating moduli of existing pavement layers and the load transfer at joints or cracks, and the rolling dynamic deflectometer (RDD) for continuously evaluating existing joints for joint concrete pavements.

The required inputs for the existing pavements are layer thickness, layer modulus, joints/crack spacing, load transfer efficiency at joints, and severity level of cracks of existing asphalt pavements.

Climatic Condition

Climatic condition has significant influence on the pavement temperature variations and consequently on both rutting and reflective cracking. The HMA overlay design system employed the enhanced integrated climatic model (EICM) to predict the pavement layer temperature based on weather station data in Texas. The only required input for climatic influence is the closest weather station to the design project. Currently, more than 80 weather station data have been included in the design system.

Traffic Loading

To be consistent to current flexible pavement design program (FPS19W), the traffic loading input in the new overlay design system is the equivalent standard axle load (18 kips). Also, the traffic input is exactly the same as that in the FPS19W program.

HMA OVERLAY THICKNESS DESIGN AND ANALYSIS SOFTWARE

Figure 4-3 shows the main screen and the layout of asphalt overlay design and analysis software. The user first provides the software with the General Information of the project and then inputs in three main categories, Traffic, Climate, and Structure & Material Properties. After all inputs are provided for the design and analysis program, the user chooses to run the analysis. The software now executes the crack propagation and rutting accumulation analysis, and the normal running time is generally less than 4 min. The user can then view input and output summaries created by the program. The program automatically creates a summary of all inputs of the analyzed overlay design project. It also provides a summary of the distress and performance prediction in both tabular and graphical formats. All charts are plotted in Microsoft Excel® and hence can be incorporated into electronic documents and reports.

The following text details the inputs in the order of General Information, Traffic, Climate, and Structure & Material Properties, and output screens of the overlay design software.
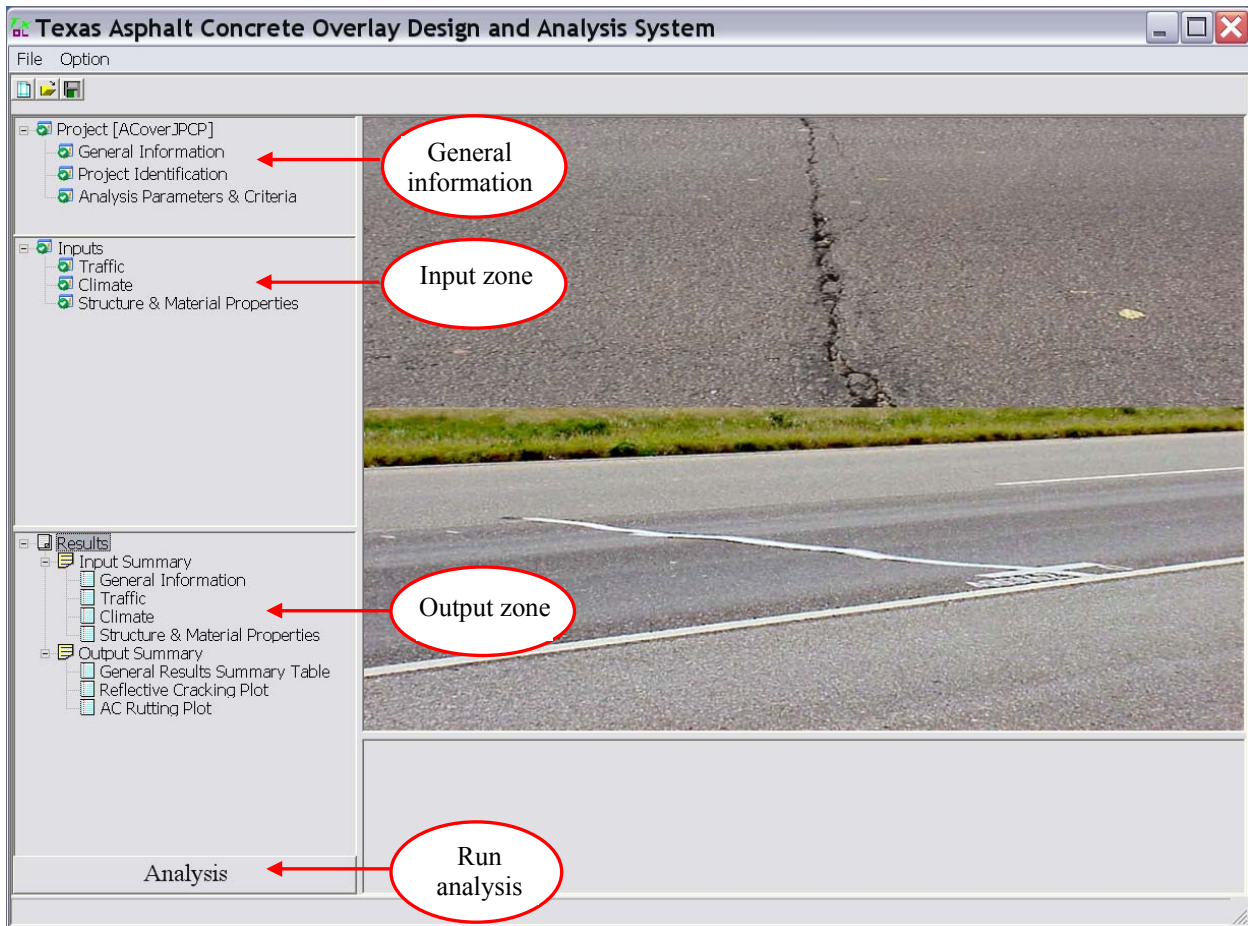
Figure 4-3. Main Screen of Asphalt Overlay Design and Analysis System.

Project General Information Inputs

Project General Information inputs include "General Information," "Project Identification," and "Analysis Parameter & Criteria." The input screens for each one of them are described below.

- "General Information" Input

Figure 4-4 shows the input screen of "General Information" in which two major inputs are "Type of AC Overlay Design" and "Design Life (years)." The user can choose three types of overlay design: 1) AC/AC, 2) AC/JCP, and 3) AC/CRCP. Additionally, the user can also specify the construction information of the overlay as shown in Figure 4-5. Note that the overlay construction information includes the overlay construction month and traffic open month, which has some influence on the EICM program but mainly affects the starting month of the asphalt overlay performance prediction. For instance, if the traffic opening date for an AC overlay was July 2000, the overlay performance prediction will start at July 2000.

Figure 4-4. Input Screen of the General Information.

Figure 4-5. Input Screen of the General Information with the Specified Construction Information.

- "Project Identification" Input

Figure 4-6 shows the input screen of the "Project Identification," which includes District, County, CSJ, Function Class, Date, Reference Mark Format, Reference Mark Begin, and Reference Mark End. The 25 districts in Texas and the counties in each district have been uploaded into the software. The user can choose the specified district and county where the AC overlay project located.
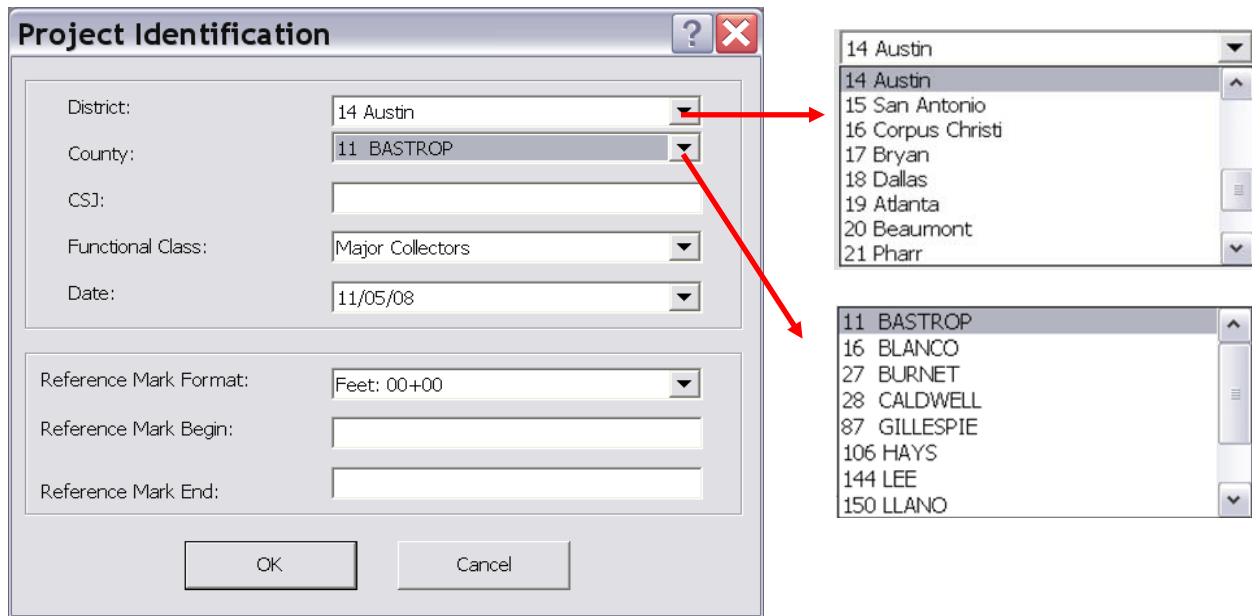
Figure 4-6. Input Screen of the Project Identification.

- "Analysis Parameters and Performance Criteria" Input

Figure 4-7 presents the input screen of the "Analysis Parameters and Performance Criteria." Two criteria included are reflective cracking rate (%) and AC rut depth. The user can specify the asphalt overlay failure criteria. The overlay design software will take the criteria the user specified as the analysis stop criteria. For example, if the user inputs 50 percent for reflective cracking rate and 0.5 inch for AC rutting, and the rutting criterion is met first, the overlay design program will stop analyzing the rutting development when the predicted rutting reaches 0.5 inch deep but continue to calculate the reflective cracking rate development until it reaches 50 percent or the analysis period reaches the pavement design life (see Figure 4-5).

63
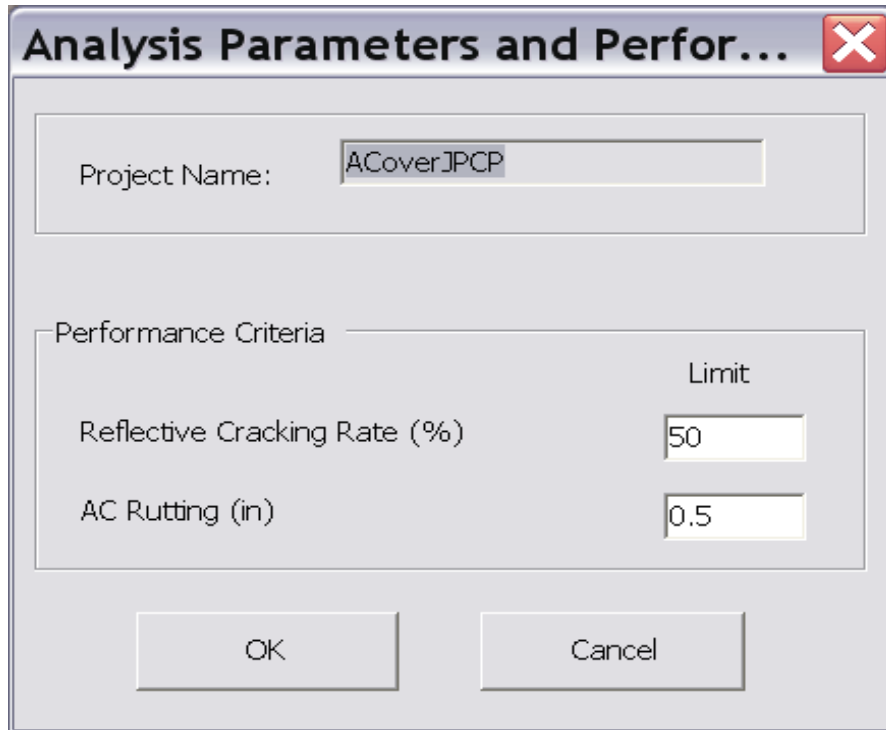
Figure 4-7. Input Screen of the Analysis Parameters and Performance Criteria.

Traffic Input

Figure 4-8 shows the traffic load input that is exactly the same as those in the FPS19W.
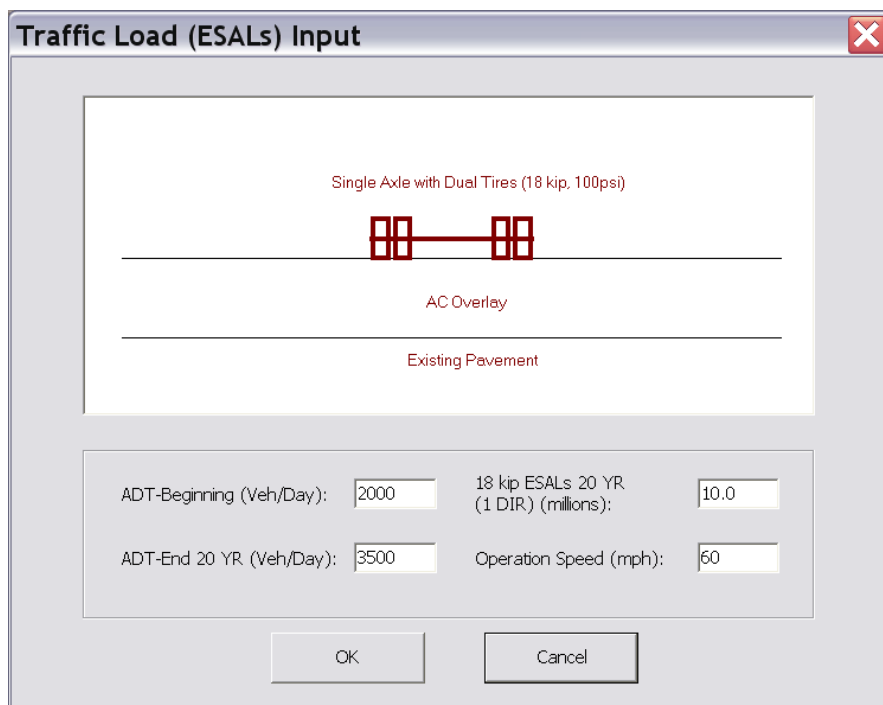
Figure 4-8. Traffic Load Input Screen.

64

Climate Input

Figure 4-9 shows the input screen of climate. The user has two major choices in Figure 4-9: Load Existing Climate Data File or Create New Climatic Data File. Further description for these two choices is provided below.

Figure 4-9. Input Screen of the Climate.

- Load Existing Climate Data File

If the user clicks the button "Load Existing Climate Data File," an opening existing climatic data file screen shown in Figure 4-10 will show up. Then the user can choose the existing climatic data files that have been generated before.
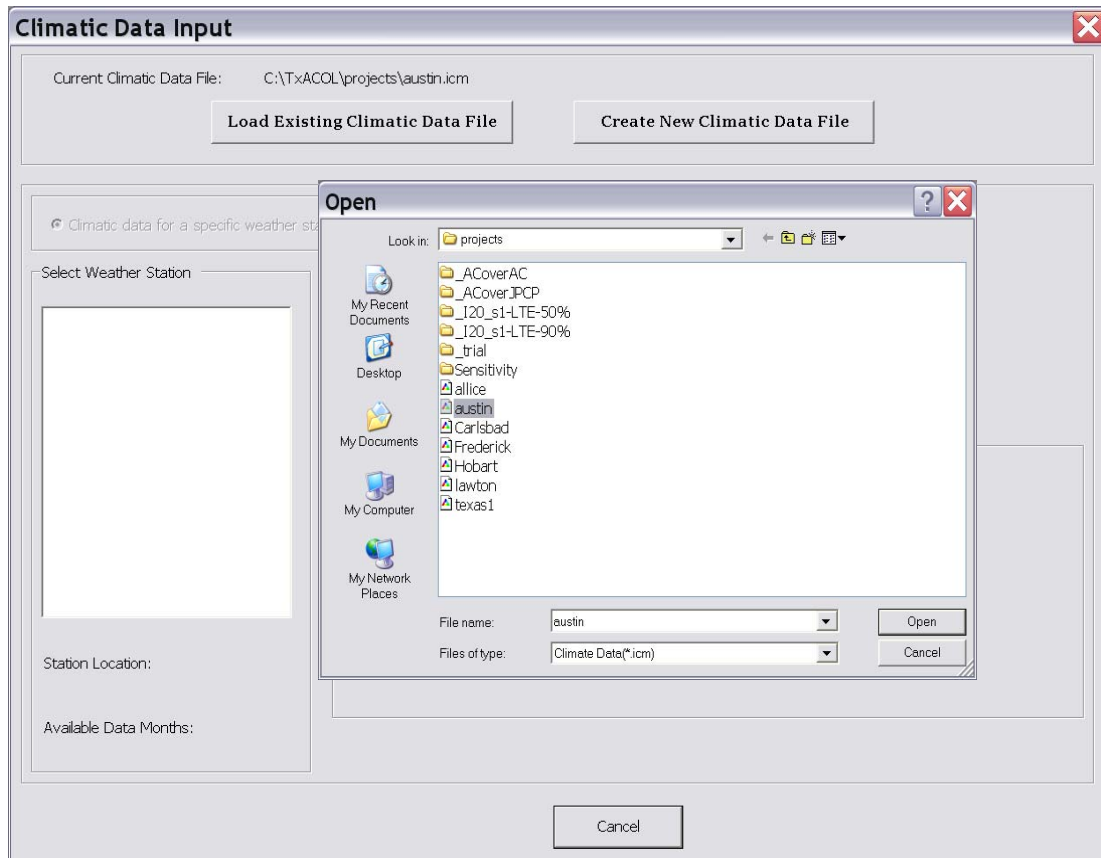
Figure 4-10. Screen of the Load Existing Climatic Data File.

- Create New Climatic Data File

If the user clicks the button "Create New Climatic Data File," the screen will become that shown in Figure 4-11. Then the user can select a specific weather station close to the asphalt overlay project, as shown in Figure 4-11. In case the asphalt overlay project is located in between several weather stations, the user can then use the function of interpolating climatic data for a given location. As shown in Figure 4-12, the closet six weather stations will show up for user selection. After selection, the program will automatically run the EICM program to generate climatic data for this specific overlay project.
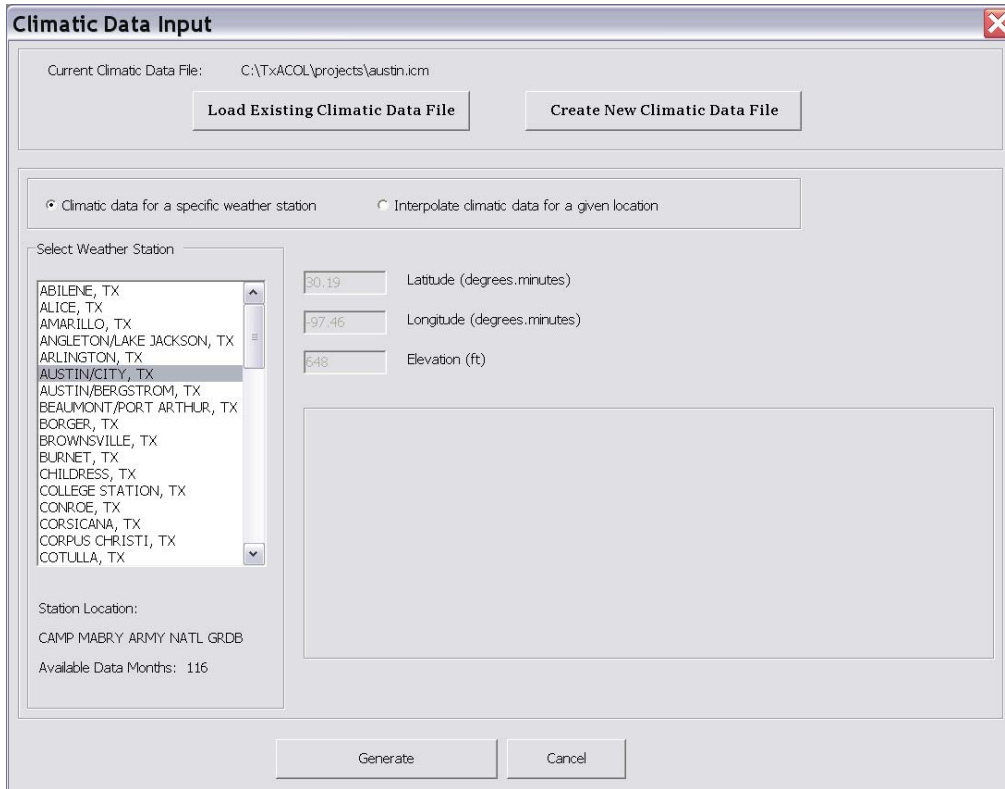
Figure 4-11. Input Screen of the Climatic Data for a Specific Weather Station.
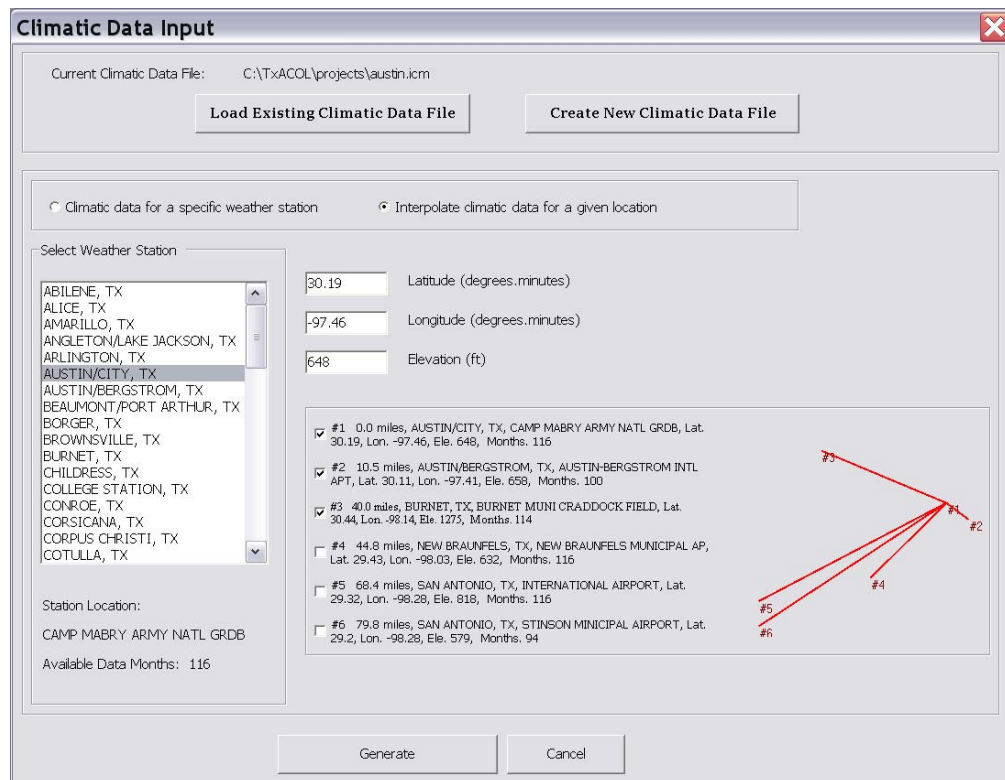
Figure 4-12. Input Screen of the Interpolate Climatic Data for a Given Weather Station.

67

Structure & Material Properties

The input screen of the Structure & Material Properties is shown in Figure 4-13. Overall the asphalt overlay pavement is composed of asphalt overlay, existing concrete layer or existing asphalt layer, existing base layer, and subgrade. For each specific pavement structural layer, different material properties are required. The following text will detail the inputs of the Structure & Material Properties.

Figure 4-13. Main Input Screen of the Structure & Material Properties.

- Asphalt Overlay

First, the user can choose either one single-layer or two-layer overlay. For each overlay, the user needs to select or input the following material information and/or properties:

a. Mix type

The user first needs to select a mix type for each asphalt overlay. The available mix types in the software are Type C, Type D, Superpave C, Superpave D, SMA-C, SMA-D, SMA-F, SMAR-C-I, SMAR-CII, SMAR-F-I, SMAR-F-II, and CAM, as shown in Figure 4-14. Then, the user can click the "Edit" or "OK" button to further describe the asphalt overlay mix that is provided below.

68
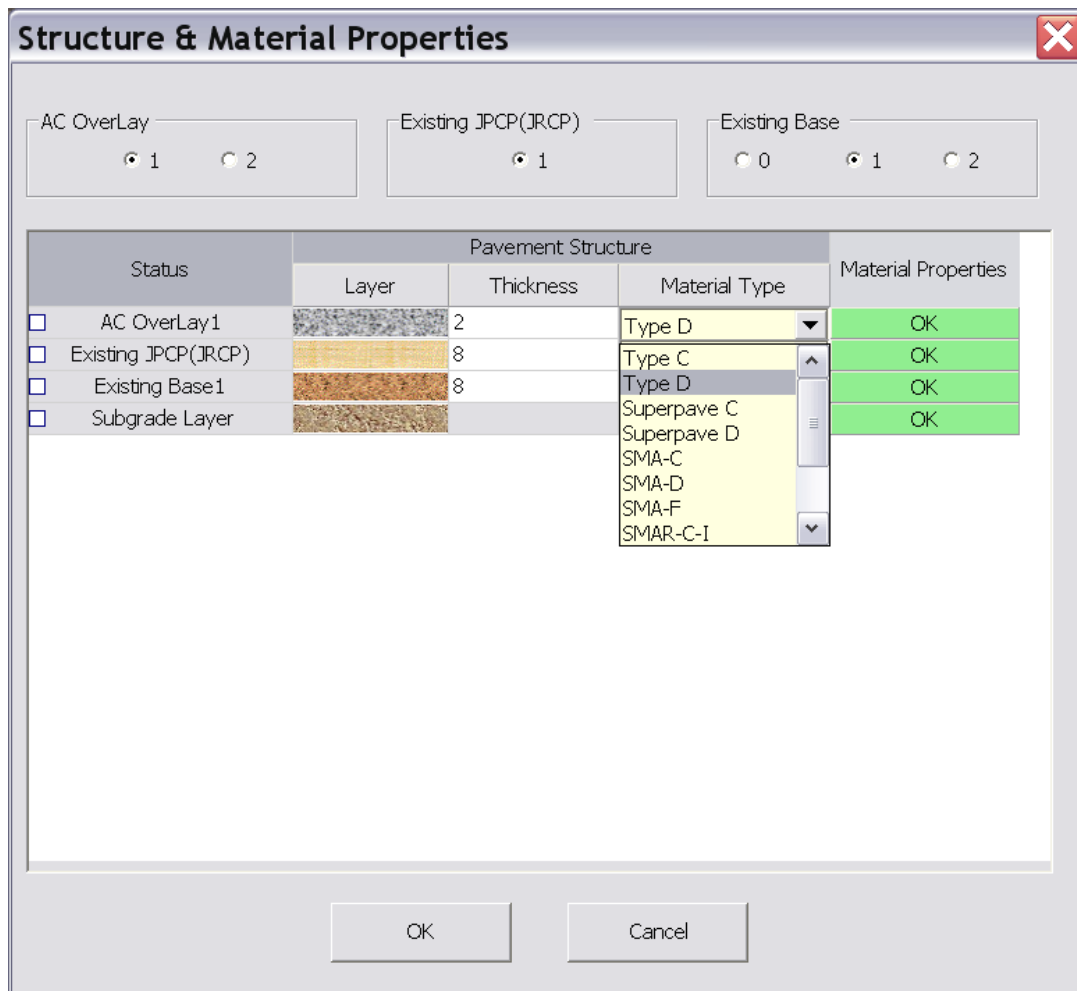
Figure 4-14. Input Screen of Mix Type of Asphalt Overlay.

b. Binder type

Figure 4-15 shows the input screen for further description of the overlay mix when the user clicks either the "OK" button for an existing project or the "Edit" button for a new project. After selecting the mix type, the next step is to determine the binder type being used with the mix. As shown in Figure 4-15, a PG76-22 binder is chosen in this case.

Figure 4-15. Input Screen of Binder Type Selection and Other Material Properties.

In the case of dense-graded mixes (Type C and D), Superpave mixes (Superpave C and D), and CAM mix, the Superpave PG binder grading system is proposed for binder type selection (see Figure 4-15). In case of SMA-C, SMA-D, and SMA-F mixes, the only binder type specified in the current specification is PG76-XX binder, which is presented in Figure 4-16. If the overlay type is an SMAR mix (SMAR-C-I, SMAR-C-II, SMAR-F-I, and SMAR-F-II), the binder type selection is not applicable and unnecessary (see Figure 4-17).

Figure 4-16. Screen of the Binder Type Selection for SMA Mixes.

Figure 4-17. Screen of the Binder Type Selection for SMAR Mixes.

c. Dynamic modulus

Dynamic moduli of asphalt overlay mixes are one of the key inputs of the overlay design and analysis software. Currently, there are two levels of dynamic modulus for each overlay mix: Levels 1 and 3 are provided in the program (see Figures 4-15, 4-16, and 4-17). Level 3 input is default values depending on the mix type and the binder type the user selected above. Note that the default dynamic modulus master curves for the overlay mixes are shown in Figure 4-2. Level 1 input needs to run the dynamic modulus test at five temperatures (14, 40, 70, 100, and 130 °F) and six frequencies (25, 10, 5, 1, 0.5, and 0.1 Hz), as indicated in Figure 4-18. Then the overlay design program will automatically generate the master curve based on the 30 dynamic modulus inputs. Note that Level 2 dynamic modulus input is currently disabled because it was found that the Witczak $E*$ model has a problem when predicting the dynamic modulus at a low temperature. The Level 2 input will be enabled when the correct Witczak $E*$ model is available.

Figure 4-18. Input Screen of the Level 1 Dynamic Modulus.

d. Fracture properties

The fracture properties (A and n) of asphalt overlay mixes are also the key inputs required by the software. For each overlay mix, default A and n values at 77 °F have been provided, as shown in Figure 4-19. Additionally, the user can run the

Overlay Test to determine the fracture properties (*A* and *n*) at different temperatures and then input the measured *A* and *n* values at the specified temperatures (see Figure 4-20).

Figure 4-19. Input Screen of the Fracture Properties of Asphalt Overlay Mixes.

Figure 4-20. Input Screen of the Fracture Properties Measured at Two Temperatures.

e. Rutting properties

Similar to fracture properties, the rutting properties of asphalt overlay mixes are also required. Again, default values for rutting properties are provided for asphalt overlay mixes. One example is shown in Figure 4-21. The user can also run the repeated load test to determine the rutting properties of asphalt overlay mixes and then load them to the program, as shown in Figure 4-22.

73

Figure 4-21. Input Screen of the Rutting Properties of Asphalt Overlay Mixes.

Figure 4-22. Input Screen of the Rutting Properties Measured at Two Temperatures.

f. Thermal coefficient of expansion

Another input parameter required is the thermal coefficient of expansion of asphalt overlay concrete. This input parameter has some influence on the thermal stress and consequently thermal related reflective cracking. Currently, default values of the thermal coefficient of expansion have been provided for the asphalt overlay mixes in the program.

74

- **Existing JPCP (JRCP) and CRCP**

The input screens for JPCP (JRCP) and CRCP are very similar, as shown in Figure 4-23. The required inputs are thermal coefficient of expansion, joint/crack spacing, modulus of concrete slab, and load transfer efficiency at joints/cracks.
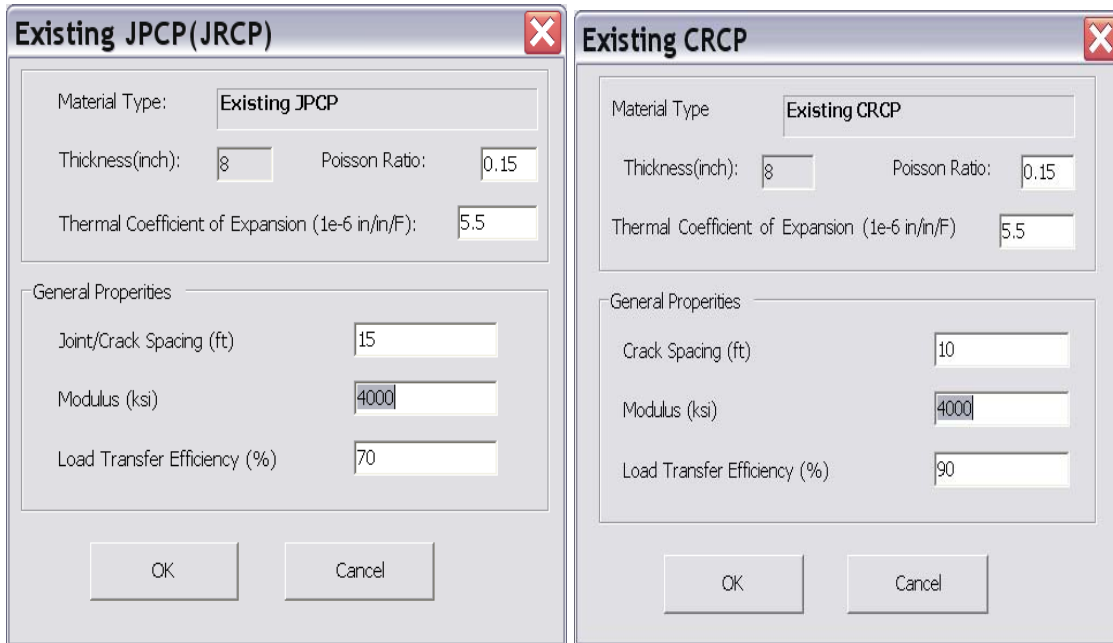
Figure 4-23. Input Screen of the Existing JPCP (JRCP) and CRCP.

- **Existing AC**

The input screen of the existing asphalt layer is shown in Figure 4-24. It can be seen that there are four types of input information required for the existing asphalt pavement: 1) thermal coefficient of expansion, 2) cracking pattern/type (alligator, longitudinal, transverse, and block cracking), 3) crack severity level (low, medium, and high), and 4) modulus. Additionally, for the transverse cracking, the crack spacing is also needed. As indicated in Figure 4-24, the modulus of existing asphalt layer is backcalculated from the FWD data, so that it is very important to evaluate the pavement structural conditions using the FWD before attempting the asphalt overlay thickness design.

Figure 4-24. Input Screen of the Existing Asphalt Layer.

- **Existing Base**

First, the user can choose the existing base layer to be none, single layer, or two layers. The base layer material can be granular base, stabilized base, or simply stabilized subgrade, as displayed in Figure 4-25.

Figure 4-25. Existing Base Type Selection Screen.

The input required for the granular base material is shown in Figure 4-26. Two levels of modulus inputs are provided in the software. For Level 2 modulus input, a typical design value is assigned to the granular base material without considering the seasonal (or monthly) variation of the modulus. Different from Level 2 input, Level 1 input requires monthly modulus of the granular base material. Again, it is recommended to conduct the FWD testing and backcalculate the modulus of the existing base layer.
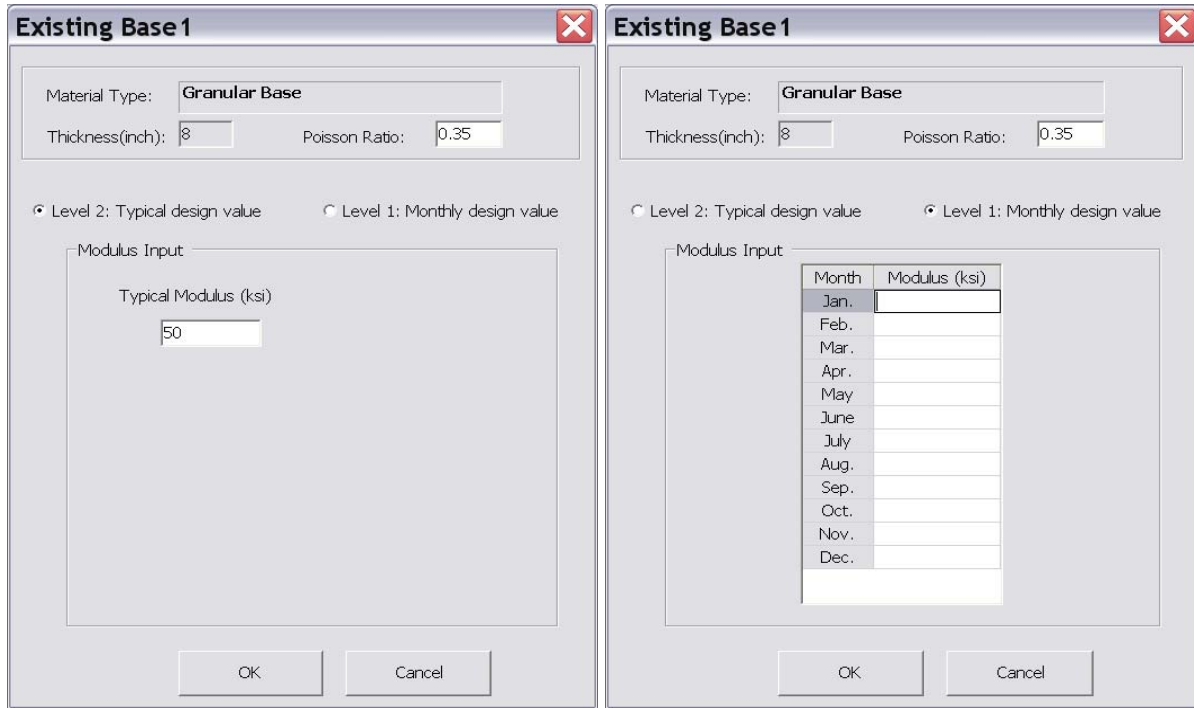
Figure 4-26. Input Screens of the Existing Granular Base Material.

In the case of a stabilized base or subgrade, the required input is simply modulus value of the stabilized base or subgrade, as displayed in Figure 4-27.
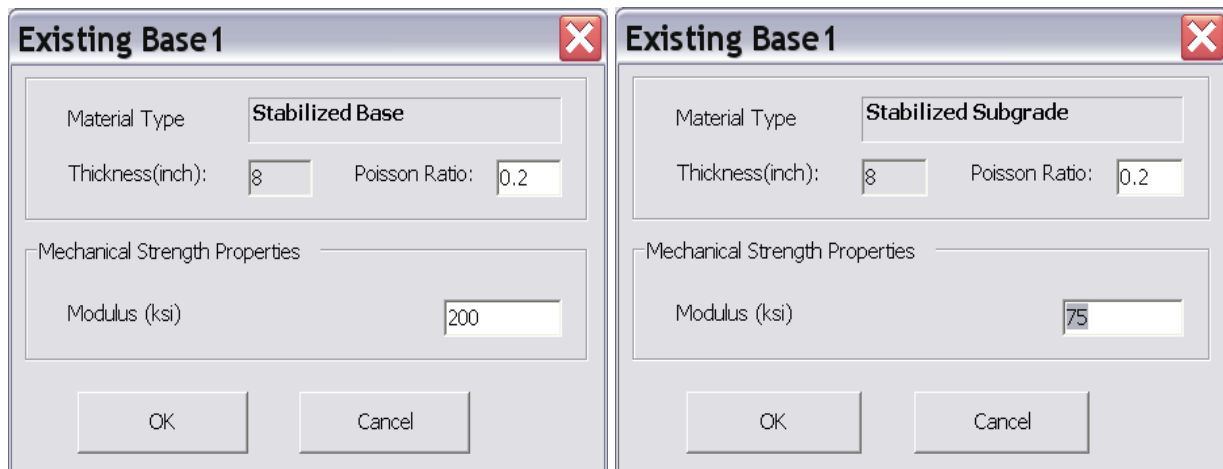
Figure 4-27. Input Screen of the Existing Stabilized Base/Subgrade.

77

- **Subgrade**

As presented in Figure 4-28, the input for Subgrade is very close to that of the granular base material.
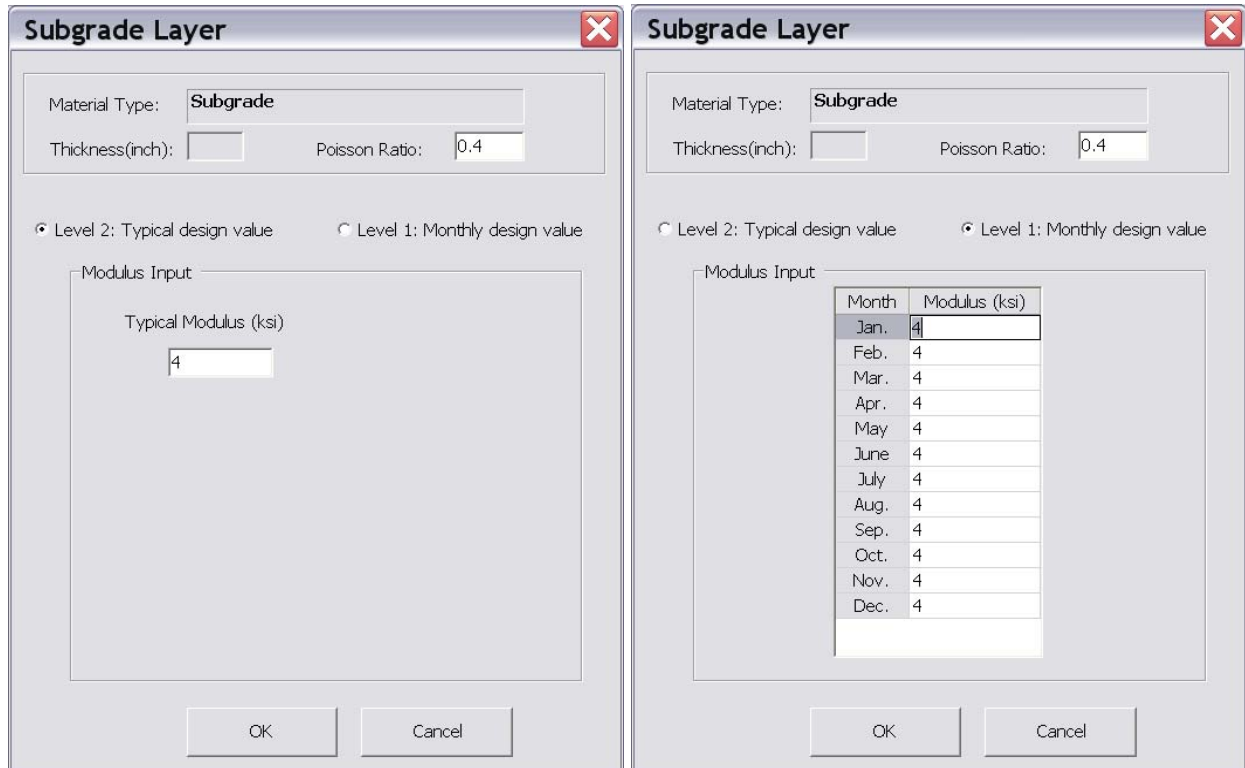
Figure 4-28. Input Screen for Subgrade Layer.

Run and Analysis Results Output

After finishing the program inputs, click the "Analysis" button (see Figure 4-3) to run the program and predict the performance of the asphalt overlay project. Figure 4-29 shows the main screen of the software after successfully running the program. As seen in Figure 4-29, the outputs of the analysis results include the input summary and output summary. An example of the input summary includes General Information, Traffic, Climate, and Structure & Material Properties is presented in Figure 4-30. The outputs of the overlay design program composed of General Results Summary Table, Reflective Cracking Plot, and Rutting Plot are shown in Figures 4-31, 4-32, and 4-33, respectively.
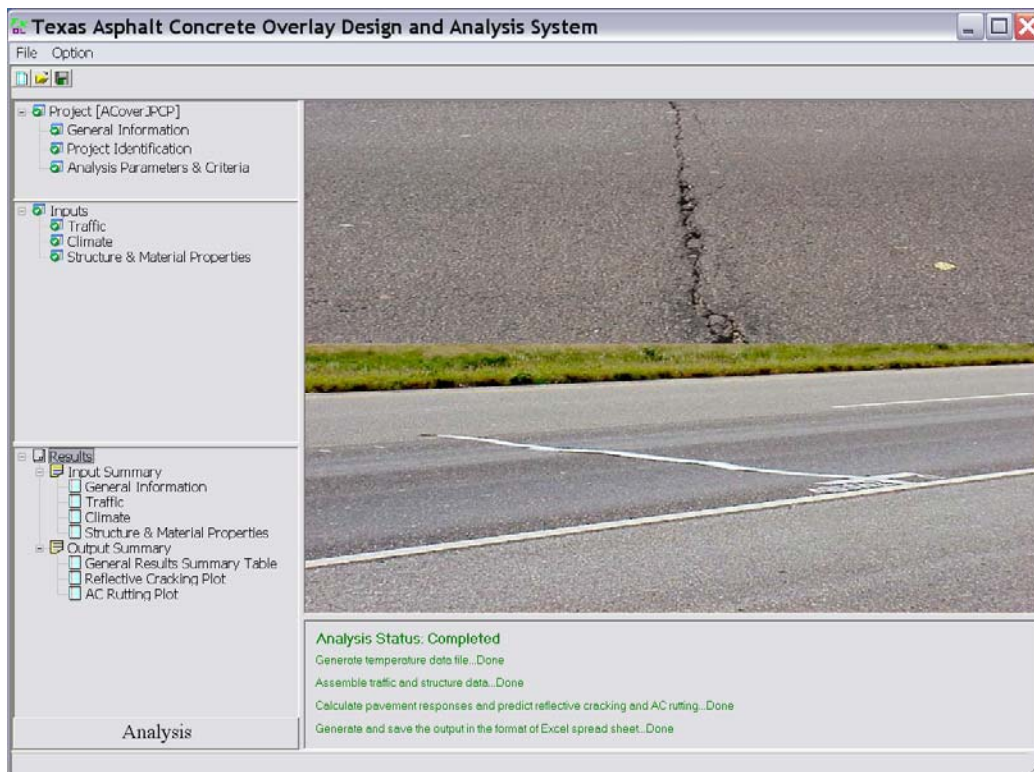
Figure 4-29. Main Output Screen of the Overlay Design and Analysis Program.

Figure 4-30. Input Summary Table.

Figure 4-31. General Output Results Summary Table.
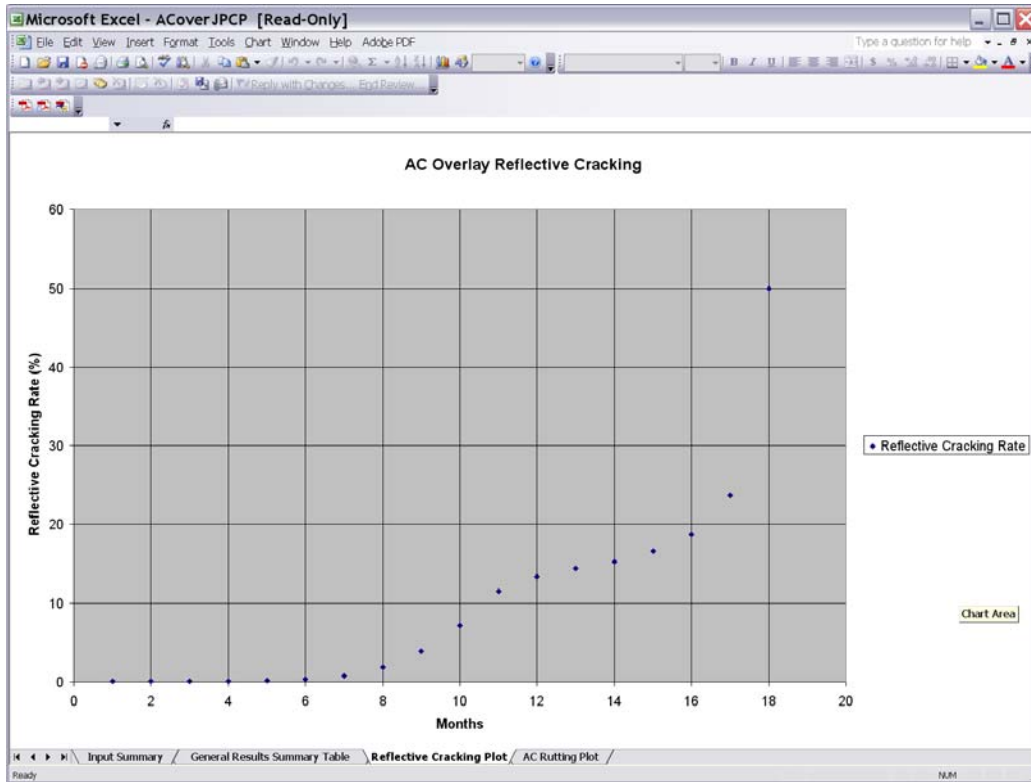
Figure 4-32. Reflective Cracking Plot.
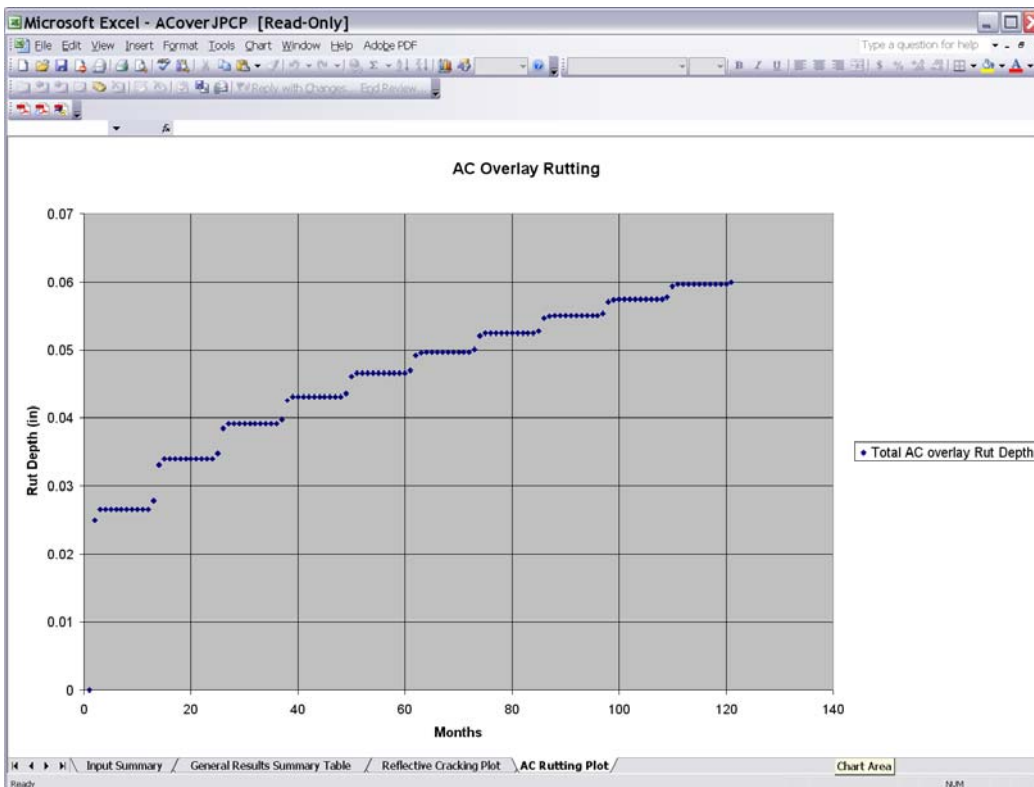
Figure 4-33. Rutting Plot.

81

SUMMARY AND CONCLUSIONS

This chapter describes the asphalt overlay design and analysis system and associated software in which the calibrated reflective cracking and rutting models discussed in previous chapters are integrated. The main feathers of the asphalt overlay design and analysis system include:

- Traffic input is compatible to the current flexible pavement design software, FPS19W.

- Pavement temperature is automatically predicted from the EICM model.

- Two levels of inputs of material properties are required. Specifically, default input values are provided for asphalt overlay mixes. Additionally, if Level 1 inputs are preferred, a series of lab test procedures were recommended or developed.

- The program automatically creates a summary of all inputs of the asphalt overlay design project. It also provides a summary of the distress and performance prediction in both tabular and graphical formats. All charts are plotted in Microsoft Excel and hence can be incorporated into electronic documents and reports.

CHAPTER 5

SENSITIVITY ANALYSIS OF THE ASPHALT OVERLAY DESIGN AND ANALYSIS SYSTEM

INTRODUCTION

The asphalt overlay design and analysis system and related software developed previously provide methodologies for the analysis and performance prediction of asphalt overlays over existing flexible and rigid pavements. The performance predicted by these methodologies (in terms of distresses such as reflective cracking and rutting) for the anticipated climatic and traffic conditions depends on the values of input parameters that characterize asphalt overlay and existing pavement materials, layers, design features, and condition. However, these input parameter values are expected to differ to varying degrees and, therefore, the predicted performance may also vary to some degree depending on the input parameter values. Thus, it is necessary to determine the degree of sensitivity of the performance (in terms of reflective cracking and rutting) predicted by the asphalt overlay design and analysis program relative to input parameter values. This information will help identify, for specific climatic regions and traffic conditions, the input parameters that appear to substantially influence predicted performance. In this manner, users can focus efforts on those input parameters that will greatly influence the asphalt overlay design. This chapter will conduct the sensitivity analysis and identify the significantly influential input parameters affecting the asphalt overlay performance in terms of reflective cracking and rutting.

SENSITIVITY ANALYSIS ON REFLECTIVE CRACKING AND RUTTING OF ASPHALT OVERLAY

As noted above, the objective of the sensitivity analysis is to investigate how the reflective cracking prediction of an asphalt overlay is influenced by changes in magnitude of several key input variables. To do so, the asphalt overlay design and analysis program was run using several factorial combinations of the input parameters. In general, the sensitivity study of reflective cracking was not intended to cover a complete full factorial matrix of all parameters. Rather, the intent was to investigate the effect of varying one parameter at a time, while keeping as many of the other variables as constant input parameters.

Design Parameters and Pavement Structure

To study the effect of the desired sensitivity of input parameters on reflective cracking, the key input parameters were usually selected from one of three different levels of the parameter under study. In certain special cases, a fourth or fifth level was employed to ensure that an adequate range of the variable can be evaluated. In general, most of the program runs were conducted using the "medium" inputs, while varying the key parameter being investigated. The key input parameters and associated input values used in this study are listed below:

- Influence of traffic (ESALs 20 YR, millions): 3, 5, **10**, 30;

- Influence of climate: Amarillo (cold), **Austin** (intermediate), McAllen (hot);

- Influence of asphalt overlay thickness (inch): 1.5, **3**, 5, 6, 9;

- Influence of mix type: Type C, **Type D**, SMA D, SMA C;

- Influence of binder type (or mix stiffness): PG64-22, PG70-22, **PG76-22**;

- Influence of thermal coefficient of expansion of the asphalt overlay (10^{-6} in/in/°F): 10, **13.5**, 17;

- In case of AC/JPCP:

  a. Influence of existing JPCP slab modulus (ksi): 3000, **4000**, 5000;

  b. Influence of existing JPCP slab thickness (inch): 8, **10**, 12;

  c. Influence of the load transfer efficiency at joints/cracks: 30, 50, **70**, 90;

  d. Influence of thermal coefficient of expansion of existing JPCP (10^{-6} in/in/°F): 4.0, **5.5**, 7.0;

  e. Influence of joints/cracking spacing of existing JPCP (ft): 5, **15**, 25;

  f. Influence of existing base layer modulus (ksi): 100, **300**, 500;

  g. Influence of existing base layer thickness (inch): **4**, 6, 8;

- In case of AC/AC:

  a. Influence of existing asphalt layer modulus (ksi): 200, **500**, 800;

  b. Influence of existing asphalt layer thickness (inch): 2, 4, **6**, 8;

  c. Influence of the severity level of existing cracks: low, **medium**, high;

  d. Influence of thermal coefficient of expansion of existing asphalt layer (10^{-6} in/in/°F): 10, **13.5**, 17;

  e. Influence of transverse cracking spacing of existing asphalt pavement (ft): 5, **15**, 25;

  f. Influence of existing base layer modulus (ksi): 20, **50**, 100;

  g. Influence of existing base layer thickness (inch): 4, **6**, 8;

- Influence of the modulus of existing subgrade (ksi): 5, **8**, 15.

As one example, Figure 5-1 shows the basic (or "medium" bolded above) pavement structure used in the sensitivity study for AC/JPCP pavements that are under 10 million ESALs of traffic loading within a 20-year design period with a climate of Austin, Texas. Similar pavement structures with 10 million ESALs of traffic loading within a 20-year design period with a climate of Austin, Texas were used for sensitivity analysis on AC/AC pavements. Detailed sensitivity analysis results are presented next.

Climate: Austin, Texas ↓↓↓↓↓↓↓↓↓ 10 million ESALs, 20 YR

3" Asphalt Overlay, Type D, PG76-22 binder

| 8" PCC, 15 ft slab | E=4000 ksi, LTE=70 % |

4" asphalt layer, E=300 ksi

Subgrade, E=8 ksi
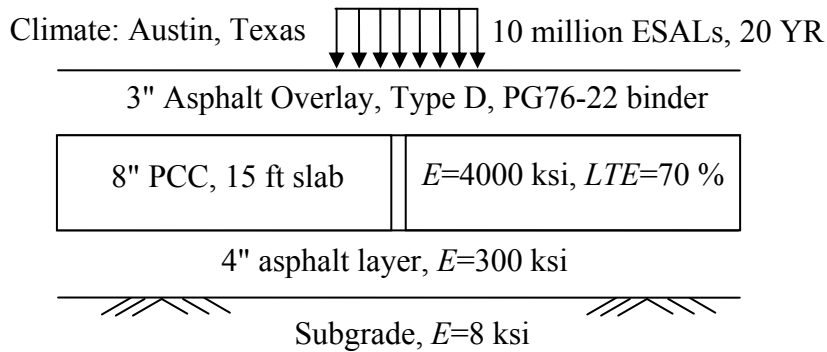
Figure 5-1. Basic AC/JPCP Pavement Structure for Sensitivity Analysis.

Sensitivity Analysis on Reflective Cracking of Asphalt Overlay

- In case of AC/JPCP pavements:

A total of 34 asphalt overlay cases have been run, and the influences of the 14 input parameters listed previously on reflective cracking of asphalt overlay are shown in Figures 5-2 to 5-15. It is clear that the influence of those 14 input parameters can be divided into three categories: significant, minor, and tiny or none. These three categories and associated input parameters are listed below:

    a. Significant input parameters: 1) traffic loading level, 2) climate, 3) asphalt overlay thickness, 4) load transfer efficiency, 5) asphalt overlay mix type, and 6) existing base layer modulus;

    b. Intermediate influential parameters: 1) asphalt binder type, 2) PCC slab thickness, 3) joints/crack spacing, and 4) thermal coefficient of expansion of PCC slab; and

    c. Minor influential parameters: 1) thermal coefficient of expansion of asphalt overlay, 2) existing PCC slab modulus, 4) existing base layer thickness, and 5) subgrade modulus.

Dividing the relevance of input parameters into three categories is beneficial in evaluating an asphalt overlay thickness design. It is apparent that the six significant input parameters must be considered when designing an asphalt overlay. Then the intermediate influential parameters should be taken into account if possible. Finally, the minor influential parameters can be ignored for asphalt overlay design in terms of reflective cracking.

Specifically, asphalt overlay life in terms of reflective cracking is not linearly proportional to asphalt overlay thickness, as clearly shown in Figure 5-4. In the case shown in Figure 5-4, a 4 inch asphalt overlay has more than two times the life of a 3 inch asphalt overlay. This finding means that asphalt overlays must have a minimum, cost-effective thickness in order to have longer life, and below such a minimum asphalt overlay, the reflective cracking will quickly show up; such a design is not economical.

Another interesting finding regarding the load transfer efficiency is shown in Figure 5-8. Figure 5-8 clearly indicates the importance of having good load transfer efficiency at joints/cracks. As seen in Figure 5-8, the reflective cracking will quickly occur when the load transfer efficiency is below 70 percent. However, the asphalt overlay will have no reflective cracking when the load transfer efficiency is 90 percent. This observation indicates that it is

better to have an overlay before the PCC pavements deteriorate very badly; it is important to treat the bad joints/cracks where the load transfer efficiency is below 70 percent before the asphalt overlay.

Influence of Traffic Level (ESALs) on Reflective Cracking
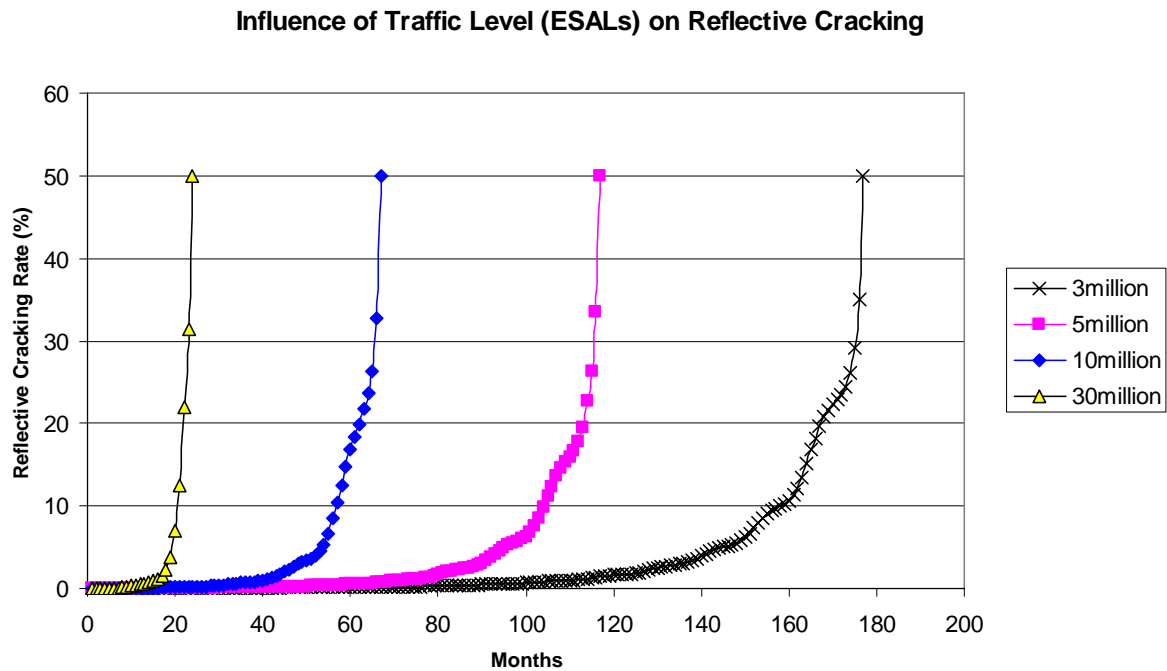
Figure 5-2. AC/JPCP: Influence of Traffic Level on Reflective Cracking.

Influence of Climate on Reflective Cracking
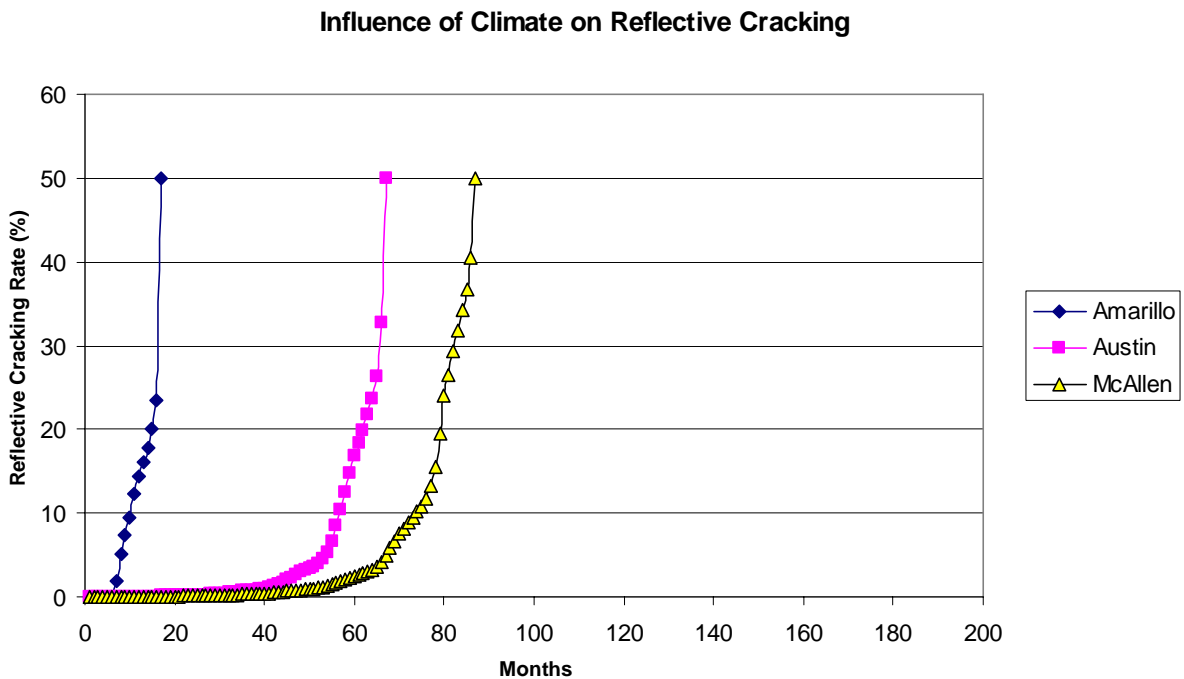
Figure 5-3. AC/JPCP: Influence of Climate on Reflective Cracking.

86

Influence of Overlay Thickness on Reflective Cracking
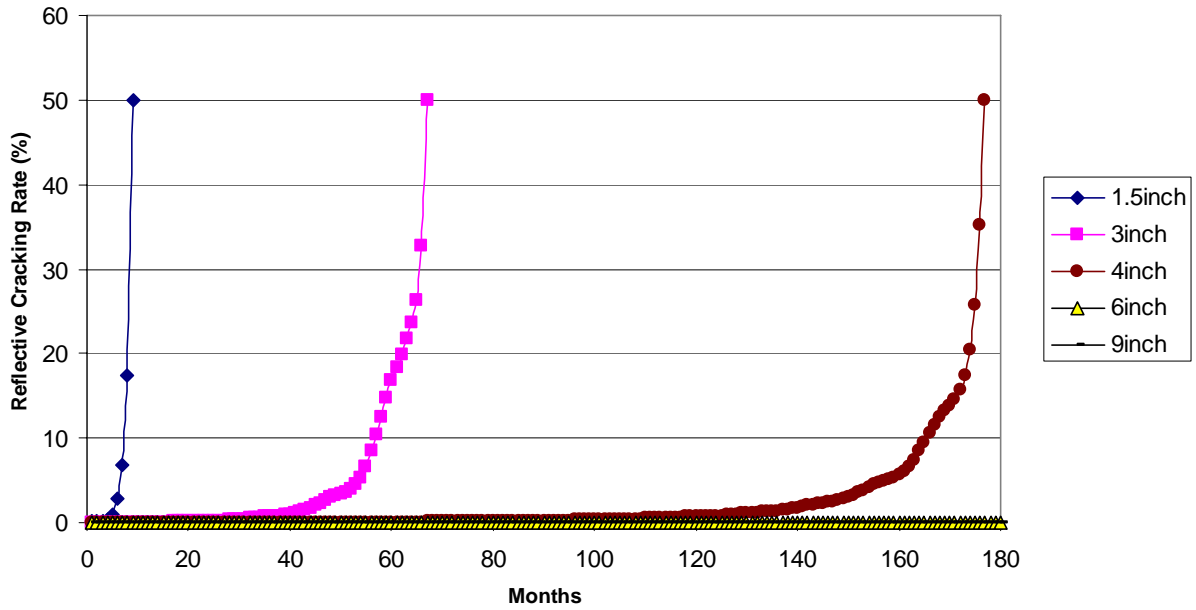
Figure 5-4. AC/JPCP: Influence of Asphalt Overlay Thickness on Reflective Cracking.

Influence of Overlay Mix Type on Reflective Cracking
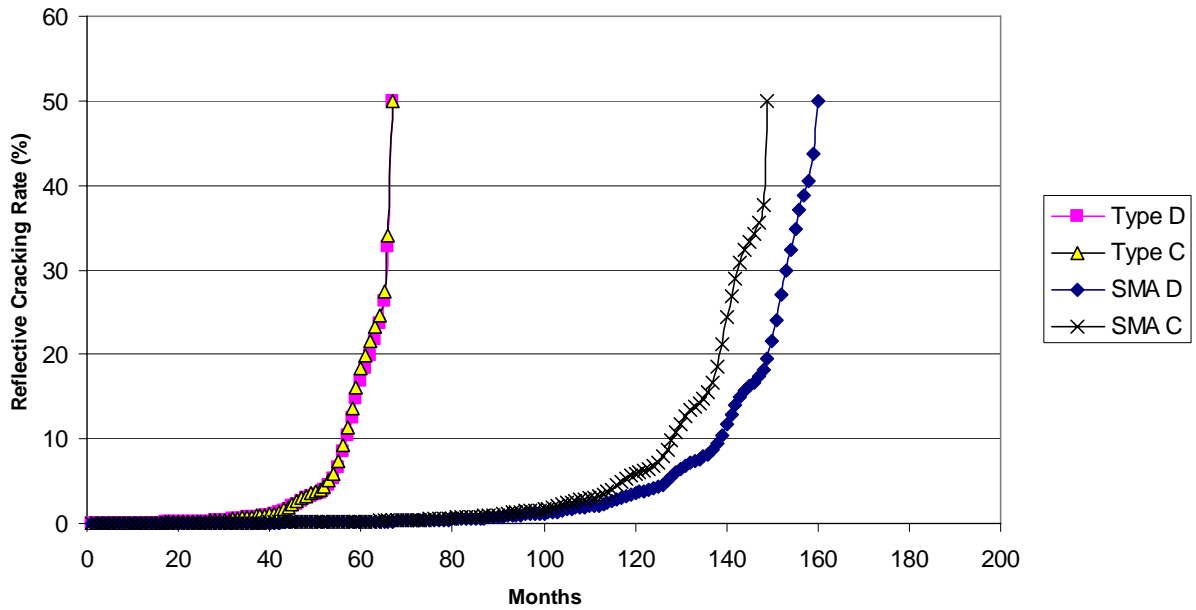
Figure 5-5. AC/JPCP: Influence of Mix Type on Reflective Cracking.

Influence of Binder Type on Reflective Cracking
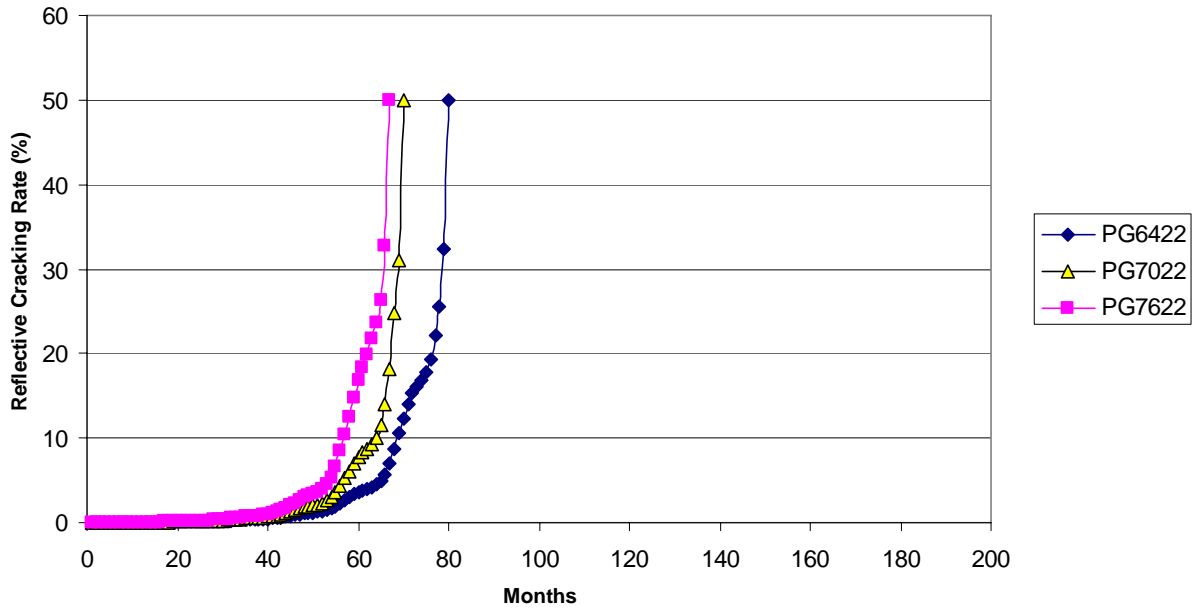
Figure 5-6. AC/JPCP: Influence of Asphalt Binder Type on Reflective Cracking.

Influence of Aspalt Overlay Thermal Coefficient of Expansion on Reflective Cracking
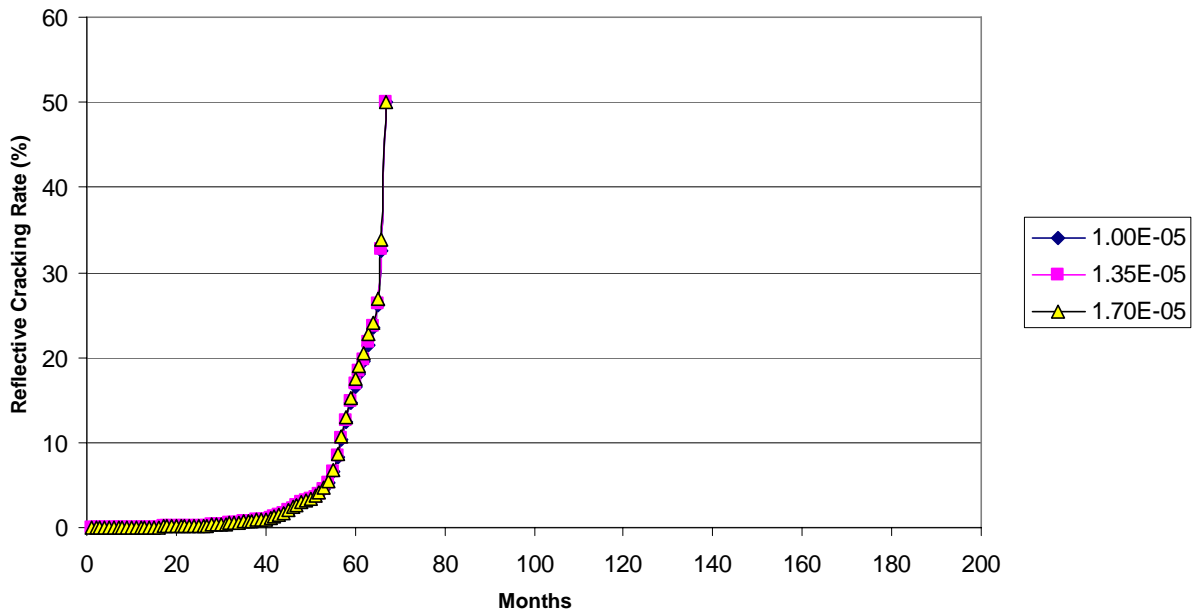
Figure 5-7. AC/JPCP: Influence of Asphalt Overlay Thermal Coefficient of Expansion on Reflective Cracking.

Influence of LTE on Reflective Cracking
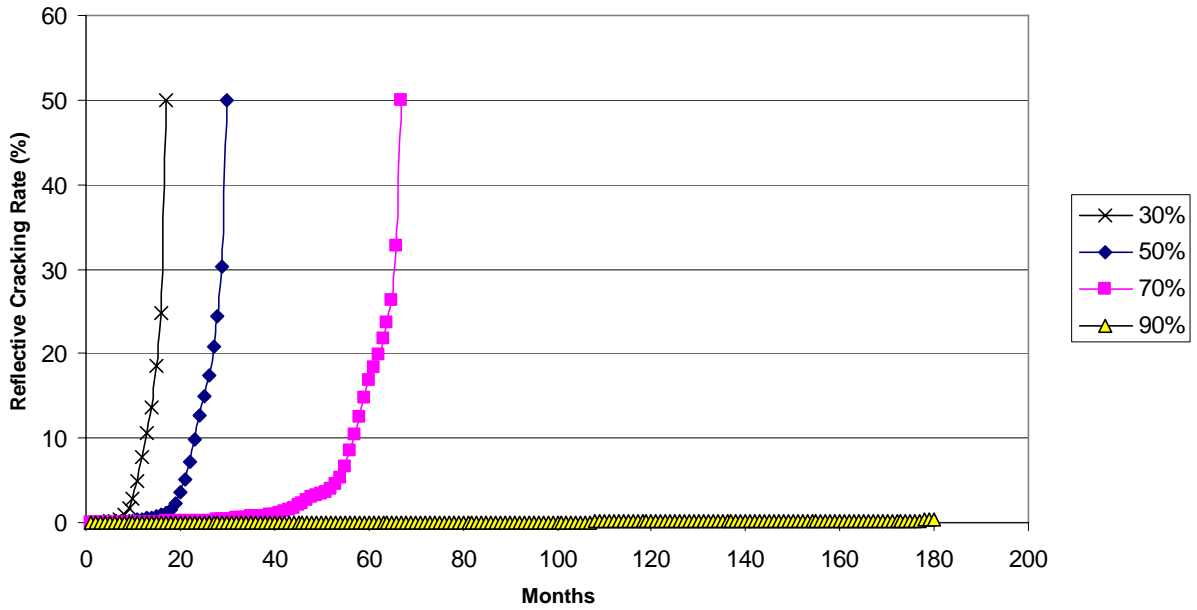
Figure 5-8. AC/JPCP: Influence of Load Transfer Efficiency at Joints/Crack on Reflective Cracking.

Influence of PCC Modulus on Reflective Cracking
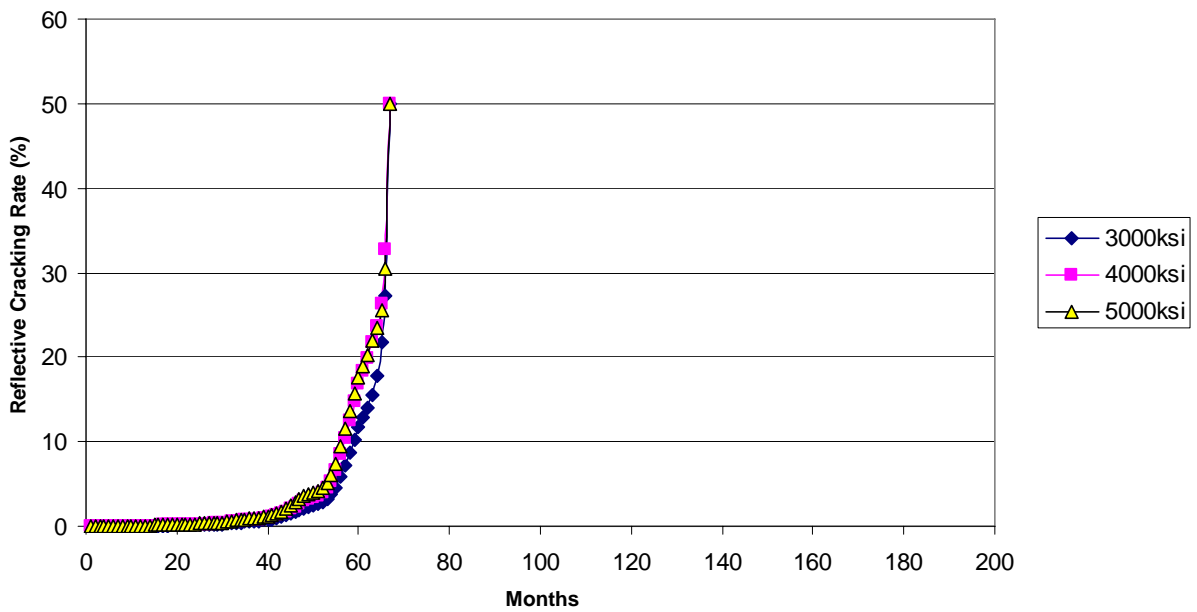
Figure 5-9. AC/JPCP: Influence of Existing PCC Slab Modulus on Reflective Cracking.
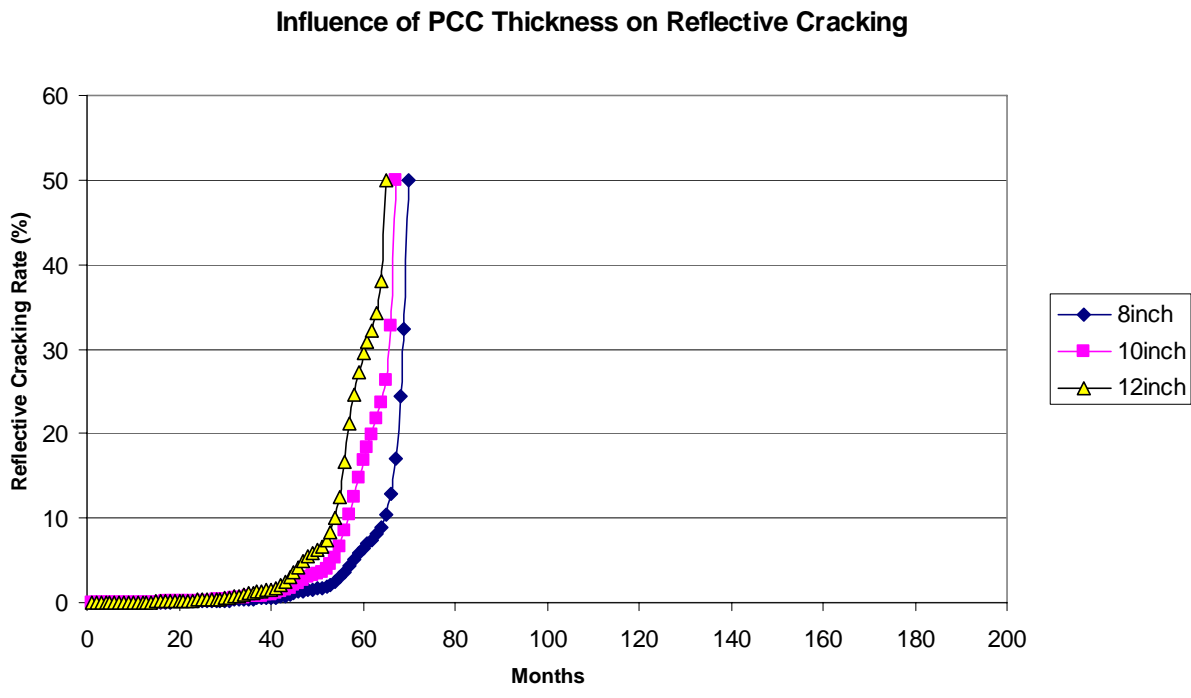
Figure 5-10. AC/JPCP: Influence of Existing PCC Slab Thickness on Reflective Cracking.
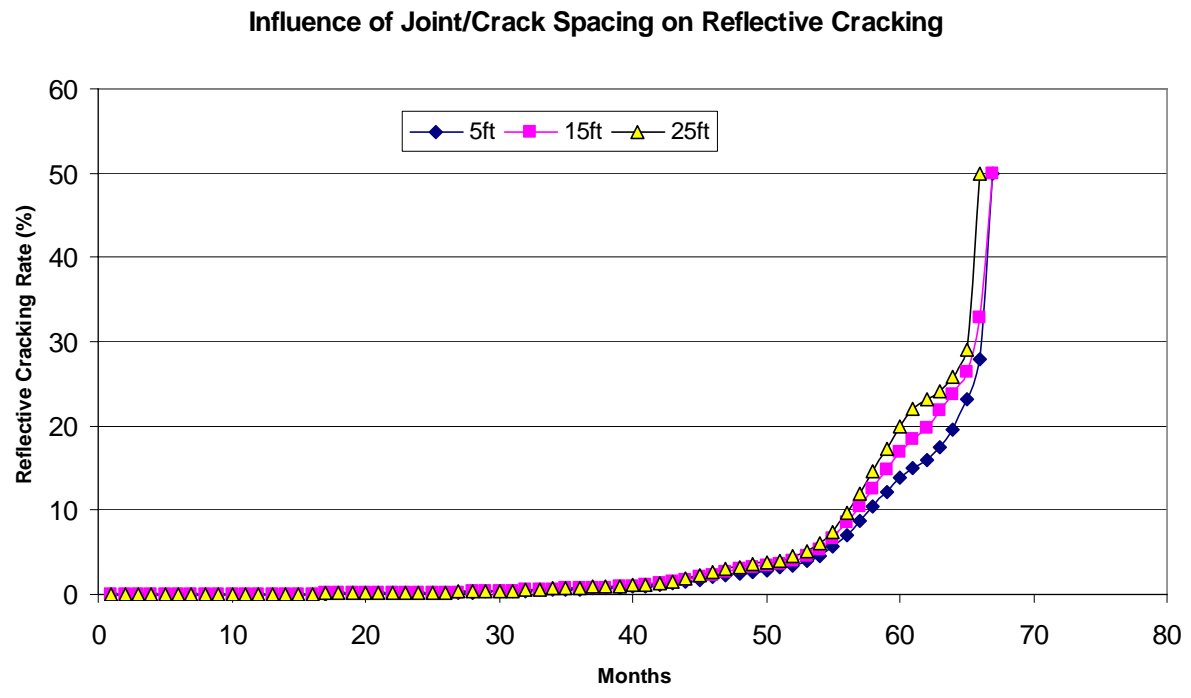
Figure 5-11. AC/JPCP: Influence of Existing Joints/Cracking Spacing on Reflective Cracking.

90

Influence of PCC Concrete Thermal Coefficient of Expansion on Reflective Cracking
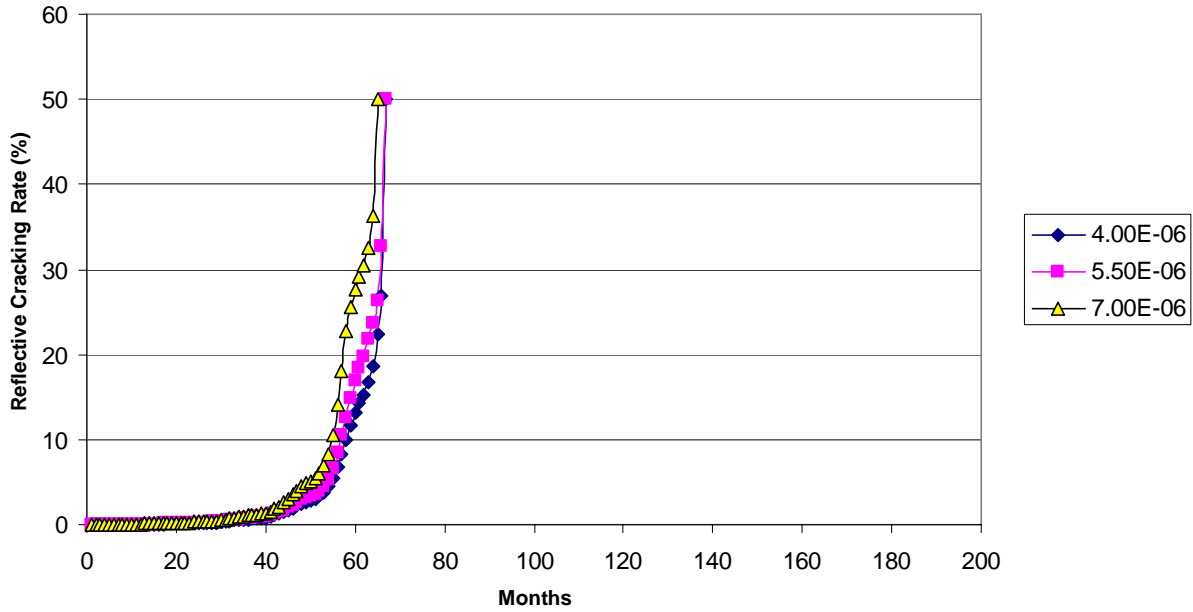
Figure 5-12. AC/JPCP: Influence of Existing PCC Concrete Thermal Coefficient of Expansion on Reflective Cracking.

Influence of Base Layer Thickness on Reflective Cracking
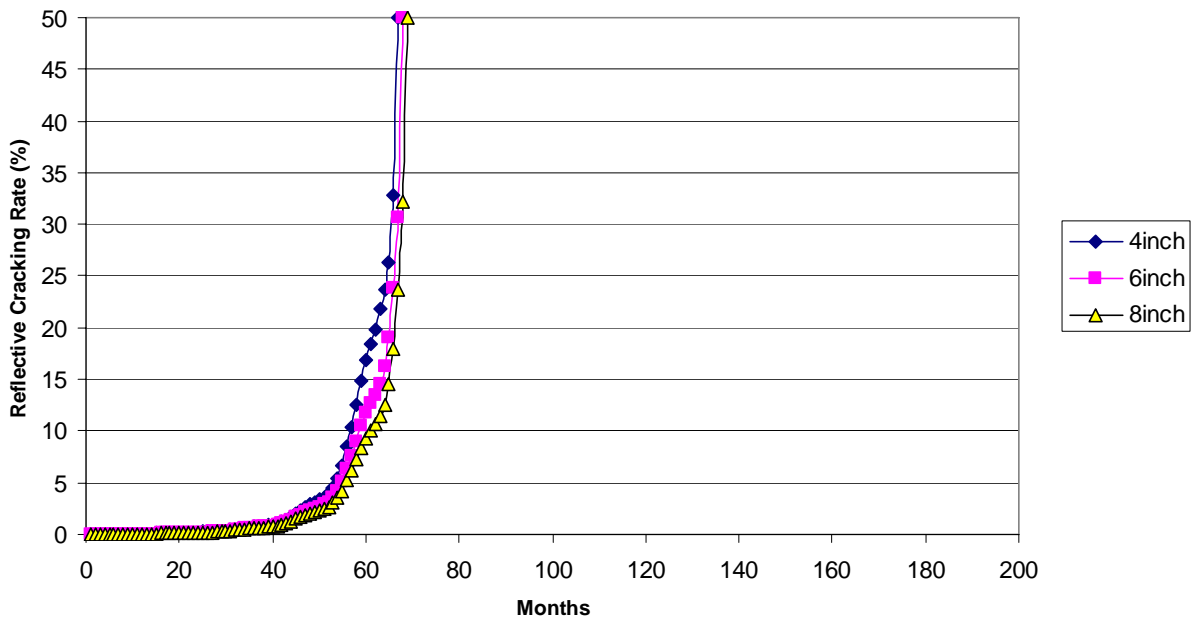
Figure 5-13. AC/JPCP: Influence of Existing Base Layer Thickness on Reflective Cracking.

91

Influence of Base Layer Modulus on Reflective Cracking
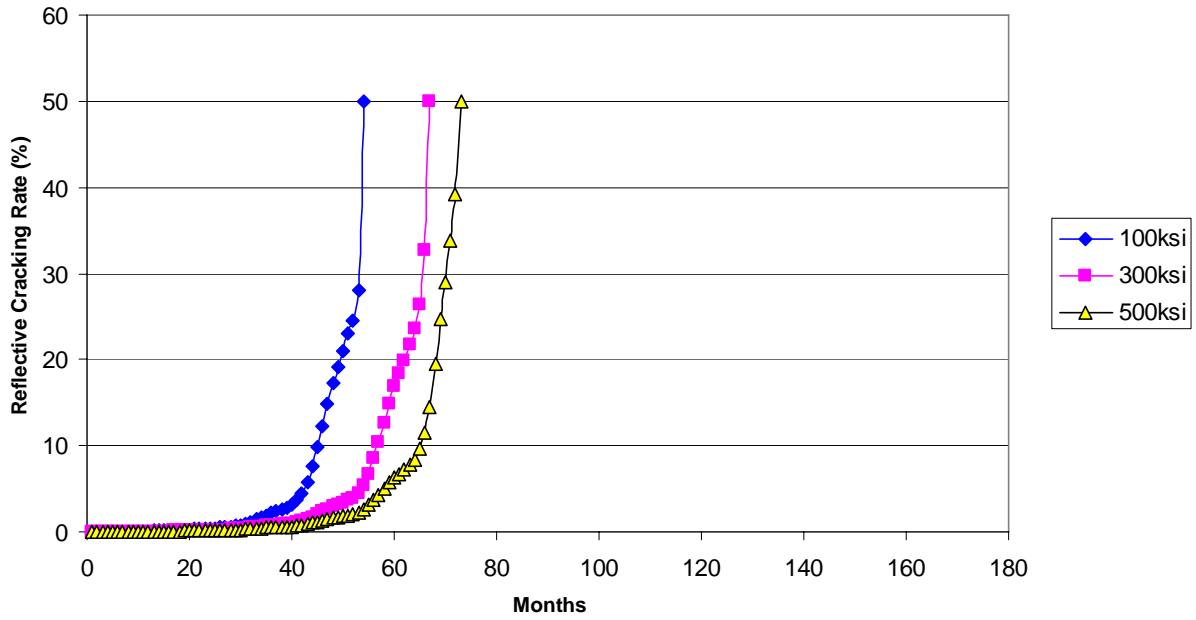
Figure 5-14. AC/JPCP: Influence of Existing Base Layer Modulus on Reflective Cracking.

Influence of Subgrade Modulus on Reflective Cracking
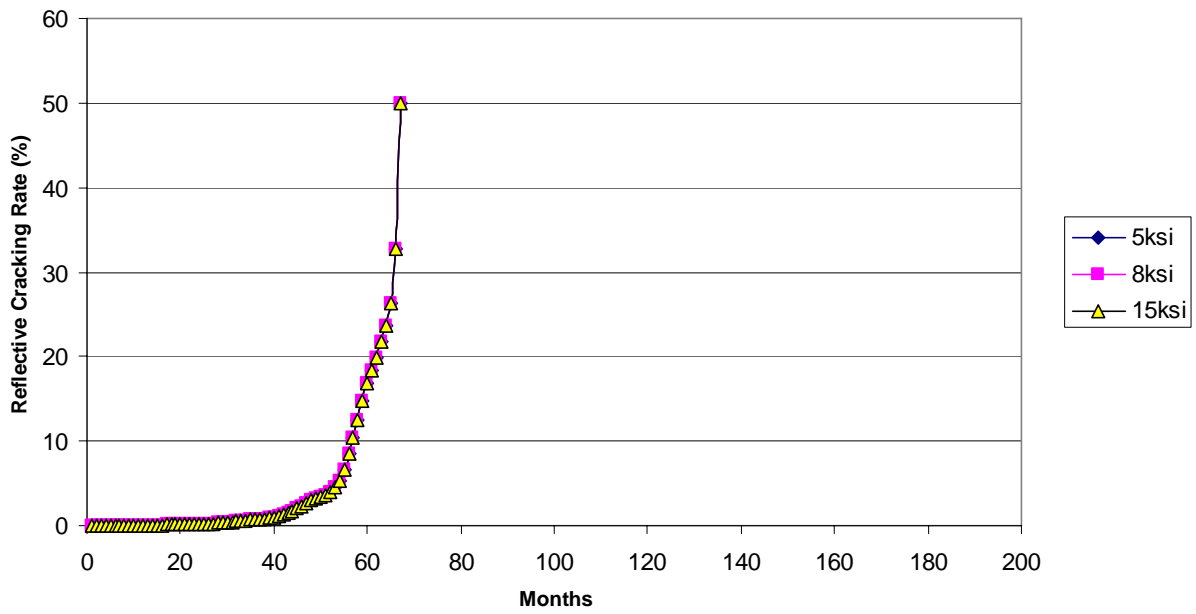
Figure 5-15. AC/JPCP: Influence of Subgrade Modulus on Reflective Cracking.

92

- In case of AC/AC pavements:

Similar runs have been conducted for AC/AC pavements. The influences of the 14 input parameters listed previously on reflective cracking of asphalt overlay are shown in Figures 5-16 to 5-29. Similarly, the influence of those 14 input parameters can be divided into three categories: significant, minor, and tiny or none. These three categories and associated input parameters are listed below:

   a. Significant input parameters: 1) traffic loading level, 2) climate, 3) asphalt overlay thickness, 4) asphalt overlay mix type, 5) asphalt binder type, 6) crack severity level, 7) existing AC layer modulus, 8) existing AC layer thickness, and 9) existing based layer modulus;

   b. Intermediate influential parameters: 1) existing base layer thickness; and

   c. Minor influential parameters: 1) thermal coefficient of expansion of asphalt overlay, 2) thermal coefficient of expansion of existing AC layer, 3) crack spacing, and 4) subgrade modulus.

Again, the nine significant input parameters must be considered when designing an asphalt overlay. Then the intermediate influential parameter should be taken into account if possible. Finally, the minor influential parameters can be ignored for asphalt overlay design in terms of reflective cracking.

Influence of Traffic Level (ESALs) on Reflective Cracking
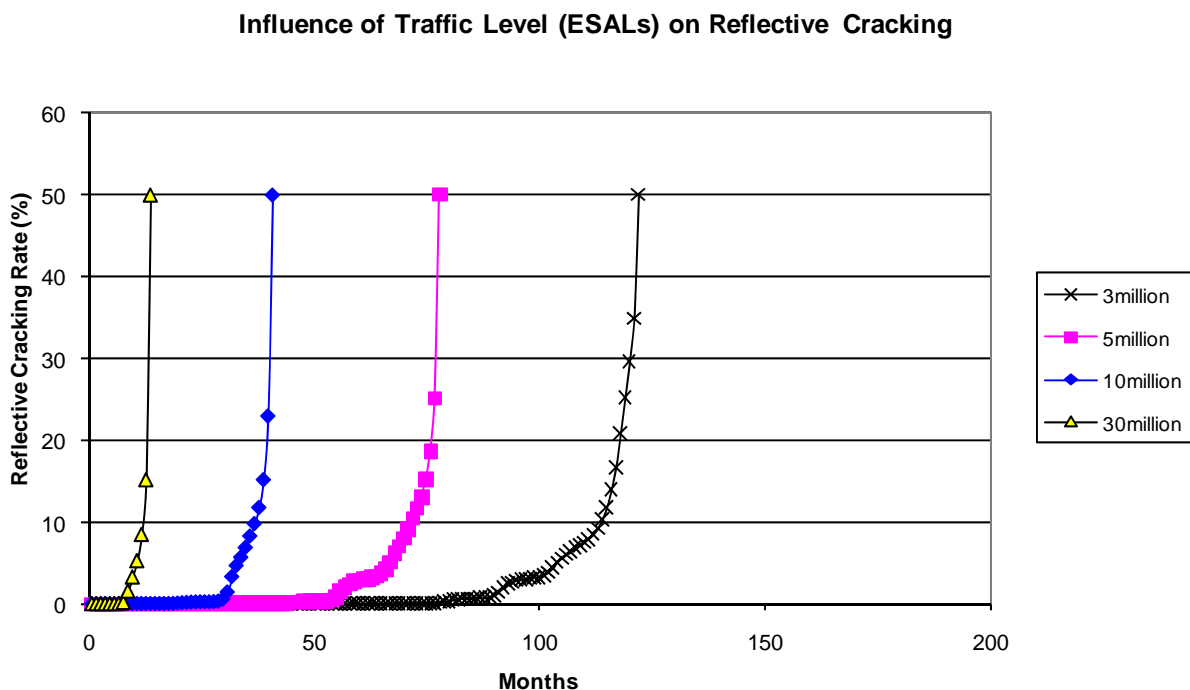
Figure 5-16. AC/AC: Influence of Traffic Level on Reflective Cracking.

93

Influence of Climate on Reflective Cracking
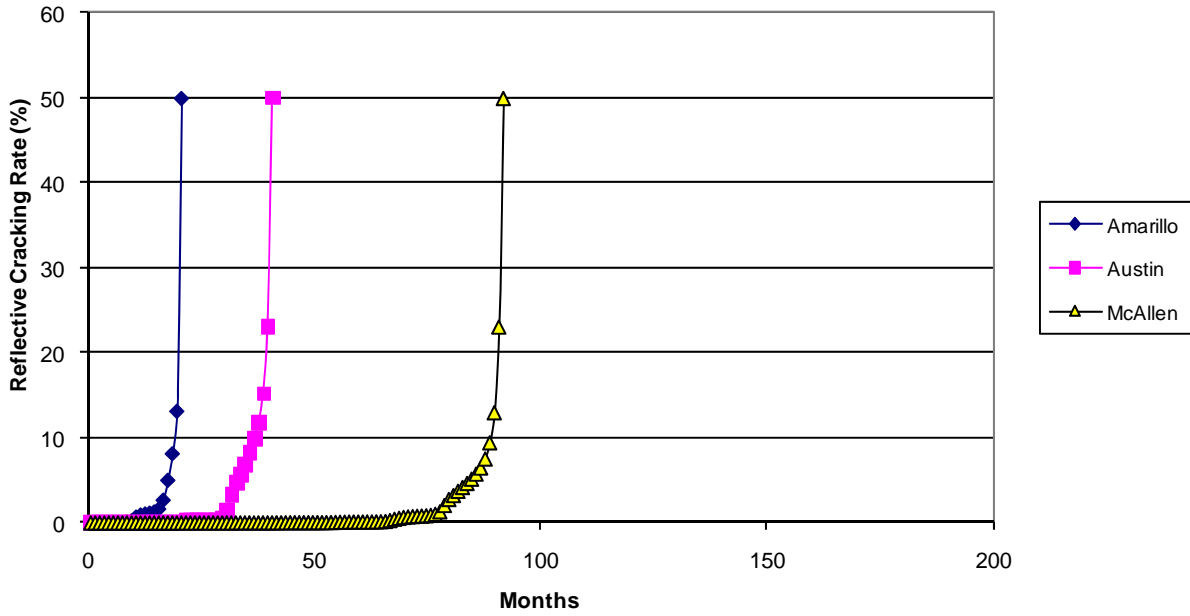
Figure 5-17. AC/AC: Influence of Climate on Reflective Cracking.

Influence of Overlay Thickness on Reflective Cracking
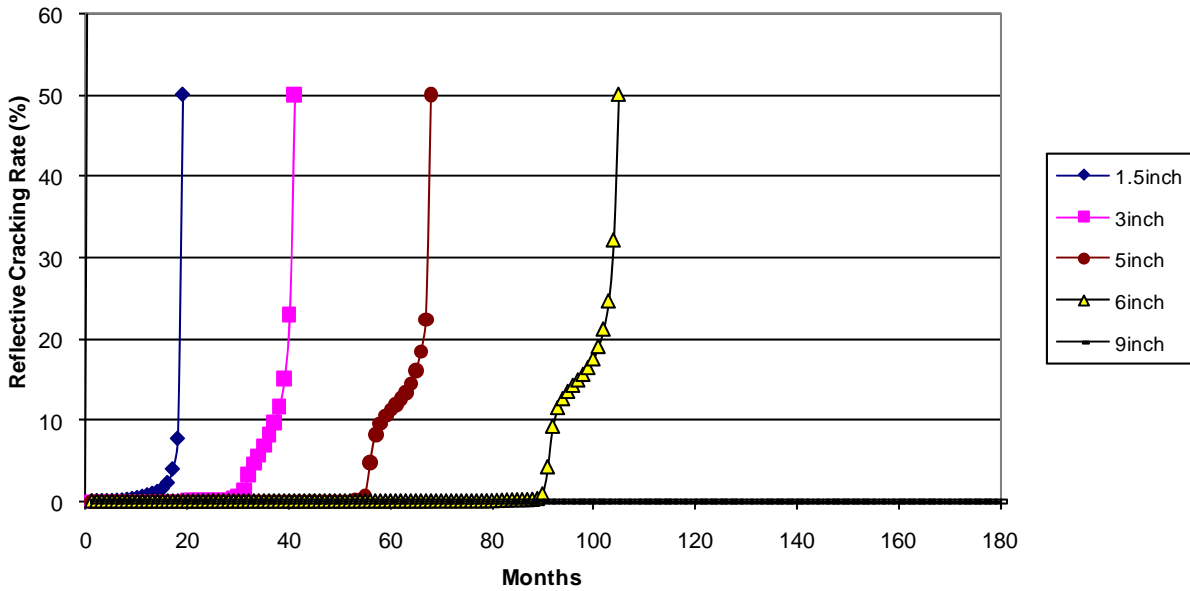
Figure 5-18. AC/AC: Influence of Asphalt Overlay Thickness on Reflective Cracking.

Influence of Overlay Mix Type on Reflective Cracking
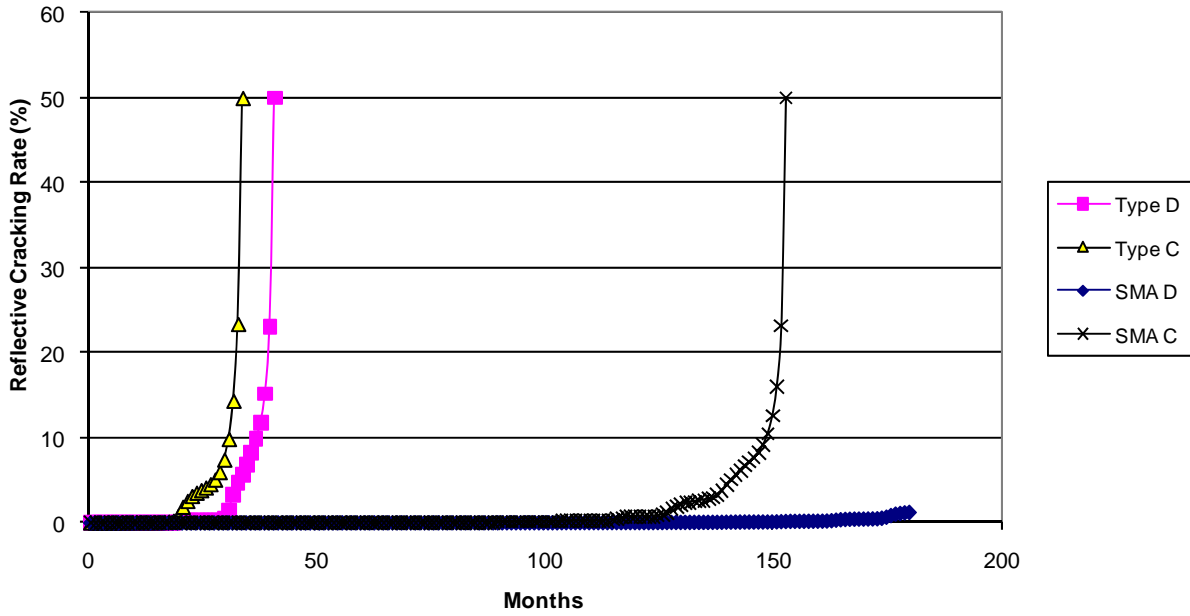
Figure 5-19. AC/AC: Influence of Mix Type on Reflective Cracking.

Influence of Binder Type on Reflective Cracking
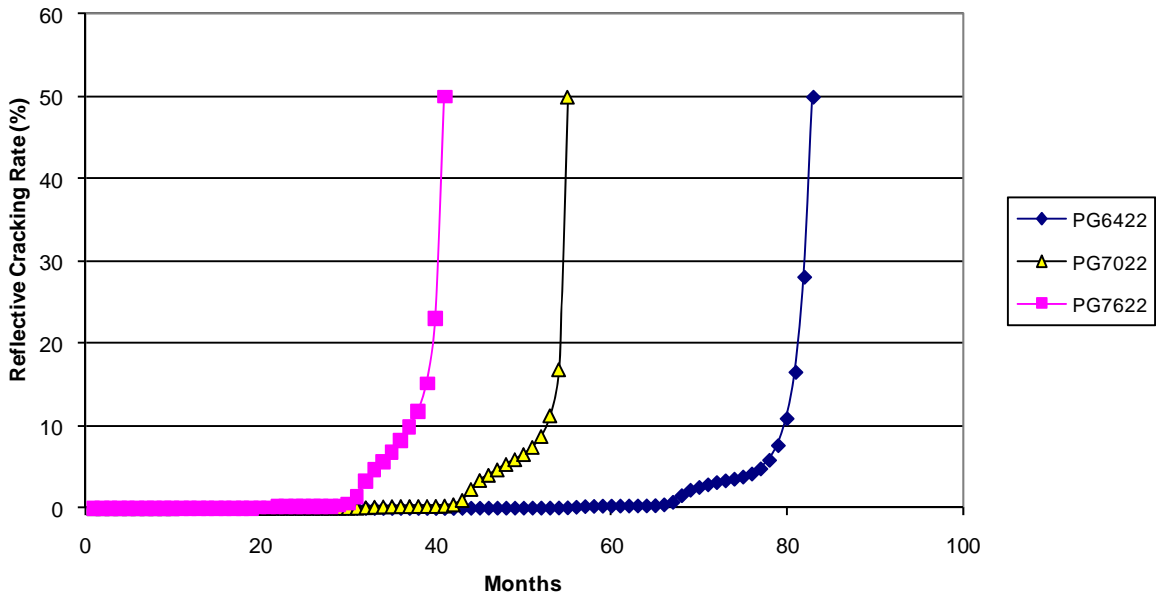
Figure 5-20. AC/AC: Influence of Asphalt Binder Type on Reflective Cracking.

95
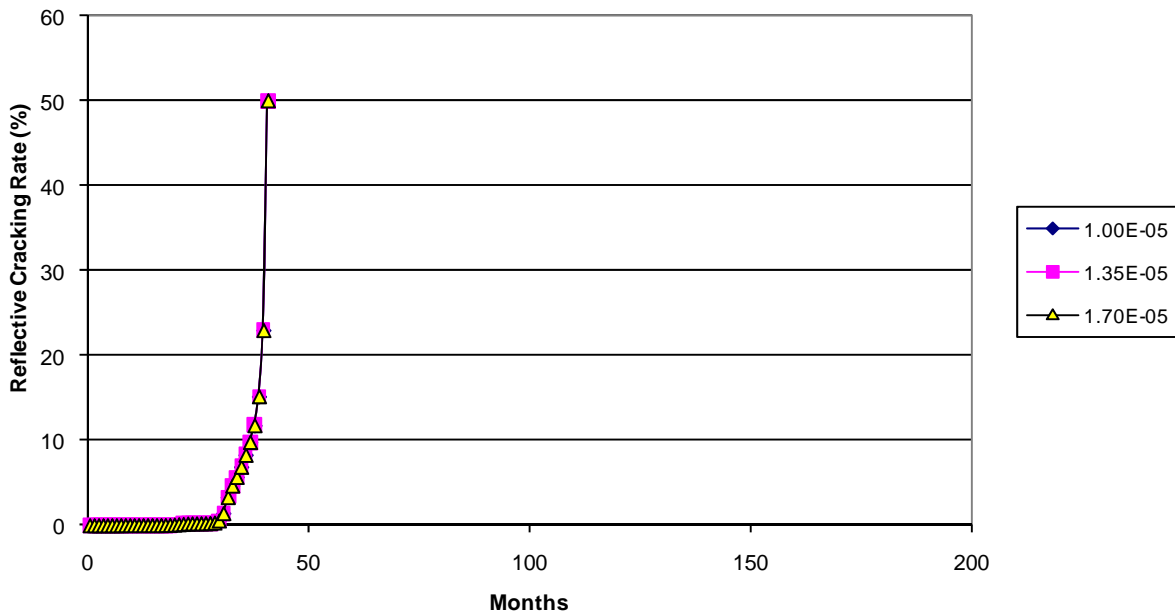
Figure 5-21. AC/AC: Influence of Asphalt Overlay Thermal Coefficient of Expansion on Reflective Cracking.

Influence of Severity Level on Reflective Cracking
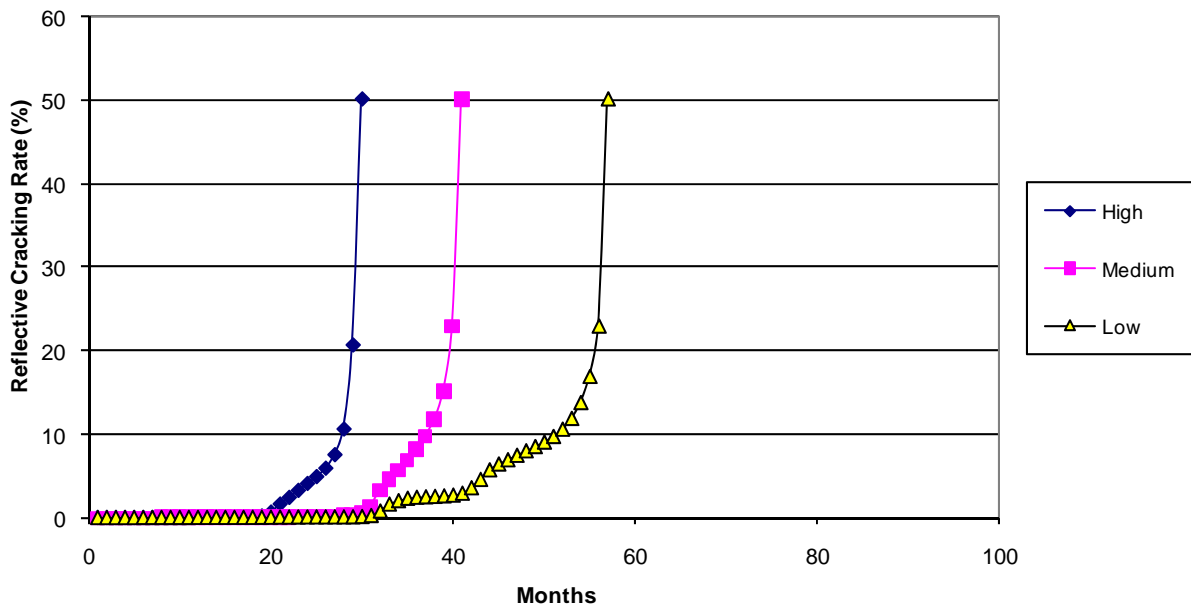
Figure 5-22. AC/AC: Influence of Crack Severity Level on Reflective Cracking.

Influence of Existing AC Modulus on Reflective Cracking
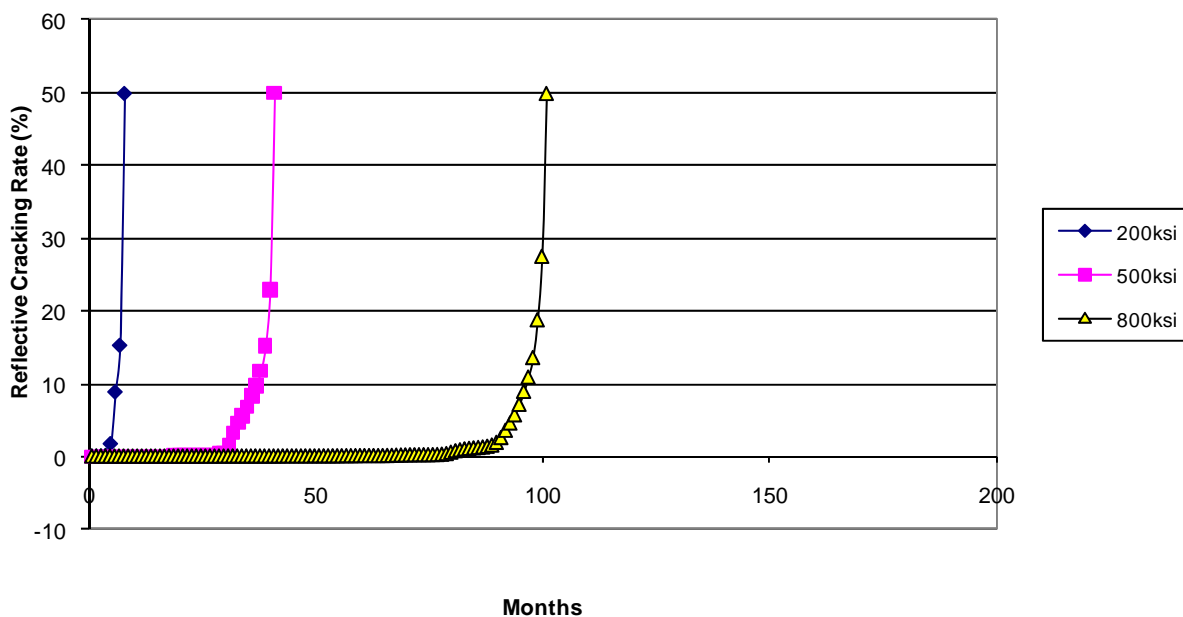
Figure 5-23. AC/AC: Influence of Existing AC Modulus on Reflective Cracking.

Influence of Exisitn AC Layer Thickness on Reflective Cracking

Figure 5-24. AC/AC: Influence of Existing AC Layer Thickness on Reflective Cracking.

Figure 5-25. AC/AC: Influence of Existing Crack Spacing on Reflective Cracking.

Figure 5-26. AC/AC: Influence of Existing AC Thermal Coefficient of Expansion on Reflective Cracking.

98

Influence of Base Layer Thickness on Reflective Cracking
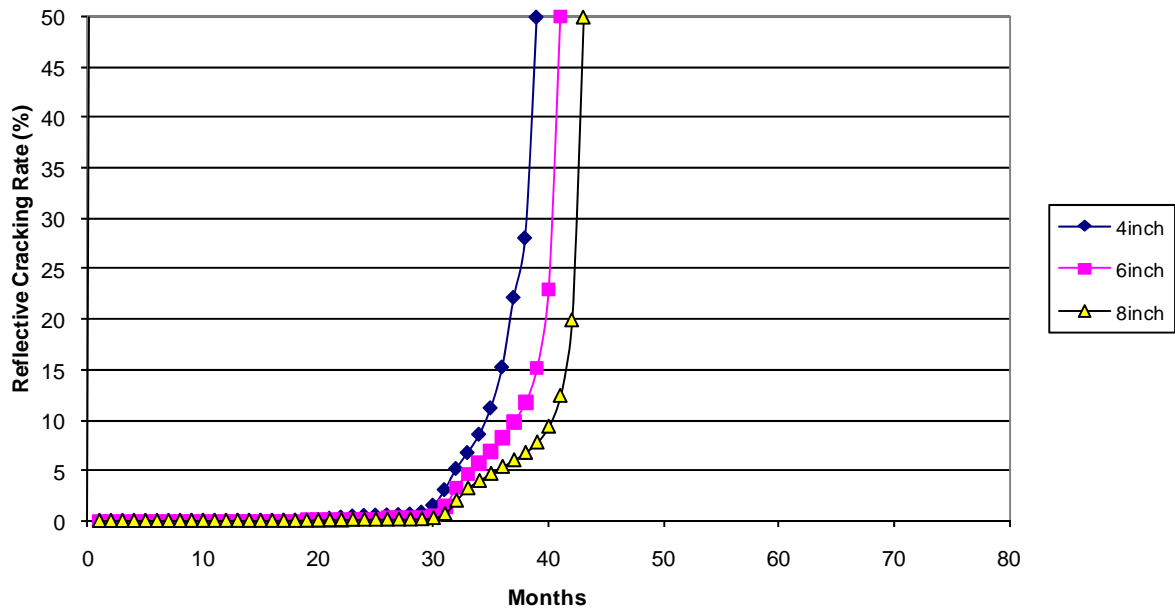
Figure 5-27. AC/AC: Influence of Existing Base Layer Thickness on Reflective Cracking.

Influence of Base Layer Modulus on Reflective Cracking
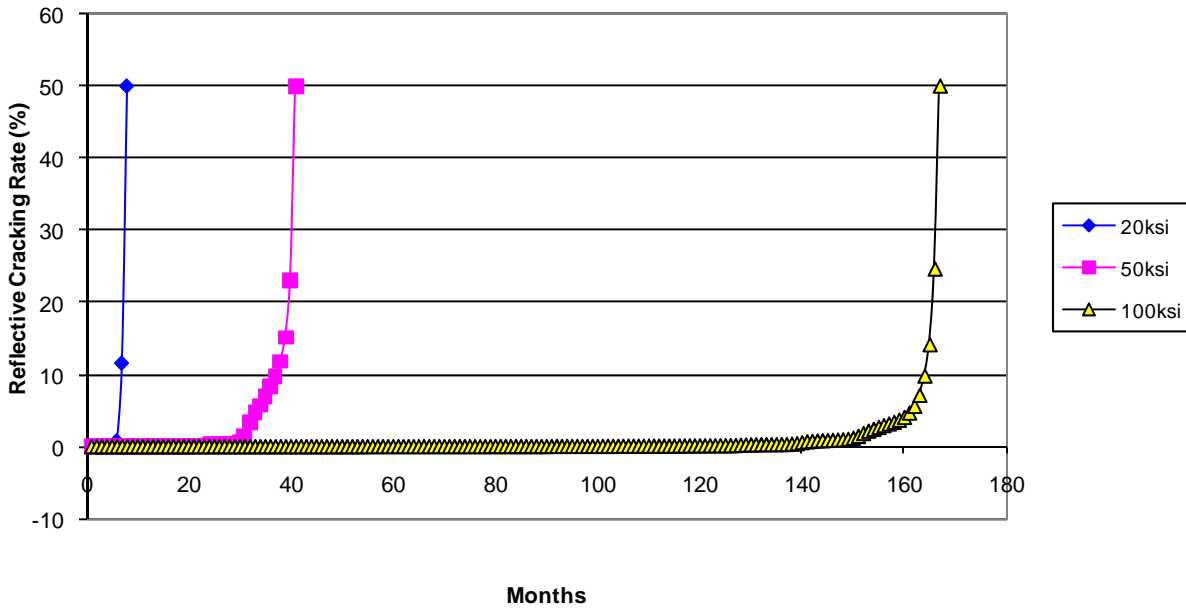
Figure 5-28. AC/AC: Influence of Existing Base Layer Modulus on Reflective Cracking.

99

Influence of Subgrade Modulus on Reflective Cracking
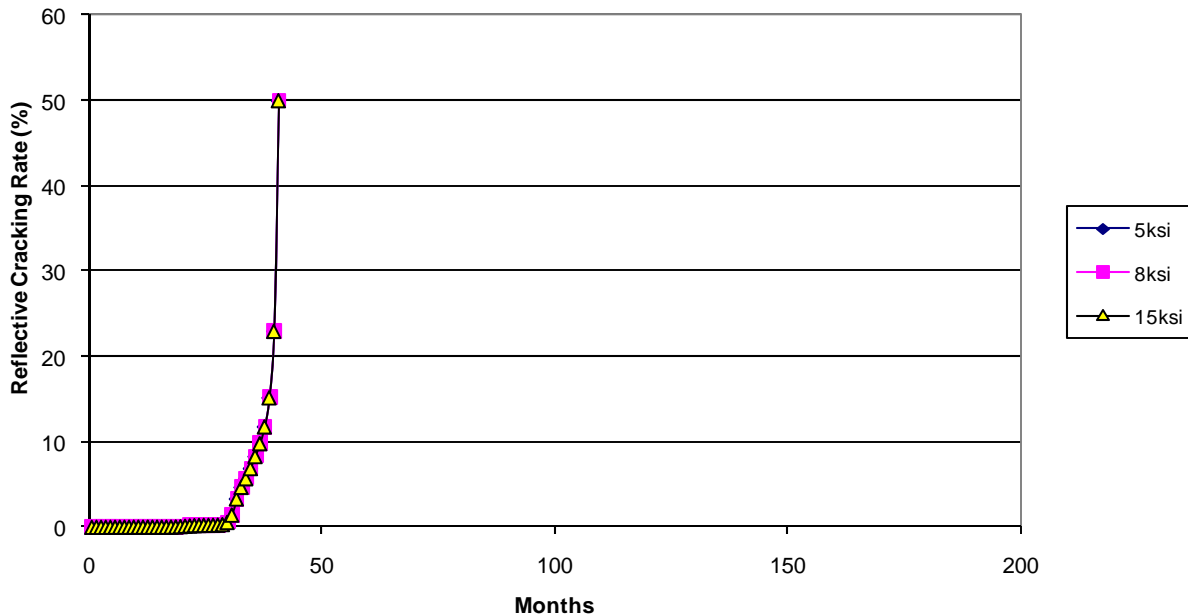
Figure 5-29. AC/AC: Influence of Subgrade Modulus on Reflective Cracking.

Sensitivity Analysis on Asphalt Overlay Rutting

- In case of AC/JPCP pavements:

A total of 34 asphalt overlay cases have been run, and the influences of the 14 input parameters listed previously on asphalt overlay rutting are shown in Figures 5-30 to 5-43. Similar to reflective cracking, the influence of those 14 input parameters can also be divided into three categories: significant, minor, and tiny or none. These three categories and associated input parameters are listed below:

a. Significant input parameters: 1) traffic loading level, 2) climate, 3) asphalt overlay thickness, 4) asphalt binder type, and 5) asphalt overlay mix type;

b. Intermediate influential parameters: 1) PCC slab thickness and 2) existing PCC slab modulus; and

c. Minor/none influential parameters: 1) thermal coefficient of expansion of asphalt overlay, 2) joints/crack spacing, 3) thermal coefficient of expansion of PCC slab, 4) load transfer efficiency of PCC slab at joints/cracks, 5) existing base layer thickness, 6) existing base layer modulus, and 7) subgrade modulus.

100

Dividing the relevance of input parameters into three categories is beneficial in evaluating an asphalt overlay thickness design. It is apparent that in terms of asphalt overlay rutting, the most significant five parameters are 1) traffic loading level, 2) climate, 3) asphalt overlay thickness, 4) asphalt binder type, and 5) asphalt overlay mix type, which must be considered when designing an asphalt overlay. Generally, all other parameters can be ignored.

Specifically, it is worth mentioning that the asphalt overlay rutting does not proportionally increase to the overlay thickness, which is displayed in Figure 5-32. Initially, the asphalt overlay rutting will increase with thicker asphalt overlay; then reaches its maximum value when the overlay is around 5 inches thick. Beyond that, the rutting will slowly decrease. For example, a 4 inch asphalt overlay has more rutting than a 1.5 inch asphalt overlay; a 6 inch asphalt overlay has similar rutting development to that of a 4 inch asphalt overlay, and a 9 inch asphalt overlay has relatively smaller rutting depth than that of 6 inch asphalt overlay. As noted previously, this prediction is consistent with the field observation, and it is due to the difference in the deviatoric stress depth distribution patterns between thin, moderate, and thick asphalt overlays.
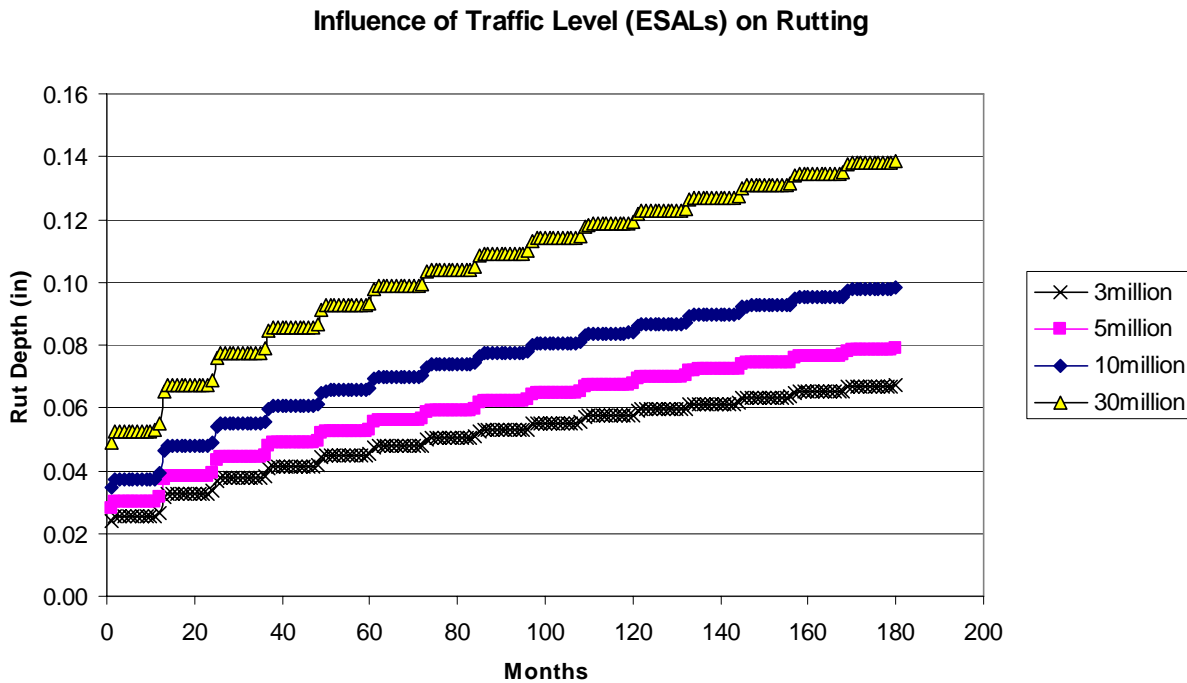
Figure 5-30. AC/JPCP: Influence of Traffic Level on Rutting.

Influence of Climate on Rutting
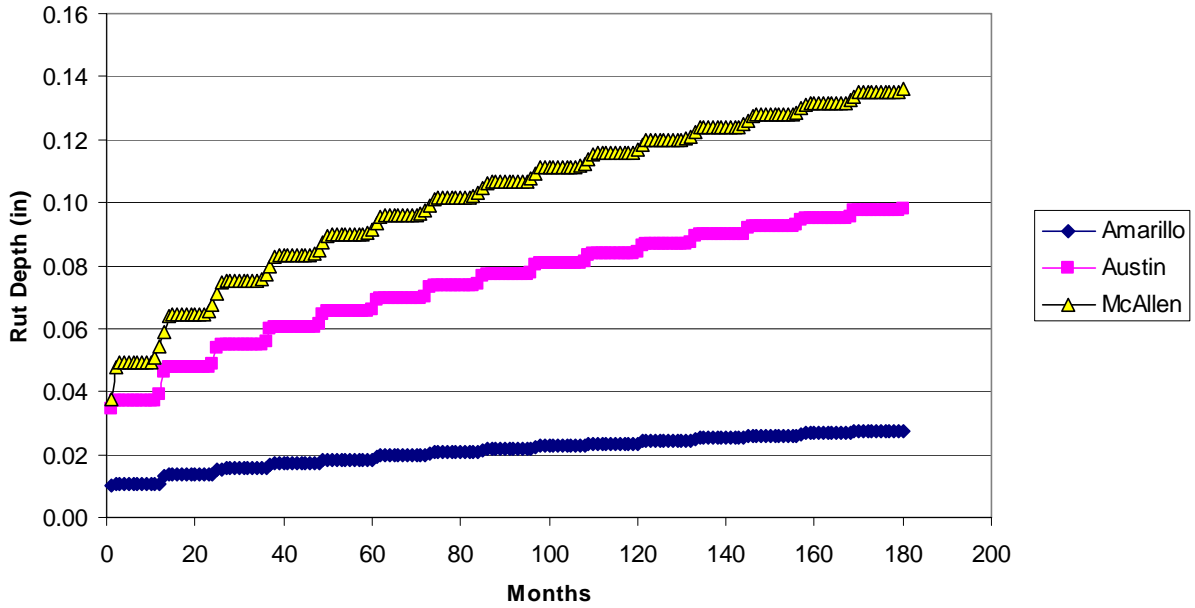
Figure 5-31. AC/JPCP: Influence of Climate on Rutting.

Influence of Overlay Thickness on Rutting
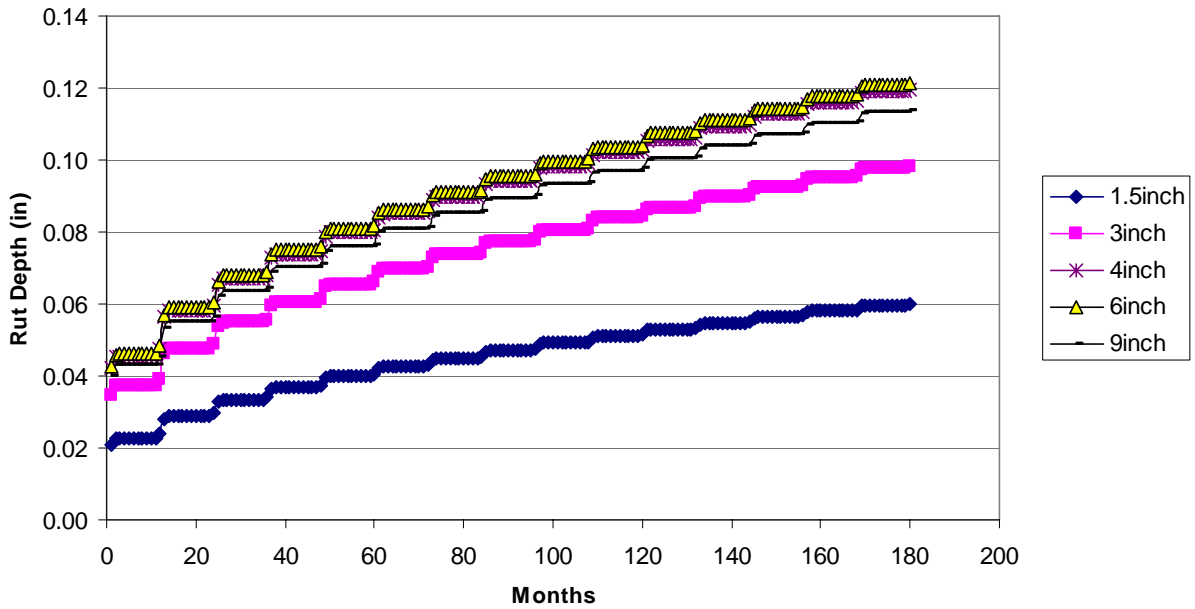
Figure 5-32. AC/JPCP: Influence of Asphalt Overlay Thickness on Rutting.

102

Influence of Overlay Mix Type on Rutting
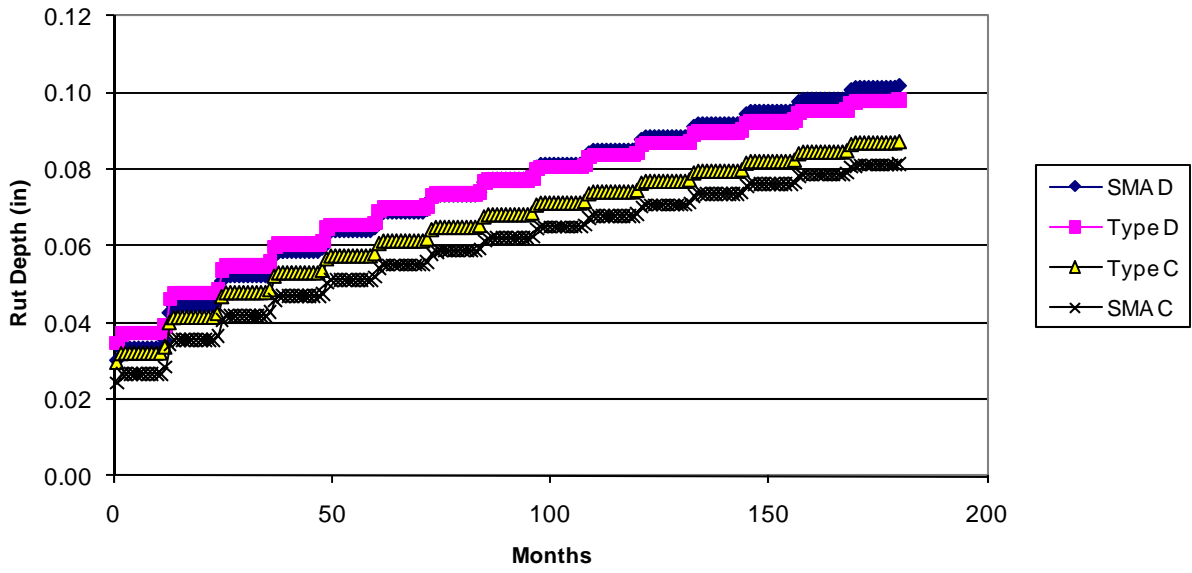
Figure 5-33. AC/JPCP: Influence of Overlay Mix Type on Rutting.

Influence of Binder Type on Rutting
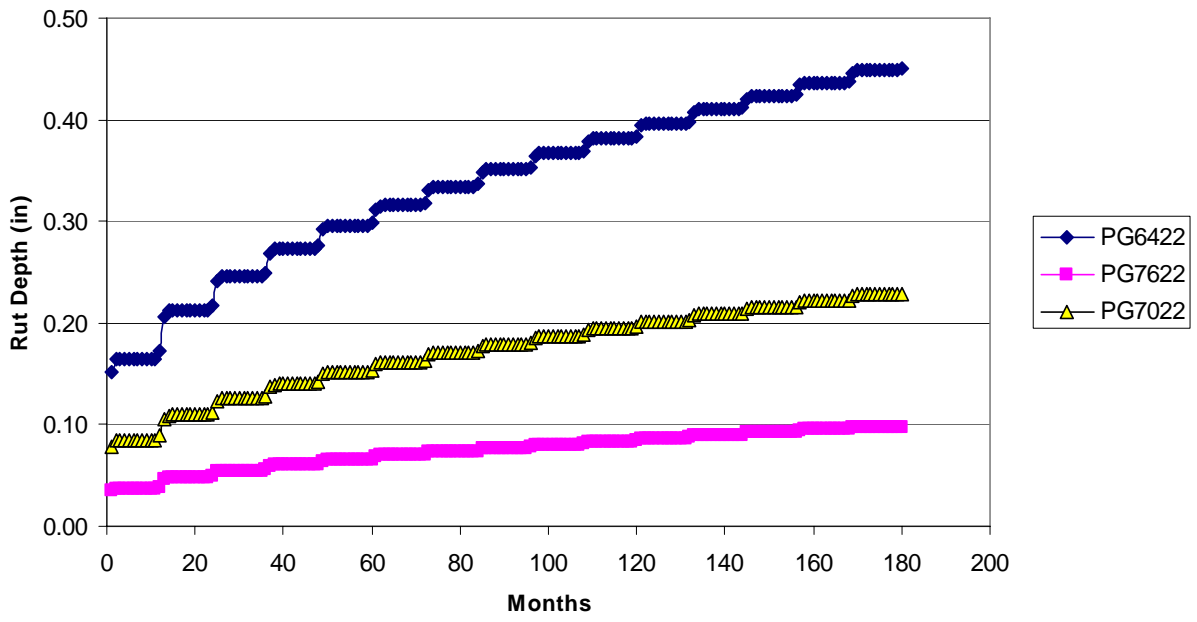
Figure 5-34. AC/JPCP: Influence of Asphalt Binder Type on Rutting.

Influence of Aspalt Overlay Thermal Coefficient of Expansion on Rutting
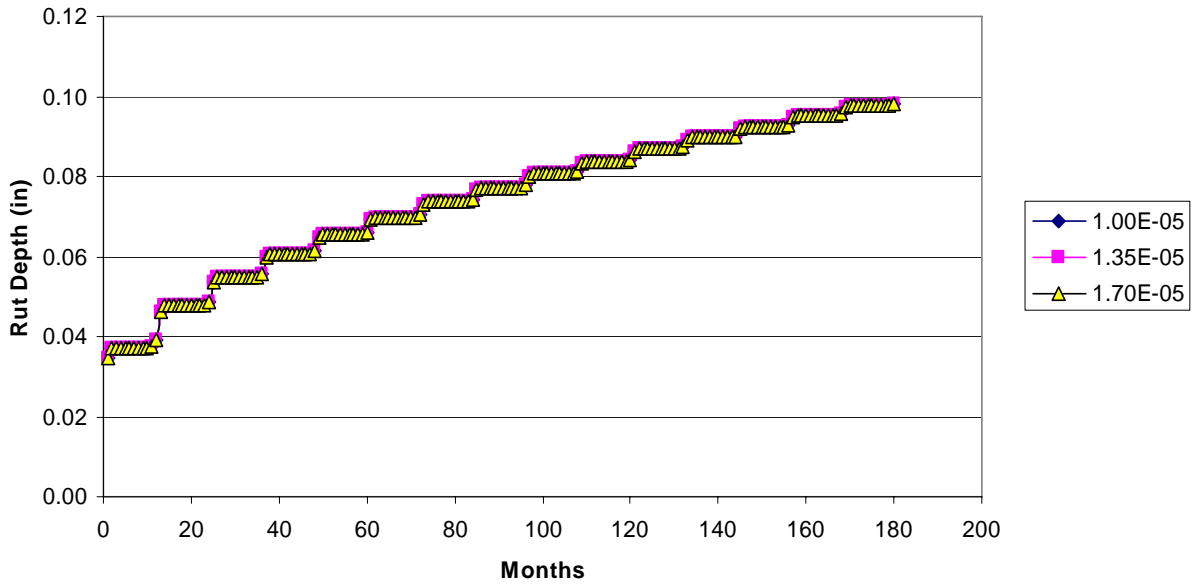
Figure 5-35. AC/JPCP: Influence of Asphalt Overlay Thermal Coefficient of Expansion on Rutting.

Influence of LTE on Rutting
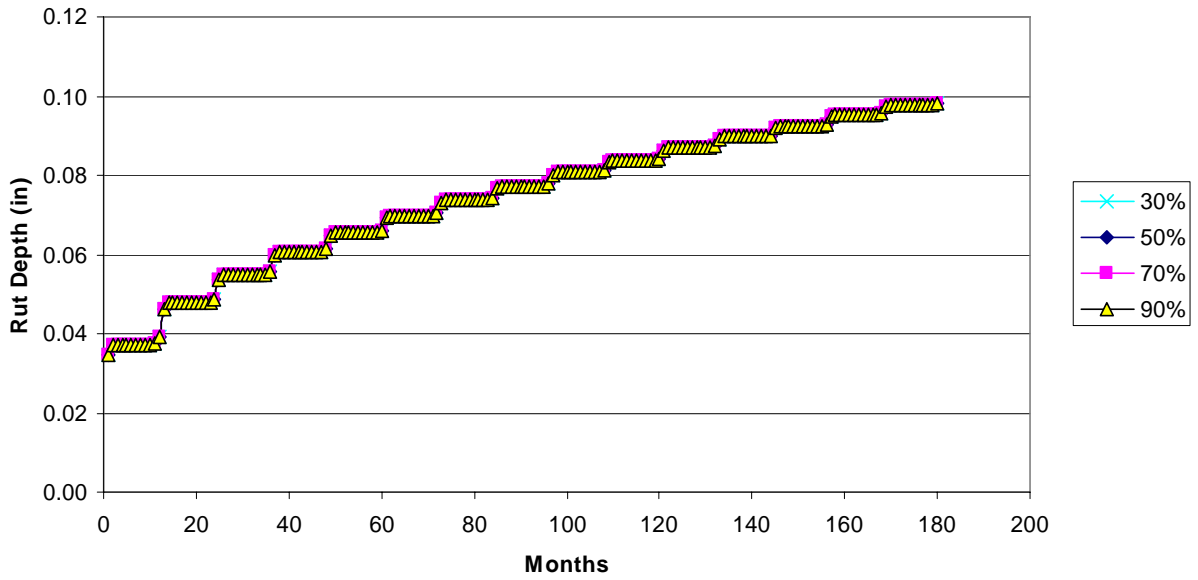
Figure 5-36. AC/JPCP: Influence of Load Transfer Efficiency at Joints/Crack on Rutting.

104

Influence of PCC Modulus on Rutting
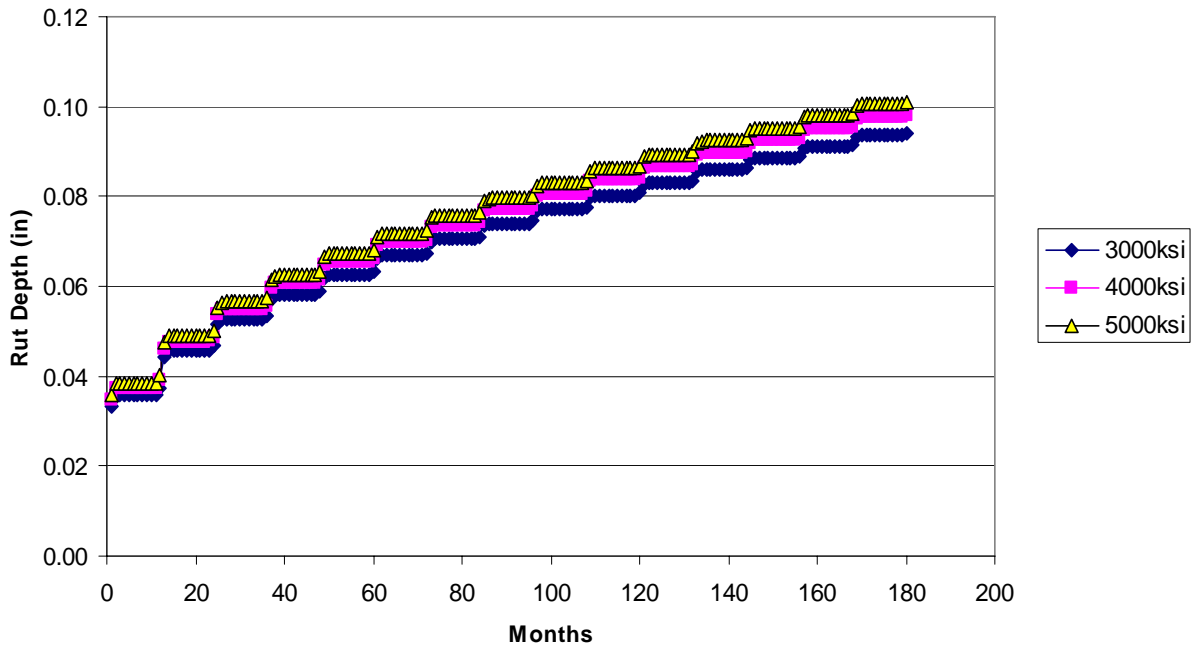
Figure 5-37. AC/JPCP: Influence of Existing PCC Slab Modulus on Rutting.

Influence of PCC Thickness on Rutting
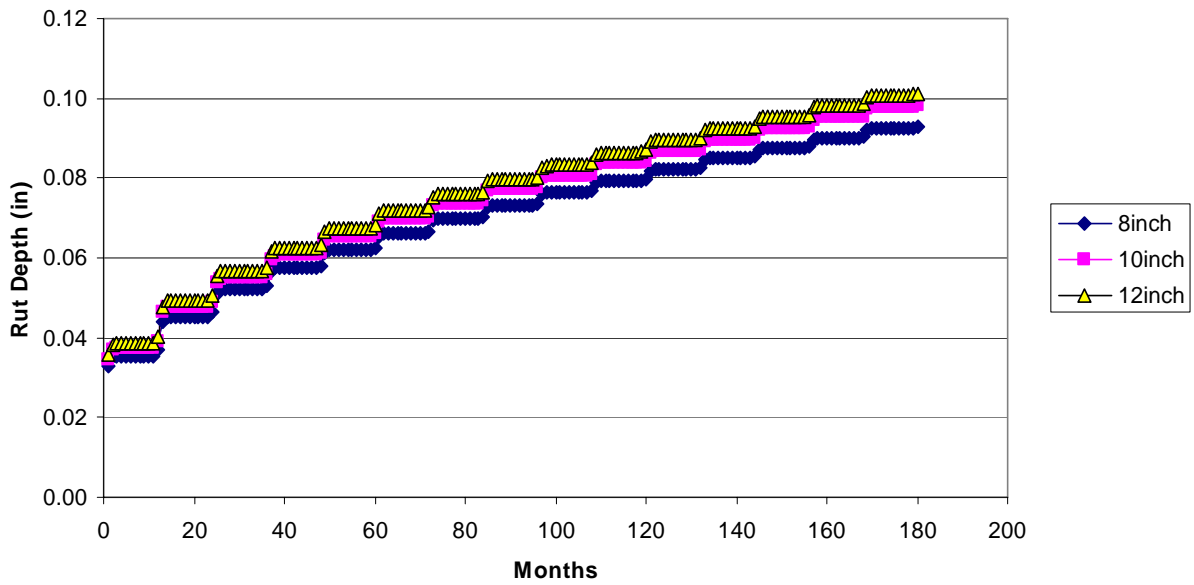
Figure 5-38. AC/JPCP: Influence of Existing PCC Slab Thickness on Rutting.

105

Influence of Joint/Crack Spacing on Rutting
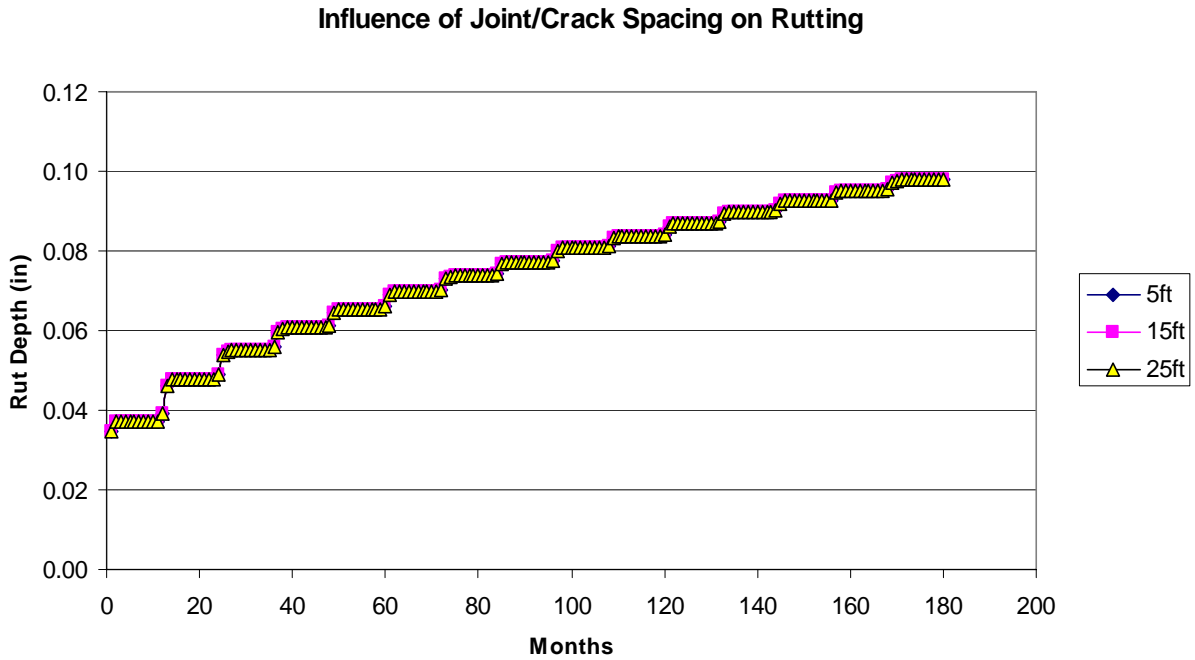
Figure 5-39. AC/JPCP: Influence of Existing Joints/Cracking Spacing on Rutting.

Influence of PCC Concrete Thermal Coefficient of Expansion on Rutting
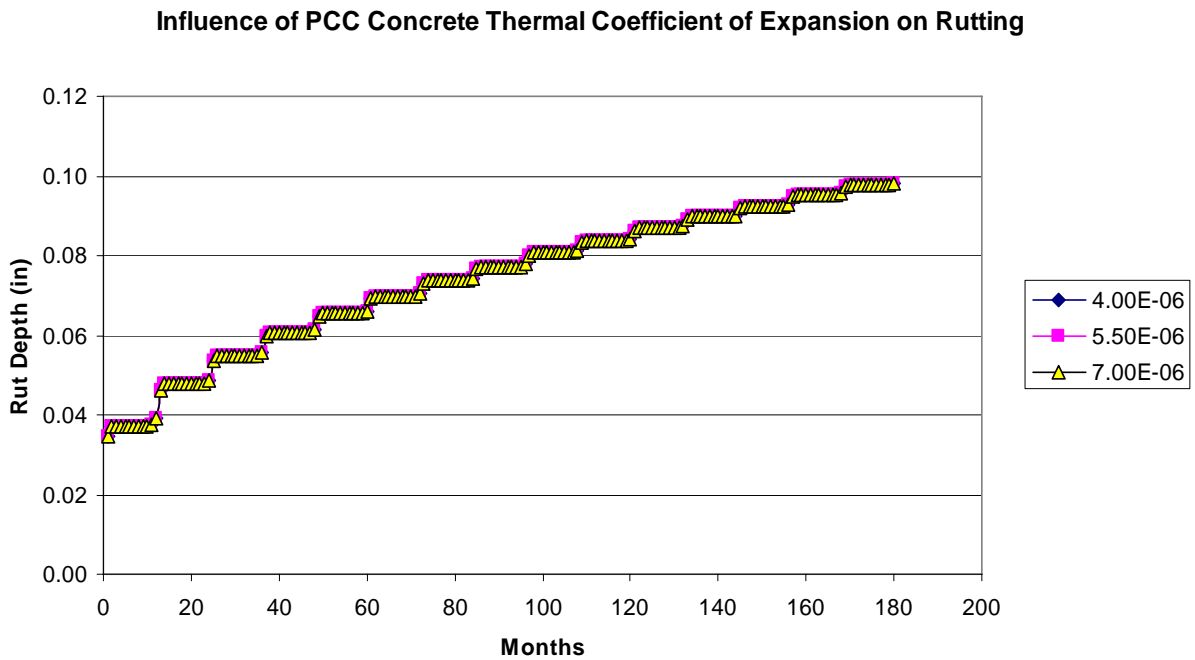
Figure 5-40. AC/JPCP: Influence of Existing PCC Concrete Thermal Coefficient of Expansion on Rutting.

106
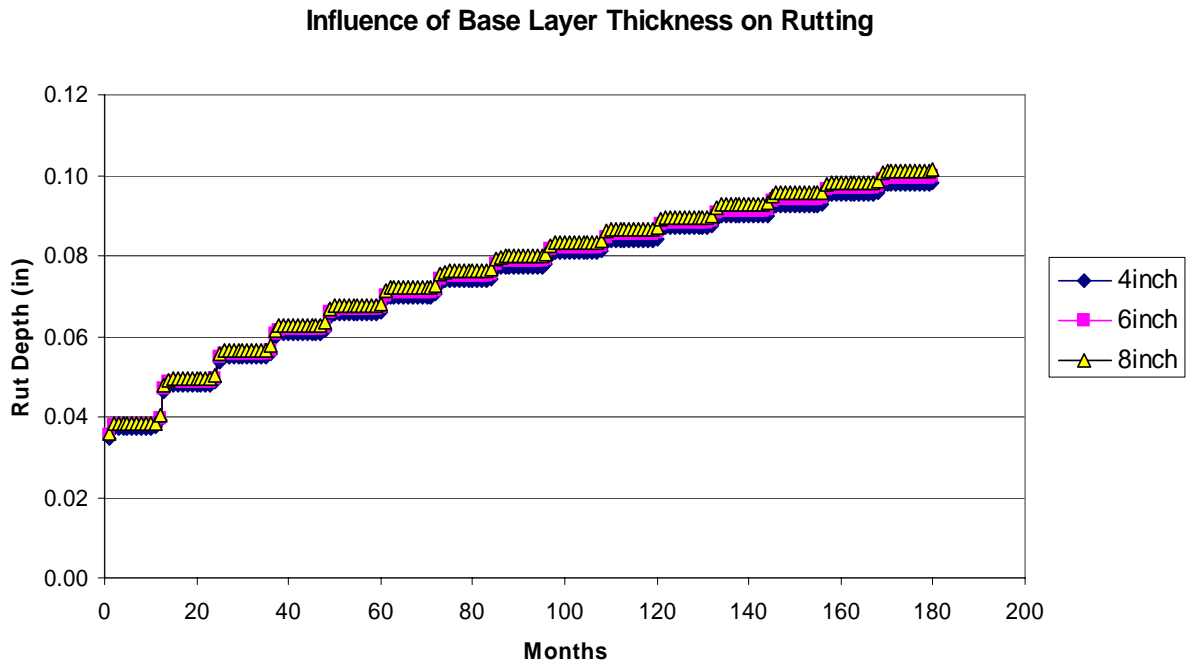
Figure 5-41. AC/JPCP: Influence of Existing Base Layer Thickness on Rutting.
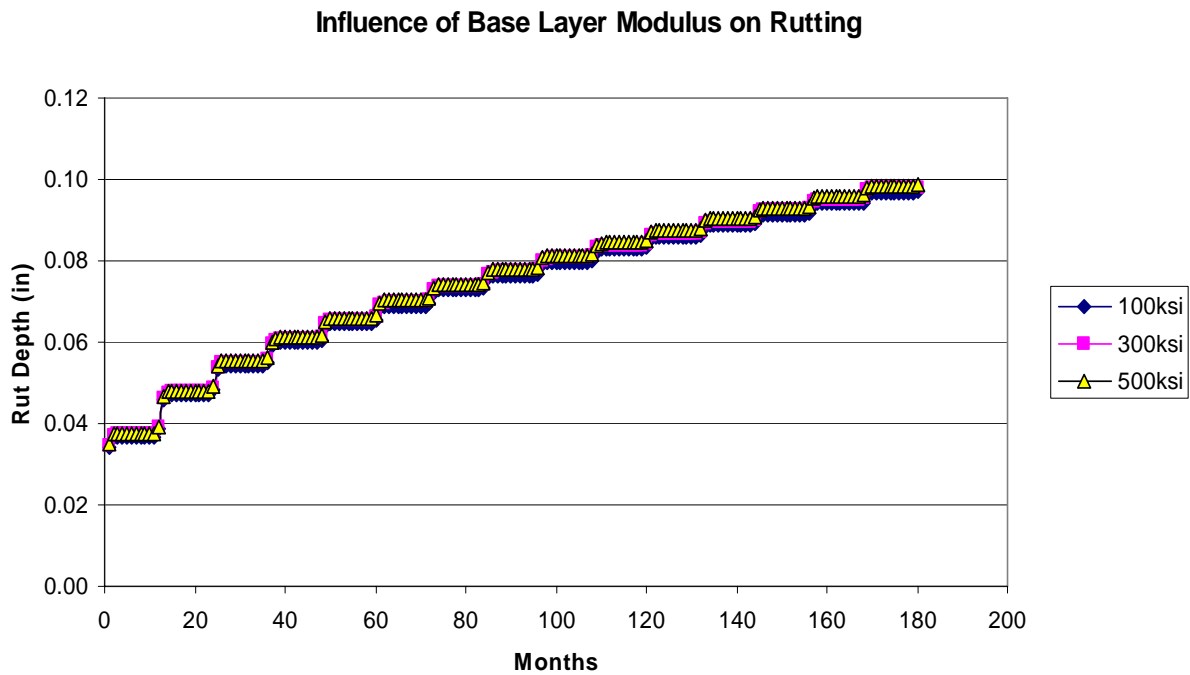
Figure 5-42. AC/JPCP: Influence of Existing Base Layer Modulus on Rutting.

Influence of Subgrade Modulus on Rutting
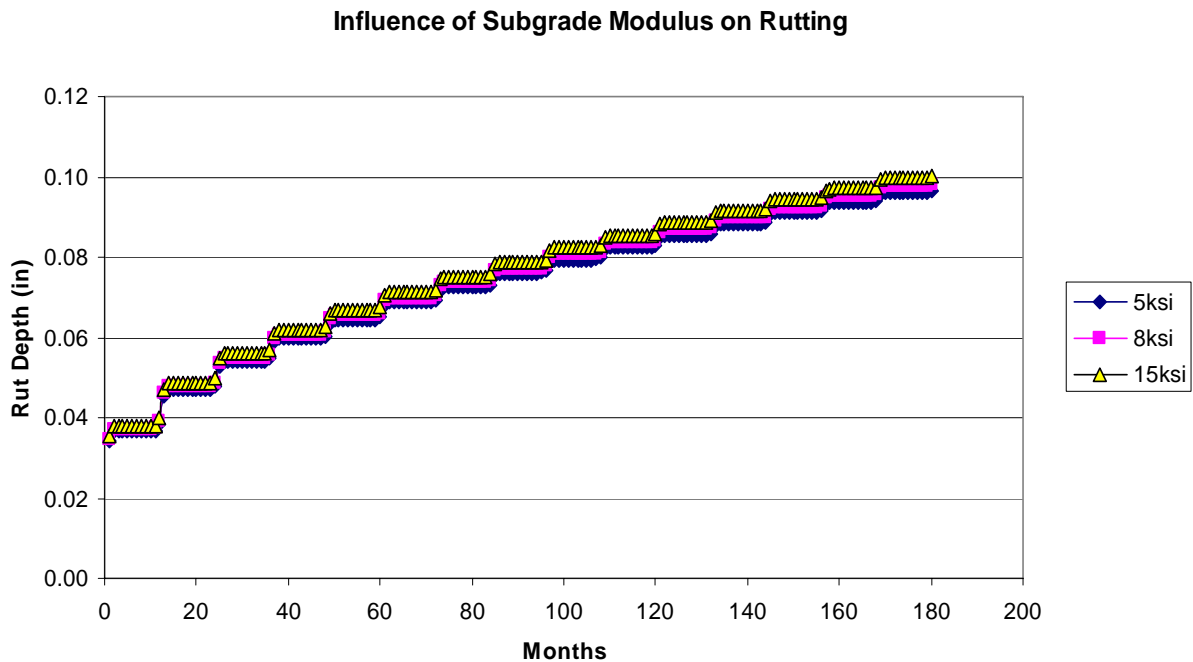
Figure 5-43. AC/JPCP: Influence of Subgrade Modulus on Rutting.

- In case of AC/AC pavements:

Again, similar runs have been conducted for AC/AC pavements, and the influences of the 14 input parameters listed previously on asphalt overlay rutting are similar to those on AC/JPCP pavements. Therefore, the influential graphs, for brevity, are omitted here. Only these three categories and associated input parameters are listed below:

   a. Significant input parameters: 1) traffic loading level, 2) climate, 3) asphalt overlay thickness, 4) asphalt binder type, and 5) asphalt overlay mix type;

   b. Intermediate influential parameters: 1) existing AC layer thickness, 2) existing AC layer modulus, 3) existing base layer thickness, 4) existing base layer modulus, and 5) subgrade modulus; and

   c. Minor/none influential parameters: 1) thermal coefficient of expansion of asphalt overlay, 2) joints/crack spacing, 3) thermal coefficient of expansion of existing AC layer, and 4) crack severity level.

Again, the five significant input parameters must be considered when designing an asphalt overlay. Then the intermediate influential parameter should be taken into account if possible. Finally, the minor influential parameters can be ignored for asphalt overlay design in terms of rutting.

Discussion

To perform well in the field an asphalt overlay must have balanced rutting and reflective cracking performances. Therefore, the significant input parameters to both rutting and reflective cracking should be well taken into account when designing an asphalt overlay. Combining both rutting and reflective cracking influential parameters, the most important factors for asphalt overlay design are:

1. traffic loading level,
2. climate,
3. asphalt overlay thickness,
4. asphalt overlay mix type,
5. asphalt binder type,
6. load transfer efficiency for JPCP pavements
7. crack severity level for existing AC pavements,
8. existing base layer modulus, and
9. existing AC layer thickness in case of asphalt overlay over existing AC pavements.

Therefore, it is critical for a good asphalt overlay design to accurately collect all of these nine input parameters. To extend performance life, it is worth emphasizing that the asphalt overlay should be designed as thick as possible and to treat the poor joints/cracks.

SUMMARY AND CONCLUSIONS

This chapter summarizes the sensitivity analysis conducted on the asphalt overlay thickness design and analysis program. It was found that not all of the input parameters have significant influence on the asphalt overlay performance in terms of the reflective cracking and rutting. The nine most important input parameters identified for asphalt overlay design are 1) traffic loading level, 2) climate, 3) asphalt overlay thickness, 4) overlay mix type, 5) asphalt binder type, 6) load transfer efficiency for JPCP pavements, 7) crack severity level for existing AC pavements, 8) existing base layer modulus, and 9) existing AC layer thickness in case of asphalt overlay over existing AC pavements. Specifically, it is worth noting that asphalt overlay life in terms of reflective cracking is not linearly proportional to overlay thickness. A 4 inch asphalt overlay can have more than two times the life of a 3 inch overlay. Additionally, it is always beneficial to treat the joints/cracks before placing an asphalt overlay. Specifically, the bad joints/cracks where the load transfer efficiency is below 70 percent must be treated in order to have a longer overlay life.

CHAPTER 6

CONCLUSIONS AND RECOMMENDATIONS

This report documents the asphalt overlay thickness design and analysis system and associated software. Based on the research presented in this report, the following conclusions and recommendations are made.

CONCLUSIONS

- o For simplicity and practical routine applications, the well-known Paris' law-based fracture mechanics model still is a rational choice to model reflective cracking induced by both traffic loading (bending and shearing) and thermal effects. This was the basis of the M-E models proposed in this study for modelling reflective cracking in HMA overlays.

- o Based on extensive SIF computations and statistical analysis, a total of 32 SIF regression equations were developed for asphalt overlays over existing flexible pavements and asphalt overlays over existing PCC pavements with three levels of load transfers efficiencies (10, 50, and 90 percent) at joints/cracks. These developed equations make it possible and practical to directly analyze the reflective crack propagation caused by ESALs or variable traffic load spectrum. It was also found that the MET approach is valid for multi-layered asphalt overlays and bases (and/or subbases).

- o For the thermal reflective cracking, a "hybrid" approach, similar to the SHRP low temperature cracking model, was proposed. In this hybrid approach, the viscoelastic properties of asphalt overlay mixes are considered through the thermal stress at the far field ($\sigma_{VE\text{-}far}$), which then ties with the stress intensity factor ($K_{thermal}$). Regression equations were accordingly developed for asphalt overlays over existing flexible pavements and asphalt overlays over existing PCC pavements.

- o The HMA fracture properties (*A* and *n*), which are some of the fundamental input parameters required in the proposed M-E reflective cracking model, can be easily and directly determined in the laboratory using the simple and rapid OT test. The main innovative features of the OT for fracture property determination are the moderately small and convenient specimen size, easy specimen preparation, and short testing time (within 15 minutes). For simplicity and convenience, the default values of fracture parameters (*A* and *n*) have been provided for typical overlay mixes (such as Type C, D, and SMAs).

- o The proposed reflective cracking model was preliminarily calibrated using three HMA overlay field case studies, and the calibrated model has been verified using the reflective cracking data of six asphalt overlay sections collected from California's HVS test site. Thus far, satisfactory results have been obtained.

- o After reviewing existing rutting models in the literature, it was found that the well-known VESYS layer rutting model still is a rational choice to model HMA overlay rutting development. The main feature of the VESYS layer rutting model is to

characterize layer properties rather than global parameters used in the MEPDG. For each layer, the VESYS rutting model requires rutting parameters: α_i and μ_i. The HMA rutting parameters (α and μ), which are some of the fundamental input parameters required in the proposed M-E rutting model, can be directly determined from the repeated load test. For simplicity and convenience, default values of rutting parameters α and μ have been provided for typical overlay mixes (such as Type C, D, and SMAs).

o The proposed HMA overlay rutting model was preliminarily calibrated using 11 test sections of the NCAT Test Track 2006, and the calibrated model was further verified using the rutting data of 3 test sections of the NCAT Test Track 2000. Thus far, satisfactory results have been obtained.

o Both calibrated reflective cracking and rutting models have been integrated into an asphalt overlay thickness design and analysis system and associated software. The four input categories required include 1) the General Information of the project, 2) Traffic, 3) Climate, and 4) Structure & Material Properties. To assist in implementation, default values of pavement material properties have been provided in the software. The running time of the software is generally less than 4 min., and the software program automatically creates a summary of all inputs of the analyzed overlay design project. It also provides a summary of the distress and performance prediction in both tabular and graphical formats. All charts are plotted in Microsoft Excel and hence can be incorporated into electronic documents and reports.

o The sensitivity analysis conducted on the asphalt overlay thickness design and analysis software indicated that not all of the input parameters have significant influence on the asphalt overlay performance in terms of the reflective cracking and rutting. The nine most important input parameters identified for asphalt overlay design are 1) traffic loading level, 2) climate, 3) asphalt overlay thickness, 4) overlay mix type, 5) asphalt binder type, 6) load transfer efficiency for JPCP pavements, 7) crack severity level for existing AC pavements, 8) existing base layer modulus, and 9) existing AC layer thickness in case of asphalt overlay over existing AC pavements. Specifically, it is worth noting that asphalt overlay life in terms of reflective cracking is not linearly proportional to overlay thickness. A 4 inch asphalt overlay can have more than two times the life of a 3 inch overlay. Additionally, it is always beneficial to treat the joints/cracks before placing an asphalt overlay. Specifically, the bad joints/cracks where the load transfer efficiency is below 70 percent must be treated in order to have a longer overlay life.

RECOMMENDATIONS

Overall, the M-E reflective cracking and rutting models developed in this study offer great promise for rationally modelling and accurately predicting the reflective cracking and rutting of asphalt overlays. The asphalt overlay thickness design and analysis program is user-friendly and available to TxDOT pavement engineers, and its prediction is rational and reasonable. Therefore, it is strongly recommended to use this program to design asphalt overlays for state-wide pilot implementation, follow up the performance of these overlays, and finally further calibrate/refine the reflective cracking and rutting models used in the program.

REFERENCES

1. NCHRP 1-37A Mechanistic-Empirical Design of New and Rehabilitated Pavement Structures, 2004. http://www.trb.org/mepdg/guide.htm.

2. Nunn, M., An investigation of reflection cracking in composite pavements in the United Kingdom, *Proceedings of 1st International RILEM Conference on Reflective Cracking in Pavements, Assessment and Control,* Liege University, Belgium, Edited by J. M. Rigo et al., March 1989.

3. Lytton, R.L. Use of Geotextiles for Reinforcement and Strain Relief in Asphaltic Concrete. *Geotextiles and Geomembranes*, Vol. 8, pp. 217-237, 1989.

4. Gary, B. E. and G. E. Martin, Resurfacing with Bituminous Types of Surfaces, *Proceedings of Highway Research Board*, National Research Council, Washington D.C., Vol. 12, 1932, pp. 177-192.

5. Hall, K. T., M. Connor, M. I. Darter, and S. H. Carpenter, *Rehabilitation of Concrete Pavements, Vol. 3: Concrete Pavement Evaluation and Rehabilitation System*, Publication FHWA-RD-88-073, FHWA, U.S. Department of Transportation, 1989.

6. Eckman, B., ESSO MOEBIUS Computer Software for Pavement Design Calculations, User's Manual, Centre de Recherche ESSO, Mont. Saint Aignan, France, June, 1990.

7. Van Gurp, A. P. M., and A. A. A. Molenaar, "Simplified Method to Predict Reflective Cracking in Asphalt Overlays," RILEM Conference on Reflective Cracking in Pavements, Leige, Belgium, pp. 190-198, 1989.

8. Treybig, H. J., B. F. McCullough, P. Smith, and H. Von Quintus, Overlay Design and Reflection Cracking Analysis for Rigid Pavements, Vols. 1 and 2. U.S. Federal Highway Administration Report Nos. FHWA-RD-77-66 and 67, 1977.

9. Seeds, S. B., B. F. McCullough, and F. Carmichael, "Asphalt Concrete Overlay Design Procedure for Portland Cement Concrete Pavements," Transportation Research Record 1007, Washington, D.C., pp. 26-36, 1985.

10. Monismith, C. L. and N. F. Coetzee, Reflection Cracking: Analysis, Laboratory Studies and Design Consideration, *Proceedings of Association of Asphalt Paving Technologists*, Vol. 49, pp. 268-313, 1980.

11. Sousa, J. B., J. C. Pais, R. Saim, G. B. Way, and R. N. Stubstad, Mechanistic- Empirical Overlay Design Method for Reflective Cracking, *Transportation Research Record*, No. 1809, pp. 209-217, 2002.

12. Wu, R., *Finite Element Analysis of Reflective Cracking in Asphalt Concrete Overlays*, Ph.D. Dissertation, University of California, Berkeley, December 2005.

13. Majidzadeh, K., E. M. Kaufmann, and D. V. Ramsamooj, Application of Fracture Mechanics in the Analysis of Pavement Fatigue, *Proceedings of Association of Asphalt Pavement Technologists*, Vol. 40, pp. 227-246, 1970.

14. Paris, P. C. and E. Erdogan, A Critical Analysis of Crack Propagation Laws, *Journal of Basic Engineering,* Transaction of the American Society of Mechanical Engineering, Series D., Vol. 85, pp. 528-883, 1963.

15. Schapery, R. A., *A Theory of Crack Growth in Visco-Elastic Media*, Report MM 2764-73-1, Mechanics and Materials Research Centre, Texas A&M University, 1973.

16. Schapery, R. A., A Method for Predicting Crack Growth in Nonhomogeneous Visco-Elastic Media, *International Journal of Fracture*, Sijthoff and Noordhoff International Publishers, Vol.14, No. 3, pp. 293-309, 1978.

17. Chang H. S., R. L. Lytton, and S. H. Carpenter, *Prediction of Thermal Reflection Cracking in West Texas*, Texas Transportation Institute, Research Report 18-3, Study 2-8-73-18, March 1976.

18. Germann, F. P., and R. L. Lytton, *Methodology for Predicting the Reflection Cracking Life of Asphalt Concrete Overlays*, Research report FHWA/TX-79/09+207-5, College Station, Texas, March 1979.

19. Molenaar, A. A. A., Fatigue and Reflection Cracking due to Traffic Loads, *Proceedings of the Association of Asphalt Paving Technologists*, Vol. 53, pp. 440-474, 1984.

20. Jayawickrama, P.W., and R. L. Lytton, Methodology for Predicting Asphalt Concrete Overlay Life Against Reflection Cracking, *Proceedings 6th International Conference on Structural Design of Asphalt Pavements*, Volume I, pp. 912-924, 1987.

21. de Bondt, A.H., *Anti-Reflective Cracking Design of (Reinforced) Asphaltic Overlays*, Ph.D. Thesis, Delft University of Technology, 1997.

22. Owusu-Antwi, E. B., L. Khazanovich, and L. Titus-Glover, Mechanistic-Based Model for Predicting Reflective Cracking in Asphalt Concrete-Overlaid Pavements, *Transportation Research Record 1629*, Transportation Research Board, Washington D.C., pp. 234-241, 1998.

23. Al-Qadi, I. L., M. A. Elseifi, and D. Leonard, Development of an Overlay Design Model for Reflective Cracking with and without Steel Reinforcement, *Journal of the Association of Asphalt Pavement Technologists*, Volume 72, pp. 388-423, 2004.

24. Elseifi, M. A. and I. L. Al-Qadi, A Simplified Overlay Design Model Against Reflective Cracking Utilizing Service Life Prediction, *Road Materials and Pavement Design*, Vol. 5, No. 2, pp. 169-192, 2004.

25. Hiltumen, D., and R. Roque, A Mechanics-Based Prediction Model for Thermal Cracking of Asphaltic Concrete Pavements, *Proceedings of Association of Asphalt Paving Technologists*, Vol. 63, pp. 81-117, 1994.

26. Jenq, Y. S. and J. D. Perng, Analysis of Crack Propagation in Asphalt Concrete Using a Cohesive Crack Model, *Transportation Research Record*, TRB, 1317, pp. 90-99, 1991.

27. Jenq, Y. S., C. J. Liaw, and P. Liu, Analysis of Crack Resistance of Asphalt Concrete Overlays − A Fracture Mechanics Approach, *Transportation Research Record*, No. 1388, pp. 160-166, 1993.

28. Scarpas, A., R. Al-Khoury, C. A. P. M. Gurp, and S. M. J. G. Erkens, Finite Element Simulation of Damage Development in Asphalt Concrete Pavements, *8th Int. Conf. on Asphalt Pavements, Volume 1 Proceeding*, University of Washington, Seattle, Washington, pp 673-692, 1997.

29. Superpave model team, Advanced AC Mixture Material Characterization Models Framework and Laboratory Test Plan Final Report, NCHRP 9-19, *Superpave Support and Performance Models Management,* Tempe, AZ, 1999.

30. Uzan, J. and E. Levenberg, Strain Measurements in Asphalt Concrete Specimens towards the Development of a Fracture Model, *International Journal of Pavement Engineering*, Vol. 2, No. 4, pp. 243-258, 2001.

31. Soares, J. B., F. A. C. de Freitas, and D. H. Allen, Considering Material Heterogeneity in Crack Modeling of Asphaltic Mixtures, *Transportation Research Record*, No. 1832, pp. 113-120, 2003.

32. Seo, Y., Y. R. Kim, R. A. Schapery, M. W. Witczak, and R. Bonaquist, A Study of Crack-Tip Deformation and Crack Growth in Asphalt Concrete Using Fracture Mechanics, *Journal of Association of Asphalt Paving Technologists*, Vol. 74, pp. 697-730, 2004.

33. Paulina, G. H., S. H. Song, and W. G. Buttlar, Cohesive Zone Modeling of Fracture in Asphalt Concrete, *Proceedings of the 5th International Conference on Cracking in Pavements*, May 5-7, Lemoges, France, pp. 63-70, 2004.

34. Wagoner, M. P., W. G. Buttlar, and G. H. Paulino, Disk-shaped Compact Tension Test for Asphalt Concrete Fracture, *Journal of Society for Experimental Mechanics*, Vol. 45, No. 3, pp. 270-277, 2005.

35. Dave, E. V., S. H. Song, W. G. Buttlar, and W. G. Paulino, Reflective and Thermal Cracking Modeling of Asphalt Concrete Overlays, *Proceedings of Advanced Characterisation of Pavement and Soil Engineering Materials*, Edited by Loizos, Scarpas, and Al-Qadi, 2007, pp. 1241-1252, 2007.

36. Wu, R., J. T. Harvey, and C. L. Monismith, Towards a Mechanistic Model for Reflective Cracking in Asphalt Concrete Overlays, *Journal of Association of Asphalt Paving Technologists*, Vol. 75, pp. 491-534, 2006.

37. Bazant, Z. P., and M. Jirasek, Nonlocal Integral Formulations of Plasticity and Damage: Survey of Progress. *Journal of Engineering Mechanics*, Vol. 128, No.11, pp. 1119–1149, 2002.

38. Hu, S., X. Hu, F. Zhou, L., and Walubita, *SA-CrackPro*: A New Finite Element Analysis Tool for Pavement Crack Propagation, TRB2008.

39. Zhou, F., S. Hu, T. Scullion, D. Chen, X. Qi, and G. Claros, Development and Verification of the Overlay Tester Based Fatigue Cracking Prediction Approach, *Journal of Association of Asphalt Paving Technologists*, Vol. 76, pp. 627-662, 2007.

40. ANSYS 9.0. User Manual, Ansys Inc., Canonsburg, PA, 2004.

41. Huang Y. H., *Pavement Analysis and Design*, Prentice-Hall, Inc., 1993.

42. Odemark, N., *Undersökning av elasticitetsegenskaperna hos olika jordartersamt teori för beräkning av beläggningar enligt elasticitetsteorin*. StatensVäginstitut, Meddelande 77, Sweden, 1949.

43. Ullidtz, P., Pavement Analysis, 1987.

44. Ullidtz, P., Modelling Flexible Pavement Response and Performance, 1998.

45. Jordahl, P. R., and J. B. Rauhut, *Flexible Pavement Model VESYS IV-B*, Report prepared for Federal Highway Administration under Contract DTFH61-C-00175, 1983.

46. Fernando, E. G., D. Musani, D-W. Park, and W. Liu, *Evaluation of Effects of Tire Size and Inflation Pressure on Tire Contact Stresses and Pavement Response*, FHWA/TX-06/0-4361-1, Texas Transportation Institute, College Station, Texas, August 2006.

47. S. W. Park and R. A. Schapery, Methods of Interconversion between Linear Visco-elastic Material Functions, Part I: A Numerical Method Based on Prony Series, *International Journal of Solid and Structure*, Vol. 36, No. 11, pp1653-1675, 1999.

48. J. C. Simo and T. J. R. Hughes, *Computational Inelasticity*, Springer-Verlag, New York, 2000.

49. Salam, Y. M. and C. L. Monismith, Fracture Characteristics of Asphalt Concrete, *Proceedings of Association of Asphalt Paving Technologists*, Vol. 41, pp. 215-256, 1972.

50. Button, J. W., and R. L. Lytton, Evaluation of Fabrics, Fibers, and Grids in Overlays, *Proceedings of the Sixth International Conference on Structural Design of Asphalt Pavements*, The University of Michigan, Vol. 1, pp. 925-934, 1987.

51. Jacobs, M. M. J., P. C. Hopman, and A. A. A. Molenaar, Application of Fracture Mechanics in Principles to Analyze Cracking in Asphalt Concrete, *Journal of the Association of Asphalt Paving Technologists*, Vol. 65, pp. 1-39, 1996.

52. Roque, R., Z. Zhang, and B. Sankar, Detaremination of Crack Growth Rate Parameters of Asphalt Mixtures Using the Superpave IDT, *Journal of the Association of Asphalt Paving Technologists,* Vol. 68, pp. 404-433, 1999.

53. Seo,Y., Y. R. Kim, R. A. Schapery, M. W. Witczak, and R. Bonaquist, A Study of Crack-Tip Deformation and Crack Growth in Asphalt Concrete Using Fracture Mechanics, *Journal of the Association of Asphalt Paving Technologists,* Vol. 73, pp. 200-228, 2004.

54. van Rooijen, R. C., and A. H. de Bondt, Crack propagation performance evaluation of asphaltic mixes using a new procedure based on cyclic semicircular bending tests, *6th Rilem Conference on Cracking in Pavements*, Chicago, Illinois, June 16-18, 2008.

55. Buttlar, W. G., S. M. Smith, W. R. Vavrik, and D. S. Sherman, Rehabilitation Alternatives for Runway 18-36 at Rantoul, Phase 2: Report on Construction, Materials Testing, Field Instrumentation, and Post-Construction Distress Survey, June 2000.

56. Buttlar, W. G., Reflective Crack Relief Interlayers, Presentation at *Cracking in Pavements Symposium*, Laramie, Wyoming, July 19, 2007.

57. Zhou, F., and T. Scullion, Type F Mix Design, Research report FHWA/TX-07/5-5123-1, College Station, Texas, July 2007.

58. Chen, D. H., F. Zhou, J. L. Lee, S. Hu, K. H. Stokoe II, and J. Yang, Threshold values for reflective cracking based on continuous deflection measurements, *Canadian Journal of Civil Engineering*, Vol. 34, pp. 1257-1266, 2007.

59. Chowdhury, A. A. Bhasin, and J. W. Button, *As-Built Properties of Test Pavements on IH-20 in Atlanta District*, FHWA/TX-03/0-4203-2, Texas Transportation Institute, College Station, Texas, March 2003.

60. Jones, D., J. Harvey, and C. Monismith, Reflective Cracking Study: Summary Report, UCPRC-SR-2007-01, CA091073N, University of California, Pavement Research Center, UC Davis, UC Berkeley, December 2007.

61. Jones, D., B. Steven, and J. Harvey, Reflective Cracking Study: HVS Test Section Forensic Investigation, Research Report: UCPRC-RR-2007-05, CA091073I, University of California, Pavement Research Center, UC Davis, UC Berkeley, July 2007.

62. Huekelom, W., and A. J. G. Klomp, Consideration of Calculated Strains at Various Depths in Connection with the Stability of Asphalt Pavements, *Proceedings of the 2nd International Conference on the Structural Design of Asphalt Pavements*, Vol. I, Ann Arbor, Michigan, 1967.

63. Monismith, C. L., Permanent Deformation Studies of Pavements, FCP Research Progress Review Report, San Francisco, California, 1973.

64. McLean, D. B., Permanent Deformation Characteristics of Asphalt Concrete, Ph.D. Dissertation, University of California, Berkeley, California, 1973.

65. Romain, J. E., Rut Depth Prediction in Asphalt Pavements, Research Report No. 150, Centre de Recherches Routieres, Brasseks, Belgium, 1969.

66. Barksdale, R. D., Laboratory Evaluation of Rutting in Base Course Materials, *Proceedings of the 3rd International Conference on the Structural Design of Asphalt Pavements*, Vol. I, London, England, 1972.

67. Morris, J., and R. C. G. Haas, Designing for Rutting in Asphalt Pavements, Canadian Technical Asphalt Association Annual Meeting, 1972.

68. *Guide for Mechanistic–Empirical Design of New and Rehabilitated Pavement Structures.* Final Report, NCHRP Project 1-37A. Transportation Research Board, National Research Council, Washington, D.C., March 2004. http://trb.org/mepdg/guide.htm.

69. Schwartz, C., Improving Mechanistic-Empirical Models for Predicting HMA Rutting, Presented at 2006 Symposium on Models Used to Predict Pavement Performance, Laramie, Wyoming.
http://www.petersenasphaltconference.org/download/Schwartz%20Improving%20Mechanistic-Empirical%20Models%20for%20Predicting%20HMA%20Rutting.pdf.

70. Kenis, W. J., *Predictive Design Procedure, VESYS User's Manual: An Interim Design Method for Flexible Pavement Using the VESYS Structural Subsystem.* Final Report No. FHWA-RD-77-154, FHWA, Washington D.C., 1978.

71. Kenis, W. J., and W. Wang, "Calibrating Mechanistic Flexible Pavement Rutting Models From Full Scale Accelerated Tests, *Proceedings of the Eighth International Conference on Asphalt Pavements*, Vol. I, pp. 663-672, Seattle, Washington, 1997.

72. Epps, J. A., A. Hand, S. Seeds, T. Scholz, S. Alavi, C. Ashmore, C. L. Monismith, J. A. Deacon, J. T. Harvey, and R. B. Leahy, Recommended Performance-Related Specifications for Hot-Mix Asphalt Construction. *NCHRP Report 455,* National Cooperative Highway Research Program, Transportation Research Board, National Research Council, Washington, D.C., pp. 496, 2002.

73. Zhou, F. and T. Scullion, Guidelines for Development Input Parameters of Enhanced VESYS5 Program, FHWA/TX-05/9-1502-01-P5, Texas Transportation Institute, College Station, Texas 77843-3135, August 2004.

74. Lytton, R. L., et al., Development and Validation of Performance Prediction Model and Specifications for Asphalt Binders and Paving Mixes. The Strategic Highway Research Program Project Report SHRP-A-357, 1993.

75. Brown, S. F., et al., Independent Review of the Mechanistic-Empirical Pavement Design Guide and Software, Research Results Digest 307, Transportation Research Board, September 2006.

76. Brown, E. R., and S. Cross, A National Study of Rutting in Asphalt Pavement, Proceedings of AAPT, Vol. 61, pp. 535-582, 1992.

77. Witczak, M. W., K. Kaloush, T. Pellinen, M. El-Basyouny, and H. Von Quintus, Simple Performance Test for Superpave Mix Design, NCHRP Report 465, Washington D.C., 2002.

78. Witczak, M. W., Simple Performance Tests: Summary of Recommended Methods and Database, NCHRP Report 547, Washington D.C., 2005.

APPENDIX A:
SIF REGRESSION EQUATIONS

The traffic induced SIF regression equations for $K_{bending}$ and $K_{shearing}$ have the same general format but with different coefficients. The detailed 28 regression equations are listed below:

$$K_{bending\,/\,shearing} = K_a\left[K_b\left(\frac{c}{H_1}\right)^3 + K_c\left(\frac{c}{H_1}\right)^2 + K_d\left(\frac{c}{H_1}\right) + K_e\right]$$

1. HMA/PCC: $K_{bending}$ under single axle load of 4 kip

$K_a = \left(-1.90348\ \log H_3 + 8.53231\ (\log E_3)^{-0.70929} + 2.28183\ (\log H_2)^2 - 19.80025\ \log H_2 - 0.62639\ (\log E_2)^2 + 5.17435\ \log E_2 + 31.58444\ \right) \times \left(1.96417\ \log H_1 - 0.22034\ (\log E_1)^2 + 1.18929\ \log E_1 - 7.08381\ \right)$

$K_b = 2.31189 \times 10^{-6}\left(11.54921\,(\log E_1)^2 - 77.21657\ \log E_1 + 0.09053\ f_1^{\ 2} - 16.77605\ f_1 + 110.24069\ \right) \times \left((\log E_3)^{-0.23146} \times (\log E_2)^{9.69177} \times (\log E_1)^{-5.09839} - 22.27888\ \right) \times \left(-6.19651\,(f_0 c)^{-0.766641} + 0.82856\ \right) \times \left(-18.46802\ f_0 - 1.43824 \times 10^{-6}\right)$

$K_c = 0.00848\left(-9.40303\,(\log E_1)^2 + 102.07343\ \log E_1 - 3.80752\ f_1^{\ 2} + 17.65776\ f_1 - 196.75557\ \right) \times \left((\log E_3)^{-2.38626} \times (\log E_2)^{-9.20678} \times (\log E_1)^{7.85167} - 0.02482\ \right) \times \left(0.06128\,(f_0 c)^{1.08723} + 0.41757\ \right) \times \left(27.62788\ f_0 + 4.08544\ \right)$

$K_d = 0.00038\left(-15.38743\,(\log E_1)^2 + 57.02739\ \log E_1 + 4.40866\ f_1^{\ 2} - 90.1837\ f_1 - 89.21533\ \right) \times \left((\log E_3)^{-0.34882} \times (\log E_2)^{5.49464} \times (\log E_1)^{-3.18461} + 21.2543\ \right) \times \left(-0.55426\,(f_0 c)^{0.03018} + 0.61211\ \right) \times \left(9.12541\ f_0 - 0.4001\ \right)$

$K_e = \left(0.00230\,(\log E_1)^2 - 0.01449\ \log E_1 + 0.01279\ \right) \times \left((\log E_3)^{-0.89426} \times (\log E_2)^{-8.21743} \times (\log E_1)^{10.32711} - 2.73609\ \right) + 0.01602$

$$f_0 = (H_1 + H_2)^2 \times \left(1 - \frac{c + H_2}{(H_1 + H_2)}\right)^2 \times \left(\frac{YE_1}{6I}\right),$$

$$f_1 = YE_1\frac{(H_1 + H_2)^2}{I},$$

$$Y = \frac{0.5E_1 H_1^{\ 2} + E_2 H_2 H_1 + 0.5E_2 H_2^{\ 2}}{E_1 H_1 + E_2 H_2},\ \text{and}$$

$$I = E_1\left(\frac{H_1^{\ 3}}{12} + H_1(Y - 0.5H_1)^2\right) + E_2\left(\frac{H_2^{\ 3}}{12} + H_2(Y - H_1 - 0.5H_2)^2\right)$$

2. HMA/PCC: $K_{shearing}$@LTE=0.1 under single axle load of 4 kip

$K_a = \left(-0.01698\ \log H_3 + 10.16702\,(\log E_3)^{-0.01396} - 0.36739\,(\log H_2)^2 + 1.90553\ \log H_2 - 0.23793\,(\log E_2)^2 + 1.99507\ \log E_2 - 16.28099\ \right) \times \left(-3.50564\ \log H_1 + 0.35377\,(\log E_1)^2 - 3.48917\ \log E_1 + 19.35167\ \right)$

$K_b = 0.070\left(20.10845\,(\log E_1)^2 - 116.4504\ \log E_1 - 1.54262\ f_1^{\ 2} + 47.42258\ f_1 + 187.64653\ \right) \times \left((\log E_3)^{-6.05012} \times (\log E_2)^{-2.20509} \times (\log E_1)^{-9.24089} + 1.15895\ \right) \times \left(-8.64519\,(f_0 c)^{-0.00277} \times (f_0(c + H_2))^{0.00555} + 8.62122\ \right)$

$K_c = 0.02168\left(0.08821\,(\log E_1)^2 - 0.82399\ \log E_1 + 0.00671\ f_1^{\ 2} - 0.10975\ f_1 + 2.44584\ \right) \times \left((\log E_3)^{0.56996} \times (\log E_2)^{-0.13358} \times (\log E_1)^{4.78212} + 21.8005\ \right) \times \left(1.10425\,(f_0 c)^{1.84449} \times (f_0(c + H_2))^{-2.08269} - 0.13258\ \right)$

$K_d = 0.00272\left(6.66449\,(\log E_1)^2 + 4.52789\ \log E_1 + 0.22973\ f_1^{\ 2} - 4.82278\ f_1 - 35.56252\ \right) \times \left((\log E_3)^{1.85797} \times (\log E_2)^{-3.52876} \times (\log E_1)^{1.79093} + 5.21028\ \right) \times \left(-0.15933\,(f_0 c)^{-0.67316} \times (f_0(c + H_2))^{1.26974} + 1.44605\ \right)$

$K_e = \left(18.85868\,(\log E_1)^2 - 99.67187\ \log E_1 + 141.55189\ \right) \times \left((\log E_3)^{0.00415} \times (\log E_2)^{-0.04388} \times (\log E_1)^{-0.00805} - 0.90891\ \right) - 0.07492$

3. HMA/PCC: $K_{shearing}$@LTE=0.5 under single axle load of 4 kip

$K_a = \left(-0.0048\ \log H_3 + 5.58859\,(\log E_3)^{-0.0075} - 0.17263\,(\log H_2)^2 + 1.03667\ \log H_2 - 0.12994\,(\log E_2)^2 + 1.14186\ \log E_2 - 9.19424\ \right) \times \left(-1.81576\ \log H_1 + 0.19202\,(\log E_1)^2 - 1.72349\ \log E_1 + 9.54219\ \right)$

$$K_b = 0.02961 \left(9.96516 \left(\log E_1\right)^2 - 62.93739 \log E_1 - 1.35185 f_1^2 + 20.67767 f_1 + 112.17681\right) \times$$
$$\left(\left(\log E_3\right)^{-6.04797} \times \left(\log E_2\right)^{-2.19593} \times \left(\log E_1\right)^{-9.23976} + 0.87743\right) \times \left(-1.03197 \left(f_0 c\right)^{-0.433601} \times \left(f_0 (c + H_2)\right)^{0.73934} + 0.00066\right)$$

$$K_c = 0.07465 \left(-0.24334 \left(\log E_1\right)^2 + 0.33125 \log E_1 + 0.00161 f_1^2 - 0.32309 f_1 + 6.73046\right) \times$$
$$\left(\left(\log E_3\right)^{0.1630} \times \left(\log E_2\right)^{-0.73015} \times \left(\log E_1\right)^{3.79783} + 20.34663\right) \times \left(0.45148 \left(f_0 c\right)^{1.45083} \times \left(f_0 (c + H_2)\right)^{-1.63532} - 0.018633\right)$$

$$K_d = 0.04720 \left(0.85135 \left(\log E_1\right)^2 - 9.85986 \log E_1 - 0.15306 f_1^2 + 2.4536 f_1 + 30.3381\right) \times$$
$$\left(\left(\log E_3\right)^{0.02292} \times \left(\log E_2\right)^{-0.83047} \times \left(\log E_1\right)^{2.61975} - 1.72539\right) \times \left(-0.04471 \left(f_0 c\right)^{-0.69506} \times \left(f_0 (c + H_2)\right)^{1.28512} + 0.64384\right)$$

$$K_e = \left(0.16479 \left(\log E_1\right)^2 - 1.08487 \log E_1 + 3.75761\right) \times \left(\left(\log E_3\right)^{0.03420} \times \left(\log E_2\right)^{-3.83124} \times \left(\log E_1\right)^{3.65864} + 1.09348\right) - 2.29727$$

4. HMA/ PCC: $K_{shearing}$@LTE=0.9 under single axle load of 4 kip

$$K_a = \left(-0.00059 \log H_3 - 0.43625 \left(\log E_3\right)^{-0.24184} + 2.37738 \left(\log H_2\right)^2 - 9.03341 \log H_2 - 0.26536 \left(\log E_2\right)^2 + 1.8638 \log E_2 + 7.28379\right) \times$$
$$\left(-0.62502 \log H_1 + 0.01979 \left(\log E_1\right)^2 - 0.19287 \log E_1 + 2.40979\right)$$

$$K_b = 0.01901 \left(7.38052 \left(\log E_1\right)^2 - 58.53132 \log E_1 - 1.34395 f_1^2 + 14.96708 f_1 + 140.99498\right) \times$$
$$\left(\left(\log E_3\right)^{-6.04734} \times \left(\log E_2\right)^{-2.19439} \times \left(\log E_1\right)^{-9.23887} + 0.49875\right) \times \left(-0.38001 \left(f_0 c\right)^{-0.81122} \times \left(f_0 (c + H_2)\right)^{0.86449} - 0.4158\right)$$

$$K_c = 0.09602 \left(0.92097 \left(\log E_1\right)^2 - 8.95566 \log E_1 + 0.01468 f_1^2 - 0.20671 f_1 + 24.14328\right) \times$$
$$\left(\left(\log E_3\right)^{-0.04331} \times \left(\log E_2\right)^{-0.88889} \times \left(\log E_1\right)^{3.76038} - 1.98467\right) \times \left(0.65317 \left(f_0 c\right)^{2.84659} \times \left(f_0 (c + H_2)\right)^{-3.30948} + 0.10573\right)$$

$$K_d = 0.08609 \left(1.63114 \left(\log E_1\right)^2 - 17.3251 \log E_1 - 0.25799 f_1^2 + 3.54743 f_1 + 41.42112\right) \times$$
$$\left(\left(\log E_3\right)^{0.00269} \times \left(\log E_2\right)^{0.59553} \times \left(\log E_1\right)^{0.51861} - 3.10907\right) \times \left(-0.95472 \left(f_0 c\right)^{0.03744} \times \left(f_0 (c + H_2)\right)^{0.13717} + 1.29626\right)$$

$$K_e = \left(-0.00412 \left(\log E_1\right)^2 + 0.03816 \log E_1 - 0.08359\right) \times \left(\left(\log E_3\right)^{-0.0165} \times \left(\log E_2\right)^{0.02652} \times \left(\log E_1\right)^{2.26417} - 9.4295\right) + 0.05599$$

5. HMA/PCC: $K_{bending}$ under single axle load of 11 kip

$$K_a = \left(-0.02755 \log H_3 + 1.2005 \left(\log E_3\right)^{-0.06237} - 0.07116 \left(\log H_2\right)^2 + 0.29274 \log H_2 - 0.04486 \left(\log E_2\right)^2 + 0.37154 \log E_2 - 2.01772\right) \times$$
$$\left(-7.45084 \log H_1 + 0.67288 \left(\log E_1\right)^2 - 4.77465 \log E_1 + 32.0413\right)$$

$$K_b = 2.56854 \left(-0.6184 \left(\log E_1\right)^2 + 4.10714 \log E_1 + 0.09638 f_1^2 - 0.95616 f_1 - 9.91166\right) \times$$
$$\left(\left(\log E_3\right)^{4.51108} \times \left(\log E_2\right)^{1.16882} \times \left(\log E_1\right)^{-11.32865} + 0.24365\right) \times \left(-0.01556 \left(f_0 c\right)^{-0.28307} + 2.59638\right) \times \left(-62.56222 f_0 + 3.71047\right)$$

$$K_c = 0.22231 \left(10.0003 \left(\log E_1\right)^2 - 49.74886 \log E_1 - 3.64464 f_1^2 + 32.13186 f_1 + 148.15694\right) \times$$
$$\left(\left(\log E_3\right)^{30.45054} \times \left(\log E_2\right)^{-28.08729} \times \left(\log E_1\right)^{-14.7846} + 3.49588\right) \times \left(0.83890 \left(f_0 c\right)^{0.01557} - 1.60196\right) \times \left(6.20685 f_0 - 0.35705\right)$$

$$K_d = 1.1130 \left(-1.79983 \left(\log E_1\right)^2 + 12.56055 \log E_1 - 0.26283 f_1^2 + 3.05612 f_1 - 16.5248\right) \times$$
$$\left(\left(\log E_3\right)^{0.07654} \times \left(\log E_2\right)^{1.44539} \times \left(\log E_1\right)^{0.92036} - 4.67752\right) \times \left(0.69123 \left(f_0 c\right)^{0.01879} - 0.78295\right) \times \left(-8.25861 f_0 + 0.33939\right)$$

$$K_e = \left(-0.45676 \left(\log E_1\right)^2 + 7.68609 \log E_1 - 19.10122\right) \times \left(\left(\log E_3\right)^{-0.59534} \times \left(\log E_2\right)^{-3.26749} \times \left(\log E_1\right)^{3.37262} - 0.42322\right) - 1.43345$$

6. HMA/PCC: $K_{shearing}$@LTE=0.1 under single axle load of 11 kip

$$K_a = \left(-0.07338 \log H_3 + 11.5598 \left(\log E_3\right)^{-0.0644} - 0.45611 \left(\log H_2\right)^2 + 2.43515 \log H_2 - 0.26619 \left(\log E_2\right)^2 + 2.20123 \log E_2 - 17.54896\right) \times$$
$$\left(-3.07743 \log H_1 + 0.8723 \left(\log E_1\right)^2 - 7.52269 \log E_1 + 26.31639\right)$$

$$K_b = 0.13312 \left(23.97659 \left(\log E_1\right)^2 - 126.6412 \log E_1 - 0.95469 f_1^2 + 19.63692 f_1 + 181.49265\right) \times$$
$$\left(\left(\log E_3\right)^{-6.05012} \times \left(\log E_2\right)^{-2.20509} \times \left(\log E_1\right)^{-9.2409} + 1.12153\right) \times \left(-7.1194 \left(f_0 c\right)^{-0.00358} \times \left(f_0 (c + H_2)\right)^{0.00582} + 7.12957\right)$$

$$K_c = 0.07434 \left(-0.11639 \left(\log E_1\right)^2 + 0.95917 \log E_1 + 0.01197 f_1^2 - 0.18571 f_1 - 1.14364\right) \times$$
$$\left(\left(\log E_3\right)^{1.65343} \times \left(\log E_2\right)^{-0.73973} \times \left(\log E_1\right)^{3.30556} + 23.93773\right) \times \left(1.11321 \left(f_0 c\right)^{2.72233} \times \left(f_0 (c + H_2)\right)^{-2.94526} - 0.06675\right)$$

$$K_d = 0.00187 \left(3.53411 \left(\log E_1\right)^2 + 4.74239 \log E_1 - 0.25776 f_1^2 + 4.91515 f_1 - 26.16564\right) \times$$
$$\left(\left(\log E_3\right)^{3.00132} \times \left(\log E_2\right)^{-0.78685} \times \left(\log E_1\right)^{-1.79301} + 4.01988\right) \times \left(-0.11235 \left(f_0 c\right)^{-0.72874} \times \left(f_0 (c + H_2)\right)^{1.44027} + 1.81869\right)$$

$$K_e = \left(18.71178 \left(\log E_1\right)^2 - 102.3362 \log E_1 + 142.82877\right) \times \left(\left(\log E_3\right)^{0.00854} \times \left(\log E_2\right)^{-0.03333} \times \left(\log E_1\right)^{-0.03037} - 0.90116\right) + 0.07349$$

7. HMA/ PCC: $K_{shearing}$@LTE=0.5 under single axle load of 11 kip

$$K_a = \left(-0.00946 \log H_3 + 5.11984 (\log E_3)^{-0.03218} - 0.02057 (\log H_2)^2 + 0.26911 \log H_2 - 0.12821 (\log E_2)^2 + 1.09361 \log E_2 - 7.46192\right) \times$$
$$\left(-1.39658 \log H_1 + 0.29149 (\log E_1)^2 - 3.0240 \log E_1 + 12.21873\right)$$

$$K_b = 0.04913 \left(15.26372 (\log E_1)^2 - 74.11115 \log E_1 - 1.06922 f_1^2 + 11.50655 f_1 + 104.83138\right) \times$$
$$\left((\log E_3)^{-6.04798} \times (\log E_2)^{-2.19593} \times (\log E_1)^{-9.23976} + 0.66497\right) \times \left(-0.95548 (f_0 c)^{-0.69803} \times (f_0 (c + H_2))^{0.96948} - 0.21787\right)$$

$$K_c = 0.13661 \left(-0.47692 (\log E_1)^2 + 4.72075 \log E_1 + 0.18432 f_1^2 - 2.32695 f_1 - 1.76428\right) \times$$
$$\left((\log E_3)^{0.83666} \times (\log E_2)^{-1.07145} \times (\log E_1)^{3.69412} + 11.08637\right) \times \left(0.51909 (f_0 c)^{2.83096} \times (f_0 (c + H_2))^{-3.13385} + 0.00909\right)$$

$$K_d = 0.06424 \left(1.67047 (\log E_1)^2 - 11.6463 \log E_1 - 0.16176 f_1^2 + 2.53335 f_1 + 22.25945\right) \times$$
$$\left((\log E_3)^{0.13258} \times (\log E_2)^{0.33365} \times (\log E_1)^{1.39081} - 1.25694\right) \times \left(-0.06646 (f_0 c)^{-0.57463} \times (f_0 (c + H_2))^{1.18273} + 1.02267\right)$$

$$K_e = \left(0.35632 (\log E_1)^2 - 1.73122 \log E_1 + 2.97347\right) \times \left((\log E_3)^{0.25322} \times (\log E_2)^{-2.10802} \times (\log E_1)^{2.12638} + 0.62706\right) - 0.77658$$

8. HMA/ PCC: $K_{shearing}$@LTE=0.9 under single axle load of 11 kip

$$K_a = \left(-0.00971 \log H_3 - 0.00464 (\log E_3)^{0.64487} + 3.4415 (\log H_2)^2 - 13.86985 \log H_2 - 0.09482 (\log E_2)^2 + 1.34923 \log E_2 + 11.52375\right) \times$$
$$\left(-0.93071 \log H_1 - 0.01349 (\log E_1)^2 + 0.0653 \log E_1 + 3.03339\right)$$

$$K_b = 0.02219 \left(1.36927 (\log E_1)^2 - 43.05297 \log E_1 - 0.98982 f_1^2 + 17.12105 f_1 + 150.10326\right) \times$$
$$\left((\log E_3)^{-6.04736} \times (\log E_2)^{-2.19444} \times (\log E_1)^{-9.23560} + 0.33702\right) \times \left(-0.68725 (f_0 c)^{-0.77567} \times (f_0 (c + H_2))^{0.88305} - 0.81795\right)$$

$$K_c = 0.05985 \left(1.2762 (\log E_1)^2 - 12.51763 \log E_1 - 0.00547 f_1^2 + 0.15191 f_1 + 31.38033\right) \times$$
$$\left((\log E_3)^{-0.00667} \times (\log E_2)^{-1.68585} \times (\log E_1)^{4.74602} + 7.19175\right) \times \left(0.66964 (f_0 c)^{2.73678} \times (f_0 (c + H_2))^{-3.04236} + 0.13023\right)$$

$$K_d = 0.06683 \left(0.47621 (\log E_1)^2 - 14.22563 \log E_1 - 0.36992 f_1^2 + 6.31936 f_1 + 40.58116\right) \times$$
$$\left((\log E_3)^{0.00844} \times (\log E_2)^{0.44572} \times (\log E_1)^{0.12298} - 0.91092\right) \times \left(-0.2315 (f_0 c)^{0.27788} \times (f_0 (c + H_2))^{0.14655} + 0.68522\right)$$

$$K_e = \left(-0.00386 (\log E_1)^2 + 0.02977 \log E_1 - 0.04738\right) \times \left((\log E_3)^{-0.02376} \times (\log E_2)^{0.8960} \times (\log E_1)^{1.11034} - 14.15467\right) + 0.05449$$

9. HMA/PCC: $K_{bending}$ under single axle load of 25 kip

$$K_a = \left(-1.59009 \log H_3 + 7.56701 (\log E_3)^{-0.6674} + 2.96893 (\log H_2)^2 - 20.28556 \log H_2 - 0.60999 (\log E_2)^2 + 4.03891 \log E_2 + 31.07212\right) \times$$
$$\left(1.98818 \log H_1 - 0.19079 (\log E_1)^2 + 1.00802 \log E_1 - 7.69635\right)$$

$$K_b = 2.96229 \times 10^{-6} \left(12.49745 (\log E_1)^2 - 76.53276 \log E_1 + 0.25022 f_1^2 - 16.96003 f_1 + 110.57392\right) \times$$
$$\left((\log E_3)^{0.53825} \times (\log E_2)^{7.75828} \times (\log E_1)^{-3.68777} - 22.2688\right) \times \left(-5.90562 (f_0 c)^{-0.8594} + 1.08551\right) \times \left(-18.40929 f_0 - 1.19046 \times 10^{-6}\right)$$

$$K_c = 0.00347 \left(-8.99407 (\log E_1)^2 + 102.19211 \log E_1 - 3.43843 f_1^2 + 17.73529 f_1 - 196.72086\right) \times$$
$$\left((\log E_3)^{-1.64403} \times (\log E_2)^{-9.21831} \times (\log E_1)^{7.88917} - 0.05954\right) \times \left(0.16176 (f_0 c)^{1.12729} + 1.07685\right) \times \left(27.62636 f_0 + 4.48997\right)$$

$$K_d = 0.00142 \left(-13.66821 (\log E_1)^2 + 57.58068 \log E_1 + 3.02126 f_1^2 - 90.3137 f_1 - 89.04471\right) \times$$
$$\left((\log E_3)^{0.05349} \times (\log E_2)^{4.72188} \times (\log E_1)^{-2.01601} + 21.39837\right) \times \left(-0.36117 (f_0 c)^{0.02547} + 0.40018\right) \times \left(9.05141 f_0 - 0.32865\right)$$

$$K_e = \left(0.02531 (\log E_1)^2 - 0.20209 \log E_1 + 0.37035\right) \times \left((\log E_3)^{-1.66115} \times (\log E_2)^{-7.57507} \times (\log E_1)^{9.82117} - 2.85009\right) + 0.10129$$

10. HMA/PCC: $K_{shearing}$@LTE=0.1 under single axle load of 25 kip

$$K_a = \left(-0.15141 \log H_3 + 17.27324 (\log E_3)^{-0.05921} - 0.77445 (\log H_2)^2 + 3.89532 \log H_2 - 0.37381 (\log E_2)^2 + 2.99431 \log E_2 - 25.66764\right) \times$$
$$\left(-2.56313 \log H_1 + 0.55994 (\log E_1)^2 - 4.32846 \log E_1 + 16.82001\right)$$

$$K_b = 0.17922 \left(37.40871 (\log E_1)^2 - 146.1245 \log E_1 + 0.28832 f_1^2 - 2.32051 f_1 + 149.86813\right) \times$$
$$\left((\log E_3)^{-6.05023} \times (\log E_2)^{-2.20538} \times (\log E_1)^{-9.2411} + 0.98371\right) \times \left(-7.24765 (f_0 c)^{-0.00251} \times (f_0 (c + H_2))^{0.00453} + 7.26426\right)$$

$$K_c = 0.07439 \left(-0.16083 (\log E_1)^2 + 1.2743 \log E_1 + 0.01111 f_1^2 - 0.17319 f_1 - 1.66228\right) \times$$
$$\left((\log E_3)^{2.03291} \times (\log E_2)^{0.19706} \times (\log E_1)^{1.73272} + 56.0789\right) \times \left(1.75965 (f_0 c)^{2.91739} \times (f_0 (c + H_2))^{-3.01957} - 0.11298\right)$$

$$K_d = 0.00184 \left(1.88959 (\log E_1)^2 + 17.33004 \log E_1 - 0.42874 f_1^2 + 5.34377 f_1 - 46.98889\right) \times$$
$$\left((\log E_3)^{3.85238} \times (\log E_2)^{1.17442} \times (\log E_1)^{-5.22868} + 2.75652\right) \times \left(-0.06939 (f_0 c)^{-0.83202} \times (f_0 (c + H_2))^{1.73672} + 3.01159\right)$$

$$K_e = \left(22.82762 \left(\log E_1\right)^2 - 126.2408 \log E_1 + 160.40173\right) \times \left(\left(\log E_3\right)^{0.01281} \times \left(\log E_2\right)^{-0.0005} \times \left(\log E_1\right)^{-0.04283} - 0.93745\right) + 0.73842$$

11. HMA/ PCC: $K_{shearing}$@LTE=0.5 under single axle load of 25 kip

$$K_a = \left(-0.0660 \log H_3 + 17.28467 \left(\log E_3\right)^{-0.01470} - 0.52463 \left(\log H_2\right)^2 + 2.5511 \log H_2 - 0.40555 \left(\log E_2\right)^2 + 3.34952 \log E_2 - 25.81724\right) \times \left(-2.9872 \log H_1 + 2.62969 \left(\log E_1\right)^2 - 23.62902 \log E_1 + 63.6796\right)$$

$$K_b = 0.17909 \left(24.54804 \left(\log E_1\right)^2 - 150.8949 \log E_1 - 0.23748 f_1^2 + 5.5174 f_1 + 241.12163\right) \times \left(\left(\log E_3\right)^{-6.0506} \times \left(\log E_2\right)^{-2.20642} \times \left(\log E_1\right)^{-9.24186} + 1.65719\right) \times \left(-3.82811 \left(f_0 c\right)^{-0.00529} \times \left(f_0 \left(c + H_2\right)\right)^{0.00801} + 3.86846\right)$$

$$K_c = 0.13278 \left(-0.20525 \left(\log E_1\right)^2 + 1.78258 \log E_1 + 0.00466 f_1^2 - 0.11348 f_1 - 3.15131\right) \times \left(\left(\log E_3\right)^{0.59268} \times \left(\log E_2\right)^{-3.2592} \times \left(\log E_1\right)^{5.59839} + 16.78488\right) \times \left(1.19673 \left(f_0 c\right)^{3.15696} \times \left(f_0 \left(c + H_2\right)\right)^{-3.3472} - 0.17659\right)$$

$$K_d = 0.00075 \left(17.21511 \left(\log E_1\right)^2 - 82.03649 \log E_1 - 0.58655 f_1^2 + 3.25517 f_1 + 95.8283\right) \times \left(\left(\log E_3\right)^{0.78578} \times \left(\log E_2\right)^{6.0915} \times \left(\log E_1\right)^{-7.79742} + 2.9515\right) \times \left(-0.06766 \left(f_0 c\right)^{-0.82468} \times \left(f_0 \left(c + H_2\right)\right)^{1.81307} + 4.22114\right)$$

$$K_e = \left(21.72316 \left(\log E_1\right)^2 - 119.8385 \log E_1 + 193.74629\right) \times \left(\left(\log E_3\right)^{-0.00018} \times \left(\log E_2\right)^{-0.00172} \times \left(\log E_1\right)^{-0.02064} - 0.95273\right) - 0.58969$$

12. HMA/ PCC: $K_{shearing}$@LTE=0.9 under single axle load of 25 kip

$$K_a = \left(-0.03405 \log H_3 - 0.22615 \left(\log E_3\right)^{0.46541} + 3.45056 \left(\log H_2\right)^2 - 14.46716 \log H_2 - 0.10155 \left(\log E_2\right)^2 + 1.51617 \log E_2 + 12.62436\right) \times \left(-0.84665 \log H_1 - 0.06379 \left(\log E_1\right)^2 + 0.36125 \log E_1 + 2.58712\right)$$

$$K_b = 0.02751 \left(1.79237 \left(\log E_1\right)^2 - 43.49006 \log E_1 - 0.94816 f_1^2 + 15.65179 f_1 + 149.21072\right) \times \left(\left(\log E_3\right)^{-6.04733} \times \left(\log E_2\right)^{-2.19437} \times \left(\log E_1\right)^{-9.23885} + 0.33926\right) \times \left(-0.33469 \left(f_0 c\right)^{-1.02115} \times \left(f_0 \left(c + H_2\right)\right)^{1.25486} - 2.31003\right)$$

$$K_c = 0.05469 \left(1.8317 \left(\log E_1\right)^2 - 17.1901 \log E_1 - 0.00156 f_1^2 - 8.925 \times 10^{-5} f_1 + 42.14414\right) \times \left(\left(\log E_3\right)^{0.04507} \times \left(\log E_2\right)^{-2.60217} \times \left(\log E_1\right)^{5.65211} + 12.8759\right) \times \left(0.64273 \left(f_0 c\right)^{2.06494} \times \left(f_0 \left(c + H_2\right)\right)^{-2.18302} + 0.13399\right)$$

$$K_d = 0.07208 \left(-0.54590 \left(\log E_1\right)^2 - 12.16223 \log E_1 - 0.52686 f_1^2 + 9.34756 f_1 + 42.86897\right) \times \left(\left(\log E_3\right)^{0.01368} \times \left(\log E_2\right)^{-0.49886} \times \left(\log E_1\right)^{1.04254} - 0.47491\right) \times \left(-0.15545 \left(f_0 c\right)^{1.36823} \times \left(f_0 \left(c + H_2\right)\right)^{-0.86179} + 0.41446\right)$$

$$K_e = \left(-0.00767 \left(\log E_1\right)^2 + 0.06934 \log E_1 - 0.14319\right) \times \left(\left(\log E_3\right)^{-0.04974} \times \left(\log E_2\right)^{1.09889} \times \left(\log E_1\right)^{0.96178} - 14.04835\right) + 0.05136$$

13. HMA/HMA: $K_{bending}$ under single axle load of 4 kip

$$K_a = \left(-0.05252 \log H_3 - 1.22 \times 10^{-5} \left(\log E_3\right)^{5.87798} + 0.08591 \left(\log H_2\right)^2 - 0.74272 \log H_2 + 0.00943 \left(\log E_2\right)^2 - 0.26356 \log E_2 + 2.67176\right) \times \left(4.75148 \log H_1 - 0.03872 \left(\log E_1\right)^2 + 0.5046 \log E_1 - 15.90641\right)$$

$$K_b = -0.00357 \left(277.45557 \left(\log E_1\right)^3 - 496.33983 \left(\log E_1\right)^2 + 2054.87873 \log E_1 - 0.48288 f_1^3 + 36.40586 f_1^2 - 449.1456 f_1 + 1710.69965\right) \times \left(\left(\log E_3\right)^{-0.0019} \times \left(\log E_2\right)^{-1.05248} \times \left(\log E_1\right)^{1.03537} - 0.83397\right) \times \left(-2.82254 \left(f_0 c\right)^{-0.01342} + 2.67325\right) \times \left(4.2345 f_0 + 0.41274\right)$$

$$K_c = 0.02381 \left(-243.66645 \left(\log E_1\right)^3 + 860.45943 \left(\log E_1\right)^2 + 68.23062 \log E_1 + 0.18133 f_1^3 - 8.43428 f_1^2 - 344.0575 f_1 - 157.29354\right) \times \left(\left(\log E_3\right)^{-2.28688} \times \left(\log E_2\right)^{1.76479} \times \left(\log E_1\right)^{2.00905} + 0.32747\right) \times \left(-0.03229 \left(f_0 c\right)^{-0.19854} + 0.01580\right) \times \left(-0.48647 f_0 - 0.00156\right)$$

$$K_d = -0.4741 \left(71.7148 \left(\log E_1\right)^3 - 591.50861 \left(\log E_1\right)^2 + 1697.46024 \log E_1 - 0.0083 f_1^3 + 0.51104 f_1^2 + 13.54099 f_1 - 1613.60936\right) \times \left(\left(\log E_3\right)^{-0.14965} \times \left(\log E_2\right)^{1.038382} \times \left(\log E_1\right)^{-0.78104} - 1.01793\right) \times \left(-0.8808 \left(f_0 c\right)^{-0.01078} + 0.85126\right) \times \left(-1.46977 f_0 + 0.63205\right)$$

$$K_e = \left(0.96428 \left(\log E_1\right)^3 - 11.00938 \left(\log E_1\right)^2 + 40.08213 \log E_1 - 47.88308\right) \times \left(\left(\log E_3\right)^{-0.18548} \times \left(\log E_2\right)^{-0.30224} \times \left(\log E_1\right)^{0.78683} - 1.61323\right) - 0.16397$$

14. HMA/HMA: $K_{shearing}$@LTE=0.1 under single axle load of 4 kip

$$K_a = \left(-0.25362 \log H_3 + 2.08167 \left(\log E_3\right)^{2.39253} - 0.20728 \left(\log H_2\right)^2 - 1.62929 \log H_2 - 0.33835 \left(\log E_2\right)^2 + 3.10054 \log E_2 + 0.45613\right) \times \left(-1.03698 \log H_1 + 0.22059 \left(\log E_1\right)^2 - 2.03303 \log E_1 + 8.05821\right)$$

$$K_b = 0.08749 \left(-0.69774 \left(\log E_1\right)^2 + 4.12232 \log E_1 + 0.00063 f_1^2 + 0.02119 f_1 - 2.03969\right) \times \left(\left(\log E_3\right)^{-2.38414} \times \left(\log E_2\right)^{1.59461} \times \left(\log E_1\right)^{2.05104} + 0.30209\right) \times \left(1.30786 \left(f_0 c\right)^{-0.00622} \times \left(f_0 \left(c + H_2\right)\right)^{-0.00034} - 1.25464\right)$$

$$K_c = 0.00133 \left(11.65096 \left(\log E_1\right)^2 - 124.9557 \log E_1 - 0.00291 f_1^2 + 0.18944 f_1 + 340.9923\right) \times \left(\left(\log E_3\right)^{-2.34487} \times \left(\log E_2\right)^{1.01147} \times \left(\log E_1\right)^{5.02187} - 0.12645\right) \times \left(-0.5756 \left(f_0 c\right)^{-0.0058} \times \left(f_0 \left(c + H_2\right)\right)^{-0.0023} + 0.54927\right)$$

$$K_d = 0.42122 \left(-3.6588 \left(\log E_1\right)^2 + 30.26805 \log E_1 - 0.00655 f_1^2 + 0.31109 f_1 - 48.71764\right) \times$$
$$\left(\left(\log E_3\right)^{-2.25754} \times \left(\log E_2\right)^{0.06008} \times \left(\log E_1\right)^{0.97808} - 0.02683\right) \times \left(-0.84733 \left(f_0 c\right)^{0.00045} \times \left(f_0(c + H_2)\right)^{0.02479} + 0.94873\right)$$

$$K_e = \left(0.00134 \left(\log E_1\right)^2 - 0.00899 \log E_1 + 0.03398\right) \times$$
$$\left(\left(\log E_3\right)^{-1.71559} \times \left(\log E_2\right)^{-0.56227} \times \left(\log E_1\right)^{1.13325} + 0.38264\right) - 0.00946$$

15. HMA/HMA: $K_{shearing}$@LTE=0.5 under single axle load of 4 kip

$$K_a = \left(-0.00986 \log H_3 + 0.90734 \left(\log E_3\right)^{0.38274} + 0.14388 \left(\log H_2\right)^2 - 0.70405 \log H_2 - 0.07086 \left(\log E_2\right)^2 + 1.02384 \log E_2 - 1.32321\right) \times$$
$$\left(-2.85633 \log H_1 + 0.28584 \left(\log E_1\right)^2 - 4.18151 \log E_1 + 22.11071\right)$$

$$K_b = 0.06254 \left(19.68167 \left(\log E_1\right)^2 - 120.1195 \log E_1 - 0.40874 f_1^2 + 18.46264 f_1 + 178.11897\right) \times$$
$$\left(\left(\log E_3\right)^{-0.47287} \times \left(\log E_2\right)^{-5.97146} \times \left(\log E_1\right)^{5.86281} - 2.72206\right) \times \left(0.00060 \left(f_0 c\right)^{1.54963} \times \left(f_0(c + H_2)\right)^{-2.67645} + 0.00054\right)$$

$$K_c = 0.17937 \left(-5.74041 \left(\log E_1\right)^2 + 30.51131 \log E_1 + 0.00479 f_1^2 - 1.29726 f_1 - 56.7776\right) \times$$
$$\left(\left(\log E_3\right)^{-0.67941} \times \left(\log E_2\right)^{0.95432} \times \left(\log E_1\right)^{-0.13189} + 0.23393\right) \times \left(-0.65909 \left(f_0 c\right)^{0.02416} \times \left(f_0(c + H_2)\right)^{-0.02814} + 0.66709\right)$$

$$K_d = 0.03634 \left(20.31178 \left(\log E_1\right)^2 - 116.6417 \log E_1 - 0.04763 f_1^2 + 4.3878 f_1 + 210.44556\right) \times$$
$$\left(\left(\log E_3\right)^{-0.45885} \times \left(\log E_2\right)^{-0.76856} \times \left(\log E_1\right)^{1.03117} + 0.08379\right) \times \left(-0.24762 \left(f_0 c\right)^{0.01587} \times \left(f_0(c + H_2)\right)^{0.07734} + 0.39141\right)$$

$$K_e = \left(-0.0077 \left(\log E_1\right)^2 + 0.06989 \log E_1 - 0.12825\right) \times$$
$$\left(\left(\log E_3\right)^{-0.90917} \times \left(\log E_2\right)^{-0.01008} \times \left(\log E_1\right)^{0.46891} + 0.22915\right) - 0.00633$$

16. HMA/HMA: $K_{shearing}$@LTE=0.9 under single axle load of 4 kip

$$K_a = \left(-0.00448 \log H_3 + 1.12399 \left(\log E_3\right)^{-0.01381} + 0.49475 \left(\log H_2\right)^2 - 1.64397 \log H_2 + 0.30167 \left(\log E_2\right)^2 - 3.17681 \log E_2 + 9.2747\right) \times$$
$$\left(-3.87817 \log H_1 + 0.19054 \left(\log E_1\right)^2 - 2.93382 \log E_1 + 22.19114\right)$$

$$K_b = 0.02779 \left(20.72526 \left(\log E_1\right)^2 - 132.8729 \log E_1 + 0.46138 f_1^2 + 0.10336 f_1 + 212.10945\right) \times$$
$$\left(\left(\log E_3\right)^{-0.06044} \times \left(\log E_2\right)^{-3.32362} \times \left(\log E_1\right)^{3.42512} - 4.54379\right) \times \left(0.00083 \left(f_0 c\right)^{2.46450} \times \left(f_0(c + H_2)\right)^{-4.37909} - 2.297 \times 10^{-5}\right)$$

$$K_c = 0.10617 \left(-7.43314 \left(\log E_1\right)^2 + 38.07914 \log E_1 + 0.05375 f_1^2 - 1.56131 f_1 - 51.7185\right) \times$$
$$\left(\left(\log E_3\right)^{-0.07207} \times \left(\log E_2\right)^{4.58804} \times \left(\log E_1\right)^{-3.68022} + 1.09586\right) \times \left(-0.76512 \left(f_0 c\right)^{0.02549} \times \left(f_0(c + H_2)\right)^{-0.03206} + 0.75805\right)$$

$$K_d = 0.02946 \left(30.21583 \left(\log E_1\right)^2 - 163.4199 \log E_1 - 0.09617 f_1^2 + 3.00014 f_1 + 234.61604\right) \times$$
$$\left(\left(\log E_3\right)^{-0.05277} \times \left(\log E_2\right)^{2.79352} \times \left(\log E_1\right)^{-3.13565} + 0.42444\right) \times \left(-0.08229 \left(f_0 c\right)^{0.14776} \times \left(f_0(c + H_2)\right)^{0.05842} + 0.25152\right)$$

$$K_e = \left(-0.00099 \left(\log E_1\right)^2 + 0.00528 \log E_1 - 0.00181\right) \times$$
$$\left(\left(\log E_3\right)^{-4.94006} \times \left(\log E_2\right)^{0.27836} \times \left(\log E_1\right)^{-1.06115} + 3.95376\right) - 0.02872$$

17. HMA/HMA: $K_{bending}$ under single axle load of 11 kip

$$K_a = \left(-0.06872 \log H_3 - 4.61 \times 10^{-5} \left(\log E_3\right)^{6.63409} - 0.0185 \left(\log H_2\right)^2 - 0.18205 \log H_2 + 0.05116 \left(\log E_2\right)^2 - 0.58393 \log E_2 + 2.58659\right) \times$$
$$\left(3.22083 \log H_1 + 0.65928 \left(\log E_1\right)^2 - 4.85795 \log E_1 - 1.53084\right)$$

$$K_b = -0.00684 \left(190.99435 \left(\log E_1\right)^3 - 490.41877 \left(\log E_1\right)^2 + 2065.3912 \log E_1 - 0.13116 f_1^3 + 13.83791 f_1^2 - 537.9968 f_1 + 1716.0663\right) \times$$
$$\left(\left(\log E_3\right)^{-0.03204} \times \left(\log E_2\right)^{-1.72406} \times \left(\log E_1\right)^{2.07277} - 0.99741\right) \times \left(-2.08483 \left(f_0 c\right)^{-0.01541} + 1.85738\right) \times \left(-1.08727 f_0 + 0.17316\right)$$

$$K_c = 0.05271 \left(-313.83408 \left(\log E_1\right)^3 + 858.12774 \left(\log E_1\right)^2 + 73.53398 \log E_1 - 0.62939 f_1^3 + 32.43389 f_1^2 - 344.3485 f_1 - 153.9022\right) \times$$
$$\left(\left(\log E_3\right)^{-2.40412} \times \left(\log E_2\right)^{-0.2302} \times \left(\log E_1\right)^{4.66286} - 65.7832\right) \times \left(-0.02337 \left(f_0 c\right)^{-0.47477} + 0.00521\right) \times \left(-0.17784 f_0 - 6.25 \times 10^{-5}\right)$$

$$K_d = -0.6025 \left(63.42146 \left(\log E_1\right)^3 - 555.5775 \left(\log E_1\right)^2 + 1657.60956 \log E_1 + 0.01294 f_1^3 - 0.63723 f_1^2 + 17.72297 f_1 - 1658.08317\right) \times$$
$$\left(\left(\log E_3\right)^{-0.65526} \times \left(\log E_2\right)^{2.55849} \times \left(\log E_1\right)^{-1.92916} - 0.49831\right) \times \left(-1.14686 \left(f_0 c\right)^{-0.00825} + 1.10105\right) \times \left(-14.51306 f_0 + 0.50026\right)$$

$$K_e = \left(-2.10048 \left(\log E_1\right)^3 + 20.58267 \left(\log E_1\right)^2 - 70.0502 \log E_1 + 77.34962\right) \times$$
$$\left(\left(\log E_3\right)^{-0.06565} \times \left(\log E_2\right)^{-0.32633} \times \left(\log E_1\right)^{0.90833} - 2.4995\right) - 2.60032$$

18. HMA/HMA: $K_{shearing}$@LTE=0.1 under single axle load of 11 kip

$$K_a = \left(- 0.15651 \log H_3 + 3.52591 \left(\log E_3\right)^{0.82285} + 0.15122 \left(\log H_2\right)^2 - 2.3658 \log H_2 - 0.26456 \left(\log E_2\right)^2 + 1.36357 \log E_2 + 1.36517\right) \times$$
$$\left(- 2.16584 \log H_1 + 3.06563 \left(\log E_1\right)^2 - 27.65561 \log E_1 + 71.29689\right)$$

$$K_b = -0.54747 \left(- 70.5829 \left(\log E_1\right)^2 + 511.24369 \log E_1 - 3.5442 f_1^2 + 21.64672 f_1 - 951.3629\right) \times$$
$$\left(\left(\log E_3\right)^{-0.50272} \times \left(\log E_2\right)^{1.71319} \times \left(\log E_1\right)^{-0.06992} - 2.18504\right) \times \left(- 0.46422 \left(f_0 c\right)^{-0.00022} \times \left(f_0\left(c + H_2\right)\right)^{0.00029} + 0.46445\right)$$

$$K_c = 2.41178 \left(- 31.10325 \left(\log E_1\right)^2 + 256.18702 \log E_1 + 0.03917 f_1^2 - 4.50218 f_1 - 466.8060\right) \times$$
$$\left(\left(\log E_3\right)^{0.96032} \times \left(\log E_2\right)^{-0.97178} \times \left(\log E_1\right)^{-1.65793} - 0.17048\right) \times \left(0.17264 \left(f_0 c\right)^{-0.0306} \times \left(f_0\left(c + H_2\right)\right)^{0.02872} - 0.17143\right)$$

$$K_d = -0.00457 \left(133.14801 \left(\log E_1\right)^2 - 555.9144 \log E_1 - 0.22595 f_1^2 + 14.03909 f_1 - 891.1816\right) \times$$
$$\left(\left(\log E_3\right)^{-1.35729} \times \left(\log E_2\right)^{-0.08878} \times \left(\log E_1\right)^{5.4597} - 30.21462\right) \times \left(- 0.00254 \left(f_0 c\right)^{0.01727} \times \left(f_0\left(c + H_2\right)\right)^{-0.00643} + 0.00264\right)$$

$$K_e = \left(0.00584 \left(\log E_1\right)^2 + 0.00554 \log E_1 + 0.11714\right) \times$$
$$\left(\left(\log E_3\right)^{-0.06402} \times \left(\log E_2\right)^{0.0141} \times \left(\log E_1\right)^{0.42134} - 2.26398\right) + 0.14679$$

19. HMA/HMA: $K_{shearing}$@LTE=0.5 under single axle load of 11 kip

$$K_a = \left(- 0.03927 \log H_3 + 5.14713 \left(\log E_3\right)^{0.18757} + 1.68261 \left(\log H_2\right)^2 - 10.67113 \log H_2 + 0.41443 \left(\log E_2\right)^2 - 3.70245 \log E_2 + 20.49937\right) \times$$
$$\left(3.47168 \log H_1 + 1.11061 \left(\log E_1\right)^2 - 4.27671 \log E_1 + 0.96995\right)$$

$$K_b = -0.19635 \left(3.62164 \left(\log E_1\right)^2 - 35.03714 \log E_1 + 0.02328 f_1^2 - 0.9523 f_1 + 91.14535\right) \times$$
$$\left(\left(\log E_3\right)^{-0.60378} \times \left(\log E_2\right)^{0.95087} \times \left(\log E_1\right)^{4.13961} - 53.31032\right) \times \left(- 0.0003 \left(f_0 c\right)^{0.08425} \times \left(f_0\left(c + H_2\right)\right)^{0.01613} + 0.00051\right)$$

$$K_c = 3.08003 \left(9.65988 \left(\log E_1\right)^2 - 115.5829 \log E_1 + 0.23496 f_1^2 - 7.19689 f_1 + 333.9242\right) \times$$
$$\left(\left(\log E_3\right)^{-0.48091} \times \left(\log E_2\right)^{0.52344} \times \left(\log E_1\right)^{3.27608} - 9.1144\right) \times \left(- 8.8301 \times 10^{-5} \left(f_0 c\right)^{0.03716} \times \left(f_0\left(c + H_2\right)\right)^{-0.02033} + 9.41802 \times 10^{-5}\right)$$

$$K_d = -0.00094 \left(37.68645 \left(\log E_1\right)^2 - 67.13976 \log E_1 - 3.05399 f_1^2 + 111.03316 f_1 + 213.90082\right) \times$$
$$\left(\left(\log E_3\right)^{-1.04923} \times \left(\log E_2\right)^{1.81707} \times \left(\log E_1\right)^{-0.33607} + 2.01981\right) \times \left(- 0.24201 \left(f_0 c\right)^{-0.05853} \times \left(f_0\left(c + H_2\right)\right)^{0.01783} + 0.20469\right)$$

$$K_e = \left(0.12189 \left(\log E_1\right)^2 - 0.3135 \log E_1 + 1.54335\right) \times$$
$$\left(\left(\log E_3\right)^{-0.00079} \times \left(\log E_2\right)^{0.00068} \times \left(\log E_1\right)^{0.26661} - 1.78338\right) + 0.75669$$

20. HMA/HMA: $K_{shearing}$@LTE=0.9 under single axle load of 11 kip

$$K_a = \left(0.03448 \log H_3 + 3.78722 \left(\log E_3\right)^{0.15242} + 1.65821 \left(\log H_2\right)^2 - 11.12548 \log H_2 - 0.21417 \left(\log E_2\right)^2 + 2.16612 \log E_2 + 11.43144\right) \times$$
$$\left(6.14065 \log H_1 + 0.93017 \left(\log E_1\right)^2 - 6.05325 \log E_1 + 3.29689\right)$$

$$K_b = -0.28207 \left(3.42472 \left(\log E_1\right)^2 - 32.98212 \log E_1 - 0.01671 f_1^2 + 0.71427 f_1 + 78.74759\right) \times$$
$$\left(\left(\log E_3\right)^{-0.16967} \times \left(\log E_2\right)^{-1.7177} \times \left(\log E_1\right)^{6.94307} - 69.12079\right) \times \left(0.00011 \left(f_0 c\right)^{0.36575} \times \left(f_0\left(c + H_2\right)\right)^{-0.39758} - 6.6169 \times 10^{-5}\right)$$

$$K_c = 1.45531 \left(4.63236 \left(\log E_1\right)^2 - 87.85419 \log E_1 + 0.68142 f_1^2 - 22.8454 f_1 + 350.2079\right) \times$$
$$\left(\left(\log E_3\right)^{-0.08514} \times \left(\log E_2\right)^{-1.46708} \times \left(\log E_1\right)^{4.28468} + 50.40254\right) \times \left(- 7.1 \times 10^{-5} \left(f_0 c\right)^{0.08161} \times \left(f_0\left(c + H_2\right)\right)^{-0.07609} + 6.74149 \times 10^{-5}\right)$$

$$K_d = -0.00036 \left(- 0.72079 \left(\log E_1\right)^2 - 10.25049 \log E_1 - 4.34197 f_1^2 + 172.50213 f_1 + 248.75293\right) \times$$
$$\left(\left(\log E_3\right)^{-0.41439} \times \left(\log E_2\right)^{-2.74040} \times \left(\log E_1\right)^{3.12917} + 2.29387\right) \times \left(- 0.45963 \left(f_0 c\right)^{-0.04875} \times \left(f_0\left(c + H_2\right)\right)^{0.00278} + 0.36963\right)$$

$$K_e = \left(0.18945 \left(\log E_1\right)^2 - 0.58631 \log E_1 + 2.07336\right) \times$$
$$\left(\left(\log E_3\right)^{-0.0004} \times \left(\log E_2\right)^{0.00033} \times \left(\log E_1\right)^{0.28628} - 1.81235\right) + 0.89414$$

21. HMA/HMA: $K_{bending}$ under single axle load of 18 kip

$$K_a = \left(- 0.09242 \log H_3 - 1.18 \times 10^{-5} \left(\log E_3\right)^{6.48058} - 0.10454 \left(\log H_2\right)^2 + 0.18417 \log H_2 + 0.02864 \left(\log E_2\right)^2 - 0.40149 \log E_2 + 1.97797\right) \times$$
$$\left(3.1272 \log H_1 + 0.93548 \left(\log E_1\right)^2 - 6.91426 \log E_1 + 1.95471\right)$$

$$K_b = -0.00882 \left(165.0092 \left(\log E_1\right)^3 - 524.89385 \left(\log E_1\right)^2 + 2046.214 \log E_1 - 0.17238 f_1^3 + 17.5757 f_1^2 - 649.209 f_1 + 1707.6908\right) \times$$
$$\left(\left(\log E_3\right)^{-0.07881} \times \left(\log E_2\right)^{-2.34961} \times \left(\log E_1\right)^{2.71773} - 0.76178\right) \times \left(- 2.29903 \left(f_0 c\right)^{-0.01144} + 2.13106\right) \times \left(- 1.69078 f_0 + 0.15602\right)$$

$K_c = 0.06041 \left(-271.68023 \left(\log E_1\right)^3 + 872.97923 \left(\log E_1\right)^2 + 276.70882 \log E_1 - 0.32215 f_1^3 + 21.28383 f_1^2 - 338.1063 f_1 - 153.6350\right) \times$
$\left(\left(\log E_3\right)^{-2.48261} \times \left(\log E_2\right)^{0.25563} \times \left(\log E_1\right)^{4.15246} - 70.7501\right) \times \left(-0.04634 \left(f_0 c\right)^{-0.45602} + 0.01059\right) \times \left(-0.17169 f_0 - 6.62 \times 10^{-5}\right)$

$K_d = -0.5376 \left(63.7932 \left(\log E_1\right)^3 - 558.7085 \left(\log E_1\right)^2 + 1658.59933 \log E_1 - 0.00454 f_1^3 + 0.14485 f_1^2 + 12.62481 f_1 - 1648.59158\right) \times$
$\left(\left(\log E_3\right)^{-0.81483} \times \left(\log E_2\right)^{2.9928} \times \left(\log E_1\right)^{-2.40889} - 0.22738\right) \times \left(-1.36094 \left(f_0 c\right)^{-0.0084} + 1.30369\right) \times \left(-16.91574 f_0 + 0.54281\right)$

$K_d = -0.5376 \left(63.7932 \left(\log E_1\right)^3 - 558.7085 \left(\log E_1\right)^2 + 1658.59933 \log E_1 - 0.00454 f_1^3 + 0.14485 f_1^2 + 12.62481 f_1 - 1648.59158\right) \times$
$\left(\left(\log E_3\right)^{-0.81483} \times \left(\log E_2\right)^{2.9928} \times \left(\log E_1\right)^{-2.40889} - 0.22738\right) \times \left(-1.36094 \left(f_0 c\right)^{-0.0084} + 1.30369\right) \times \left(-16.91574 f_0 + 0.54281\right)$

$K_e = \left(-2.31219 \left(\log E_1\right)^3 + 22.71251 \left(\log E_1\right)^2 - 76.8795 \log E_1 + 84.89029\right) \times \left(\left(\log E_3\right)^{-0.09898} \times \left(\log E_2\right)^{-0.37026} \times \left(\log E_1\right)^{0.89553} - 2.19459\right) - 1.3488$

22. HMA/HMA: $K_{shearing}$@LTE=0.1 under single axle load of 18 kip

$K_a = \left(-0.18193 \log H_3 + 1.2049 \left(\log E_3\right)^{1.5888} - 0.1285 \left(\log H_2\right)^2 - 1.1777 \log H_2 - 0.2594 \left(\log E_2\right)^2 + 1.7982 \log E_2 + 1.1992\right) \times$
$\left(-1.0568 \log H_1 + 0.3687 \left(\log E_1\right)^2 - 3.2755 \log E_1 + 10.9943\right)$

$K_b = 0.20052 \left(-1.3169 \left(\log E_1\right)^2 + 8.7084 \log E_1 - 0.0014 f_1^2 + 0.0667 f_1 - 9.0007\right) \times$
$\left(\left(\log E_3\right)^{-1.26714} \times \left(\log E_2\right)^{-1.19578} \times \left(\log E_1\right)^{3.7822} - 0.26406\right) \times \left(1.41502 \left(f_0 c\right)^{0.02073} \times \left(f_0 \left(c + H_2\right)\right)^{-0.1102} - 1.0240\right)$

$K_c = 0.00399 \left(9.0683 \left(\log E_1\right)^2 - 103.134 \log E_1 - 0.0063 f_1^2 + 0.27698 f_1 + 294.593\right) \times$
$\left(\left(\log E_3\right)^{-1.2782} \times \left(\log E_2\right)^{-1.1283} \times \left(\log E_1\right)^{6.37136} - 5.1019\right) \times \left(-0.5775 \left(f_0 c\right)^{0.0192} \times \left(f_0 \left(c + H_2\right)\right)^{-0.0823} + 0.47432\right)$

$K_d = 0.49627 \left(-5.2237 \left(\log E_1\right)^2 + 43.2265 \log E_1 - 0.00388 f_1^2 + 0.12413 f_1 - 71.5511\right) \times$
$\left(\left(\log E_3\right)^{-1.46209} \times \left(\log E_2\right)^{-0.60894} \times \left(\log E_1\right)^{1.36839} - 0.05645\right) \times \left(-0.86322 \left(f_0 c\right)^{0.00337} \times \left(f_0 \left(c + H_2\right)\right)^{0.08527} + 1.11734\right)$

$K_e = \left(-0.03035 \left(\log E_1\right)^2 + 0.24665 \log E_1 - 0.36381\right) \times \left(\left(\log E_3\right)^{-1.8449} \times \left(\log E_2\right)^{0.24161} \times \left(\log E_1\right)^{1.35257} - 0.32039\right) + 0.00631$

23. HMA/HMA: $K_{shearing}$@LTE=0.5 under single axle load of 18 kip

$K_a = \left(-0.003698 \log H_3 + 2.81679 \left(\log E_3\right)^{1.25962} + 0.65865 \left(\log H_2\right)^2 - 3.3641 \log H_2 + 0.05146 \left(\log E_2\right)^2 - 0.57978 \log E_2 + 1.80579\right) \times$
$\left(-1.15567 \log H_1 + 2.27401 \left(\log E_1\right)^2 - 21.38891 \log E_1 + 54.4086\right)$

$K_b = 0.06385 \left(19.27122 \left(\log E_1\right)^2 - 115.1545 \log E_1 + 0.02078 f_1^2 + 2.36956 f_1 + 169.5806\right) \times$
$\left(\left(\log E_3\right)^{-2.35593} \times \left(\log E_2\right)^{-0.42318} \times \left(\log E_1\right)^{3.68446} - 2.21843\right) \times \left(0.00085 \left(f_0 c\right)^{0.59864} \times \left(f_0 \left(c + H_2\right)\right)^{-1.37151} + 0.00566\right)$

$K_c = 0.19779 \left(-4.70092 \left(\log E_1\right)^2 + 22.66984 \log E_1 + 0.00432 f_1^2 - 0.42336 f_1 - 26.6458\right) \times$
$\left(\left(\log E_3\right)^{-2.89578} \times \left(\log E_2\right)^{2.37071} \times \left(\log E_1\right)^{0.06911} - 0.17879\right) \times \left(-1.11596 \left(f_0 c\right)^{0.03845} \times \left(f_0 \left(c + H_2\right)\right)^{-0.04555} + 1.18087\right)$

$K_d = 0.06217 \left(33.31007 \left(\log E_1\right)^2 - 187.3846 \log E_1 - 0.04581 f_1^2 + 1.56132 f_1 + 268.966\right) \times$
$\left(\left(\log E_3\right)^{-3.36822} \times \left(\log E_2\right)^{0.94154} \times \left(\log E_1\right)^{0.18367} + 0.02315\right) \times \left(-0.14565 \left(f_0 c\right)^{0.11908} \times \left(f_0 \left(c + H_2\right)\right)^{0.25023} + 0.9608\right)$

$K_e = \left(0.06685 \left(\log E_1\right)^2 - 0.38486 \log E_1 + 0.55959\right) \times \left(\left(\log E_3\right)^{-2.98043} \times \left(\log E_2\right)^{2.23116} \times \left(\log E_1\right)^{-0.53536} - 0.01971\right) + 0.00061$

24. HMA/HMA: $K_{shearing}$@LTE=0.9 under single axle load of 18 kip

$K_a = \left(-0.03372 \log H_3 + 3.61517 \left(\log E_3\right)^{0.39514} + 0.69029 \left(\log H_2\right)^2 - 4.5708 \log H_2 + 0.08537 \left(\log E_2\right)^2 - 0.54853 \log E_2 + 5.59021\right) \times$
$\left(1.38326 \log H_1 + 0.44852 \left(\log E_1\right)^2 - 2.02384 \log E_1 + 0.82749\right)$

$K_b = -1.16296 \left(-0.19772 \left(\log E_1\right)^2 + 3.59637 \log E_1 - 0.08219 f_1^2 + 3.18523 f_1 - 7.44357\right) \times$
$\left(\left(\log E_3\right)^{-0.82282} \times \left(\log E_2\right)^{-1.06221} \times \left(\log E_1\right)^{-0.31239} - 0.01514\right) \times \left(-0.01003 \left(f_0 c\right)^{-0.59021} + 0.15167\right)$

$K_c = 0.48455 \left(10.15602 \left(\log E_1\right)^2 - 109.6302 \log E_1 - 0.09097 f_1^2 + 4.05044 f_1 + 298.3276\right) \times$
$\left(\left(\log E_3\right)^{-0.89979} \times \left(\log E_2\right)^{-0.8055} \times \left(\log E_1\right)^{1.37894} + 0.07573\right) \times \left(1.71143 \left(f_0 c\right)^{-0.0027} - 1.69622\right)$

$K_d = -0.0181 \left(22.15799 \left(\log E_1\right)^2 - 151.9949 \log E_1 + 0.55888 f_1^2 - 22.28526 f_1 + 231.7873\right) \times$
$\left(\left(\log E_3\right)^{-0.56642} \times \left(\log E_2\right)^{-0.49595} \times \left(\log E_1\right)^{0.14085} - 0.15326\right) \times \left(-0.12396 \left(f_0 c\right)^{-0.43348} + 0.58385\right)$

$K_e = \left(0.20972 \left(\log E_1\right)^2 - 0.99724 \log E_1 + 1.97168\right) \times \left(\left(\log E_3\right)^{0.00593} \times \left(\log E_2\right)^{0.02992} \times \left(\log E_1\right)^{0.32181} - 1.91878\right) + 0.37692$

25. HMA/HMA: $K_{bending}$ under single axle load of 25 kip

$$K_a = \left(-0.14151 \log H_3 - 3.735 \times 10^{-5} (\log E_3)^{6.08041} - 0.222136 (\log H_2)^2 + 0.63096 \log H_2 + 0.02262 (\log E_2)^2 - 0.39024 \log E_2 + 1.95566 \right) \times$$
$$\left(3.01154 \log H_1 + 1.21346 (\log E_1)^2 - 9.10516 \log E_1 + 6.13147 \right)$$

$$K_b = -0.01521 \left(216.98134 (\log E_1)^3 - 604.20498 (\log E_1)^2 + 2007.9248 \log E_1 - 0.10538 f_1^3 + 15.56618 f_1^2 - 764.8393 f_1 + 1694.4212 \right) \times$$
$$\left((\log E_3)^{-0.06823} \times (\log E_2)^{-2.69978} \times (\log E_1)^{2.62246} - 0.45315 \right) \times \left(-4.09712 (f_0 c)^{-0.00815} + 3.91613 \right) \times (-1.52785 f_0 + 0.08451)$$

$$K_c = 0.07888 \left(-292.33899 (\log E_1)^3 + 949.0045 (\log E_1)^2 + 116.6365 \log E_1 - 0.28598 f_1^3 + 18.33145 f_1^2 - 313.4977 f_1 - 138.63055 \right) \times$$
$$\left((\log E_3)^{-2.26532} \times (\log E_2)^{0.63254} \times (\log E_1)^{3.40458} - 48.74302 \right) \times \left(-0.04807 (f_0 c)^{-0.43897} + 0.01113 \right) \times (-0.20257 f_0 - 8.192 \times 10^{-5})$$

$$K_d = -0.51204 \left(63.17429 (\log E_1)^3 - 559.09684 (\log E_1)^2 + 1677.3344 \log E_1 + 0.00279 f_1^3 - 0.06646 f_1^2 + 12.64402 f_1 - 1687.81813 \right) \times$$
$$\left((\log E_3)^{-0.85202} \times (\log E_2)^{2.97766} \times (\log E_1)^{-2.52145} - 0.11653 \right) \times \left(-1.50679 (f_0 c)^{-0.00846} + 1.44086 \right) \times (-15.95577 f_0 + 0.56149)$$

$$K_e = \left(-2.2869 (\log E_1)^3 + 22.42583 (\log E_1)^2 - 75.4725 \log E_1 + 82.61074 \right) \times$$
$$\left((\log E_3)^{-0.0866} \times (\log E_2)^{-0.23452} \times (\log E_1)^{0.85983} - 2.61035 \right) - 2.09231$$

26. HMA/HMA: $K_{shearing}$@LTE=0.1 under single axle load of 25 kip

$$K_a = \left(-0.3871 \log H_3 + 2.6905 (\log E_3)^{1.4727} - 0.6216 (\log H_2)^2 - 0.1397 \log H_2 - 0.5264 (\log E_2)^2 + 3.6743 \log E_2 - 1.9082 \right) \times$$
$$\left(-1.4546 \log H_1 + 0.1887 (\log E_1)^2 - 1.8289 \log E_1 + 9.7058 \right)$$

$$K_b = 0.05338 \left(-1.11005 (\log E_1)^2 + 3.73399 \log E_1 - 0.00305 f_1^2 + 0.14486 f_1 + 11.0707 \right) \times$$
$$\left((\log E_3)^{-1.43494} \times (\log E_2)^{-0.73357} \times (\log E_1)^{4.31732} - 0.2651 \right) \times \left(0.87894 (f_0 c)^{0.00209} \times (f_0 (c + H_2))^{-0.04327} - 0.76963 \right)$$

$$K_c = 0.00275 \left(21.8434 (\log E_1)^2 - 235.7621 \log E_1 - 0.01369 f_1^2 + 0.6156 f_1 + 642.0770 \right) \times$$
$$\left((\log E_3)^{-1.44449} \times (\log E_2)^{-0.63819} \times (\log E_1)^{6.42022} - 2.90489 \right) \times \left(-0.30462 (f_0 c)^{0.00349} \times (f_0 (c + H_2))^{-0.02913} + 0.28339 \right)$$

$$K_d = 0.38664 \left(-6.5291 (\log E_1)^2 + 54.4341 \log E_1 - 0.00305 f_1^2 + 0.09749 f_1 - 94.18648 \right) \times$$
$$\left((\log E_3)^{-1.66122} \times (\log E_2)^{-0.28884} \times (\log E_1)^{0.9949} - 0.01403 \right) \times \left(-0.98922 (f_0 c)^{0.00953} \times (f_0 (c + H_2))^{0.05199} + 1.16833 \right)$$

$$K_e = \left(0.00190 (\log E_1)^2 + 0.00533 \log E_1 + 0.13048 \right) \times$$
$$\left((\log E_3)^{-2.08728} \times (\log E_2)^{0.23067} \times (\log E_1)^{0.61965} + 0.31873 \right) - 0.0669$$

27. HMA/HMA: $K_{shearing}$@LTE=0.5 under single axle load of 25 kip

$$K_a = \left(-0.04862 \log H_3 - 0.36443 (\log E_3)^{-0.1.0435} + 0.23028 (\log H_2)^2 - 1.02157 \log H_2 + 0.01471 (\log E_2)^2 + 0.06963 \log E_2 + 2.02486 \right) \times$$
$$\left(-6.09196 \log H_1 + 7.76307 (\log E_1)^2 - 73.28617 \log E_1 + 194.48495 \right)$$

$$K_b = 0.05997 \left(84.64725 (\log E_1)^2 - 450.7625 \log E_1 + 0.07066 f_1^2 + 4.34521 f_1 + 583.3783 \right) \times$$
$$\left((\log E_3)^{-0.26273} \times (\log E_2)^{-1.12901} \times (\log E_1)^{1.45638} - 0.86080 \right) \times \left(0.00281 (f_0 c)^{0.92701} \times (f_0 (c + H_2))^{-1.90795} + 0.02504 \right)$$

$$K_c = 0.31318 \left(-52.21494 (\log E_1)^2 + 296.48271 \log E_1 + 0.11422 f_1^2 - 2.67739 f_1 - 424.64773 \right) \times$$
$$\left((\log E_3)^{-0.59618} \times (\log E_2)^{0.56993} \times (\log E_1)^{-0.82417} - 0.23234 \right) \times \left(-2.8877 (f_0 c)^{0.01666} \times (f_0 (c + H_2))^{-0.02046} + 2.95702 \right)$$

$$K_d = 0.06778 \left(57.95241 (\log E_1)^2 - 330.7743 \log E_1 - 0.15410 f_1^2 + 3.51775 f_1 + 479.54338 \right) \times$$
$$\left((\log E_3)^{-0.13699} \times (\log E_2)^{0.02797} \times (\log E_1)^{-0.12679} - 0.66708 \right) \times \left(-0.07519 (f_0 c)^{-0.03623} \times (f_0 (c + H_2))^{0.54188} + 1.21492 \right)$$

$$K_e = \left(1.34232 (\log E_1)^2 - 8.1839 \log E_1 + 12.47348 \right) \times$$
$$\left((\log E_3)^{-0.58497} \times (\log E_2)^{0.71435} \times (\log E_1)^{-2.52283} - 0.00056 \right) + 0.00529$$

28. HMA/HMA: $K_{shearing}$@LTE=0.9 under single axle load of 25 kip

$$K_a = \left(-0.03372 \log H_3 + 3.61517 (\log E_3)^{0.39514} + 0.69029 (\log H_2)^2 - 4.5708 \log H_2 + 0.08537 (\log E_2)^2 - 0.54853 \log E_2 + 5.59021 \right) \times$$
$$\left(1.38326 \log H_1 + 0.44852 (\log E_1)^2 - 2.02384 \log E_1 + 0.82749 \right)$$

$$K_b = -1.16296 \left(-0.19772 (\log E_1)^2 + 3.59637 \log E_1 - 0.08219 f_1^2 + 3.18523 f_1 - 7.44357 \right) \times$$
$$\left((\log E_3)^{-0.82282} \times (\log E_2)^{-1.06221} \times (\log E_1)^{-0.31239} - 0.01514 \right) \times \left(-0.01003 (f_0 c)^{-0.59021} + 0.15167 \right)$$

$$K_c = 0.48455 \left(10.15602 (\log E_1)^2 - 109.6302 \log E_1 - 0.09097 f_1^2 + 4.05044 f_1 + 298.3276 \right) \times$$
$$\left((\log E_3)^{-0.89979} \times (\log E_2)^{-0.8055} \times (\log E_1)^{1.37894} + 0.07573 \right) \times \left(1.71143 (f_0 c)^{-0.0027} - 1.69622 \right)$$

$$K_d = -0.0181 \left(22.15799 \left(\log E_1 \right)^2 - 151.9949 \log E_1 + 0.55888 f_1^2 - 22.28526 f_1 + 231.7873 \right) \times$$
$$\left(\left(\log E_3 \right)^{-0.56642} \times \left(\log E_2 \right)^{-0.49595} \times \left(\log E_1 \right)^{0.14085} - 0.15326 \right) \times \left(-0.12396 \left(f_0 c \right)^{-0.43348} + 0.58385 \right)$$

$$K_e = \left(0.20972 \left(\log E_1 \right)^2 - 0.99724 \log E_1 + 1.97168 \right) \times \left(\left(\log E_3 \right)^{0.00593} \times \left(\log E_2 \right)^{0.02992} \times \left(\log E_1 \right)^{0.32181} - 1.91878 \right) + 0.37692$$

APPENDIX B:
OVERLAY TEST PROTOCOL FOR HMA FRACTURE PROPERTIES

1. SCOPE

    1.1. This test method determines the fatigue fracture properties of bituminous mixtures. This test method is very similar to the regular overlay test procedure, Tex-248-F, but not exactly the same.

    1.2 The values given in parentheses (if provided) are not standard and may not be exact mathematical conversions. Use each system of units separately. Combining values from the two systems may result in nonconformance with the standard.

2. APPARATUS

    2.1 *Overlay Tester*—The device is an electro-hydraulic system that applies repeated direct tension loads to specimens. The machine features two blocks. One is fixed and the other slides horizontally. The device automatically measures and records load, displacement, and temperature every 0.1 sec.

    The sliding block applies tension in a cyclic triangular waveform to a constant maximum displacement of 0.025 in. (0.63 mm). The sliding block reaches the maximum displacement and then returns to its initial position in 10 sec. (one cycle).

    Note 1 —the constant maximum opening displacement of 0.025 in. (0.63 mm) may need to be reduced to be 0.015 in. (0.38 mm), depending on how stiff the bituminous mixtures are.

    Additionally, the device includes:

    - an air bath chamber that controls the test temperature,

    - a linear variable differential transducer to measure the displacement of the block,

    - an electronic load cell to measure the load resulting from the displacement,

    - aluminum or steel base plates to restrict shifting of the specimen during testing, and

    - a mounting jig to align the two base plates for specimen preparation.

    Refer to manufacturer for equipment range and accuracy for LVDT and load cell.

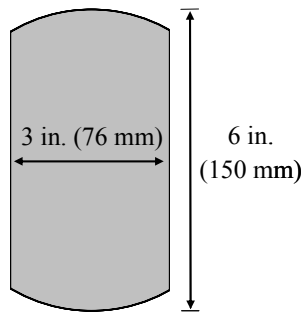   2.2 *Cutting Template*—Refer to Figure B1.

Figure B1. Cutting Template.

2.3 *3/8-in. Socket Drive Handle with a 3-in. (7.6 cm) extension.*

2.4 *Hacksaw with carbide grit blade.*

3. MATERIALS

3.1 *Two-part epoxy with a minimum 24 hr. tensile strength of 600 psi (4.1 MPa) and 24 hr. shear strength of 2,000 psi (13.8 MPa) according to Tex-614-J.*

3.2 *10 lb. (4.5 kg) weight.*

3.3 *1/4-in. width adhesive tape.*

3.4 *Paint or permanent marker.*

4. SPECIMENS

4.1 *Laboratory Molded Specimens*—Prepare specimens according to Tex-205-F and Tex-241-F. Specimen diameter must be 150 mm (6 in.) and specimen height should be 115 ±5 mm (4.5 ±0.2 in.). Density of the laboratory molded specimen should be targeted such that the trimmed specimen density is 93 ±1%.

Note 2 —Select molded specimen density depending on experience and knowledge of materials used, typically 92 ±1%.

Note 3 —Mixture weights for specimens prepared in the laboratory typically vary between 4500 to 4700 g to achieve density. Mixture weights for specimens prepared in the laboratory vary with different aggregate sources and with different mix types.

4.2 *Core Specimens*—Specimen diameter must be 6 ±0.1 in. (150 ±3 mm) and specimen height should be a minimum of 1.5 in. (38 mm). There is not a specific density requirement for core specimens.

5. PROCEDURE

5.1 *Sample Preparation:*

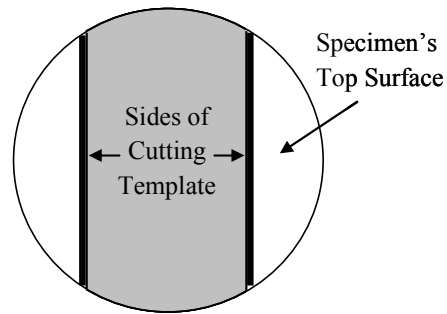5.1.1 Use three cylindrically molded specimens or collect three roadway cores according to Section 4.

5.2 *Trimming of Cylindrical Specimen:*

5.2.1 Place the cutting template on the top surface of the laboratory molded specimen or roadway core. Trace the location of the first two cuts by drawing lines using paint or a permanent marker along both sides of the cutting template.
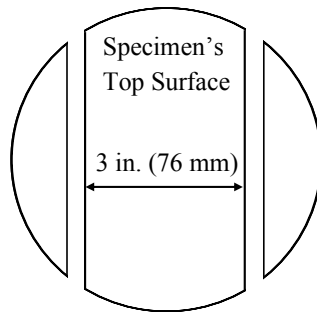
5.2.2 Trim the specimen ends by cutting the specimen perpendicular to the top surface following the traced lines. Discard specimen ends.

5.2.3 Trim off the top and bottom of the specimen to produce a sample with a height of 1.5 ±0.02 in. (38 ±0.5 mm). Discard the top and bottom parts of the specimen.
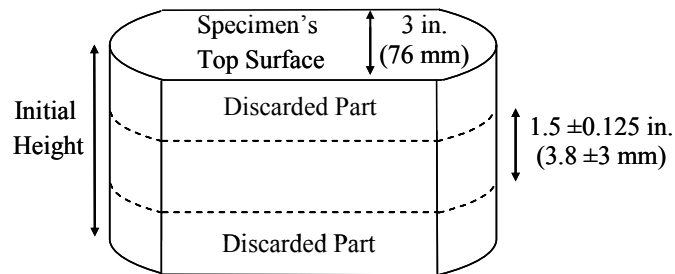
Note 4 —Refer to Figure B2.

Tracing lines using cutting template

Specimen's Top Surface

Sides of Cutting Template

Specimen's Top Surface

3 in. (76 mm)

Trimming specimen's ends

Specimen's Top Surface   3 in. (76 mm)

Initial Height

Discarded Part

1.5 ±0.125 in. (3.8 ±3 mm)

Discarded Part

Trimming specimen to required height

Figure B2. Trimming of Cylindrical Specimen.

5.2.4   Measure the relative density of the trimmed specimen according to Tex-207-F. Density for trimmed laboratory molded specimen must be 93 ±1%. Discard and prepare a new specimen if it does not meet the density requirement. Density for trimmed core specimens is for informational purposes only.

5.2.5   Dry the trimmed specimen at a maximum temperature of 140 ±5°F (60 ±3°C) to constant weight.

Note 5 —Constant weight is the weight at which further oven drying does not alter the weight by more than 0.05% in a 2-hr. interval.

5.3 *Mounting Trimmed Specimen to Base Plates:*

5.3.1   Mount and secure the base plates to the mounting jig. Cut a piece of adhesive tape approximately 4.0 in. (102 mm) in length. Center and place piece of tape over the gap between the base plates.

131

5.3.2   Prepare epoxy following manufacturer's instructions.

5.3.3   Glue the trimmed specimen to the base plates using the prepared epoxy. Cover the majority of both base plates with the epoxy including the tape.

5.3.4   Place a 10-lb. (4.5 kg) weight on top of the glued specimen to ensure full contact of the trimmed specimen to the base plates. Allow the epoxy to cure for the time recommended by the manufacturer. Remove the weight off the specimen after the epoxy has cured.

5.3.5   Use a hacksaw to cut through the tape and dry epoxy located at the gap opening between the base plates. Slightly score the test specimen to propagate a crack at the gap opening.

5.4 *Preconditioning the OT specimen*

5.4.1   Place the test sample assembly in a 77 ±1°F (25 ±0.5°C) temperature chamber and allow to remain for a minimum of 2 hours before testing.

5.5 *Starting Testing Device:*

5.5.1   Turn on the overlay tester. Turn on the computer and wait at least 1 minute to establish communication with the overlay tester. Start the overlay test software.

5.5.2   Turn on the hydraulic pump using the software after it is completely loaded on the computer. Turn the machine to load mode.

5.6 *Mounting Trimmed Test Specimen to Testing Device:*

5.6.1   Enter the required test information into the overlay test software for the specimen mounted. Mount the specimen assembly onto the machine according to the manufacturer's instructions and the following recommendations.

- Clean the bottom of the base plates and the top of the testing machine blocks before placing the specimen assembly into the blocks. If not all four surfaces are clean, damage may occur to the machine, the specimen, or the base plates when tightening the base plates.

- Apply 15 lb-in of torque for each screw when fastening the base plates to the machine.

5.7 *Testing Specimen:*

5.7.1   Turn the machine to stroke mode. Perform testing at a constant temperature of 77 ±1°F (25 ±0.5°C).

Note 6 —Ensure temperature of trimmed test specimen is 77 ±1°F (25 ±0.5°C).

5.7.2   Start the test by enabling the start button in the program. Perform testing until a 93% reduction (or more) of the maximum load measured from the first opening cycle occurs. If 93% is not reached, run the test to 100 cycles.

Note 7 —This is not a regular OT testing, a maximum of 100 cycles is enough for determining fracture properties *A* and *n*.

Note 8 —The constant maximum opening displacement of 0.025 in. (0.63 mm) may need to be reduced to be 0.015 in. (0.38 mm) if the cycles to reach 93% load reduction are less than 50 cycles. Then, repeat the test.

5.7.3   Remove specimen assembly.

Note 9 —Ensure machine is in load mode before removing specimen assembly.

6. Data Analysis and Report

An Excel© Macro has been developed to directly read the output file from the overlay test and automatically determine the fracture properties (*A* and *n*) of the specimen. Figure B3 shows the macro start window, and the *A* and *n* results from this macro are shown in Figure B4. Note that the only input the macro required is modulus of the specimen. The theoretical background and detailed steps of determining both *A* and *n* values are presented Appendix C.
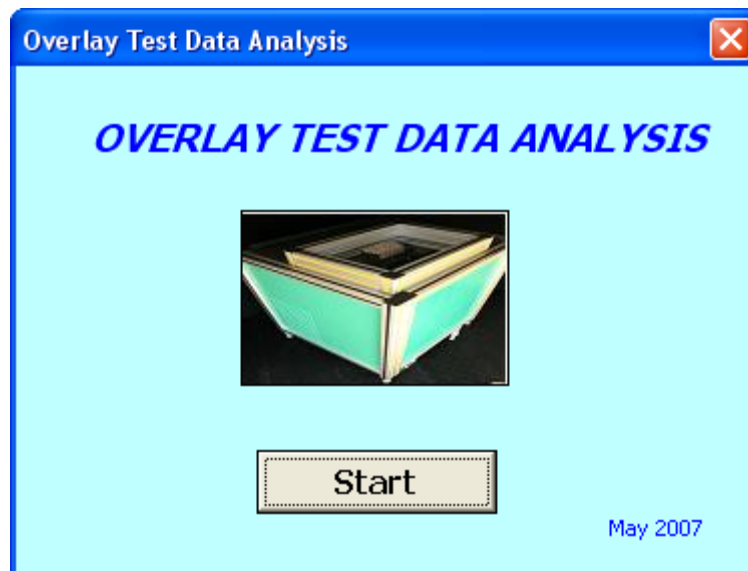

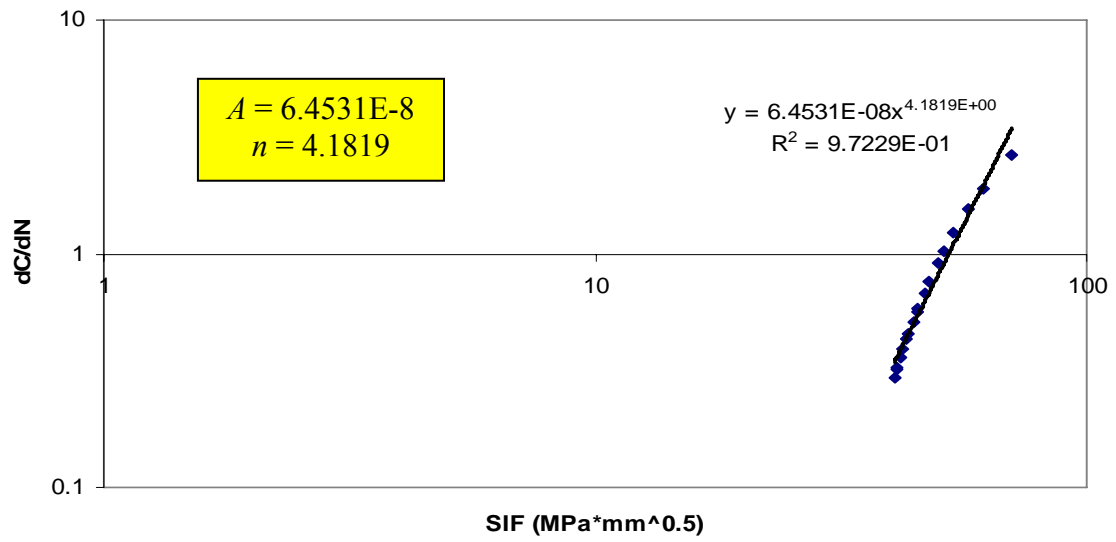**Figure B3. Macro for Fracture Properties (*A* and *n*).**

dC/dN and SIF

$A = 6.4531E-8$
$n = 4.1819$

$y = 6.4531E-08x^{4.1819E+00}$
$R^2 = 9.7229E-01$

dC/dN

SIF (MPa*mm^0.5)

Figure B4. *A* and *n* **Output from the Macro.**

APPENDIX C:
THEORETICAL BACKGROUND AND DETAILED STEPS OF DETERMINING HMA FRACTURE PROPERTIES: *A* AND *n*

It is well known that HMA mixes are complex materials. However, for simplicity and convenience, HMA mixes are often assumed to be quasi-elastic materials represented by dynamic modulus and Poisson's ratio. With this assumption, the well-known Paris' law shown in Equation 1 can be used to describe crack propagation of HMA mixes (*1*).

$$\frac{dc}{dN} = A(\Delta K)^n \tag{C-1}$$

where *c* is crack length, *N* is number of load repetitions, *dc/dN* is crack speed or rate of crack growth, ΔK is change of stress intensity factor (SIF), and *A* and *n* is fracture properties of material.

In view of Equation C-1, it can be seen that the information required for determining HMA fracture properties (*A* and *n*) includes 1) the SIF corresponding to any specific crack length (*c*) and 2) crack length (*c*) corresponding to a specific number of load repetitions (*N*). The proposed approach for determining the SIF and crack length (*c*) are discussed as follows:

- Determination of SIF

A two dimensional (2D) finite element (FE) program named *2D-CrackPro* was developed to analyze the SIF under the OT testing. In the *2D-CrackPro* program, the desired $\frac{1}{\sqrt{r}}$ stress singularity in the crack tip region was met by placing the mid-side nodes of two adjacent sides of an 8-node isoparametric element at the one-fourth distance mark from the common corner node (*2*). The accuracy of this program has been verified by comparing the computed SIFs of an infinite slab with a center crack with those given in "*the stress analysis of cracks handbook*" (*3*).

Figure C1 shows the 2D FE mesh plus the singularity elements used. Since Poisson's ratio has minor influence on SIF, a constant Poisson's ratio ($\upsilon=0.35$) was used for all the analyses. With the above quasi-elastic assumption, it has been found that the SIF is proportional to dynamic modulus (*E*) of the overlay tester (OT) specimen and the specified maximum opening displacement (MOD). Therefore, the SIFs corresponding to variable crack length (*c*) were calculated at an assumed condition: 1) dynamic modulus of the OT specimen: *E*=1 MPa, and 2) MOD = 1 mm. The results are presented in Figure C2. To facilitate implementation, a regression equation shown in Figure C2 was developed for the SIF versus crack length at the condition of *E*=1 MPa and *MOD* = 1 mm.

For any other *E* and *MOD* combination, the corresponding SIF can be determined by the following equation:

$$SIF = 0.2911 * E * MOD * c^{-0.4590} \tag{2}$$

where *SIF* is stress intensity factor (MPa*mm$^{0.5}$), *E* is dynamic modulus (MPa), *MOD* is maximum opening displacement (mm), and *c* is crack length (mm).
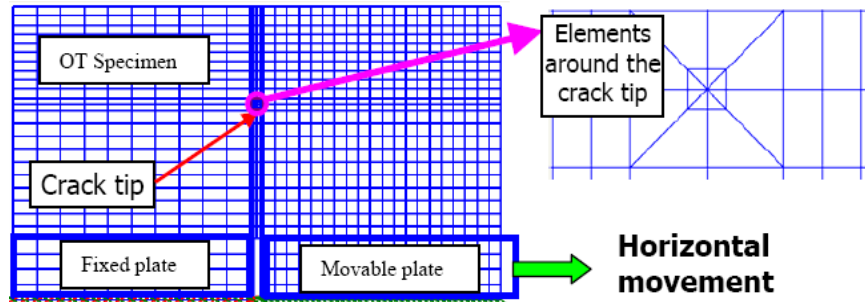
Figure C1. A 2D FE Mesh of the OT System.

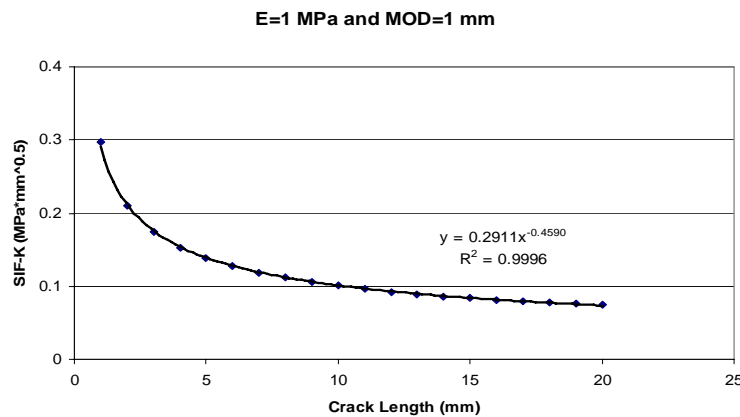**Figure C2. Calculated SIF vs. Crack Length.**

Additionally, it can be seen that the SIF shown in Figure C2 decreases rapidly at the beginning, and its decreasing rate becomes smaller and smaller with crack length growth. This observation indicates that the initial crack propagation stage is very important to determine reasonable fracture properties of HMA mixes, which means that the required fracture properties can be determined from the initial stage of the OT testing (perhaps within 15 minutes). This feature separates the OT from other types of fracture tests (such as, direct tension test [*4, 5, 6*], indirect tension test [*7*]), because the other tests often focused on the late crack propagation stage where the SIF increased rapidly so that these tests generally take a very long time (say hours).

- Determination of crack length (*c*)

To monitor crack length growth, researchers have used several different techniques such as crack foil (*5*). Recently, Seo et al. applied a Digital Image Correlation (DIC) technique to monitor crack propagation and crack length (*6*). The DIC is a non-contact, full-field displacement (or strain) measurement system that analyzes the displacement (or strain) by comparing digital images of a deformed specimen with that of an initial undeformed specimen. Compared with other techniques, the DIC is one of most advanced techniques for monitoring crack propagation. However, using the DIC system will definitely increase the difficulty and cost of running the OT. Fortunately, there is an alternative method used for estimating crack length, namely the backcalculation approach, which has been successfully used by Jacobs (*5*) and Roque et al. (*7*) to backcalculate the crack length from the recorded load or displacements.

Three assumptions listed below were made for establishing the theoretical relationship between an equivalent crack length and the maximum load required to reach a specified *MOD*.

1) An equivalent (or ideal) crack starts from the bottom at the center of the OT specimen and propagates vertically to the top surface of the specimen.
2) The reduction of maximum load from the first cycle is attributed to crack growth.
3) As assumed previously, HMA mixes are quasi-elastic and are represented by a dynamic modulus and Poisson's ratio ($\upsilon=0.35$).

With the above three assumptions, the maximum load required to reach a *MOD* is proportional to the dynamic modulus of the OT specimen and decreases with crack length growth, provided that the *MOD* is constant. To exclude the influence of the dynamic modulus and the *MOD*, the maximum load corresponding to any crack length was normalized to the maximum load corresponding to "zero" crack length which is determined through extrapolation. Figure C3 shows the relationship between the normalized maximum load (*y-axis*) and crack length (*x-axis*). A corresponding regression equation is also presented in Figure C3.

Since the maximum load at each cycle is automatically recorded during the OT testing, it is easy to develop the relationship between the normalized maximum load at each cycle and the number of cycles. Finally, combining with Figure C3, crack growth rate (d*c*/d*N*) can be calculated.

- Determination of fracture properties: *A* and *n*

With known SIF (*K*) and crack growth rate (*dc/dN*), the fracture properties (*A* and *n*) can be readily determined. Figure C4 shows the five steps of determining HMA fracture properties (*A* and *n*).
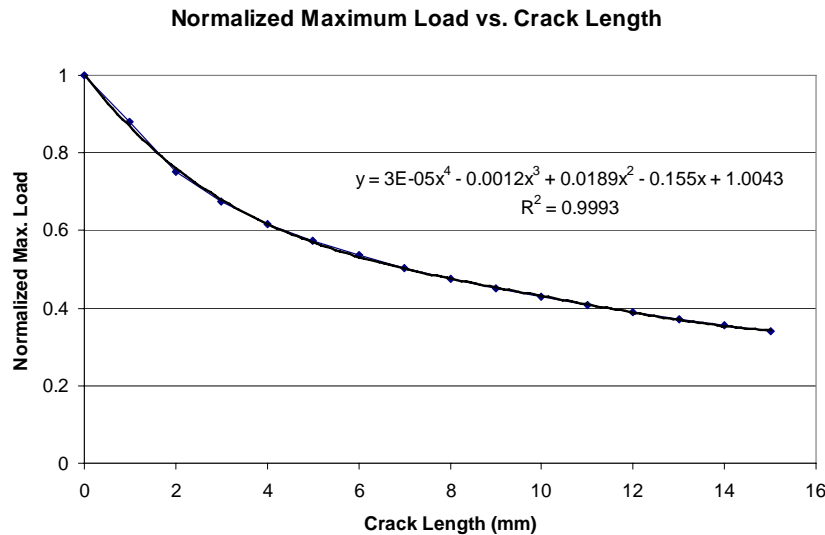
Normalized Maximum Load vs. Crack Length

$y = 3\text{E-05}x^4 - 0.0012x^3 + 0.0189x^2 - 0.155x + 1.0043$
$R^2 = 0.9993$

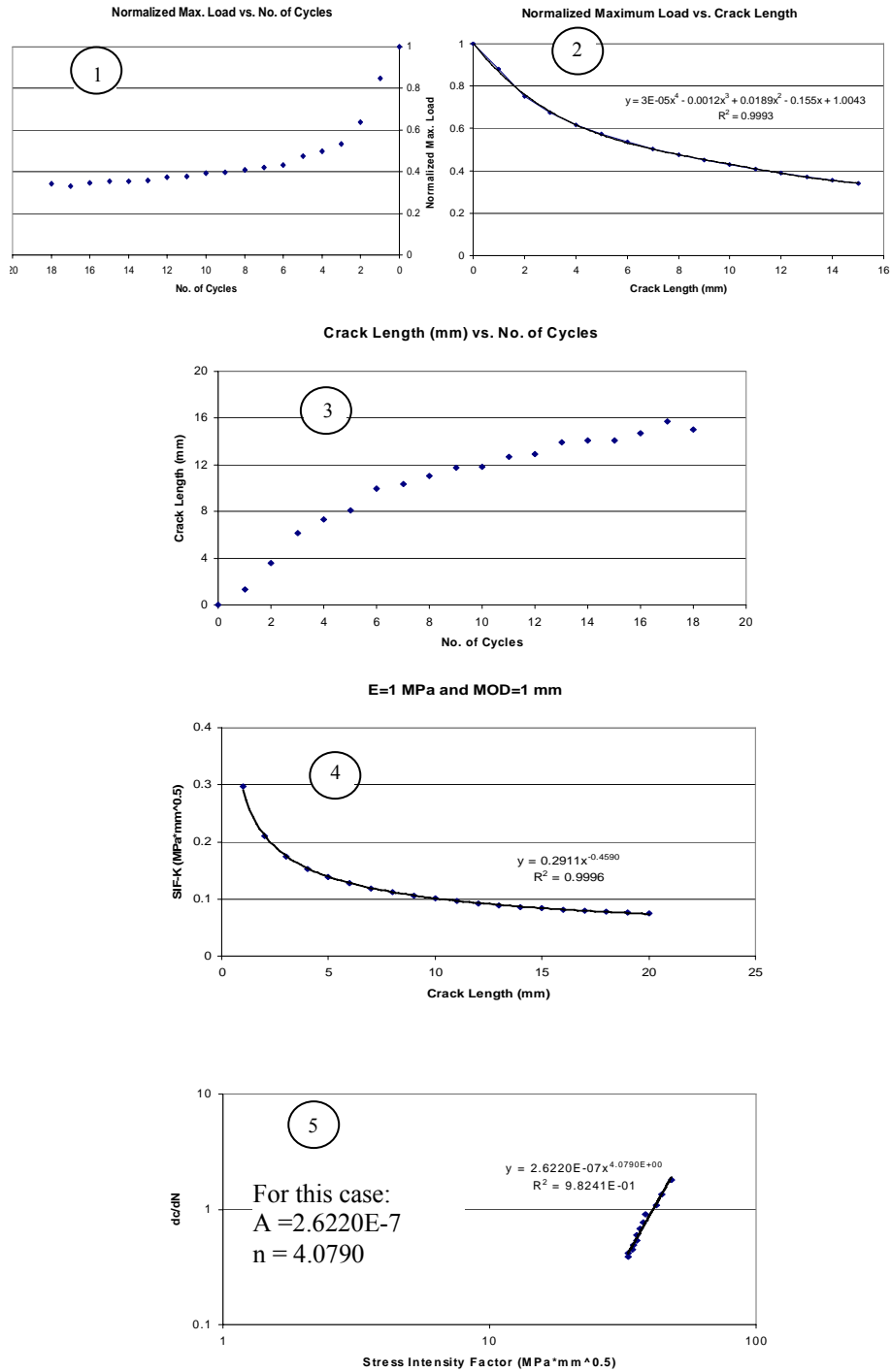**Figure C3. Normalized Maximum Load vs. Crack Length.**

Figure C4. Determination of Fracture Properties: *A* and *n*.

In summary, this appendix presented the development and detailed steps of determining HMA fracture properties (*A* and *n*) using the OT.

APPENDIX C REFERENCES

1. Paris, P. C., and F. Erdogan, A Critical Analysis of Crack Propagation Laws, *Transactions of the ASME, Journal of Basic Engineering*, Series D, 85, No. 3, 1963.
2. Barsoum, R. S., On the Use of Isoparametric Elements in Linear Fracture Mechanics, *International Journal of Numerical Methods in Engineering*, Vol. 10, pp. 25, 1976.
3. Tada, H., P. C. Paris, and G. R. Irwin, *The Stress Analysis of Cracks Handbook*, 3rd Ed., New York, ASME Press, 2000.
4. Molenaar, A. A. A., "Structural Performance and Design of Flexible Road Constructions and Asphalt Concrete Overlays," Ph.D. Dissertation, *Delft University of Technology,* 1983.
5. Jacobs, M. M. J., *Crack Growth in Asphaltic Mixes*, Ph.D. Dissertation, Delft University of Technology, Road Railraod Research Laboratory, The Netherlands, 1995.
6. Seo, Y., Y. R. Kim, R. A. Schapery, M. W. Witczak, and R. Bonaquist, A Study of Crack-Tip Deformation and Crack Growth in Asphalt Concrete Using Fracture Mechanics, *Journal of the Association of Asphalt Paving Technologists,* Vol. 73, pp. 200-228, 2004.
7. Roque, R., Z. Zhang, and B. Sankar, Determination of Crack Growth Rate Parameters of Asphalt Mixtures Using the Superpave IDT, *Journal of the Association of Asphalt Paving Technologists,* Vol. 68, pp. 404-433, 1999.